THE SYNTHESIS OF MODEL ASPHALTENES

A thesis submitted to the University of Manchester for the degree of Doctor of Philosophy in the Faculty of Science and Engineering

Barnaby T. Haire
School of Chemistry
The University of Manchester
2018

TABLE OF CONTENTS

Word Count: 33720

LIST OF FIGURES

DEFINITIONS

Acene	Linear, cata-condensed polyaromatic hydrocarbon.
Archipelago	Possible structural type for the asphaltenes. Consisting of aromatic units bridged by chain functionality.
Asphaltene	Heptane-insoluble, toluene-soluble fraction of bitumen.
Asphaltene dispersant	Compound or polymer capable of suspending asphaltene colloids in solution.
Asphaltene inhibitor	Compound or polymer capable of preventing asphaltene colloids from forming.
Benzenoid	Fully resonance stabilised π-sextet reflecting the aromatic properties of benzene.
Biodegradation	The process by which hydrocarbons formed from catagenisis are decomposed by micro-organisms to form a heavier crude oil.
Bitumen	The non-volatile fraction of crude oil distillation in the refinery.
Cata-condensed	Non-linear, stepped polyaromatic geometry where aromatic rings are connected through two common atoms.
Catagenisis	The process describing the cracking process of kerogen into lighter hydrocarbons.
Clar's Sextet	An empirical rule relating the number of benzenoid aromatic rings in a molecule to the overall stability of polyaromatics.
Colloid	A homogenous non-crystalline substance consisting of aggregated small molecules dispersed throughout a liquid.
Desalter	A process unit in an oil refinery which separate brine from petroleum before introducing the feedstock to fractional distillation.
Diagenisis	The process describing the evolution of sediments after they are deposited and buried. Can include physical, chemical and biological change.
Double bond equivalent	Value assigned to the sum of the double and triple bonds present in a molecule.

Heat exchanger	A process unit that transfers heat energy to crude oil prior to fractional distillation.
Heavy crude oil	Petroleum possessing a higher proportion of resins and asphaltenes in comparison to volatile alkanes commonly associated with difficulties regarding extraction and transport.
Island	Possible structural type for the asphaltenes. Consisting of a single, peri-condensed aromatic core with peripheral alkyl functionality.
Kerogen	A nonspecific carbonaceous deposit formed from the breakdown of organic matter under thousands of tons of pressure over millennia.
Light crude oil	Petroleum with favourable fluid properties consisting largely of light alkanes used in fuels.
Maltenes	A fraction of crude oil existing in the vacuum residue of fractional distillation. Heavier than the saturates and aromatics, but lighter than the asphaltenes. Separated from the asphaltenes by partitioning into n-heptane.
Mercaptan	Another term for thiol. Any sulfur-containing compound possessing the formula R-SH.
Peri-condensed	Non-linear condensed aromatic geometry where three rings in a condensed ring system share a single ring atom in common.
Permeability	Capacity for fluid flow.
Petroleum/Crude oil	A liquid mixture of hydrocarbons formed in sedimentary rock deposits commonly obtained by drilling and refined into fractions including gasoline, kerosene and naphtha.
Pigging	The practice of performing maintenance operations upon pipelines using ‘pig’ devices. Common uses involve cleaning and inspection.
Reservoir	A location of petroleum deposit.
Resin	A subcomponent of the maltenes. Separated through being soluble in heptane and insoluble in lighter hydrocarbons such as propane.

Specific Gravity	Ratio of density compared to a reference. Specific Gravity = density of object/density of water, for example.
Topology	Molecular structural architecture.
Tower tray	A device that facilitate the fractionation of crude oil in distillation.

GLOSSARY OF ABBREVIATIONS

AFM	Atomic Force Microscopy
APCI	Atmospheric Pressure Chemical Ionisation
API	American Petroleum Institute
ASAP	Atmospheric Solids Analysis Probe
CMC	Critical Micelle Conversation
CVD	Chemical Vapour Deposition
DBE	Double Bond Equivalent
DCM	Dichloromethane
DDQ	2,3,-Dichloro-5,6-dicyano-1,4-benzoquinone
DEPT	Distortionless Enhancement by Polarisation Transfer
DFT	Density Functional Theory
DMF	*N*,*N*-Dimethyl Formamide
ESI	Electrospray Ionisation
FAR	Fused Aromatic Region
FCS	Fluorescence Correlation Spectroscopy
FIMS	Field Ionisation Mass Spectroscopy
GC	Gas Chromatography
HBC	Hexabenzocoronene
HOPG	Highly Orientated Pyrolytic Graphite
HPB	Hexaphenylbenzene
HRTEM	High-Resolution Transmission Electron Microscopy
LDA	Lithium Diisopropylamide
LDI	Laser Desorption Ionisation
LIAD-EI	Laser-Induced Acoustic Desorption Electron Ionisation
MALDI	Matrix Assisted Laser Desorption Ionisation
MS	Mass Spectroscopy
NMR	Nuclear Magnetic Resonance
OAC	Oxidative Aromatic Coupling
OLED	Organic Light Emitting Display
PAH	Polyaromatic Hydrocarbon
PBI	Perylene *bis*-imide
PHT	Pre-Heat Train

SARA	Saturate, Aromatic, Resin, Asphaltene
SFA	Surface Force Apparatus
SG	Specific Gravity
STM	Scanning Tunnelling Microscopy
TAN	Total Acid Number
TBP	Tribenzoperylene
TCNQ	Tetracyanoquinodimethane
THAI	Toe-to-Heel Air Injection
THF	Tetrahydrofuran
TFA	Trifluoroacetic Acid
TRFD	Time Resolved Fluorescence Depolarisation
VAPEX	Vapour Extraction
XANES	X-ray Adsorption Near Edge Structure

ABSTRACT

Derivatives of polyaromatic core structures representing ‘island’ and ‘archipelago’ structural types were synthesised, functionalised and characterised for use in developing a fundamental understanding of asphaltene aggregation and deposition.

Tetraphenylcyclopentadiene derivatives were subjected to Diels-Alder cycloaddition enabling a suite of tetra- and hexaphenylbenzenes. Subsequent oxidative aromatic coupling provided a key synthetic step in the formation of functionalised tribenzopentaphene and hexabenzocoronene derivatives. The reaction procedure for isolation of 1-nitroperylene was refined and enabled the installation of thiophene, carbazole and pyridine functionalities, with alkyl functionality incorporated by Sonogashira coupling and acylation to permit solution-based analysis. Nucleophilic aromatic substitution and nucleophilic substitution chemistries were performed deliver a series of alkyl-tethered pyrene and phenanthrene derivatives.

Preliminary investigations performed by academic partners into model compounds deposition behaviour utilising atomic force microscopy and adsorption isotherms have provided information regarding substrate affinity through surface coverage and morphology analysis.

The University of Manchester, March 2018
Barnaby T. Haire

Degree Title: Doctor of Philosophy
Thesis Title: The Synthesis of Model Asphaltenes

DECLARATION

Work undertaken in collaboration with other researchers has been attributed in the text. Preliminary work on the synthesis and evaluation of 1- and 3-nitroperylene (**27** and **28**) and its derivatives (**30**) was also included in the MChem report (University of Manchester) of supervised student Eben McCabe.[1] AFM results of **32** upon various substrates included herein (**sect. 2.1.5.1**) will also be included in the PhD thesis (University of Cambridge) of Domina-Maria Kaimaki. Adsorption Isotherms calculated for **32** upon various substrates included herein (**sect. 2.1.5.2**) will also be included in the PhD thesis (University of Cambridge) of Richard Alloway.

NO OTHER PORTION OF THE WORK REFERRED TO IN THE THESIS HAS BEEN SUBMITTED IN SUPPORT OF AN APPLICATION FOR ANOTHER DEGREE OR QUALIFICATION OF THIS OR ANY OTHER UNIVERSITY OR OTHER INSTITUTE OF LEARNING.

COPYRIGHT STATEMENT

ACKNOWLEDGEMENTS

Firstly, I must thank my supervisors Dr Peter Quayle and Prof. Stephen Yeates for giving me the opportunity to pursue these studies and for providing such excellent support throughout.

This work would not have been possible without the expertise of my colleagues in the School of Chemistry. I would like thank Dr Mark Little for his tuition and guidance in dealing with stressful syntheses; Dr Adam Parry for always being available and helpful regarding topics ranging from project direction to data analysis; Dr Daniel Tate and Dr John Morrison for sharing their extensive experience with vexing materials; Dr Ralph Adams and Dr Carlo Bawn for running and processing NMR experiments; Dr Inigo Victorica-Yrezabal and Dr George Whitehead for acquiring X-ray structures from my often questionable crystals, and Gareth Smith for uncountable mass spectrometry analyses.

Much of the credit for this work is owed to my friends and peers in OMIC, who have stood with me in solidarity whether enjoying the highs of a successful project or facing a crisis of confidence in Sandbar: Josh Moore, Glenn Sunley Saez, Vaiva Nagyte, Tom Raine, Fiona Porter, Ray Marcial, Robyn Worsley, Seb Broll, Andrew Foster, Vanessa Tischler, Matt Boyes, Rich Stevenson, Daryl McManus and Kane Heard.

I would like to acknowledge BP ICAM for providing the funding for this research. Working within this group has been so enjoyable thanks to my friends and collaborators: Maria Kaimaki, Emma Antonio, Richard Alloway, Matt Acres, James Gilcrist, Pralav Shetty, Mike Odarczenko and Thu Doan.

Finally, I would like to thank my Grandad and Granduncle (Robin and Grant), who were as inspiring as they were kind; my parents; my siblings (Amy, Sam and Jim) and my new niece Annie for their constant encouragement.

1. INTRODUCTION

1.1. PETROLEUM

Petroleum, or crude oil, has been the main source of the world's energy production for over a century and demand is predicted to increase 30% from 2006 to 2030.[2] It represents a continuum of solids, liquids and gases that occur in sedimentary rock deposits with highly varied chemical compositions and physical properties. Formed over millions of years under huge pressures, organic matter is transformed, fossilised into petroleum fluids and captured in sedimentary basins.[3] From these traps, the material can be captured and refined. The fluid properties of a crude oil are of great significance in determining the necessary procedure for extraction, with heavier, more viscous sources providing numerous chemical engineering difficulties.[4] The scale of the challenge in profiting from unconventional crude oils – mainly heavy oils, extra heavy oils and bitumens - is represented clearly upon observation of activities in Venezuela and Canada, which are currently considered to possess a reserve of heavy oil comparable to the amount of conventional oil worldwide.[5] The profitable collection, transportation and conversion of these substances remains elusive however, owing namely to the challenging demands of their fluid properties. An increased viscosity, high acidity and metal content require transportation and upgrading technologies to be significantly advanced in order to maintain supplies of petroleum products (**Table 1**, **Fig. 1**), representing a major challenge regarding future energy supply and security.[6,7]

Type of Crude	Volumes in Place (Bb)	Recoverable Volumes (Bb)
Conventional heavy	1,000	200-250
Extra-heavy	1,350	40-244
Bitumen	2,650	290-450
Total heavy oils	**5,000**	**530-944**
Conventional crude	**4,800**	**1,032**

Table 1. Predicted total and recoverable conventional and unconventional crude oil rescources in billions of barrels (Bb).[2]

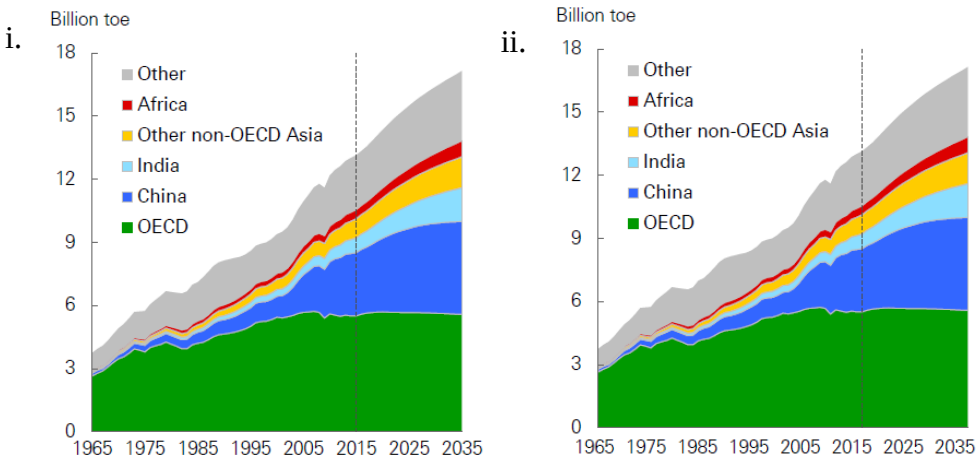

Figure 1. Past and future oil consumption by region in billion tons of oil (TOE) equivalent (part i). Primary energy consumption by fuel source (part ii).[6]

A chemical class of highly aromatic organic and inorganic compounds termed the asphaltenes are one of the components responsible for complicating the processing of heavy crude oils.[8] Their chemical composition results in instability in the liquid phase. They exist at the boundary of the solubility limit of a crude oil and are capable of aggregation, forming particles that contribute to increased viscosity levels.[9] Furthermore, the aggregation state of these species is largely impacted by changes in temperature and pressure, with precipitation a common occurrence in industrial tubing.[10] Asphaltene deposits are responsible for problems including reduced flow rate, increased maintenance costs and at its most severe, the complete shutdown of the extraction to clear a severe blockage.[11]

Attempts to mitigate the impact of asphaltenes upon the refinery process have been diverse, targeting both the solution phase and surface chemistry. In the bulk phase, aggregation prevention has been treated with a broad spectrum of asphaltene inhibitors/dispersants including anionic and ionic surfactants, polymeric and non-polymeric amphiphiles, fatty acids/esters and ionic liquids.[12] Utilising surface chemistries that aim to prevent strong interactions between the depositing species and the substrate has also been heavily invested in.[13–15] The limitations of these approaches are due to each heavy crude oil requiring specific treatments that are difficult to reproduce from laboratory scale to the reservoir.

Until recently, asphaltene science has been effectively reduced to phenomenology due to their structural and physical properties being obscured by complexity.[16,17] Despite many parameters now being largely agreed upon by the scientific community,[18] analysis of this highly

complicated mixture of compounds remains a challenge. Model compounds have been studied to some success in simplifying the complex nature of asphaltenes.[19] By identifying key structural and functional groups solution and surface experiments can be performed to probe the nature of asphaltenes adsorption.[20] With the system well defined, analysis is greatly simplified. This data can then be used to develop targeted approaches to control asphaltenes in upstream refining.

1.2. LIGHT AND HEAVY CRUDE OIL FORMATION

In order to understand how bulk properties of heavy crude oils differ from their light counterparts, an understanding of the differences in their formation is critical. Petroleum reservoirs vary widely based on the location, temperature, depth and age. These conditions define the distribution of the organics present and the overall value of a potential extraction.

Petroleum fields are created by plant life and animal organic species decaying on the sea bed where they are stripped of chemicals such as nitrogen, oxygen and phosphorous by bacteria leaving mainly carbon and hydrogen to remain.[21] This organic matter is then exposed to increasingly high pressures as billions of tons of sand and silt layer upon them. Diagenisis describes the process of heat and pressure within the first several hundred metres of burial breaking down humin and various organics including lignin, carbohydrates, proteins and lipids to geopolymers chains which lead to the formation of the heaviest components of petroleum, kerogen.[22]

Kerogen is capable of further chemistry in catagenisis (**Fig. 2**), which describes the cracking of these geopolymers at a deeper burial point to form hydrocarbon chains at higher temperatures and pressures. However, should the kerogen become trapped or not exposed to the pressures required for catagenisis, the extractable products from the reservoir will consist only of heavy hydrocarbons and bitumen. Sufficient temperatures in the catagenisis stage lead to more extensive cracking of light hydrocarbons to form shorter chained species, with methane being the end point of this mechanism.

After catagenisis aliphatic oil components can be oxidised to form an increasingly denser oil through biodegradation, creating a heavy oil. This is possible when the temperature of the hosting environment is low enough to permit anaerobic organisms to carry out microbial operations (<80 °C). Alkanes are consumed successively based on their chain length in a quasi-sequential manner, with the lightest being consumed first and followed by heavy and cyclic hydrocarbons later in the timeline. As aliphatic components of the reservoir are consumed, the relative proportion of resins and asphalt increases. This results in an increased viscosity, heteroatom content, metal content, and a higher acidity due to the presence of intermediate acid-containing chemical species from biodegradation. This is reflected in the high total acid number (TAN) seen in heavy oils.[2,23]

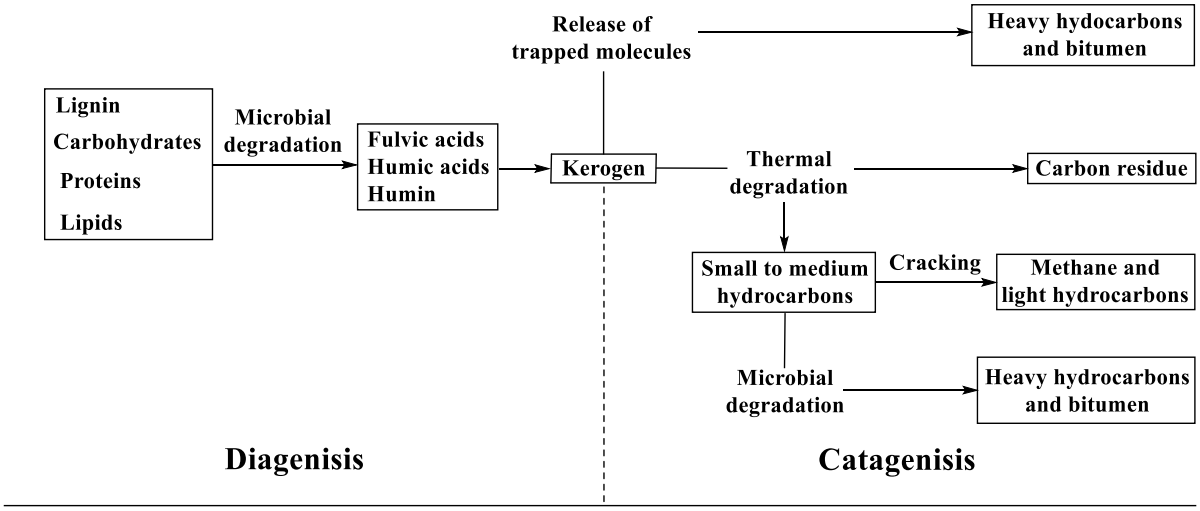

Figure 2. General scheme of petroleum formation.

Bitumen describes an unconventional crude oil that has formed as a result of incomplete catagenisis, resulting in significant quantities of soluble kerogen being present and an unfavourable distribution of valuable products. A heavy crude oil is typically produced through microbial degradation, where catagenisis is in the advanced stages and the paraffinic materials are partially converted to resins and asphaltenes by microorganisms.[24]

1.3. HEAVY CRUDE OILS – EXTRACTION AND REFINING

1.3.1. RESERVOIR

A reservoir is characterised based upon the quality of its hydrocarbon reserves. They are analysed for their quantity, composition, density, temperature of formation and permeability (capacity for fluid flow). A well can then be assigned a valuation for its contents. Following this, the potential costs of extraction are considered taking in to account depth profile, thickness, rock type, sedimentology analysis and geological history.[4,25]

Heavy crude oil analysis and extraction represents an undertaking of significantly higher complexity compared to lighter counterparts. The quality of hydrocarbons is more difficult to assess due to the wettability of rock being reduced,[26] raising the possibility of an inaccurate assessment of the reservoir contents. Furthermore, the quality of hydrocarbons is significantly poorer resulting in a less favourable distribution of commercial products.

Increased viscosity of heavy oil results in a slower flow rate. This is treated by injection of heat directly into the reservoir. This can be achieved with hot water flooding, but often results in structural deformations of the reservoir and, unsurprisingly, a much higher oil to water ratio of extracted product. Steam flooding is a significantly more effective treatment and has been used intensively due to having higher heat content and reduced volumes being required. However, the disparity between densities can often result in water or steam only being able to transfer its heat to the reservoir oil at the interface between liquids, resulting in poor heat transfer. This can be addressed with polymer injection, whereby the density of the water is increased to closer match that of oil and encourage mixing. Carbon dioxide injection, non-thermal vapour extraction (VAPEX), Toe-to-Heel air injection (THAI) and other enhanced oil recovery methods make extraction of heavy crude oils possible, but require significantly greater resources, manpower, technical expertise and carry increased financial risk.[27,28]

Even with the solution stabilised and viscosity reduced, the heaviest components of crudes can still reach their solubility limit. A drop in temperature or pressure can cause these materials to deposit in oil pipelines reducing flow rate and causing obstructions. Asphaltene, wax, gas hydrate, diamondoids, organic scale and inorganic scale are all known to form deposits and represent their own challenges in prevention and removal.[29]

The most complex and chemically diverse of the solid species mentioned above are the asphaltenes. No method for their removal is universally effective. Depending upon the location and extent of the problem, chemical or mechanical methods can be applied. The chemical solution involves injecting hot aromatic solvents, typically xylene, into pipelines in order to dissolve asphaltenes on a scale of 1000 L per meter of obstructed tubing. The costs of this method are significant and often involve the shutdown of production wells. Furthermore, this approach risks introducing previously insoluble heavy bitumen rock from the well into the extracted material.[29] This can reduce the relative permeability of the oil, resulting in more serious asphaltene deposition problems to result downline. Solvents used for this process can also damage the extraction equipment, namely through the dissolution of elastomer seals used to allow natural gases and steam to be removed selectively through a permeable membrane. The environmental impact using these solvents in high quantities is significant as alteration of the well's structural integrity can have far-reaching implications to surrounding geological sites. Asphaltene dispersants and inhibitors can be injected *via* coiled tubing which aim to stabilise or prevent flocculates in solution from forming. However, this technique has had limited success due to the additives used generally performing inconsistently.[30]

Asphaltene blockages in production tubing can also be resolved mechanically, utilising scraping devices or by 'pigging', where an internal device carries out inspection and cleaning of the pipeline. These techniques can be performed without halting flow or altering the well pressure. The limitation being that highly specific 'pigs' are required for different problems and that they are only suitable for pipelines that do not possess certain valves or internal probes.[31]

1.3.2. REFINERY

Once extracted, crude oil feedstock is transported to a refinery where it is received by a desalter (**Fig. 3**). This equipment acts to remove water and salts including sodium chloride and magnesium chloride to prevent potential corrosion and fouling upon the refinery framework. Water is also removed as its presence impacts the efficiency of distillation.[8] Following this crude oil will be heated prior to atmospheric distillation utilising a series of heat exchangers, the Preheat Train (PHT), which raises the temperature of the crude oil to the maximum temperature possible for single phase flow, around 200 °C.[32] The PHT is often fouled due to remaining inorganics not completely removed by the desalter, waxes, resins and asphaltenes.[33] The PHT serves to efficiently transfer 60-70% of the heat required for atmospheric distillation,

before introducing the crude oil to a direct fired furnace which further increases the temperature to 370 °C.[34]

The heated feedstock is then introduced to the atmospheric distillation column as a mixture of liquid and vapour. In order to achieve effective distillation, vapours rising through the liquid must be able to evaporate before transferring its heat to the surrounding liquid above it. This is achieved with utilising 'tower trays' which permit effective heat transfer between different vapour and liquids of different volatilities.[35,36] Heavy crude oils complicate each of these critical refinery stages. Insoluble organic and inorganic debris builds up in a desalter at a significantly faster rate and is very difficult to remove, often requiring large amounts of specialist solvent-based cleaning fluids, followed by an acid-surfactant to remove any inorganics. Due to the nature of every fouling deposit being unique to the petroleum source and conditions of the refinery, there is no standard protocol or specific solvent regimen to dissolve these materials. Furthermore, if any cleaning material remains in the system, oil-water emulsions can form that reduce the effectiveness of the desalter causing myriad problems in the following stages of the refinery.[37]

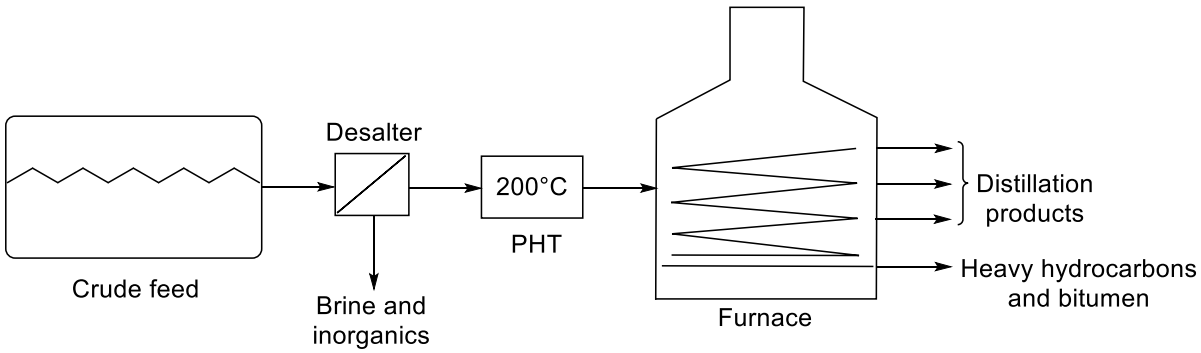

Figure 3. General scheme for petroleum refining.

The furnace and heat exchangers are susceptible to fouling in a refinery resulting in reduced effective heat transfer and consequentially greater quantities of fuel being required for feedstock to reach temperatures necessary for distillation.[38] Cleaning fouled preheat bundles and furnace tubes requires soaking the equipment in aggressive oxidising agents such as potassium permanganate. The solvation of deposited organics often proves the most technical and costly section of the cleaning process, with extreme cases requiring the mechanical removal of the material through high pressure hydroblasting.[39] An awry cleaning procedure can lead to wasted volumes of cleaning agents, increased operational outage time, reduced resource recovery and increased maintenance costs.

Asphaltenes are significantly responsible for increased viscosity, emulsion formation and precipitation in the processing and transportation of heavy crude oils. A major obstacle in controlling organic deposition is that despite decades of research, the solution and surface chemistry of the asphaltenes remains obscure.

1.4. PETROLEUM CHARACTERISATION

1.4.1. DENSITY

Light and heavy crudes oils can be simply characterised through observation of density and colour. These properties are affected by the distribution of hydrocarbons present, with a light crude oil possessing more volatile organics than a heavy crude oil. Light and heavy crudes are defined from the American Petroleum Institute (API) gravity which presents a value illustrating the density of a given oil compared to water. This is derived from the Specific Gravity (SG).[40]

$$API\ gravity = (141.5/Specific\ gravity) - 135.5$$

Equation 1. Formula for calculation of API gravity.

Light crude oil has an API of above 20 and demonstrates a low viscosity due comprising of a greater proportion of straight and branched chain hydrocarbons (paraffins) with a high C to H ratio. The highest commercial value light crudes possess 60% paraffins.[41] API interpretation varies according to region and organisation. However, generally an oil is determined to be heavy if the API is under 20, with a value of 10 expressing that the density is the same as water. An API of less than 10 defines an extra heavy oil that sinks in water. These material differences define the nature of a particular crude oil in terms of physical properties such as appearance and viscosity, as well as practical considerations including the percentage of the most valuable fractions and flow assurance.

1.4.2. HEAVY CRUDE OIL ANALYSIS

The complexity of crude oils means that basing characterisation upon individual molecular constituents is not possible. A crude oil can be fractionated on the basis of polarity to provide the ratios of classes saturates, aromatics, resins and asphaltenes (SARA, **Table 2**).[42] Saturates are apolar hydrocarbons with linear or branched alkyl chains. Aromatics generally refers to species with one aromatic ring bonded to aliphatic chains. Resins and asphaltenes, components of vacuum residue from crude oil distillation, possess polar functionality and are the heaviest fractions, distinguished on the basis of solubility with the former being soluble in heptane and the latter in toluene.[9,43]

Origin	Saturate (wt.%)	Aromatic (wt%)	Resin (wt.%)	Asphaltene (wt.%)	Density (g/mL)	API gravity
SQ-95	65.2	18.3	13.9	2.6	0.84	37.2
C-R-00	70.6	16.4	11.4	1.6	0.87	31.3
Tensleep	64.0	19.8	12.9	3.2	0.87	31.1
S-Ven-39	51.1	28.3	14.5	6.1	0.88	28.8
Russia	51.0	20.5	19.7	8.8	0.90	25.2
C-LH-99	49.4	21.5	23.9	3.4	0.92	22.6
Canada	18	27	27	15	0.99	11.3
Alaska	23	22	35	18	1.00	10.4
Utah	19	19	46	20	1.00	8.05
Venezuela	19	19	29	18	1.01	8.05
Texas	4	17	37	43	1.12	-5.00

Table 2. SARA analysis and API gravity of crude oils of various origin.[42,43]

Elemental analysis shows asphaltenes to be largely responsible for the increased amounts of sulfur, oxygen and nitrogen heteroatom functionality in heavy oils (**Table 3**).

Fraction	wt.%	Carbon	Hydrogen	Nitrogen	Oxygen	Sulfur
Asphaltene	14.1	83.8	7.5	1.3	1.7	4.8
Resin	37.3	82.8	8.9	1.5	2.0	4.3
Aromatic	37.2	84.3	10.0	<0.3	1.1	4.0
Saturate	11.4	86.6	13.0	<0.3	<0.2	<0.1

Table 3. Elemental composition for Venezuelan reserve heavy crude oil.[43]

Despite still being a minor component of heavy oils by weight percentage, the asphaltenes are recognised to have a significant bearing upon the properties of a crude oil.[18,37,40] Mercaptans, sulphides and thiophene derivatives are recognised as having a detrimental impact upon the refining process due to their ability to corrode iron used in pipelines.[44] Products of oxidation including carboxylic acids, ketones, phenolic groups, ethers and anhydrides are also present in significant quantity and greatly impact the commercial value through their effect on oil acidity, a key cost factor in refining.[45,46] Quantities of basic and non-basic forms of nitrogen are also elevated including pyridine, indole and carbazole functionality which affect oil pH and can

form salts with acidic species resulting in stabilised emulsions.[47] Porphyrins can complex to source rock metals vanadium and nickel,[48] with the resulting organometallics significantly impacting viscosity and being capable of metal corrosion and the fouling of refinery catalysts.[43]

1.5. ASPHALTENES

1.5.1. STRUCTURAL INFORMATION

The asphaltenes are a solubility class. The most well-known definition comes from the procedural guidelines IP143, which fractionates vacuum residua into maltenes and asphaltenes on the basis of their solubilities in heptane and toluene.[49] Numerous problems present themselves upon contemplating this description. Firstly, a solutes solubility is dependent upon a certain volume, which is undefined in this procedure. Asphaltenes describe a continuum of organic molecules with a range of solubilities. Increasing the volume of nonpolar solvent here will result in an increase, however small, in material otherwise considered to be insoluble. Secondly, the temperature and pressure of this process are not defined. The variation of these parameters is significant as asphaltene precipitation is well known to occur upon temperature and pressure reductions in the refinery. High resolution mass spectrometry has compared those asphaltenes deposited by pressure drop in a live crude oil with those precipitated from heptane and found significant differences in aromaticity and heteroatom content.[50] Furthermore, it has been demonstrated in SARA separation that distinction between these groups is not clear and that cross contamination is significant.[42,51] Classification of such a broad and complex range of organic compounds in this manner does not represent a scientific standard of what an asphaltene is, and should only serve to provide a non-exacting distinction between the lipophilic and toluene soluble species in the residuum remaining after vacuum distillation.[52]

1.5.2. HETEROATOM CONTENT AND FUNCTIONALITY

Understanding the structural and functional groups present in the asphaltenes is key to manipulating their solution and surface chemistries. Elemental analysis of asphaltenes provides basic chemical information about asphaltenes (**Table 4**).

Heteroatoms contribute approximately 10-20% weight to an asphaltene molecule.[53] The impact of these species on the properties of the asphaltenes is significant and must be included if any structure-function relationships are to be fully understood.

Origin	Elemental Composition (%)					H:C
	Carbon	Hydrogen	Nitrogen	Oxygen	Sulfur	
U.S.A	88.6	7.4	0.8	2.7	0.5	1.00
Kuwait	82.4	7.9	0.9	1.4	1.4	1.14
Venezuela	85.5	8.1	3.3	1.8	1.3	1.14
Mexico	81.4	8.0	0.6	1.7	8.3	1.18
Brazil	83.0	9.0	2.0	-	-	1.30
Italy	78.0	8.8	Trace	3.0	10.2	1.35
Canada	85.1	11.1	0.7	2.5	0.6	1.56

Table 4. Elemental analysis of various asphaltene sources[43].

Thermal degradation experiments show the nitrogen functionality to be very stable as little is lost (approximately 2%) upon exposure to high temperatures,[54–56] suggesting that nitrogen atoms are likely to be incorporated in aromatic rings. This is consistent with nitrogen X-ray absorption near edge structure (XANES) studies which have shown nitrogen content to be primarily pyrolic and pyridinic.[29,57] Conversely, the majority of oxygen is lost in this experiment, indicating that it is present in the form of carboxylic acids, ketones and phenols rather than in heterocyclic structures.[46] Sulphur is likely present in both the saturated and heterocyclic regions of the molecule as 23% is lost upon this analysis.[58] ^{13}C NMR shows >80% carbon to be aromatic and is consistent with IR studies showing >90% of hydrogen to be upon aliphatic groups and a more varied heteroatom weight percentage of O = 0.3-4.9%, S = 0.3-10.3% and N = 0.6-3.3%.[7,59]

1.5.3. Molecular Weight Range

The molecular weight range of asphaltenes has been the subject of debate for decades, with values ranging from 300-100,000 Da.[16,60] Mass spectrometry, the obvious choice of technique for resolving this issue, has been challenged on the accuracy of values reported. Field ionisation mass spectroscopy (FIMS) first reported weights to be approximately 1000 Da,[61] but concerns were raised over the heaviest components not being volatised and fragmentation of the compounds being studied leading to a lower weight range being reported.[62] Laser desorption

ionisation (LDI) experiments have since resolved these issues of contention to arrive at molecules having a most probable molecular weight of approximately 600 Da,[63] in strong agreement with atmosphere pressure chemical ionisation (APCI) and laser-induced acoustic desorption electron impact (LIAD-EI) mass spectrometry.[18]

Molecular diffusion experiments have been performed to resolve the values of molecular weight and are in strong agreement with those derived from mass spectrometry.[62,64,65] Time resolved fluorescence depolarisation (TRFD) uses a polarised laser to excite a molecular system which results in the absorbing species reaching a corresponding excited state. The rotational correlation time then measures how long it takes for the molecule to reorient, with the size of the molecule impacting the time taken for reorientation. With fluorescence and optical absorption spectra an estimate for the molecular weight distribution for the asphaltenes is given at 500-1000 Da.[66,67] Convergent results were also obtained from fluorescence correlation spectroscopy (FCS)[68,69] and NMR[70] measurements.

1.5.4. TOPOLOGY

The physical, elemental and structural information gathered from the asphaltenes results in two topological motifs being used to describe the asphaltenes. These are the 'island' and 'archipelago' models (**Fig. 4**). The 'island' model describes a single condensed aromatic unit with alkyl chains and heteroatoms functionalising the periphery whilst the archipelago model describes multiple polyaromatic hydrocarbon (PAH) units tethered together by alkyl chains (**Fig. 4**).[29] When asphaltene molecular weight was presumed to in the order of 10,000-100,000g/mol, there was little restraint on the number of aromatic units in each molecule. This permitted large archipelago models with FAR regions of varying aromatic size to be considered as possible asphaltenes.[71,72] However, with the average molecular weight consistently now reported as approximately 750 Da with a FAR region consisting of 4-10 aromatic rings, the possibilities for the archipelago architecture are restricted to small and medium size PAHs with only two or three interconnected aromatic systems.

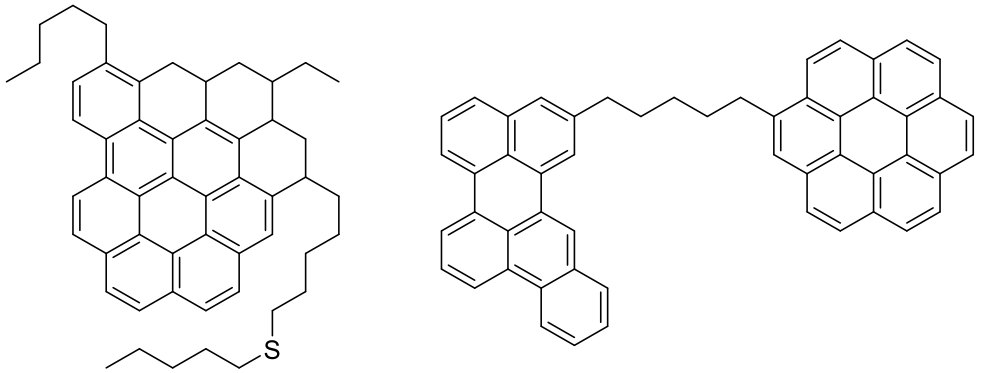

Island Archipelago

Figure 4. Structure of 'island' and 'archipelago' structural motifs for the asphaltenes. [73,74]

DFT/ZINDO molecular oribital calculations of over 3000 archipelago and island systems found that island model systems more often fall within the experimental range of fluorescence emission data of asphaltenes.[74] ^{1}H-^{13}C cross polarization with ^{13}C pulse excitation performed upon six Ecuadorian asphaltene samples have acquired carbon aromaticity values that suggest larger aromatic systems have increased aromaticity, rather than a larger number of smaller aromatic units.[75] With a certain structural type comes a particular aggregation behaviour. This relationship has been probed in molecular dynamics and found that the 'island' model most closely embodies that of the asphaltenes. [76] Behaviour of asphaltene molecular ions in fragmentation provides data consistent with these conclusions, with electrospray ionisation (ESI) and APCI patterns describing the 'island' model to more closely resemble structures in real asphaltenes.[77]

The 'archipelago' model has been prevalent for decades.[78,79] Despite the current consensus appearing to favour the alternative 'island' motif, there is still evidence of this architecture being consistent with that of the asphaltenes.[80] Catagenesis has been simulated utilising small aromatic model compounds. Cracked fragments were found to recombine and form larger molecules, likely through free-radical addition reactions to unsaturated species, to form 'archipelago' bridged addition products. These results imply the same geological conditions that generate light paraffins also create asphaltenes with this topology.[54,81,82]

Fourier transform ion cyclotron resonance mass spectrometry (FT-ICR MS) has demonstrated a strong correlation between the extent of aromaticity as a function of C to H ratio (described in terms of double bond equivalency (DBE), **Equation 2**) and number of carbon atoms in asphaltene molecules.[50,83] A spectrum is generated containing thousands of peaks each

representing a molecular formula where numerous isomers are possible. Possible structures can be generated from these data points and provide valuable information on the elucidation of structural parameters of the asphaltenes. A DBE range of 10-40 includes the majority of peaks observed for asphaltenes and can be plotted against 400-1000 $gmol^{-1}$ molecular weight distribution to define structural parameters for prospective asphaltene molecules. Both the 'island' and 'archipelago' asphaltene molecular architectures can be interpreted from these results.

$$DBE = C + \left(1 - \left(\frac{H}{2}\right) + \left(\frac{N}{2}\right)\right)$$

Equation 2. Double bond equivalent formula. C = Number of carbon atoms present; H = Number of hydrogen atoms present; N = Number of nitrogen atoms present.

1.5.5. FAR ORIENTATION

Density functional theory calculations show Clar's sextet theory to provide simple rules for the suitability of candidate asphaltene model compounds.[84] These parameters allow the stability of a particular FAR region to be qualitatively assessed in terms of π-electron distribution. Structural isomers of a PAH can be refined and generate an optimised geometry with a minimised internal energy using these parameters.

Aromatic rings with six π-electrons in a benzenoid ring capable of being drawn with Kekule resonance is a π-sextet (**Fig. 5**). A greater number of aromatic sextets in a particular FAR limit describe a system with a greater degree of aromaticity.[74,85,86] Given the geological timeframe and high temperatures of asphaltene formation, less stable structures possess a lower occurrence probability.

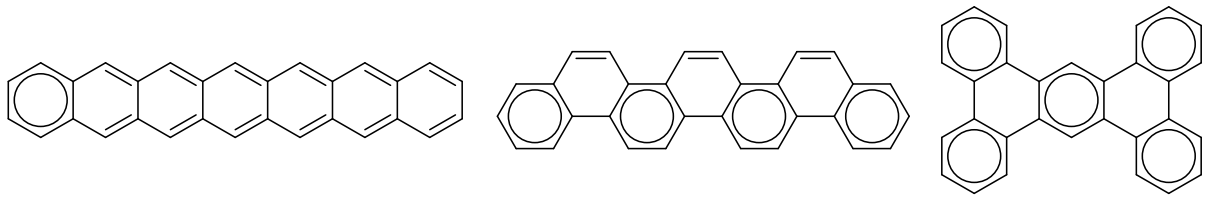

Figure 5. Resonance structures of i. Linear acene, ii. Stepped cata-condensed, iii. Peri-condensed PAHs displaying the maximal configuration of resonant sextets.

The Clar model effectively rules out the acenes, linear cata-condensed fused PAHs, as possible aromatics in asphaltene mixtures due to the series containing only one migrating π-sextet. It is well established in the field of organic electronics that acenes display an increasing sensitivity toward oxidation and dimerization when subjected to heat and light respectively.[87] Comparison of the seven FAR containing PAHs heptacene and tetrabenzoanthracene demonstrate the effect of greater aromaticity upon oxidative stability through calculation of their respective HUMO-LUMO bandgaps, with the former registering a reading of 760 nm and the latter at a markedly more stable 326 nm.[88]

The size and orientation of asphaltene PAHs has been elucidated through a molecular imaging analysis. Scanning tunnelling microscopy is capable of detailing the long axis dimensions of asphaltene PAHs giving a length of approximately 1 nm, corresponding to an aromatic structure of 7 fused rings.[89] This is in agreement with high resolution transmission electron microscopy (HRTEM).[90] ^{13}C Distortionless enhancement by polarisation transfer (DEPT) experiments describe the average asphaltene as having approximately 27 carbons, also consistent with 7 fused aromatic rings (FARs).[91] More recently, atomic resolution atom force microscopy (AFM) has been combined with STM to study over 100 asphaltene molecules, revealing the structure of the asphaltenes in detail. This showcased the extraordinary structural diversity of mean asphaltene structures and was in agreement with the values attained through analytical techniques. Due to a limited sample size and preferential selection of clear images however, the investigation of asphaltene structure is not as conclusive as these results indicate.[92]

1.6. SURFACE CHEMISTRY OF ASPHALTENES

Structural and colloidal characteristics govern the adsorption of the asphaltenes onto surfaces.[93–95] The strength of interactions between asphaltene molecules differentiates them from the other fractions of petroleum. They possess a high polarity through large aromatic units and heteroatom functionality that generate van der Waals forces,[96] hydrogen bonding[97] and charge-transfer interactions[98] which lead to self-association and ultimately facilitate asphaltene-surface adsorption. These forces combine to result in a strong supramolecular self-assembly.[99]

Monomeric solutions of asphaltenes are common at concentrations below 1 mg/L, while dimer formation occurs in the range of 5-15 mg/L.[95] Dimer pairs (nanocrystallites) form at approximately 90 mg/L, displaying a diameter of approximately 2 nm and further concentration of the solution results in 2-5nm diameter aggregate crystallites with an average of eight molecular stacking being predominate (**Fig. 6**).[100]

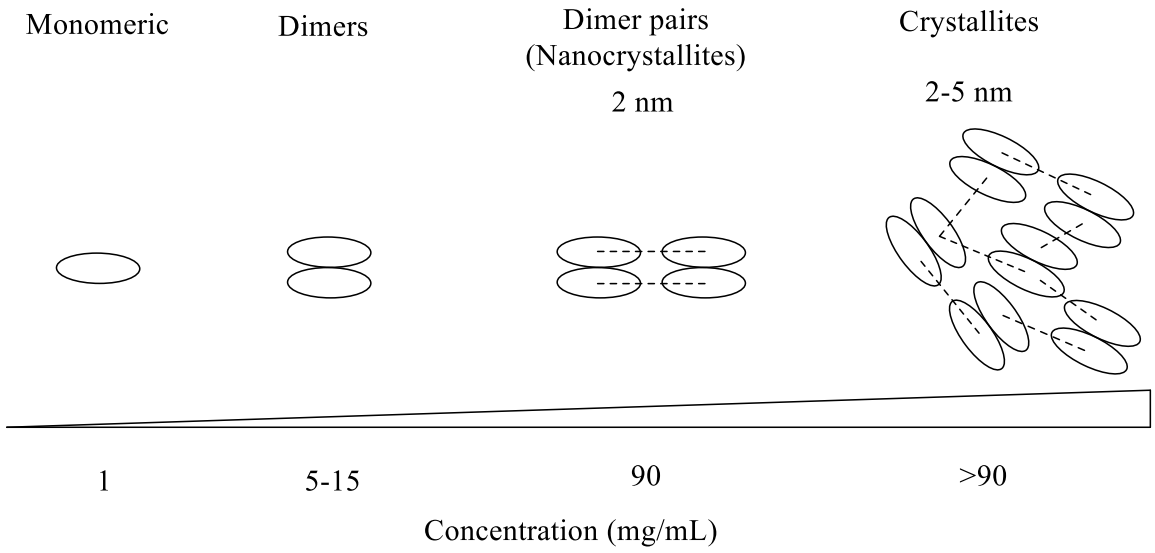

Figure 6. Representative scheme of increasing asphaltene particle size with concentration.

X-ray and small angle neutron scattering (SANS) techniques have shown crystallites can further aggregate to form larger particles possessing a diameter of 3-10 nm.[17,101,102] The aggregates are dynamic and structurally sensitive towards shear rate, solvent, temperature and pressure, with a change in one of these variables resulting in a change in the shape and structure of the particle.[103–105] Research in asphaltene aggregation has led many groups to attempt to interpret the phenomena in terms of micelles and calculate the critical micelle concentration

(CMC). This is not appropriate for the asphaltenes as micellisation describes a significant change at a certain concentration, whereas the observed behaviour here is stepwise. This explains the variance from different groups in data captured for the CMC, with values ranging from 10 mg/L[106] up to 4.9 g/L.[107]

As the solvent system becomes less stable for asphaltenes, such as upon the addition of non-polar solvent or a reduction in temperature, suspended colloids flocculate to form larger suspended particles of non-dissolved organics which lead to agglomeration and precipitation.[108,109] The colloidal status of asphaltenes strongly influences the rheological properties of their solutions, with viscosity being increased upon the liquid carrying larger particles.[110]

The source of asphaltenes produced governs their chemical and structural characteristics.[111] These properties, combined with the thermodynamics of the system from which they are precipitated details their ability to adsorb to surfaces. Adsorption can be described as a physical process whereby Van der Waals forces drive the interaction, or through chemical adsorption which sees the formation of ionic or covalent bonds, altering the electronic structure of the adsorbate.

Adsorption rate is described firstly by asphaltene diffusion from the bulk solution to the particle surface, followed by adsorption at the substrate and finally chemical reaction if chemisorption can occur. Adsorption experiments found no difference in the rate whilst static compared to under the influence of stirring, indicating that diffusion is fast compared to the adsorption step.[112] A kinetic study for asphaltene adsorption at liquid interfaces was in agreement that diffusion was rapid and subsequently led to a rate limiting multilayer build-up of organic deposits.[113]

Characterisation of sorbents offers insight into the mechanisms that inhibit or encourage asphaltene deposition. Relevant substrates include silica, alumina, glass metals, metals oxides carbon and polymers.[15] From analysis of adsorption isotherms interesting trends become apparent. For example, minerals display a noticeable adsorption capacity difference based upon the abundance of surface hydroxyl groups, with hydrophilic silica operating at 3.78 mg/m^2 and hydrophobic silica at 0.26 mg/m^2.[114] This suggests hydrogen bonding interactions of the sorbate and the asphaltenes to be significant, consistent with studies that show reservoir rocks, with high numbers of hydroxyl functionality per area, to display very high adsorption capacities. Furthermore, a series of silica substrates impregnated with increasing amounts of

alumina found surface acidity to dramatically increase PAH adsorption.[115] This mechanism is utilised in the selective removal of basic asphaltenes from Cold Lake vacuum residuum.[116]

The morphology of the surface is also regarded as highly significant.[117,118] This has been demonstrated by showing the increased adsorption capacity of asphaltenes upon colloidal alumina nanoparticles compared to equivalent micro-sized particles.[119] Comparison of various hydrophilic metals has shown surface morphology to greatly affect adsorption, with relatively rough stainless steel displaying a capacity of 2.7 mg/m^2 compared to 0.25 mg/m^2 for the smoother alumina,[120] suggesting that with a higher surface area (roughness) per gram of sorbate, adhesion is increased.[119,121] Current research points towards asphaltene adsorption being governed by physisorption due to the inability to define specific chemical-surface interactions of which the asphaltenes are capable.[14,20,122]

1.7. MODEL ASPHALTENES

The development and study of model asphaltene compounds, representing average asphaltene molecule types, offers a fundamental approach to their study.

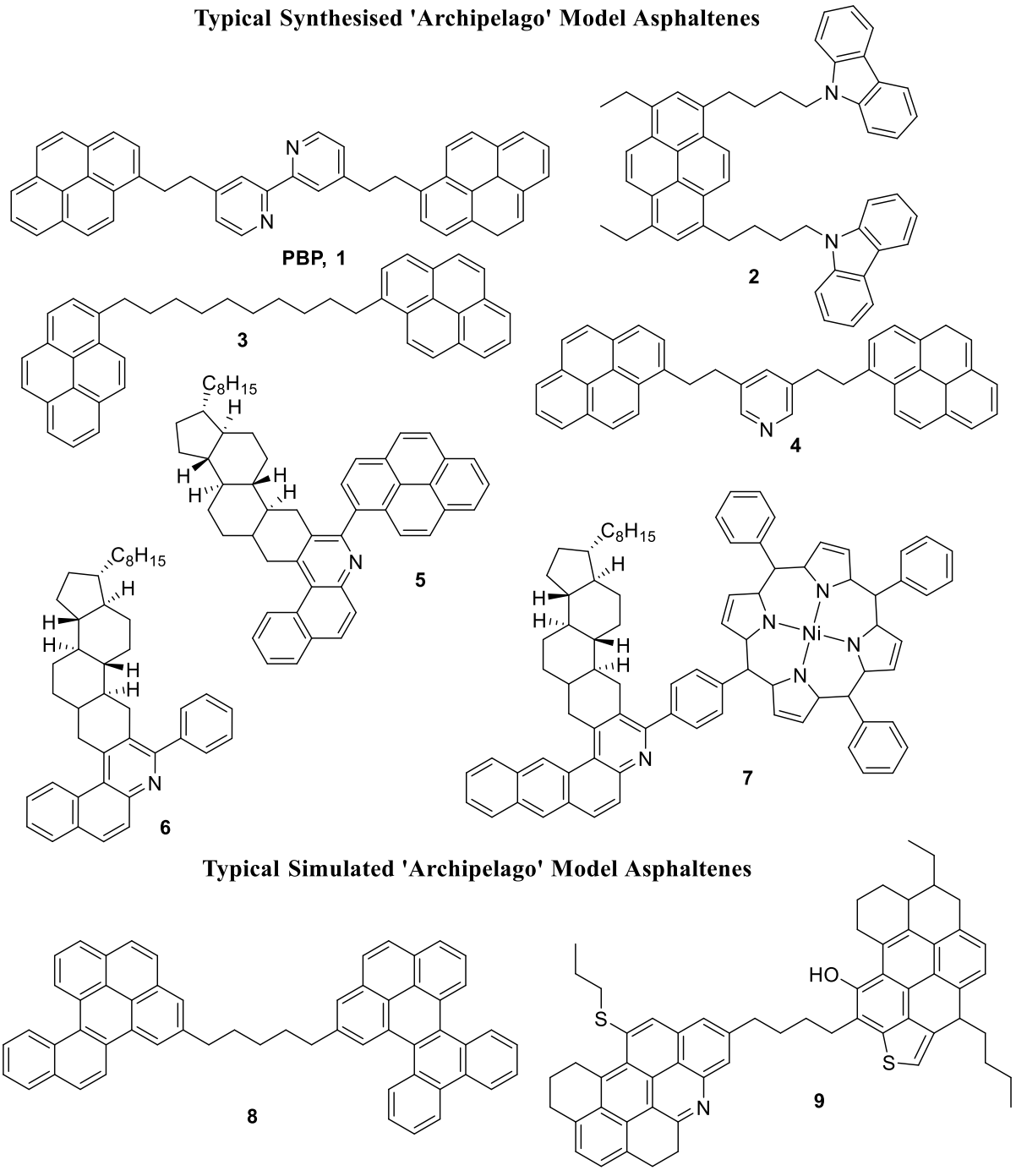

Figure 7. Representative, synthesised and simulated 'archipelago' model compounds. **1**,[123] **2**,[124] **3**,[125] **4**,[126] **5/6**,[127] **7**,[128] **8**,[74] **9**.[51]

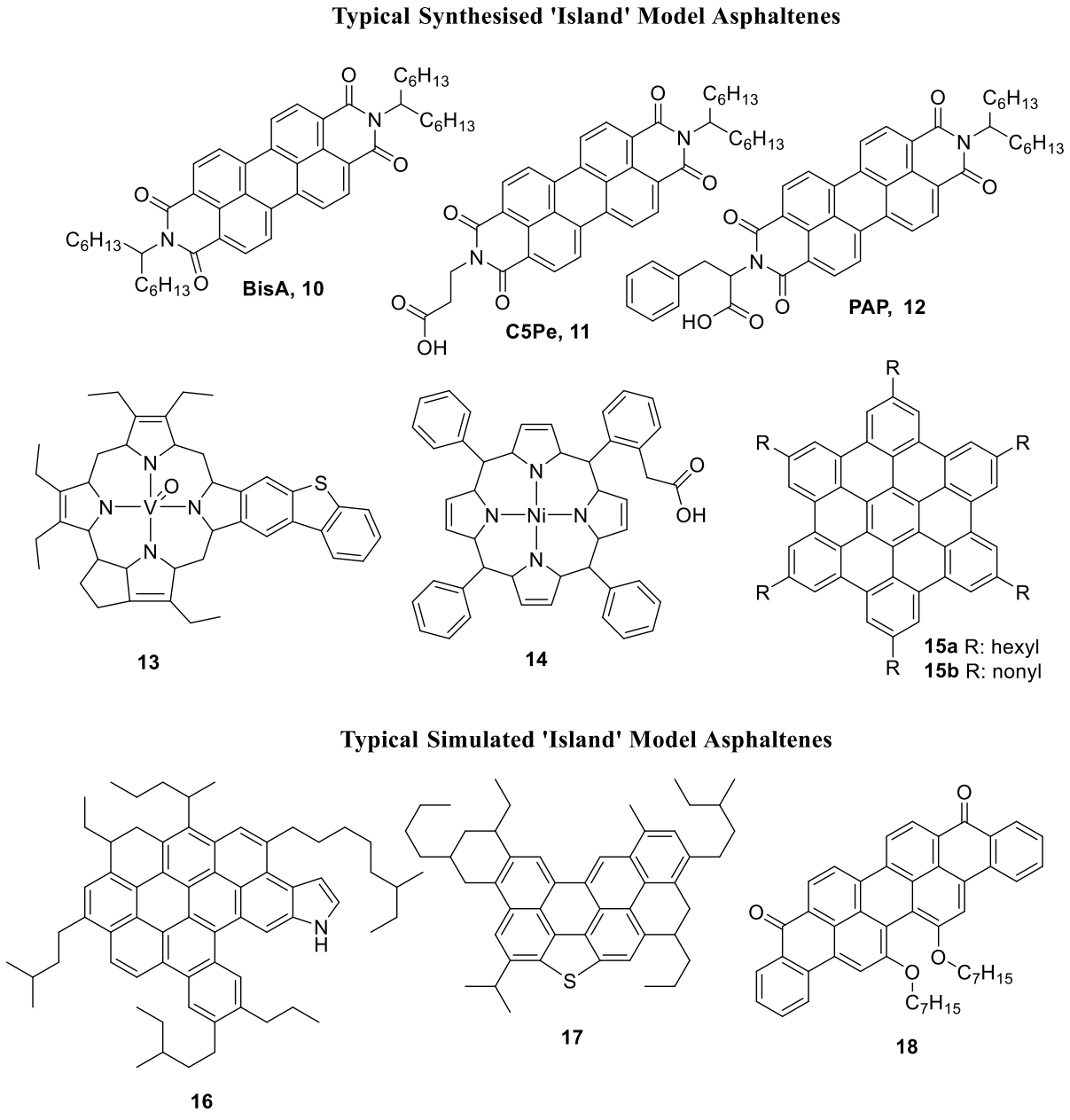

Figure 8. Representative, synthesised and modelled 'island' model compounds. **10**/**11**/**12**,[129] **13**/**14**,[128] **15**,[80] **16**/**17**,[130] **18**.[131]

The chemical diversity of the asphaltenes generally makes the interpretation of experimental analysis highly complicated. Targeting specific molecules with functionalities and topologies present in the asphaltenes allows physical properties to be studied at a molecular level. This tactic is commonly used simplify biological systems.[132–134] With molecules and substrates well defined, the deposition characteristics of asphaltenic compounds can be investigated through aggregation analysis and surface science with confidence. This approach is utilised in

computational modelling of the asphaltenes which uses idealised molecules as the subject of their investigation.

With a well-defined aggregation model, asphaltene deposition could be better controlled through methods such as concentration management or the use of targeted aggregation inhibitors. This aim has led to model compounds being the subject of investigation in self-association studies. Solution behaviours of alkyl-bridged pyrene derivatives (**3**) have been analysed through vapour pressure osmometry to find that these units alone lack the ability to aggregate.[125] However, when a similar unit 4,4'-*bis*-(2-pyren-1-yl-ethyl)-[2,2']bipyridinyl (PBP, **1**) was probed by NMR and steady state fluorescence, dimerisation was found to occur within the concentration range found for asphaltenes.[123]

The bipyridine spacer in **1** was found to be significant in the associative forces between molecules. The effect of larger aromatic molecules with extended π networks followed this work to see if a higher aggregation state could be reached with stronger π-based interactions. Hexabenzocoronene (HBC) derivatives (**15a**/**b**) have FAR of 13 and represents a boundary asphaltene molecule. However, it was found that these models were also only capable of forming dimers.[135] Molecular dynamics investigations upon violanthrone derivatives **18** found similar results with inadequate aggregation.[136] Interestingly, upon further investigations into **18** regarding the effects of peripheral alkyl chain length upon aggregation derivatives in water, it was found that this relationship was not linear. Dense aggregates were shown to form with short (butyl) and long (hexadecyl) alkyl chains, whilst lesser aggregates form with medium length (octyl and dodecyl) chains. It was concluded that when aromatic core units can approach without paying a penalty of alkyl chain steric repulsion aggregates can form. This is also the result if strong enough alkyl-alkyl interactions can exist between molecules. However, if neither the aromatic or alkyl attraction is strong enough, no aggregation is seen. The analyses upon these model molecules show that the underlying principles of asphaltene aggregation are not yet identified through this approach.

Much work surrounding asphaltene models has been focused on how molecules interact with the oil/water interface in an effort to better understand how these species stabilise emulsions. Notably, Langmuir physiochemical experiments combined with steady-state fluorescence and Brewster angle microscopy can describe a conformational orientation at the interface.[137,138] Analysis of PBI derivatives C5Pe (**11**), BisA (**10**) and PAP (**12**) found that acidic groups are of great significance regarding surface activity as they reach into the aqueous phase, with the

condensed aromatic group lying flat against the interfacial boundary. Adsorption isotherms and interfacial tension data have found **1** to form a monolayer film at the water/oil interface. At high pH **1** was in alignment with the asphaltenes ability to stabilise emulsions, indicating that a certain fraction of the asphaltenes are responsible for this behaviour.

Model molecules have also been used to develop our understanding of the deposition mechanism of asphaltenes upon surfaces. The strength of interaction between two mica surfaces coated with asphaltenes has been compared to identical surfaces with model compound C5Pe, **11** adsorbed in toluene, heptane and water.[139,140] The resulting force curve profiles captured through Surface Force Apparatus (SFA) showed model molecules and asphaltenes to display similar attraction forces, suggesting that these molecules are pertinent to the asphaltenes. Given this accurate representation, it is anticipated that further studies of specific asphaltene structures and functionalities will prove fruitful in faithfully imitating the solution and deposition behaviour of the material of interest.

1.8. BP ICAM 15

The work undertaken in this thesis is one part of a cross-university collaborative program (ICAM 15) aimed at developing an understanding of asphaltene deposition through investigation of asphaltene and model compound deposition upon materials. The main scientific challenges for the group are summarised:

1. Develop mechanisms of asphaltene deposition describing the bulk state solution chemistry that facilitate nucleation and growth of deposits.
2. Understand the role of materials composition and structure (atomic and macro) upon asphaltene deposition.
3. Design and test the effect of novel materials and coatings to inhibit or clean asphaltene deposits.
4. Select and utilise analytical tools and techniques suited for surface characterisation, detection and investigation of molecular deposits.
5. Develop computational modelling tools to allow visualisation and prediction of the various molecular interactions taking place both in solution and at fluid-substrate interfaces.

Specialist groups comprising of synthetic chemists, materials scientists, physical and theoretical chemists have been divided into 'work packages' (WP) that comprise two integrated themes of experimentalist and modelling research. The work described in this thesis falls into the remit of Work Package 1 (WP 1).

Work Package 1 (WP1) – Reference Materials and Properties

Pure compounds representing asphaltenes in terms of molecular shape, size, functionality and aggregation/adhesion behaviours are to be specifically prepared and characterised. Novel molecular cores are to be synthesised and derivatised to provide an array of new model materials which are expected to be excellent asphaltene models. These molecular cores' functional utility allows the inclusion of all chemical groups of interest to the programme. They can be readily modified to give a range of large molecular weights, variable solubility and site specific polarity.

A full description of the objectives and experimental process undertaken by each WP is detailed in the appendix of this report (**Sect. 5.1**) and is summarised (**Fig. 9)**.

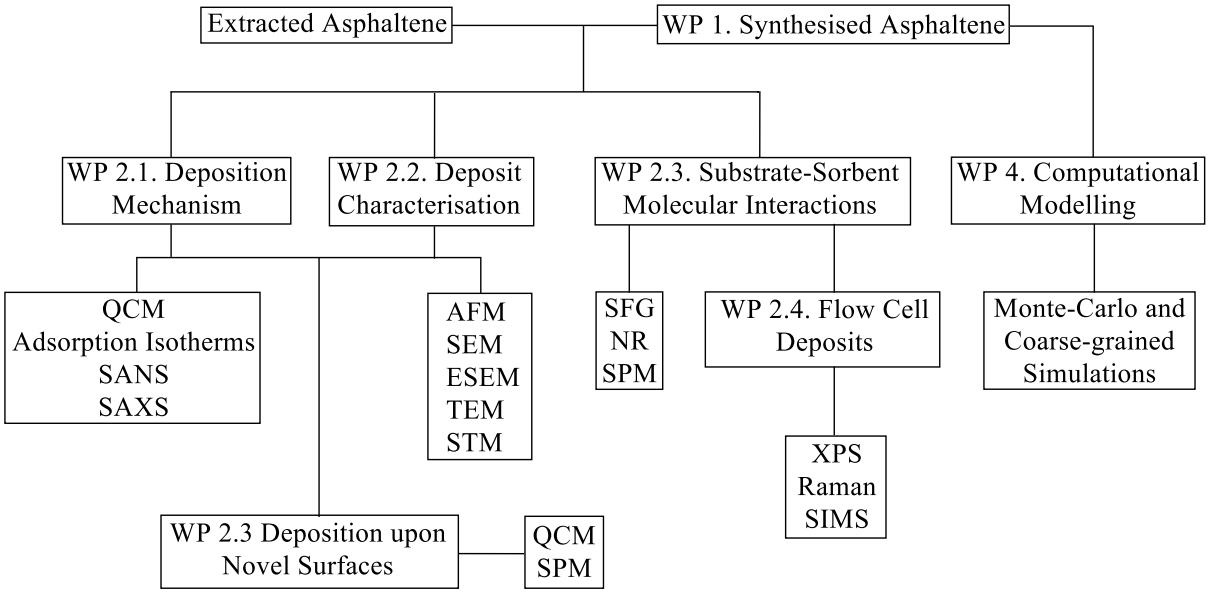

Figure 9. Flow diagram of ICAM 15 work packages.

1.9. SYNTHESISING MODEL ASPHALTENE MOLECULES

Considering the scale of resources invested in the explanation of asphaltene structural properties, the combination of known parameters to synthesise model compounds for asphaltene molecules has been inadequately explored. This is possibly due to the asphaltenes occupying an area of chemical space which is difficult to access. As a consequence of this, models used for this purpose are often selected presumably out of convenience, rather than for possessing appropriate properties. For instance, perylene *bis*-imides (PBIs, **10**-**12**) have been heavily researched as asphaltene models, yet contain a level of heteroatom content ill-fitting with known asphaltene data. Furthermore, these materials possess an intrinsic low solubility that limits the scope of their analysis.[12,90,141]

'Archipelago' models have a significantly higher occurrence rate in research despite being the less favourable of the two structural motifs. This is likely due to their synthesis being more facile. 'Archipelago' model compounds are generally acquired through tethering of often commercially available 2-4 ring aromatic units through S_N2 or other coupling chemistries.[123,124] These synthetic routes use reliable chemistry, have no issues regarding solubility and are generally acquired in 1-3 reaction steps.

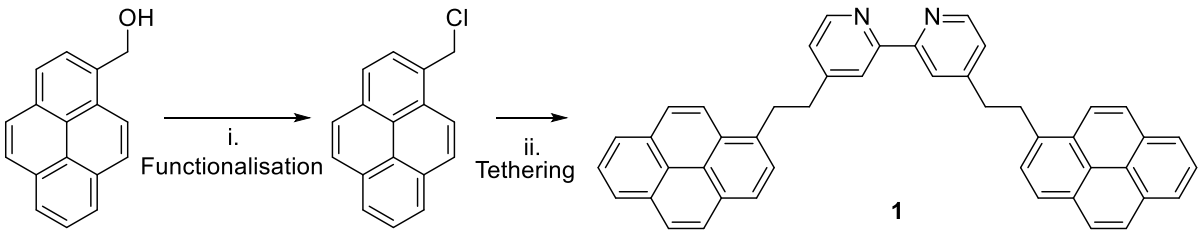

Figure 10. Representative 'archipelago' synthesis.[123] i. $SOCl_2$, pyridine, CH_2Cl_2; ii. LDA, THF, 4,4'-dimethyl2,2'-bipyridine.

'Island' model compounds however present a significantly more technical and uncertain synthetic challenge. Commercial aromatic compounds possessing ≥5 fused aromatic rings are few, expensive, have a limited potential for functionalisation and are typically inherently insoluble. Coronene, ovalene, benzoperylene and isoviolanthrone derivatives comprise the most obvious available and appropriate starting units, yet all of which are unsuitable (**Fig. 11**).

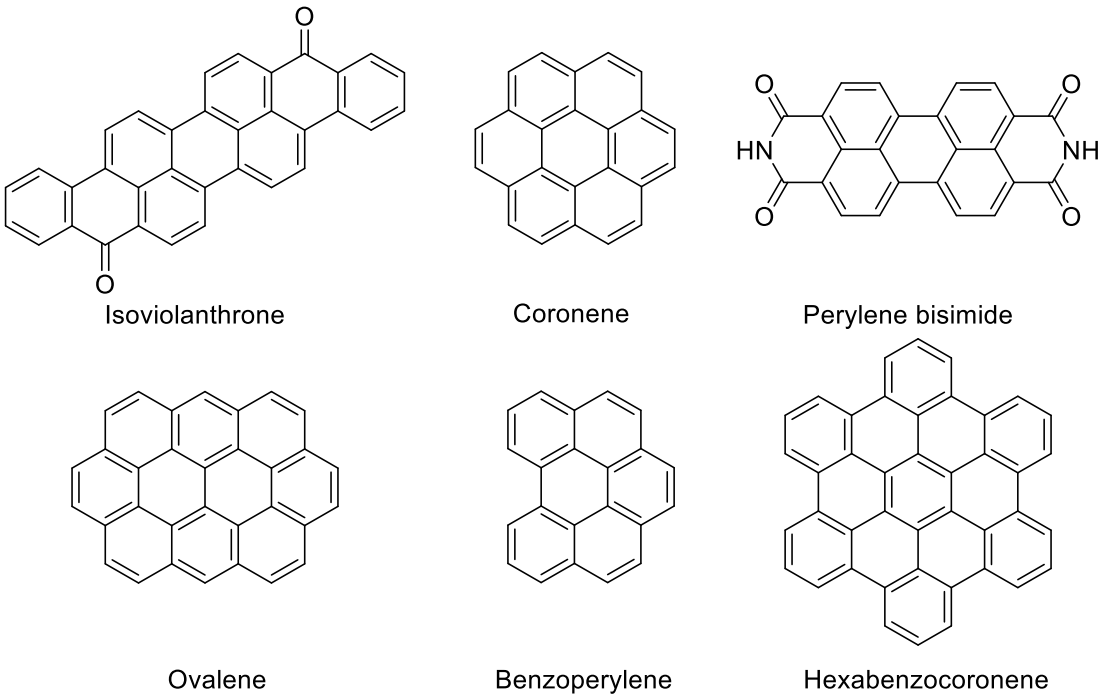

Figure 11. Commercially available PAHs.

In order to achieve a solubility level appropriate for solution based analysis for appropriate PAHs, functionalisation has to be performed. Potential chemistry is confined largely to benzene chemistry, with bromination, nitration and Freidel-Crafts reactions being the most general. These reactions are typically unselective upon multiple substitutions however. Symmetry effects allow one substitution to often be successful, but di- or tri-substitutions typically result in a statistical distribution of products. Operating with only one substitution site on these aromatics is limiting and makes including heteroatom and sufficient solubilising functionality difficult.

1.9.1. SYNTHESIS OF 'ISLAND' MODEL MOLECULES

Suitable 'island' model compounds need to include heteroatom functionality N, S and O into the aromatic framework. In order to achieve a suitable product, large aromatic units have to be made from pre-functionalised components (**19**, **21**) with an oxidative capability that allows the formation of a singly condensed aromatic molecule (**20**, **22**). This versatile approach can be described as a 'bottom-up' route to synthetic targets and permits creativity in producing suitable aromatic species.

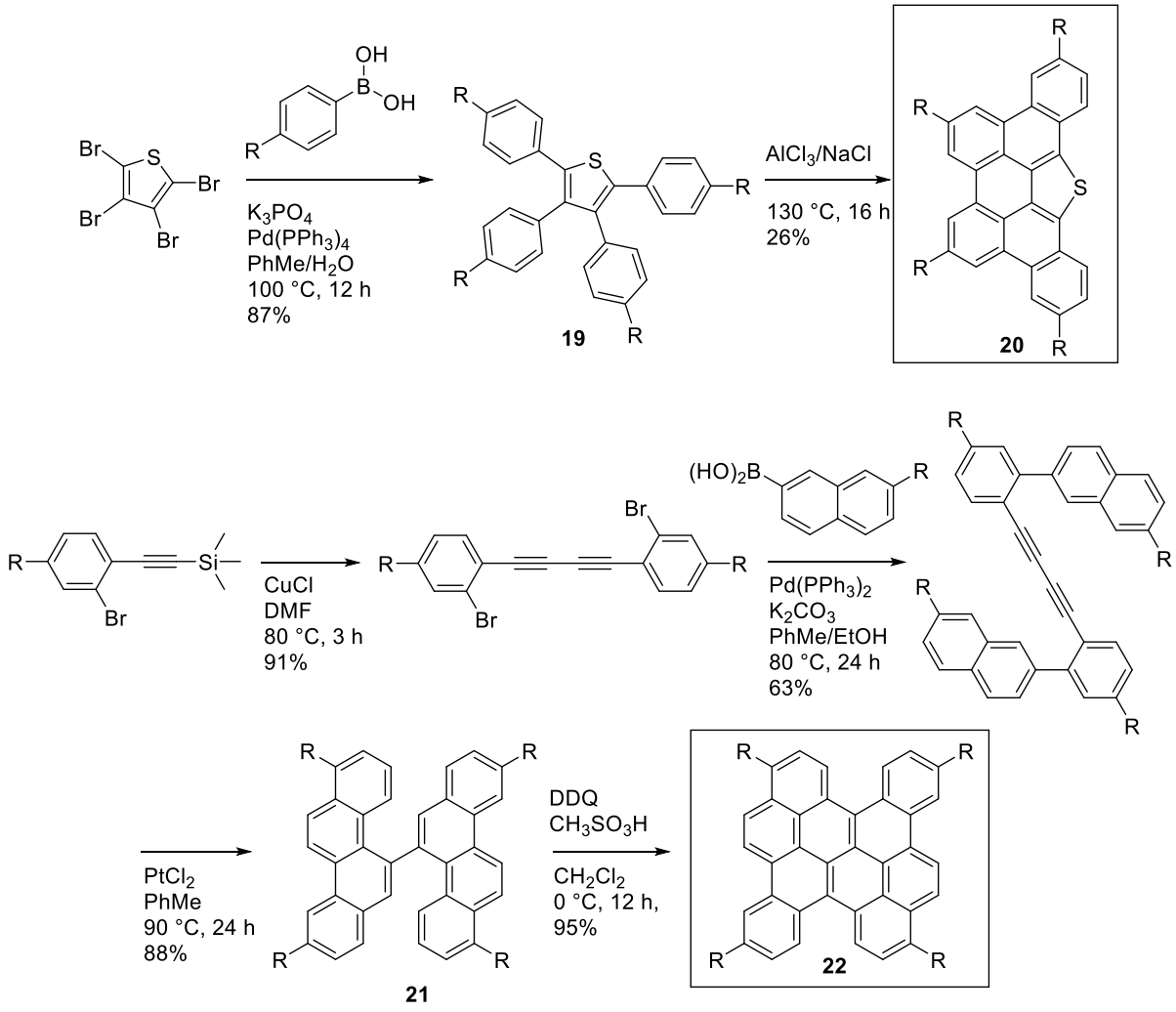

Figure 12. Representative 'bottom-up' 'island' asphaltene model syntheses.[142–144]

This synthetic approach carries significant risk due to the idiosyncratic nature of oxidative aromatic couplings (OACs). The mechanism of this reaction remains controversial and numerous articles have explored OACs high sensitivity toward subtle changes structural isomerisation.[145,146] In OAC reactions an electron-rich aromatic compound loses an electron to form a radical cation. The radical species then attacks at a susceptible second site to form a carbon-carbon bond (**Fig. 13**).[147] Where radicals form and attack is unpredictable however, and can result in the formation of oligomeric species through intermolecular coupling reactions.[148]

1.9.2. Oxidative Coupling of Electron Rich Aromatics

Suitably functionalised precursors can form intramolecular biaryl bonds giving access to a hugely diverse selection of functionalised aromatic compounds for purposes including dyes, organic light emitting diodes (OLEDs), graphene nanostructures and sensors.[146] This reaction

can be performed using a variety of conditions, but principally uses an electron-rich arene, an oxidant and a strong acid. The reaction proceeds *via* a radical cation mechanism.[147]

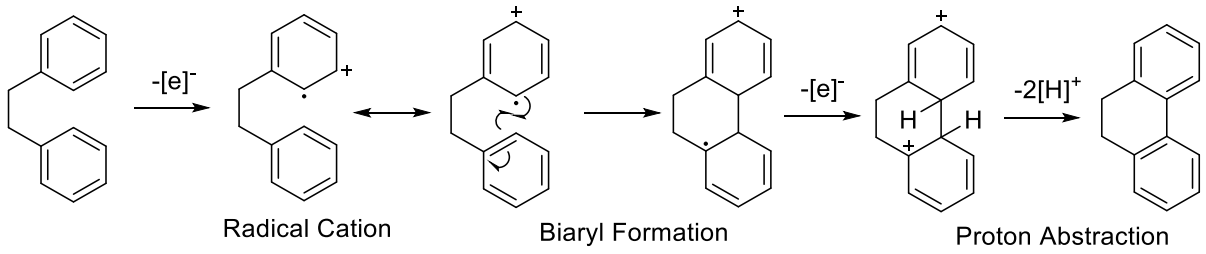

Figure 13. General scheme for the radical cation mechanism of OAC reactions.

OAC reactions are facilitated by an oxidant, typically DDQ or $FeCl_3$, capable of removing an electron from the aromatic system to form a radical cation. The intermediate is susceptible to intra- or intermolecular electrophilic attack to form a biaryl bond. DDQ and $FeCl_3$ are commonly used as the oxidant and are able to perform this reaction through variations of the same mechanism.

$FeCl_3$ acts as a strong Lewis acid capable of oxidising an aromatic unit by accepting electron density into its vacant 3d and 4p orbitals, with the electronegative chlorine substituents stabilising the negative charge and promoting the formation of a radical cation. $FeCl_3$ is a highly deliquescent material that forms hydrochloric acid upon contact with water, allowing proton abstraction to be facilitated through chloride anions.

DDQ operates differently, forming an electron donor-acceptor complex with the electron-rich arene. An acid source is then required to facilitate the electron transfer reaction resulting in oxidation of the substrate and the formation of hydroquinone (**Fig. 14**).

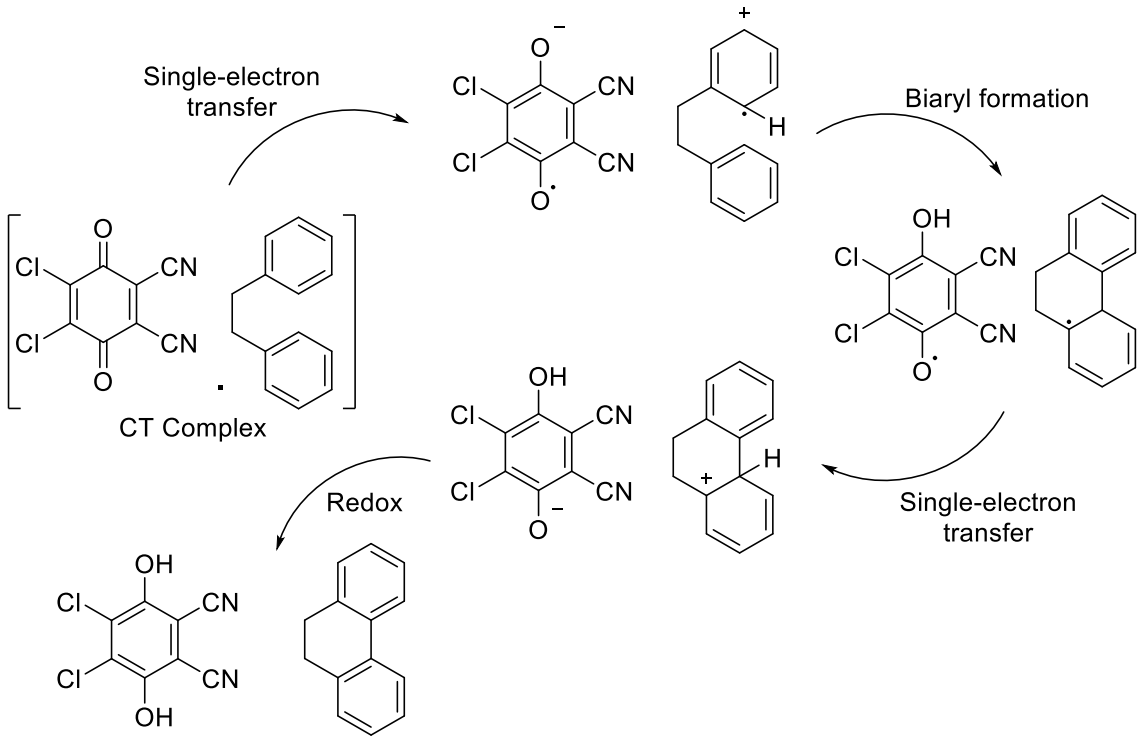

Figure 14. Reaction cycle of DDQ in OAC.

Due to the late-stage nature of OACs in these synthetic routes, time and labour intensive substrate preparation can often result in an undesired or intractable final product due to misaligned electronic distribution. Density functional theory (DFT) can help to predict whether a precursor is amenable to the desired reaction but requires lengthy simulation times. In order to acquire representative asphaltene molecules however, this chemistry cannot be avoided. HBC chemistry is well established[135,149–151] and has been successfully applied to capture a series of tribenzopentaphene (TBP) derivatives (**Fig. 15**).[152–154] By developing upon this established chemistry, the risks associated with OAC chemistry upon substrates is minimised.

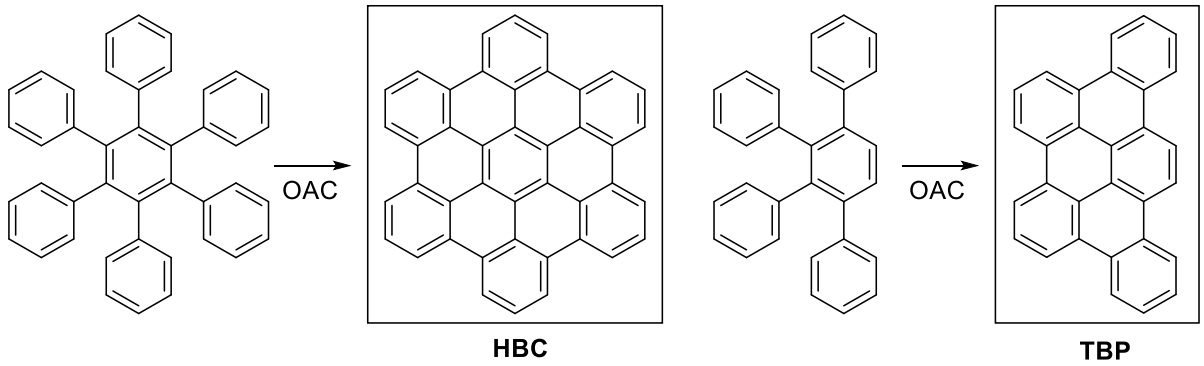

Figure 15. General reaction schemes for the synthesis of HBC and TBP derivatives.

Models synthesised *via* these routes offer extensive R-group versatility (**Fig. 16**). This allows tuneable solubility to be built into the molecule. HBC use in asphaltene modelling has been primarily focused on hexa-alkylated derivatives (**15a/b**), which possess a high degree of symmetry and self-associate in a lamellar orientation. The potential for these molecules to perform as asphaltene models has not yet been properly explored however, as their synthesis can allow for the formation asymmetric and functionalised compounds. This also applies to TBP chemical syntheses, with the added benefit of being able to utilise functionalised commercial alkynes for Diels-Alder addition chemistry. This potentially allows a library of TBP derivatives with various functionalities to be developed from a common precursor **23**.

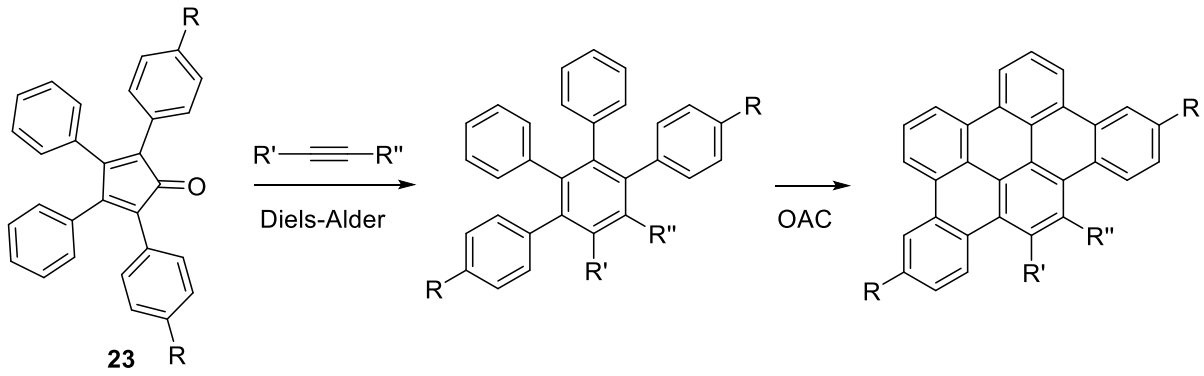

Figure 16. General reaction scheme for the preparation of functionalised TBP derivatives.

The asphaltene modelling community has invested a large amount of effort in PBIs due to their surface and solution properties aligning well with those of the asphaltenes. Perylene **24** offers a versatile starting point (**Fig. 17**) for a variety of potential asphaltene model compounds without including inappropriate heteroatom content associated with *bis*-imide functionality. **24** is highly amenable to various functionalisation mechanisms allowing a series of perylene-based derivatives to be synthesised featuring the key functional groups of interest. The risk of

producing a material with inadequate solubility for solution analysis is also mitigated due to the ability to tune alkyl functionality through cross-coupling reactions upon borylated **25** or brominated derivatives **26**.

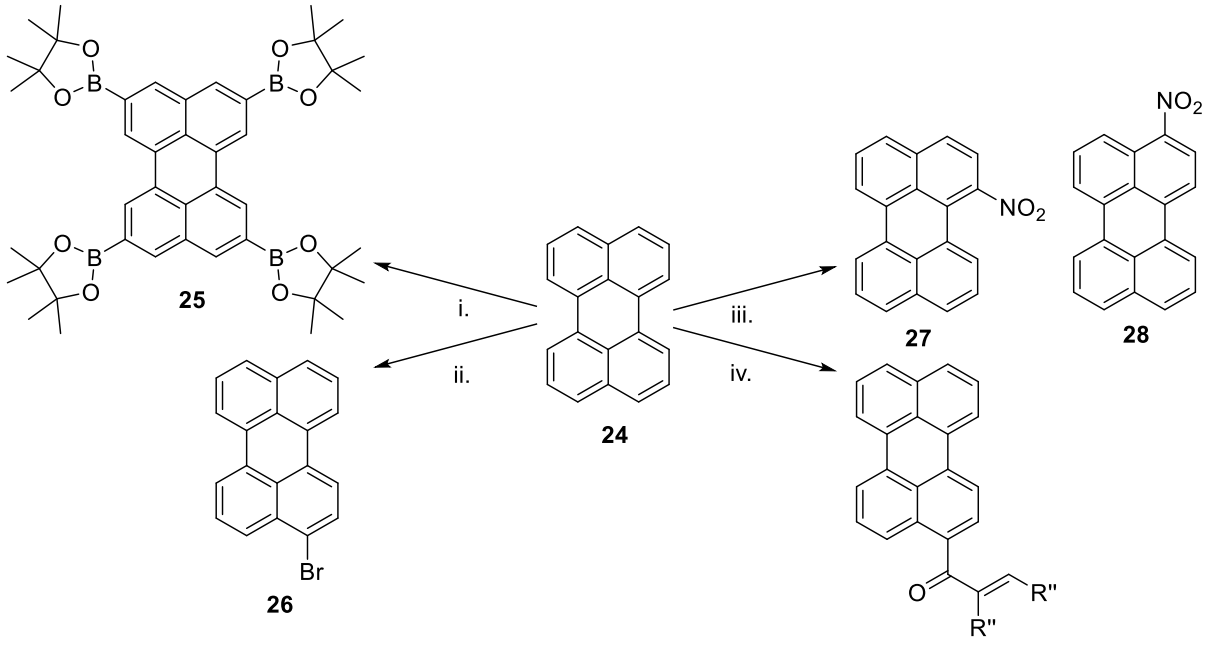

Figure 17. The versatile substitution chemistry of perylene **24**. i. B_2Pin_2, $[Ir(OMe)(COD)]_2$, DTBPY, cyclohexane;[155] ii. NBS, DMF;[156] iii. HNO_3, dioxane/water;[157] iv. $(CF_3CO)_2O$, CF_3SO_3H, α,β-unsaturated carboxylic acid.[158]

The installation of aromatic functionality is also reported for perylene **24**. This is possible due to the regioselectivity of primary nitration occuring in the 1- and 3-positions **27**/**28**. Electrophilic aromatic substitution is governed by electron density and steric effects.[159] Despite **27** appearing the less sterically available isomer in comparison to **28**, significant yields have been reported of its isolation.[157] **27** is of great value in creating asphaltene model compounds due to its ability to form thiophene **29** and carbazole **30** derivatives through oxidative cyclisation reactions.

The potential to capture a pyridinic derivative of **24** through bischler cyclisation also exists through a proposed synthetic route upon the successful reduction of **27** to 1-aminoperylene **31** (**Fig. 18**).

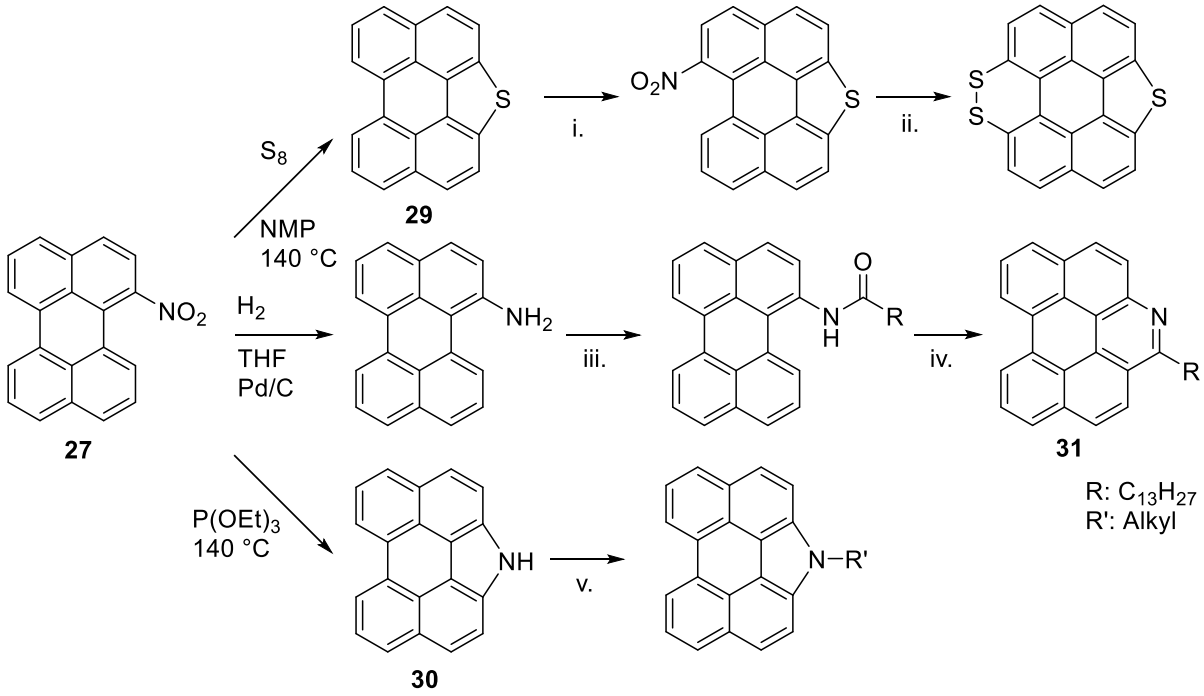

Figure 18. Synthesis of heterocyclic perylene derivatives from **27**. i. HNO_3/H_2O, 15%; ii. S powder, Cu, 88%;[160] iii. $CH_3(CH_2)_{11}COCl$, Pyridine, THF;[161] iv. P_2O_5, DCM;[162] v. $C_8H_{17}Br$, KOH, KI, THF, 78%.[163]

1.10. AIMS AND OBJECTIVES – SYNTHESIS OF ASPHALTENE MODEL MOLECULES

In this project, model molecules representing the spectrum of molecular weights, functionalities and aromatic orientation of the asphaltenes are synthesised and distributed to academic and industrial partners for solution and surface chemistry analysis. Compounds displaying the supposed asphaltene frameworks of ‘island’ and ‘archipelago’ are to be both represented.

In summary the project has the following aims:

1. Establish a protocol for the synthesis of ‘archipelago’ model compounds generated from functionalised phenanthrene and pyrene polyaromatic units tethered together utilising sulphides and alkyl spacers of various lengths.
2. Successfully synthesise 1-nitroperylene **27** to allow the preparation of novel pyridinic and carbazole containing perylene derivatives.
3. Synthesise a series of HBC derivatives of various solubilities through variation of alkyl chain length and substitution pattern to represent a reference C/H containing ‘island’ molecule.
4. Utilise the chemistry of HBC synthesis to develop a series of TBP model molecules possessing relevant functionalities and solubilities suitable for surface analysis.
5. Synthesise a geologically inspired asphaltene model molecule through coupling and subsequent oxidation of a steroid with a PAH.

2. RESULTS AND DISCUSSION

2.1. ARCHIPELAGO MODEL COMPOUNDS

2.1.1. TETHERING AROMATICS THROUGH S_NAr REACTIONS

The synthesis of a suitable archipelago compound requires two PAH groups each functionalised with single effective leaving group and a single tethering unit with a nucleophile potent enough to facilitate nucleophilic aromatic substitution (S_NAr). Initial studies utilised bromide functionalised pyrenes and alkyldithiols based upon successful reactions in the literature surrounding the use of sulfoxides as fluorescent chemosensors. [164–166]

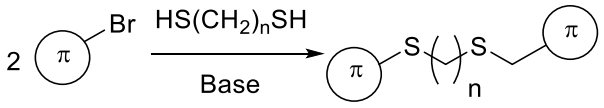

Figure 19. General route for the synthesis of aromatics tethered together by a dithiol.

The reaction is facilitated by aromatic resonance in the extended π-network in pyrene that stabilises the anionic intermediate.

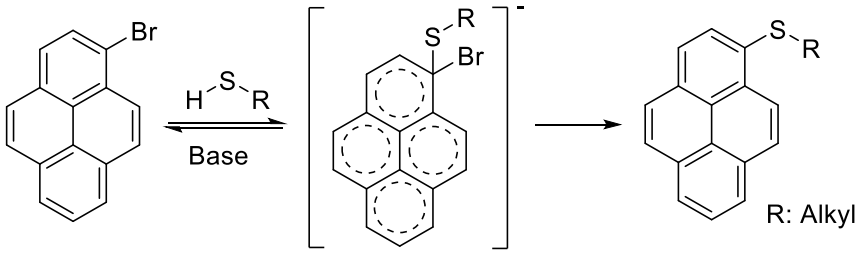

Figure 20. Example of resonance stabilised nucleophilic aromatic substitution.

The commercially available starting materials 1-bromopyrene and 9-bromophenanthrene were reacted with either 1,6-hexanedithiol or 2,2'-(ethylenedioxy)diethanethiol and potassium carbonate at high temperature to produce a series of archipelago compounds **32**-**34**.

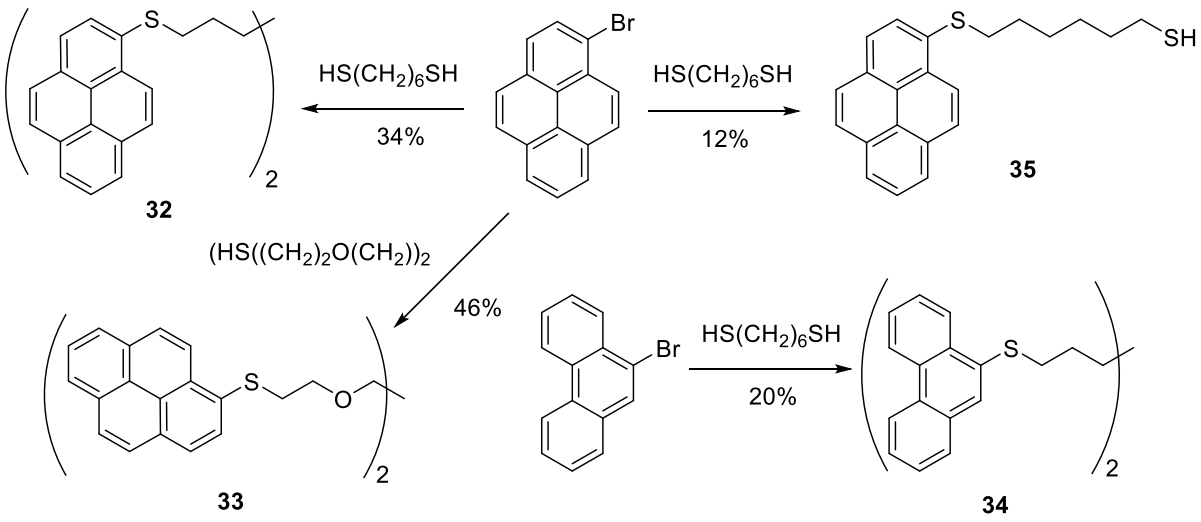

Figure 21. Arylsulfides synthesised from nucleophilic aromatic substitution. Conditions K_2CO_3, DMF, 145 °C, 16 h.

The synthesis for the production **32-34** requires one reaction step and operates within a short timescale. However, the process proved typically low-yielding and produced considerable by-products, the separation of which requires multiple recrystallisations from toluene/heptane. The result is an inconsistent procedure. It is plausible that the unintentional species produced are products of sulfur oxidation, resulting in sulfoxide and disulfoxide formation (these compounds are indistinguishable by ^{1}H NMR). The CH_2 environment α- to sulphur displays a resonance of 2.62 ppm, which is in the range of those reported for sulfoxides.[164,167]

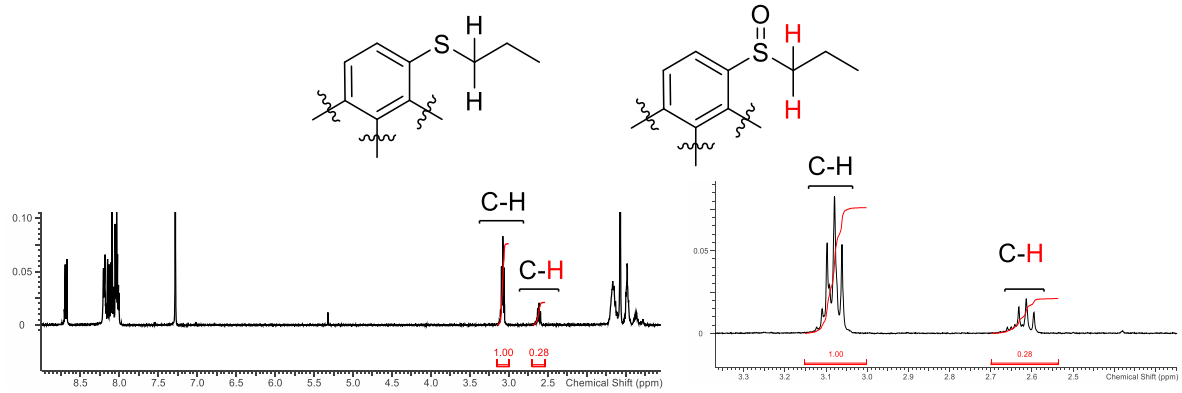

Figure 22. Crude ^{1}H NMR spectrum of **32** containing a 20% intractable impurity.

Attempts to optimise the synthesis and prevent sulfoxide from forming were initially addressed by more aggressively removing oxygen in a freeze-pump-thaw procedure but resulted in limited success. Lowering the reaction temperature in order to make the reaction conditions milder prevented bromoaromatic compounds from being consumed at all. A series of reactions

at different temperatures revealed that this procedure requires a minimum temperature of 130 °C to proceed. Given that no reaction was found to proceed in o-xylene at 144 °C, it is plausible that a highly polar solvent facilitates charge separation of the thiolate nucleophile and anionic aromatic intermediate species to permit this reaction pathway.

2.1.2. TETHERING AROMATICS THROUGH S_N2 REACTIONS

In order to avoid the formation of any potential oxidation products, the reaction procedure was altered by substituting the aromatic bromide for thiolate functionality. This allows 'archipelago' models to be synthesised under milder conditions by performing an S_N2 nucleophilic substitution upon a dibromoalkane.

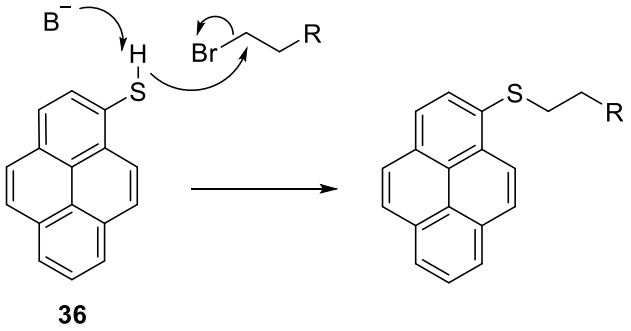

Figure 23. Mechanism for S_N2 addition upon pyrene-1-thiol **36**.

Pyrene-1-thiol **36** was synthesised from 1-bromopyrene and sodium methanethiolate, utilising a nucleophilic aromatic substitution resulting in methyl(pyren-1-yl)sulfane **37** forming as an intermediate (**Fig. 24**). With excess sodium methanethiolate the reaction continues as the thiolate species is a strong nucleophile capable of attacking **37**, resulting in the formation of **36**, methane thiol and dimethyl sulphide. This reaction requires the strictest chemical containment standards as otherwise the reaction is almost intolerable to the operator due to the potency of odour produced. In spite of these technical challenges this optimised procedure was performed at room temperature in the order of minutes and produced the desired product in a near quantitative yield.

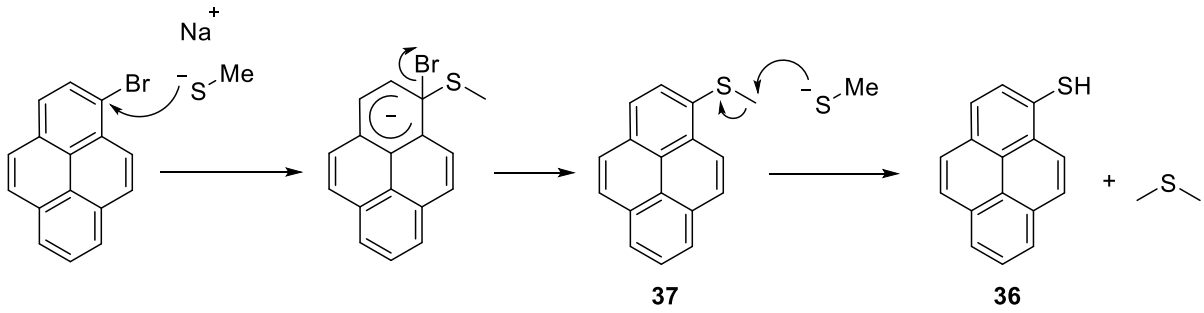

Figure 24. Mechanism for the generation of pyrene-1-thiol **36**.

Due to material demands from academic partners, this procedure was only performed upon 1-bromopyrene for the capture of **32**.

2.1.3. ALL-CARBON ANALOGUE OF 32

In order to access the impact of sulphur contained in the archipelago model series and because of recent interest in the field regarding these molecules,[168] a carbon analogue of **32** was synthesised **38** using 1-bromopyrene, 1,8-dibromooctane and *tert*-butyl lithium (**Fig. 25**).

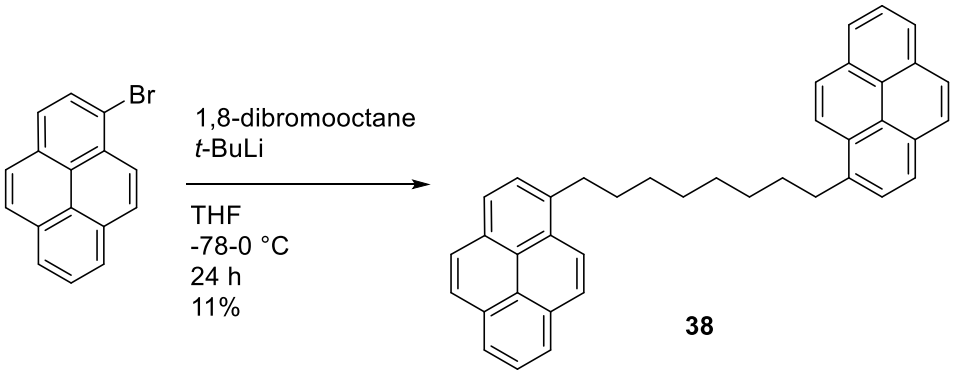

Figure 25. Reaction scheme to yield 38.

Pyrene **39** was formed as a major by-product due to the lithiated pyrene intermediate reacting with water present in the solvent and reaction vessel despite precautions being taken to keep the system moisture free.

Use of *n*-butyllithium led to the formation of 1-bromobutane, which competed directly with the intended coupling partner, resulting in a statistical distribution of inseparable products. *Tert*-butyl lithium however avoids the formation of a competing bromoalkyl species when two equivalents are used, resulting in a more facile purification and an increased yield.

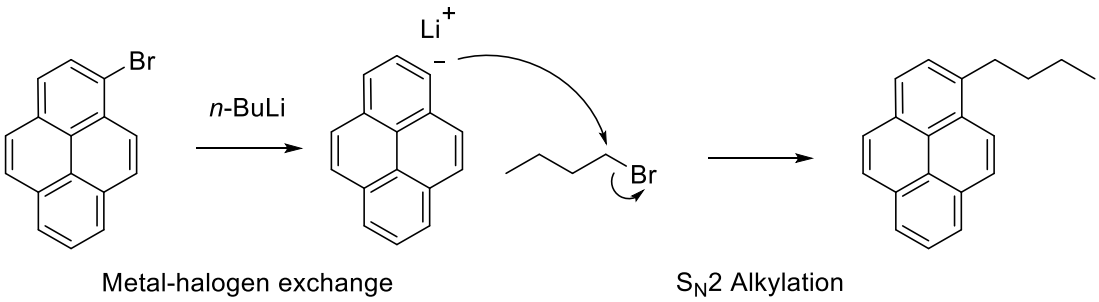

Figure 26. Mechanism of lithiation and associated by-products with *n*-Buli.

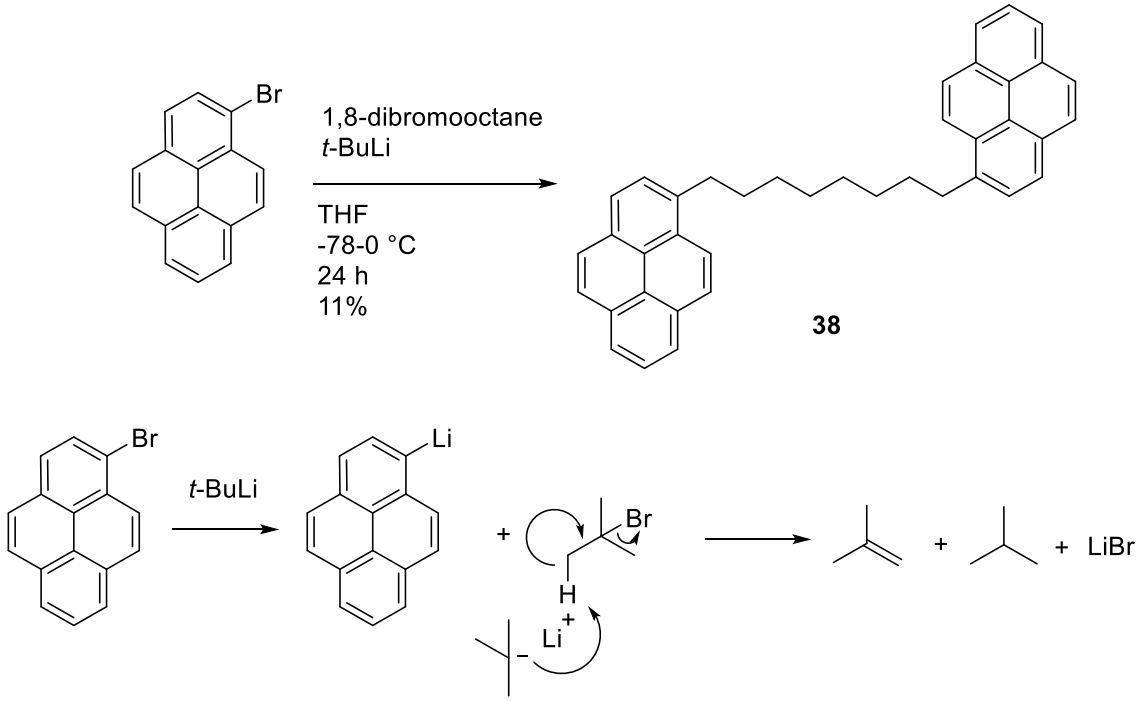

Figure 27. Mechanism of lithiation with two equivalents of *t*-BuLi.

2.1.4. SINGLE CRYSTAL X-RAY CRYSTALLOGRAPHY

Single crystals were grown throughout the project in order to acquire X-ray structures for the purpose of structure determination and to assess stacking motif. Archipelago model compounds **32-35** and **38** have been collected and analysed.

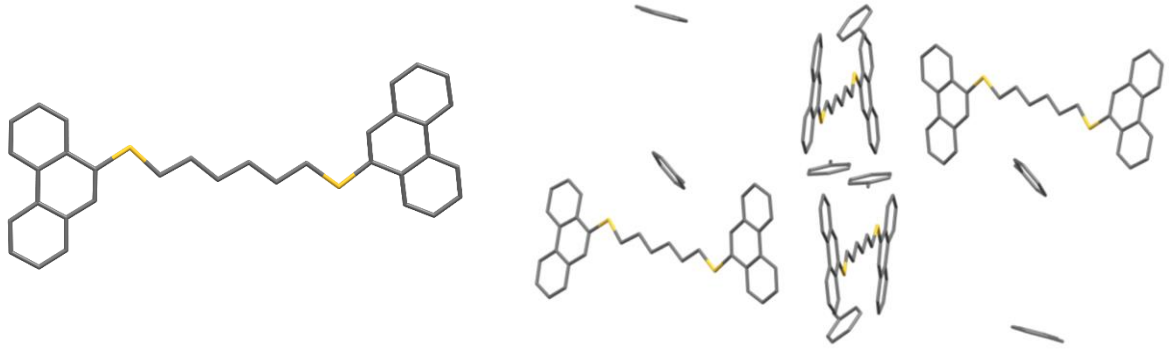

Figure 28. Crystal structure of 34.

34 co-crystallised with toluene to adopt a highly asymmetric twisted herringbone stacking orientation, dominated by CH-π interactions (short C-C contact 3.66 Å, CH-C contact 2.93 Å).

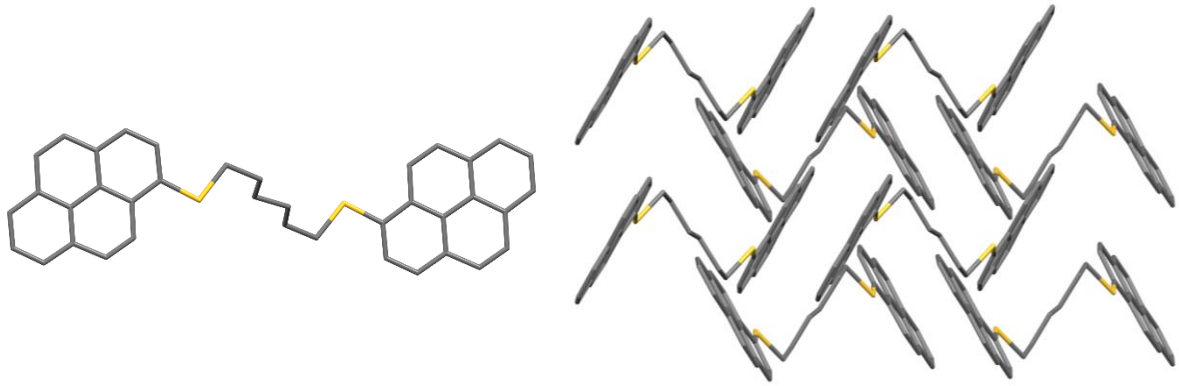

Figure 29. Crystal structure of 32.

32 crystallised in a symmetric herringbone orientation with coplanar geminal aromatic units and CH-π interactions dominating (short C-C contact 3.35 Å, CH-C contact 2.91 Å).

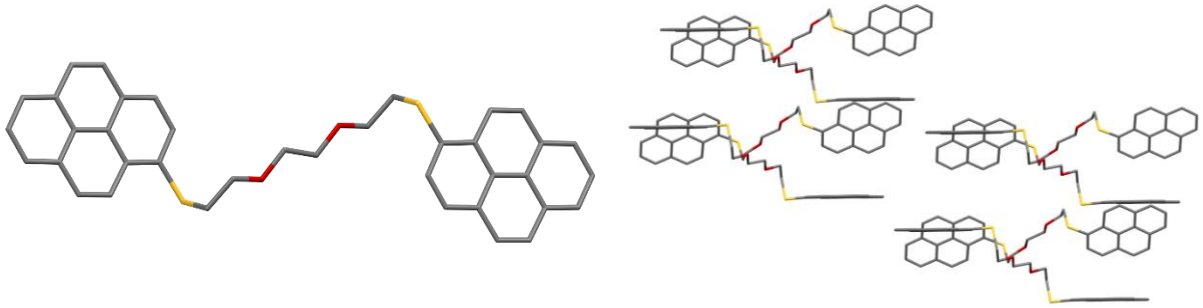

Figure 30. Crystal structure of 33.

In a similar manner to **32**, **33** crystallised in a symmetric herringbone orientation with coplanar germinal aromatic units, and CH-π interactions predominating (short C-C contact 3.55 Å, CH-C contact 2.988 Å).

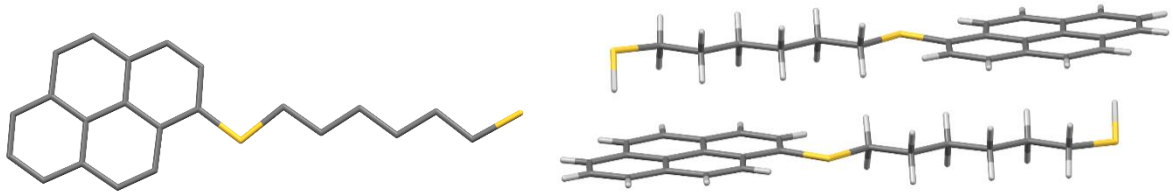

Figure 31. Crystal structure of 35.

35 stacked in a head to tail orientation with 1D stacking, dominated by alkyl-π and SH-π interactions (short CH-C contact 3.027, SH-π contact 2.79).

Figure 32. Crystal structure of 38.

38 crystallised in a herringbone orientation with orthogonal geminal aromatic units and CH-π interactions dominating (short C-C contact 3.74 Å, CH-C contact 2.90 Å). Full detail of crystal structures detailed upon in appendix (**5.3.1**-**5.3.5**).

2.1.5. PRELIMINARY ANALYSIS OF ARCHIPELAGO STRUCTURES BY ICAM EXPERIMENTALISTS

2.1.5.1. AFM STUDIES OF 32 FROM WP 2/3

All work detailed herein (**Sect. 2.1.5.1.**) was performed by Domina-Maria Kaimaki and Dr Colm Durkan at the University of Cambridge operating within WP 2 and 3. The following is a brief summary of preliminary results acquired from SPM upon 'archipelago' model **32**.

AFM studies were undertaken investigate the deposit morphology of **32** upon model surfaces Au, highly orientated pyrolytic graphite (HOPG) and Al_2O_3. These surfaces were chosen as they represent industrial steel surfaces at vairous stages of their lifecycle. Metallic Au represents a non-oxidised steel surface and alumina an oxidised steel surface. HOPG is a semi-metal and is expected to serve as a model steel surface. The different electron densities of these materials are expected to result in different adsorbate-substrate behaviour due to the potential for charge transfer varying considerably. These materials are well defined and have characteristic features that make analysis reproducible, making them preferable candidates to more complicated industrial steel surfaces. From these model systems it is anticipated that the general principles of asphaltene deposition can be investigated with confidence.

Compound **32** was deposited onto model surfaces using dropcasting, chemical vapour deposition (CVD) and immersion. Immersion (in 1 mmol toluene solution over 5 hours) was identified as the most representative of the deposition methods due to the organics being allowed to equilibrate and not being forced onto the substrates. Furthermore, experimentally this method gave the most reproducible results.

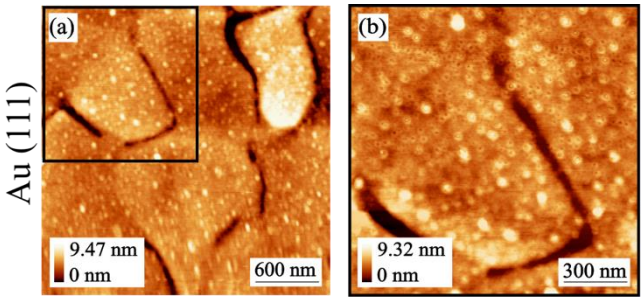

Figure 33. AFM topography images of **32** deposited upon ^{111}Au.

Circular adsorbates of ~3 nm height were found to form upon Au. The size of these deposits are much greater than the dimensions of a single molecule, indicating that deposits are forming

as molecular clusters or aggregates (**Fig.33** (a) and (b)). The molecule-surface interaction is understood to be relatively strong due upon observation that their position remains fixed through repeated imaging. Therefore, it is plausible that **32** can chemisorb to the Au surface.

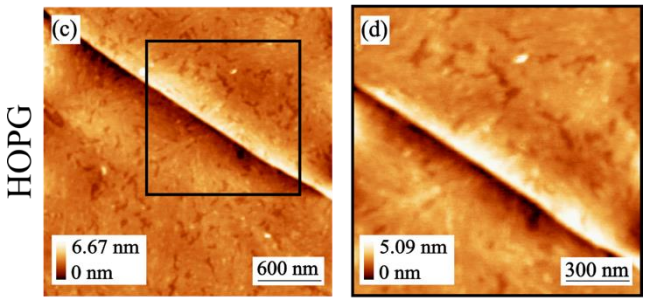

Figure 34. AFM topography images of **32** deposited upon HOPG.

Upon HOPG a self-assembled monolayer can be seen to form ~1 nm tall with no apparent preferential molecular orientation or location relative to either surface steps or atomic rows (**Fig. 34** (c and d)).

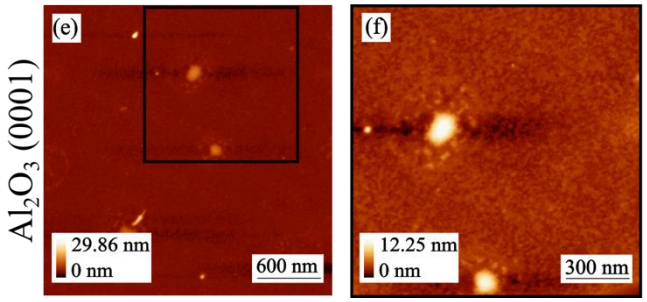

Figure 35. AFM topography images of **32** deposited upon on alumina.

Adsorption on alumina is significantly reduced in comparison to Au and HOPG (**Fig. 35** (e and f)). Weakly bound adsorbates with two different size profiles are present, with the larger adsorbates ~3 nm tall and ~200 nm wide and the smaller covering the surface as a submonolayer ~1 nm tall.

The relative strength of adsorbate interaction can be interpreted through grain analysis, with a greater surface area coverage indicating stronger adsorbate adhesion. From analysis of AFM images it is anticipated that the strength of interaction is in the order of Au>HOPG>alumina. However, surface coverage values display Au at 35%±6%, HOPG at 73%±6% and alumina at 63%±4%. It is plausible that the low surface coverage of Au is due to the analytical technique not accounting for a monolayer film underneath the observed clusters.

2.1.5.2. ADSORPTION ISOTHERMS OF 32 UPON GRAPHITE AND IRON (III) OXIDE

All work detailed herein (**Sect. 2.1.5.2.**) was performed by Richard Alloway and Dr Stuart Clarke at the University of Cambridge within WP 2. The following is a brief summary of preliminary results acquired from adsorption isotherms taken for 'archipelago' model **32**.

In these studies **32** was adsorbed from non-aqueous solvents onto graphite and iron (III) oxide.

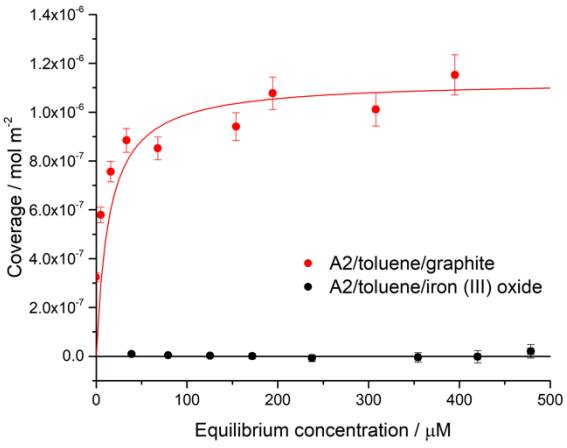

Figure 36. Adsorption isotherms of **32** (also named A2 within the scope of the project) in toluene onto graphite (red) and iron (III) oxide (black).

Experimental adsorption of **32** upon unrecompressed exfoliated graphite (**Fig. 36**) shows an increase in adsorption until a plateau is reached, demonstrating behaviour typical of a Langmuir isotherm.

$$\theta = \theta_{sat} \frac{K_{ads} c}{1 + K_{ads} c}$$

Equation 2. Langmuir adsorption isotherm as a function of surface coverage (θ) and deposition rate ($K_{ads} c$)

Linear regression can determine the values of θ_{sat} and K_{ads} to be:

θ_{sat} = (1.13 ± 0.05) x 10^{-6} mol m^{-2}

K_{ads} = (7.2 ± 4.2) x 10^{4}

Interpretation of these values suggests a strongly adsorbing chemical species onto a solid substrate. It can be calculated from the plateau region that the area per molecule is approximately 147 ± 6 $Å^2$ $molecule^{-1}$. A pyrene molecule lying flat on a surface occupies approximately 70 $Å^2$ and a C8 chain 40 $Å^2$, giving a rough total area of X as 180 $Å^2$. An upright pyrene molecule would occupy approximately 30 $Å^2$, suggesting an upright orientation for **32** of to cover approximately 30-60 $Å^2$. From these calculations it is inferred that **32** preferentially lies flat on the graphite surface, consistent with chemical intuition that would understand adsorbate-substrate π-interactions to be maximised when in parallel.

Adsorption behaviour of **32** upon iron (III) oxide (Fig. 41) is markedly different from graphite, with essentially no adsorption measurable within the given concentration range. It is plausible that this is due to differences in polarity between iron oxide and **32** making their interaction unfavourable.

2.2. Synthesis of Models from Perylene Scaffold

2.2.1. Nitration of Perylene

Perylene **24** offers a versatile substrate towards the synthesis of model asphaltene molecules through being a sufficiently soluble, 5-ring peri-condensed aromatic compound with numerous routes to functionalisation (**Fig. 17**). Asphaltene nitrogen-based functionality is understood to be largely incorporated into the aromatic framework, rather than being peripheral (see **Sect. 1.5.2**). **24** Offers access to these structural characteristics through optimally positioned nitro groups, allowing ring closures that result in structures not accessible from commercially available aromatics (**Fig. 18**).

The nitration of **24** has been utilised rarely, possibly due to difficulties in its handling. Whilst **24** is soluble enough for synthesis on an appreciable scale, its effective use generally requires large volumes of solvent per gram and an elevated temperature. **24** Was found to have a solubility limit of approximately 1.0 g per 150 mL at 70 °C in 1,4-dioxane. The desired 1-nitroperylene **27** is the less sterically available isomer due to the crowded environment of the bay region. Interpretation from ^{1}H NMR detailed an approximate 60% of conversion to produce isomer **28**. This unfavourable isomeric distribution results in multi-gram scales being necessary to produce a sufficient quantity of material. This problem is compounded by the purification process of this reaction being unavoidably wasteful.

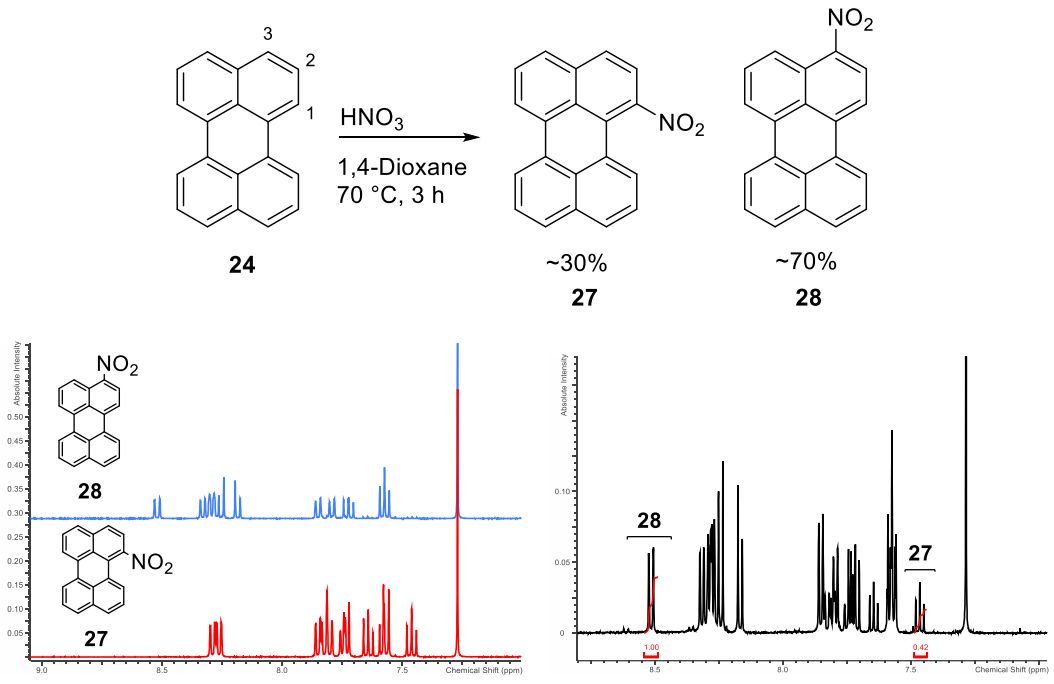

Figure 37. ^{1}H NMR spectra of purified and crude products from perylene nitration.

A serviceable reaction rate and limited unwanted additional nitro group substitutions require the correct concentration of nitric acid in the reaction. Surrounding literature for this reaction has described the need to stop the reaction whilst some perylene remains in the system, due to multiple additions upon one molecule being possible on this timescale.[157] However, using 10 mL of nitric acid per 1.5 L of solvent found 15 g of **24** to be entirely converted and the products largely limited to the two mono-substituted isomers **27** and **28**.

The work-up of and purification of this large scale reaction is demanding of time, technical ability and a hugely unfavourable ratio of solvent to product returned. The use of aqueous base to quench acid present forms an emulsion with 1,4-dioxane and low-solubility perylene products, resulting in excessive quantities of organic solvent being required to form a solvent partition.

Regioisomers **27** and **28** are separable by column chromatography, however both products possess intrinsically low solubility and share a similar polarity. The purification of >1 g of crude products required gradient chromatography to be performed in a broad bore vessel due to the high loading volume permitted per area of silica. The intrinsic low solubility of nitration products complicates loading and required 100 mL of boiling chloroform per 10 g of crude products to afford an organic solution amenable to silica loading. Dry loading, typically employed for insoluble systems of this nature, was found to be ineffective as products where introduced to the solvent system in a gradual manner, resulting in ineffective separation. Vacuum silica plug chromatography was employed due to quantity of solvent needed to achieve separation and subsequent collection.

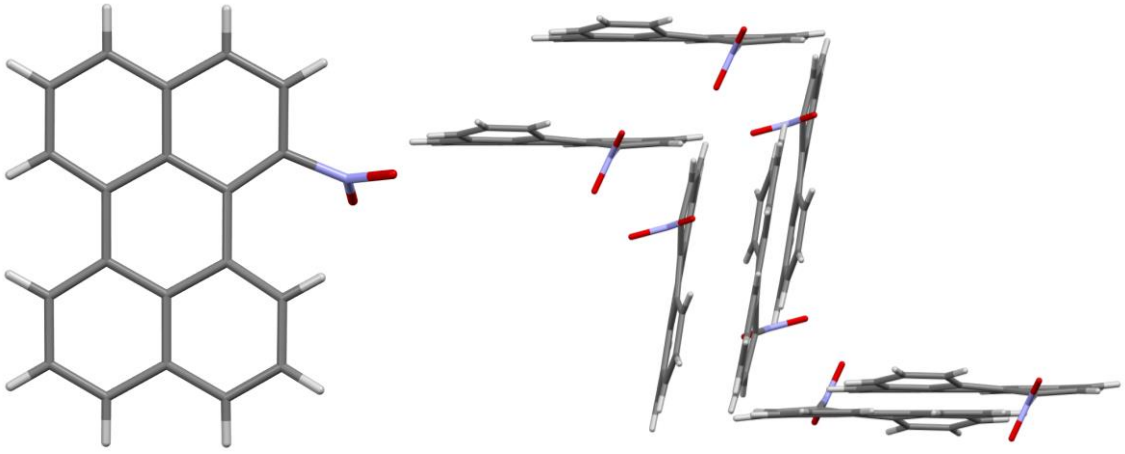

Figure 38. X-ray crystal structure of **27**. Full details in appendix (**Sect. 5.3.6**).

27 displays a herringbone packing motif with CH-π interactions dominating. The molecule is noticeably contorted due to the nitro group and C_{12}-H competing for space in the bay position. The NO_2 group is orthogonal to the perylene core. Despite numerous attempts to prepare **28** for X-ray crystallography, suitable crystals could not be grown.

2.2.2. PYRIDINE ASPHALTENE MODEL

A perylenophananthridine derivative **31** was sought as a synthetic target in order to represent a pyridinic asphaltene molecule. Given the limited availability of **27** the synthetic procedure was first examined upon (1,1'-biphenyl)-2-amine **42**. The series uses a base-mediated acylation followed by Bischler-Napieralski cyclisation (**Fig. 39**).

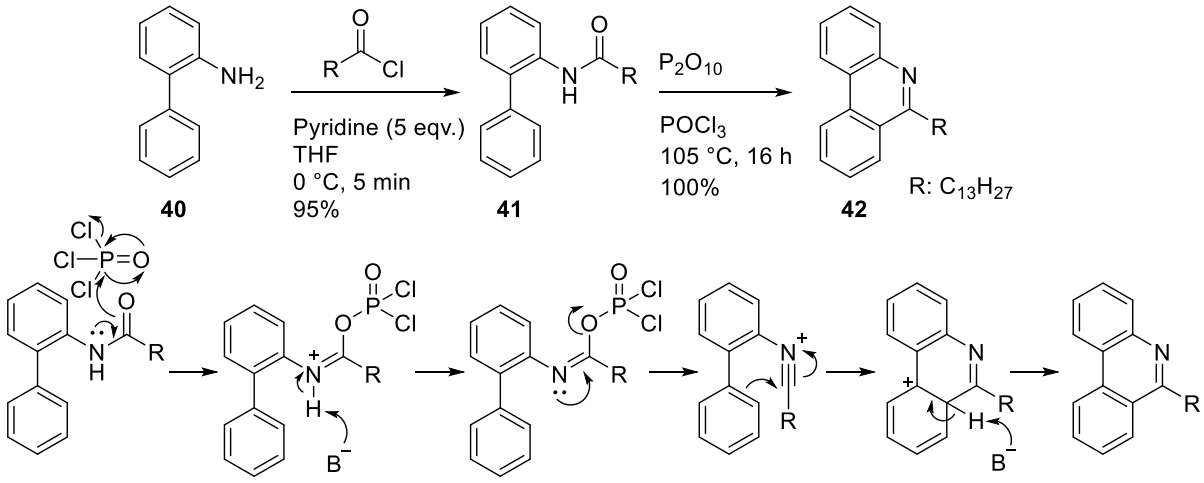

Figure 39. Synthetic route to the generation of **42** and Bischler-Napieralski cyclisation mechanism.

Acylation required investigation into the appropriate base and acylating agent. Pyridine proved to be effective in its role of activating the amine functionality as a nucleophile. Dodecanoic anhydride was selected as a mild acylating reagent, but displayed no reaction at room temperature. Myristoyl chloride was then selected as a more active reactant and was to found to perform best when used as two equivalents to capture **41**, with multiple additions frustrated by the steric demands of the amide formed. Bischler-Napieralski cyclisation proved to be a highly effective reaction, operating with a near quantitative yield to afford **42**.

This reaction sequence was then applied to the perylene derivatives following palladium catalysed hydrogen reduction of **27** to **43**.

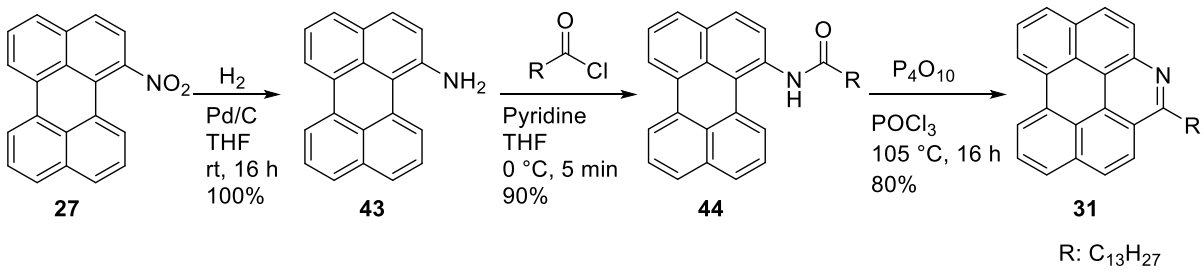

Figure 40. Synthetic route to the generation of **31**.

Analysis of **44** was complicated by solution chemistry obscuring ^{1}H NMR, implying a poorly defined mixture of products from acylation. Purification by column chromatography apparently yielded a single material. However, in chloroform-*d* at room temperature proton resonances were found to be poorly resolved. When subjected to increasing temperature in a series of variable temperature ^{1}H NMR experiments it was found that the signals changed significantly. Furthermore, when analysed in DMSO-d_6 resonances resolved at higher temperature (**Fig. 42**). This effect may be due to hindered rotation about the aryl C-N and N-acyl bonds on the NMR timescale at these temperatures. Upon hydrogen bonding to DMSO solvent this effect is significantly reduced.

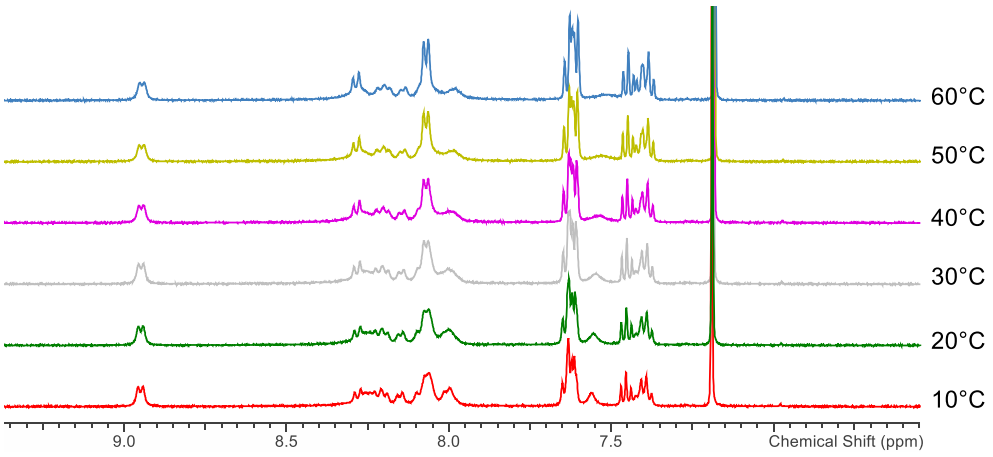

Figure 41. Variable temperature ^{1}H NMR study of **44** in chloroform-*d*.

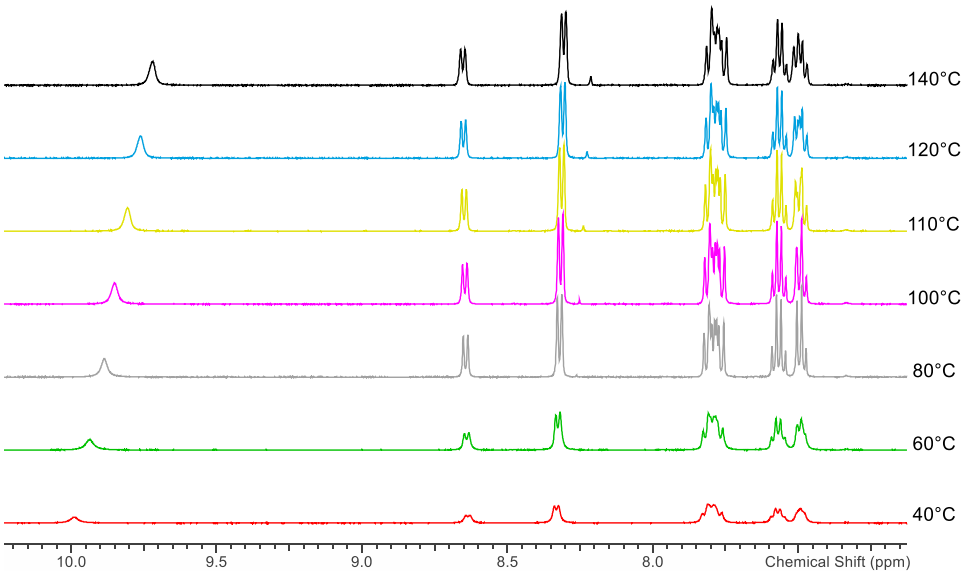

Figure 42. Variable temperature ^{1}H NMR study of **44** in DMSO-*d6*.

Upon subjection to Bischler-Napieralski cyclisation conditions it was found that the purified materials from acylation near-quantitatively returned **31** and possessed suitable solubility for use as an asphaltene model compound.

2.2.3. PERYLENOCARBAZOLE ASPHALTENE MODEL

A carbazole-containing asphaltene model was sought to investigate acidic nitrogen functionality upon surfaces. Cadogan-Sunberg indole synthesis facilitates the formation of an indole from **27** through deoxygenation to form a nitroso intermediate followed by intramolecular electrophilic attack upon the intermediate nitrene species and subsequent protonation to form **30**.

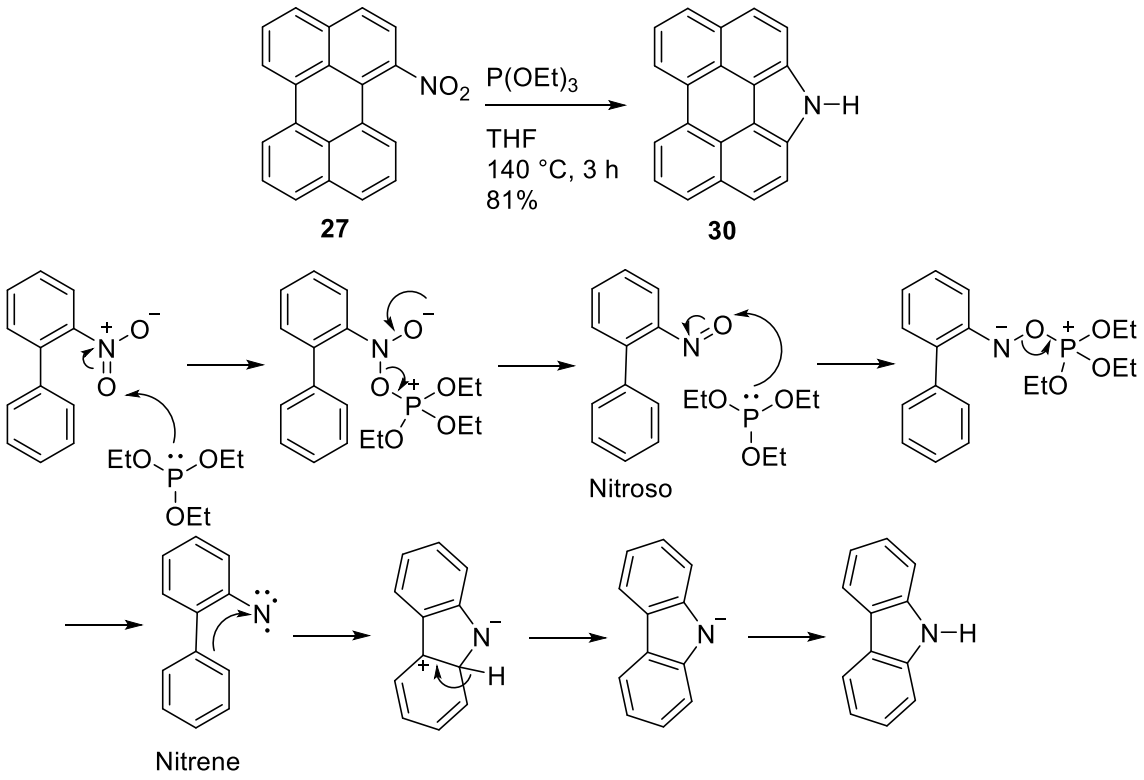

Figure 43. Cadogan-Sunberg reaction and mechanism upon **27**.

30 Would itself serve as a useful asphaltene model, however the solubility of the aromatic unit with no alkyl functionalisation is too poor for solution based analysis. **30** demonstrates acceptable solubility only in DMSO and THF. When used previously in the literature, groups tend to circumvent this problem by alkylation of the indole with sodium hydride and a haloalkane.[169] However, given that the target molecule requires N-H functionality this was not a viable solution. Bromination of **30** allows the solubility to be altered through instalment of alkyl functionality *via* cross-coupling reactions.

Mono-bromination of **30** proved complicated due to competing di-bromination in positions -3 and -10 inseparable by column chromatography. One equivalent of NBS generates unreacted, mono-brominated **45** and di-brominated **46** products in a ratio of 10:70:20 (**Fig. 44**).

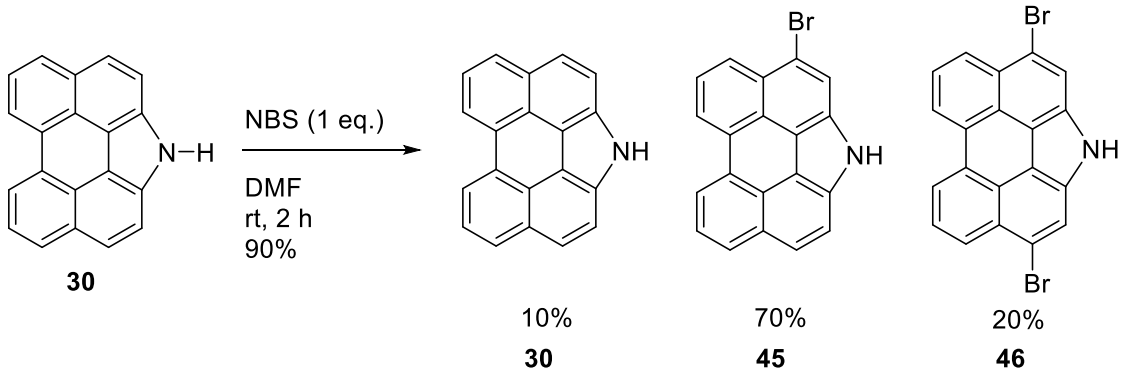

Figure 44. The bromination products of **30** with 1 equivalent of NBS.

Protection of **30** with TBDMS-ether was pursued with the intention of increasing solubility and allowing the use of column chromatography upon products of subsequent reactions. Whilst successful in increasing the solubility of **30**, subsequent bromination products of **47** were no more amenable to column chromatography than their unprotected analogues.

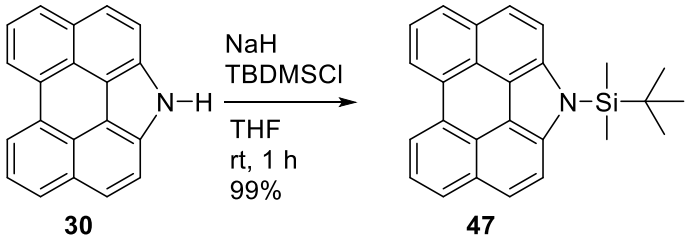

Figure 45. Reaction scheme for the protection of **30** with TBDMSCl to afford **47**.

As a result of this, di-brominated derivative **46** was selected as preferred candidate for further functionalisation and collected quantitatively after reaction with 2 equivalents of NBS (**Fig. 46**). It is notable that NBS directs electrophilic aromatic substitution to these locations. At room temperature, the second bromide substitution in unfunctionalised perylene is unselective for the -9 and -10 positions. However, instalment of the carbazole functionality apparently increases electron density at the 3- and 10- positions to direct substitution at these sites and afford one regioisomer **46**.

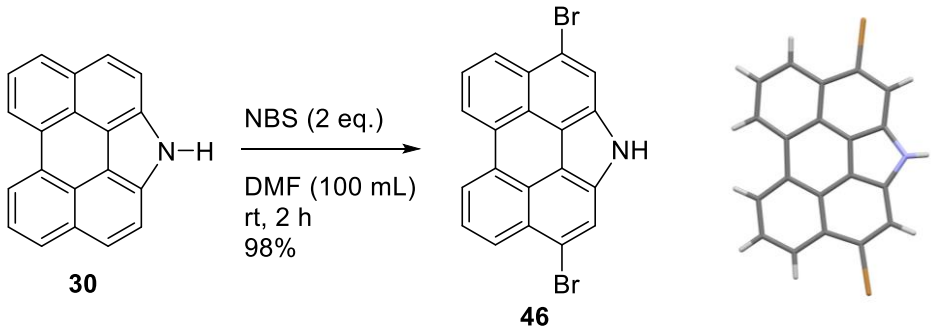

Figure 46. The bromination products of **30** with 2 equivalents of NBS and X-ray crystal structure (full detail in appendix, **Sect. 5.3.7**).

The crystal structure of **46** shows strongest interactions between orthogonal Ar-H and Ar-C (short contact 2.893 Å) and between Ar-Br and Ar-H short contact) of 2.982 Å. Two stacking motifs are present, with an offset stack of planar molecules and 125° herringbone stack laterally.

A double Sonogashira coupling upon **46** using Pd((PPh$_3$)$_4$) to afford **48** proved to be satisfactory after initial testing on 1-bromoperylene and was found to significantly increase the solubility of the material. Due to alkyne functionality being alien to asphaltene chemistry, a palladium catalysed hydrogenation was carried out with the intention of producing an alkyl derivative. An interesting consequence of this system is that these conditions reduced not only the alkyne functionality, but also two of the aromatic rings to give **49**.

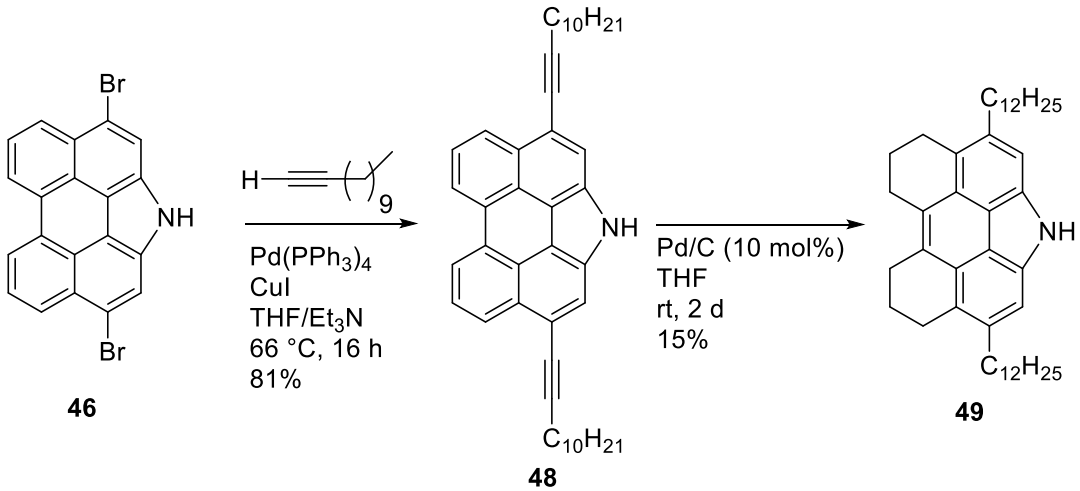

Figure 47. Reaction scheme for the Sonogashira coupling and subsequent catalytic hydrogenation to afford **51**.

Observation of the successful reduction of **27** to **43**, and attempted hydrogenation reactions performed on the unfunctionalised carbazole **30**, it is hypothesised that the alkyne functionality facilitates this further reduction. This could be made possible by subtle electronic differences in the molecule or the alkyne's approach and interaction with palladium forcing the molecule into a structural conformation whereby an aromatic reduction can take place.[170] The room temperature atmospheric pressure hydrogen reduction of aromatics mediated by palladium on charcoal is a seldom reported phenomena but has precedent in the Yeates group, with an alkylperylene derivative observed to form a hexahydroperylene under similar reducing conditions.[171] **49** Was decided to suffice as an asphaltene model compound despite the reduced aromaticity due to its FAR region, solubility and molecular range being within an acceptable range.

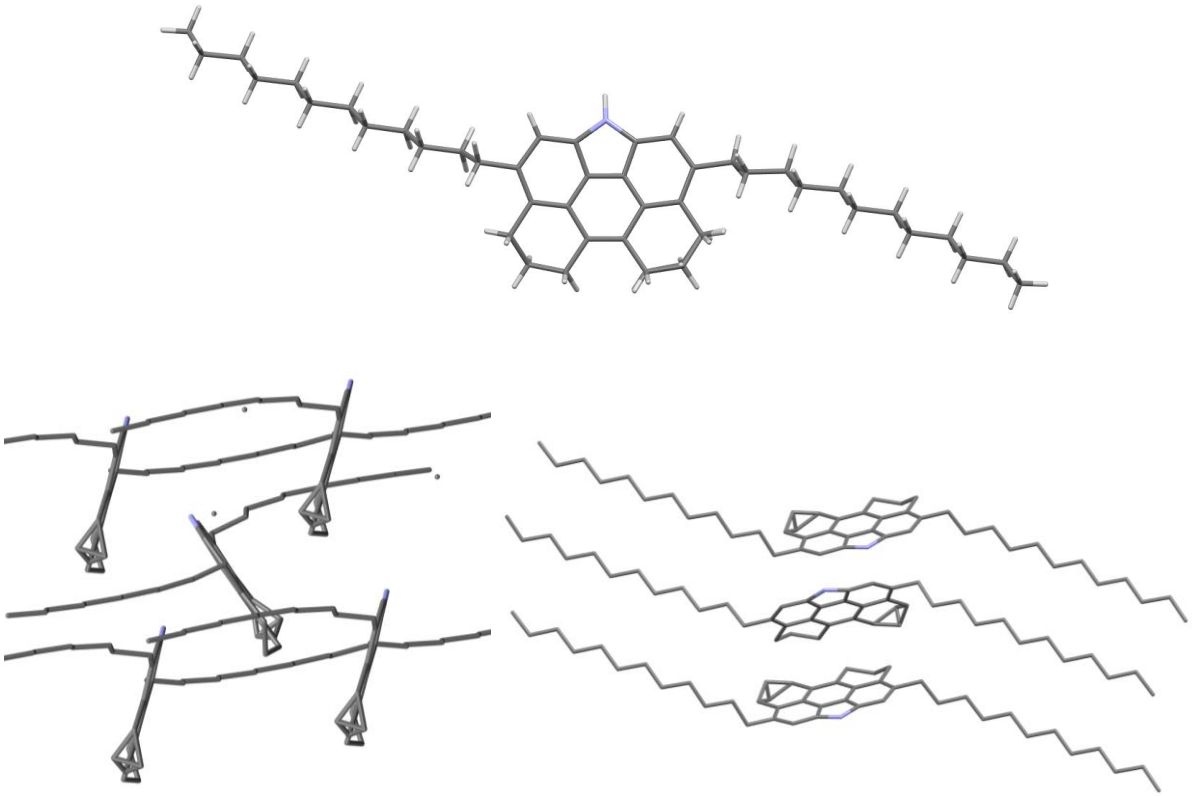

Figure 48. Crystal structure of **49**.

The crystal structure of **49** is dominated by orthogonal interactions of NH-π (short contact of 2.535 Å) and CH-π (short contact 2.840 Å).The saturated rings are evident from the tetrahedral carbons in positions -4,-5,-6 and -7,-8,-9. Full detail in appendix (**Sect. 5.3.8**).

2.2.4. A SULPHUR CONTAINING ASPHALTENE ISLAND MODEL

Thiophene functionality was incorporated into **24** *via* **27** in order to provide insight into the effect of an aromatic sulphur species in an 'island' topology upon industry surfaces. The structure of **29** and similar models have been used in experimental and computational model simulations, suggesting agreement in the field regarding its legitimacy as an asphaltene model compound.[172,173]

The condensed benzothiophene **29** was synthesised through reaction of **27** with elemental sulfur at high temperature. Whilst the reaction mechanism here is not fully understood, it is plausible that this reaction proceeds *via* electrophilic attack followed by nucleophilic aromatic substitution with elimination of NO_2.[174,175]

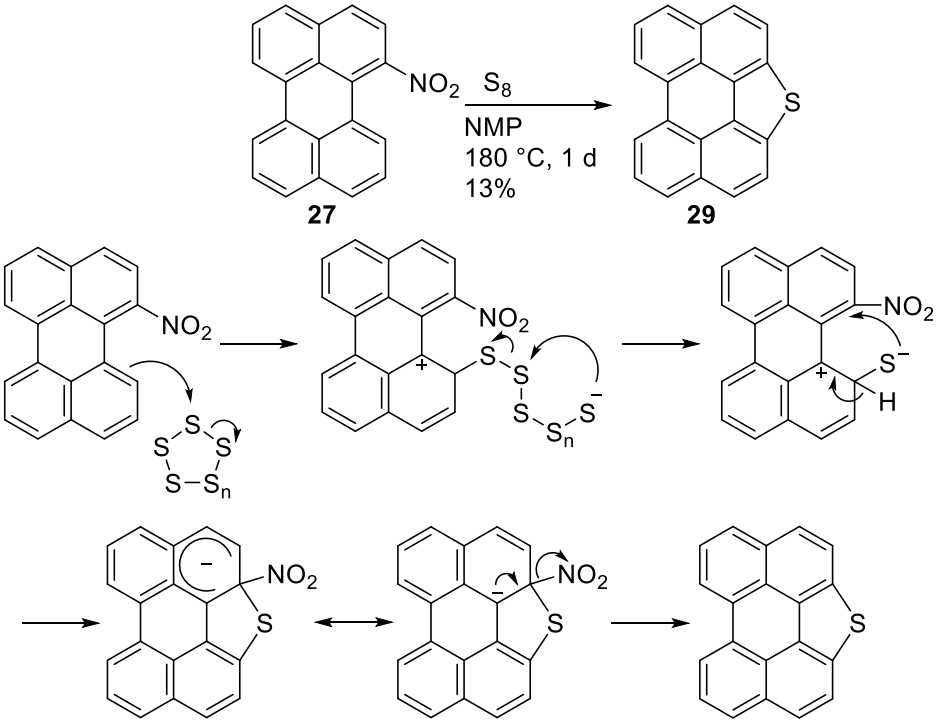

Figure 49. Reaction scheme and plausible mechanism for the conversion of **27** to **29**.

29 Was found demonstrate high solubility in toluene. Suitable solubility characteristics resulted in this molecule being serviceable as an asphaltene model without further functionalisation.

2.3. SYNTHESIS OF HEXABENZOCORONENES

2.3.1. ALKYNE PREPARATION

Alkylated HBC structures were selected as candidates to represent the heaviest 'island' structures to act as a reference point for a simple carbon and hydrogen containing asphaltene. They display versatile solubilities through the ability to tune aromatic to alkyl chain lengths. HBCs historical use as an asphaltene model allowing parallels to be drawn with the surrounding literature.[135,176]

A series of diphenylacetylenes were synthesised capable of undergoing either [4+2] Diels-Alder cycloaddition or cobalt cotrimerisation to generate hexaphenylbenzene (HPB) derivatives (**Fig. 50**).

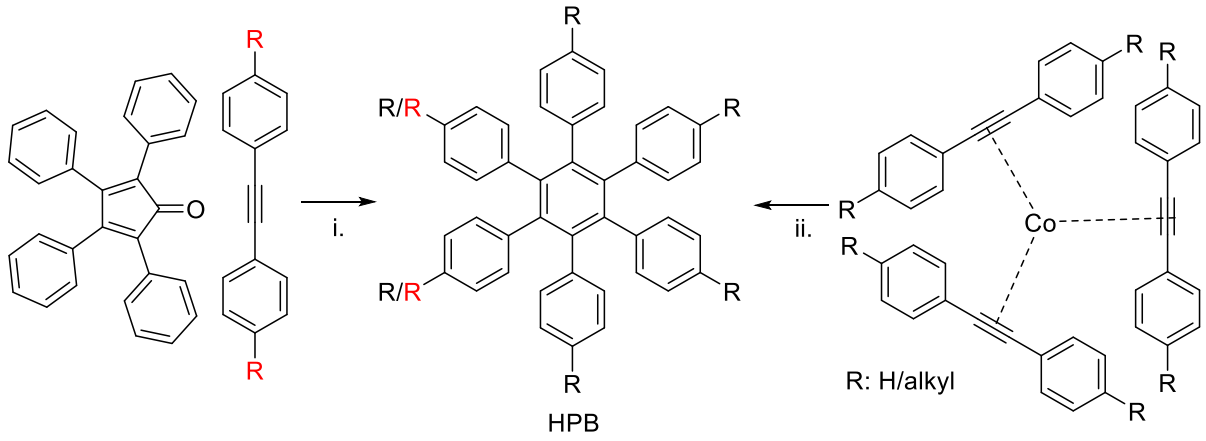

Figure 50. Route to HPB derivatives. i. 250 °C, 4 h; ii. $Co_2(CO)_8$, 250 °C, 4 h.

It was then intended to perform OAC reactions to capture a series of peri-condensed 13 aromatic ring containing HBCs (**Fig. 51**).

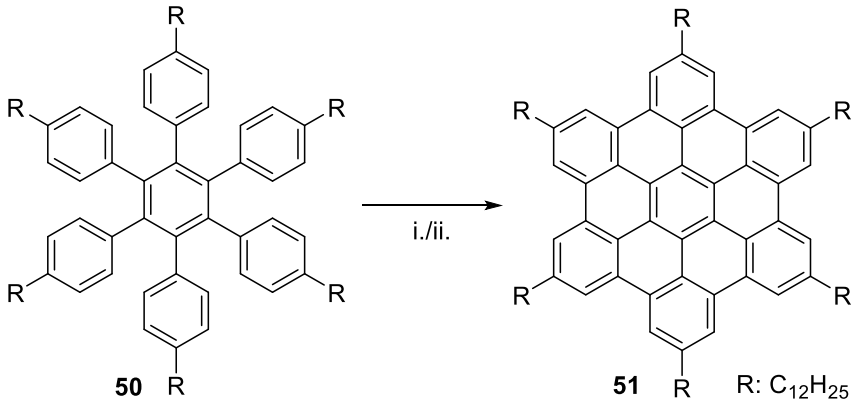

Figure 51. OAC conversion of HPB to HBC. i. $FeCl_3$. $PhNO_2$/DCM; ii. DDQ, TfOH, DCM.

A Sonogashira coupling was performed to generate asymmetric acetylene **52**. Coupling partners 1-hexyl-4-iodobenzene and 1-ethynyl-4-pentylbenzene were selected due to their commercial availability.

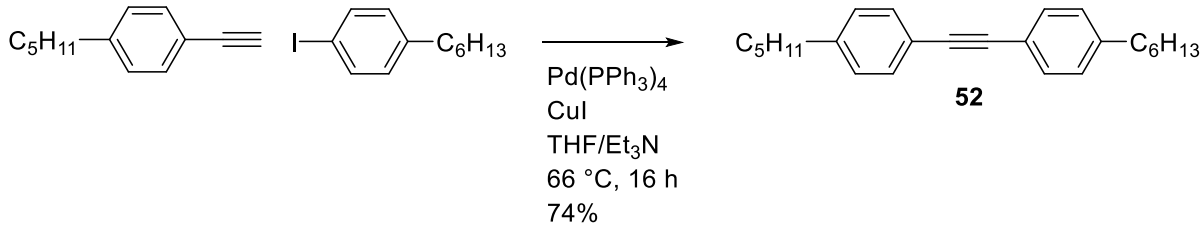

Figure 52. Reaction scheme for Sonogashira coupling to generate **52**.

In order to generate a diphenylacetylene with greater solubilising ability, an alternative synthetic route was undertaken. The ability of dodecyl alkyl groups is reported to afford HBCs with a sufficient degree of solubility in xylene.[177]

Generating a didodecyl derivative of diphenylacetylene requires an alternative synthetic route due to a lack of commercially available starting materials. A *bis*-Kumada-Corriu coupling was attempted upon **55** (**Fig. 53**). After myriad palladium and nickel catalysis conditions were employed affording a poorly defined mixture of products, it was deemed that this particular compound was not a suitable precursor towards functionalised HBCs and would not be pursued further.

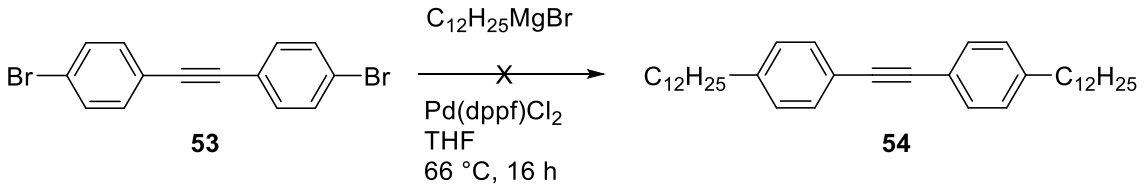

Figure 53. Attemped *bis*-Kumada-Corriu coupling performed upon **53**.

The Friedel-Crafts acylation of bromobenzene **55** and subsequent Wolff-Kishner reduction of the ketone **56** produced 1-bromo-4-dodecyl benzene **57**. A decarboxylative cross-coupling with **57** and acetylene dicarboxylic acid yielded phenylacetylene **54** (**Fig. 54**). Optimisation of the literature protocol in the conversion of **57** to **54** was attempted through use of a microwave reactor.[178] This approach was found to be unsuitable due the two equivalents of CO_2 released per successful *bis*-coupling, resulting in the pressure limits of sealed vessels being reached prior to completion.

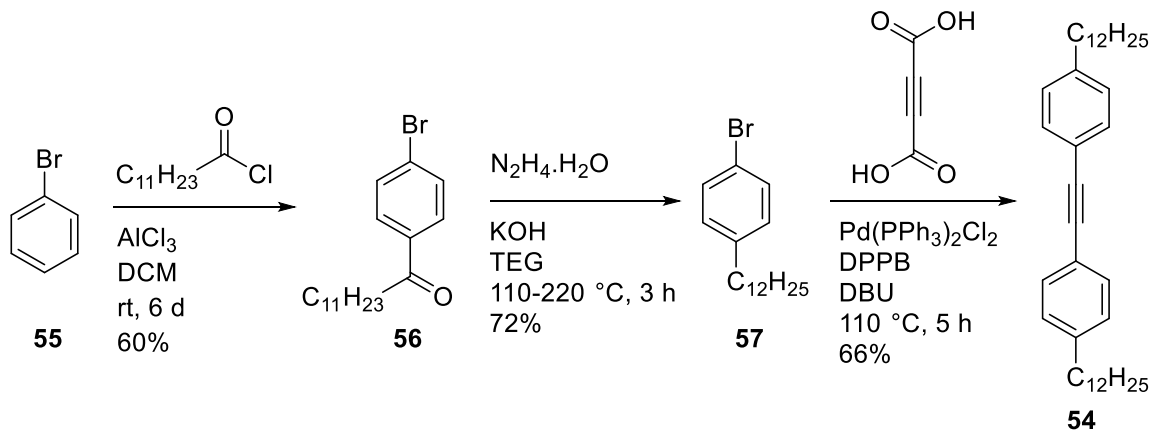

Figure 54. Synthetic route for the generation of diphenylacetylene derivative **54**.

It was found that the Huang Minlon modification of the Wolff-Kishner reduction used in the synthesis of **57** resulted in a significantly higher yield when compared to the original procedure. By establishing the equilibrium of hydrazone/carbanion, then increasing the temperature to 220 °C, excess water and hydrazine are vigorously removed driving the equilibrium towards reduction. Failure to increase the temperature results in the formation of a significant quantity of the hydrazone intermediate and approximately 25% yield of **57**.

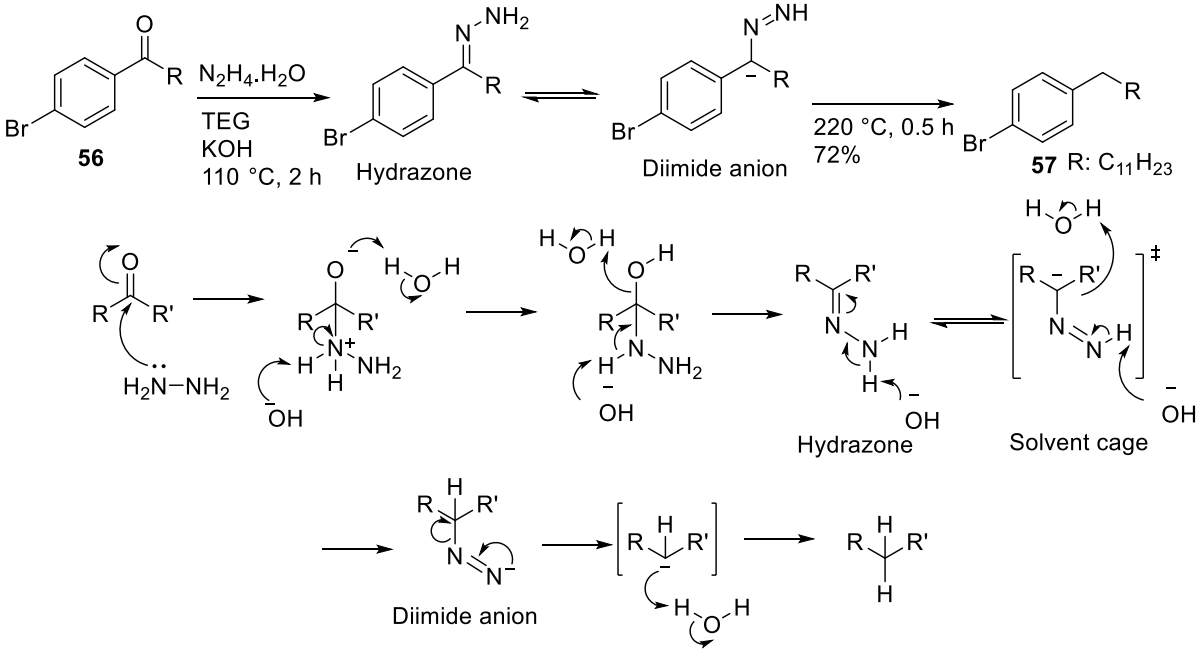

Figure 55. Scheme and Mechanism for Wolff-Kishner reduction of **56** to **57**.

Attempts to reduce this synthesis to a single reaction procedure were run by performing a Kumada-Corriu coupling upon **58** with 1-bromododecane (**Fig. 56**). It was hoped that the

inevitable statistical distribution of unreacted, mono- and di-substituted products of the reaction would be sufficiently different in solubility or polarity for a separation to be possible. High lipophilicity of all products produced rendered this approach ineffective however.

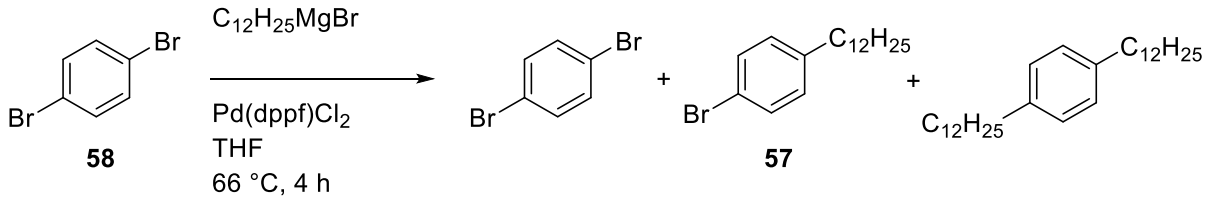

Figure 56. Unsuitable *bis*-Kumada-Corriu coupling for the generation of **57**.

2.3.2. DIELS-ALDER CYCLOADDITIONS

Diel-Alder [4+2] cycloadditions were carried out to generate HPB derivatives **60** and **61**. Some procedures for the development of these materials report significantly lower temperatures than were found to be necessary for the sought products.[149,153,179,180] All derivatives synthesised here require 250 °C for 4 hours to reach completion, comparable with alternative protocols.[181–183] It is consistent with the energetic barrier insertion of molecules possessing such steric bulk that the reaction should require high temperatures in order to proceed.

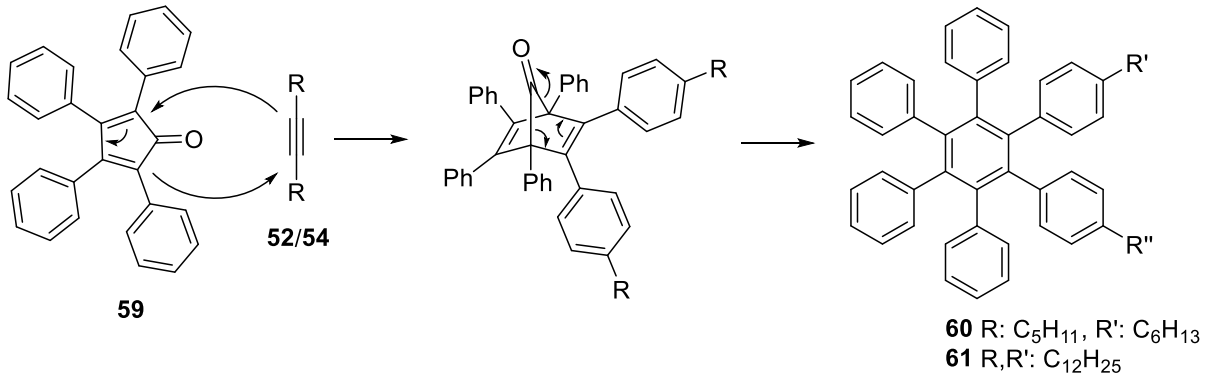

Figure 57. Mechanism for Diels-Alder [4+2]cycloaddition – chelotropic extrusion reaction of 52/54 and 59 leading to HPBs 60 and 61.

Diphenyl ether is often utilised in these reactions. Despite being an effective heat transfer medium, this solvent can significantly complicate the purification of desired products from the reaction. Removal requires trituration from methanol and dichloromethane, yet can require multiple repeats to be effective. Regarding purification, the polarity of this solvent often

coincides with HPB derivatives, resulting in difficulties when purifying *via* column chromatography. For these reasons tetradecane was selected as a superior solvent in this reaction, serviceable in promoting effective heat transfer, thermally stable and removed easily by washing with hexane.

The hexa-functionalised aromatic **50** was generated through a cobalt mediated cotrimerisation reaction. The reaction operates by forming two metal alkyne complexes which combine to afford a metallacyclopentadiene intermediate. The reaction then proceeds in an analogous manner to the formation of **60**/**61**, with insertion of a third alkyne and reductive elimination of cobalt (**Fig. 58**).

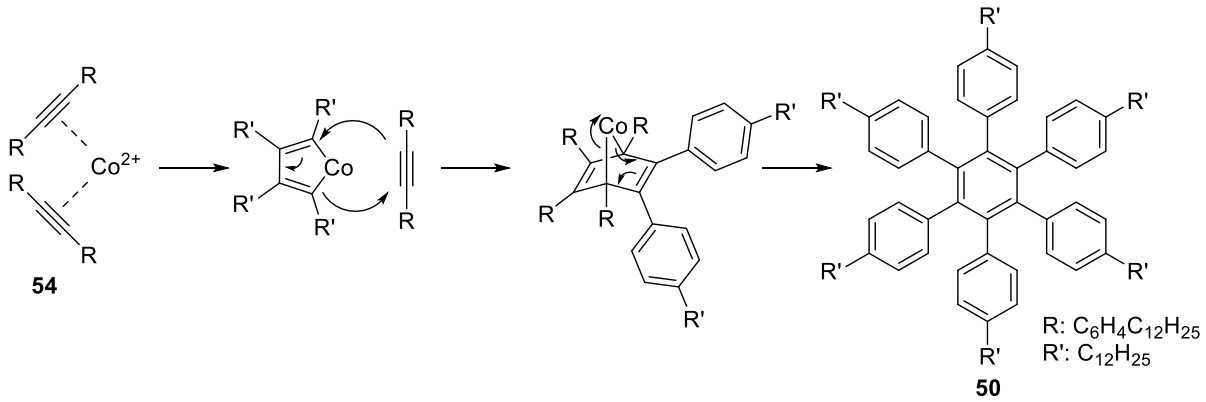

Figure 58. Reaction mechanism for acetylene co-trimeristion to generate **50**.

Further validation of the temperature requirements of these reactions is evident through observation of colour change in this reaction. Formation of the cobalt complexed CPD intermediate is seen at 140 °C through a characteristic deep purple colouration. Upon increasing the temperature to 235-250 °C the solution transitions to colourless as this intermediate is consumed.

2.3.3. OXIDATIVE AROMATIC DEHYDROGENATION OF HPBS

The transformation of HPBs to HBCs was performed utilising either $FeCl_3$ or DDQ, with technical difficulty and product yields varying significantly between the two protocols.

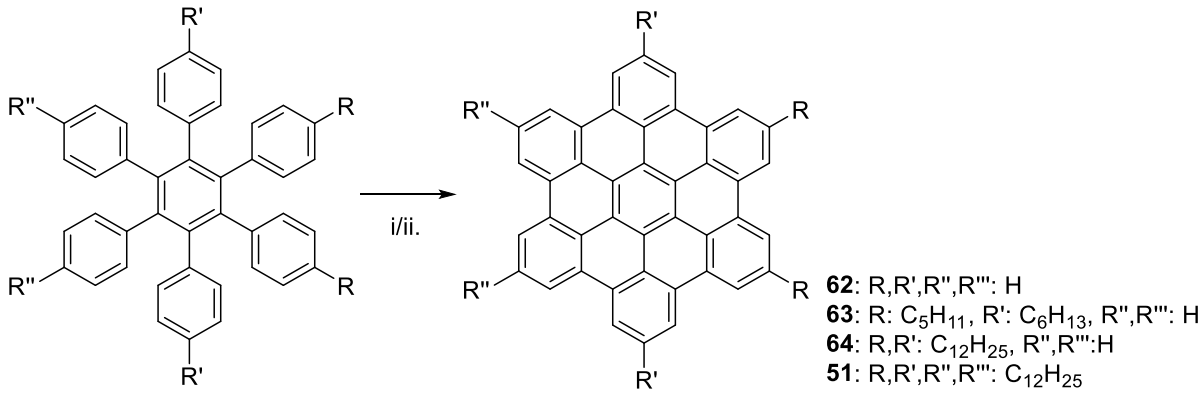

Figure 59. General scheme and products of OAC reactions upon HPB derivatives i. $FeCl_3$, $DCM/PhNO_2$, ii. DDQ, TfOH, DCM.

SUBSTRATE	PRODUCT	OXIDANT	YIELD
HPB	**62**	$FeCl_3$	10
60	**63**	$FeCl_3$	7
61	**64**	$FeCl_3$	11
50	**51**	$FeCl_3$	6
HPB	**62**	DDQ	45
60	**63**	DDQ	39
61	**64**	DDQ	32
50	**51**	DDQ	35

Table 5. Yields from OAC reactions upon HPB derivatives using $FeCl_3$ and DDQ.

Contrary to a variety of literature sources, reactions with $FeCl_3$ consistently yielded less than 15% of desired products.[148,152,184,185] Using DDQ as an oxidant proved to be generally more successful with higher yields and fewer complications in work-up.

The deliquescent oxidising agent $FeCl_3$ generates a number of problems when used in these cyclisation reactions. Often a significant excess of the material is employed in relation to the

substrate. However, the reactivity of $FeCl_3$ is such that when used in excess upon an OAC precursor, multiple oxidations can occur upon the same molecule. Large aromatic compounds are often difficult to purify, with low solubilities and a tendency to chromatograph poorly. This makes significant proportions of unwanted by-products problematic due to an inability to separate them from the desired material.

OACs with $FeCl_3$ require a reductive workup using methanol to quench the reagent through donation of a lone pair into the orbitals of Fe.[184] It was commonplace in these reactions for the aqueous workup to be complicated due to ferric species and methanol stabilising emulsions and preventing phase separation. This resulted in the process requiring a disproportionate quantity of solvents in order to satisfactorily remove inorganic species from the organic phase, inevitably leading to a significant loss of material.

Attempted oxidative cyclisation using DDQ in the presence of triflic acid provides many advantages over $FeCl_3$. DDQ is able to be used in stoichiometric equivalents in OACs reducing the potential for multiple couplings upon a single reactant. This makes the reaction and workup significantly more manageable and is a possible contributor to the increased yields seen consistently among various substrates.

In proton-coupled electron transfer the LUMO of the electrophile is lowered through coordination of the proton to a carbonyl bond, resulting in a lower activation energy (see charge transfer complex **Fig. 15**, **Sect. 1.9.**). It is noteworthy that acids including trifluoroacetic acid (TFA) and methane sulfonic acid are commonly utilised for this reaction, yet only with superacid triflic acid was acceptable conversion achieved in all cases.

The PAHs **62**, **63** and **64** all proved to have solubilities too low for NMR analysis, rendering them unsuitable for solution analysis as asphaltene model compounds. The difficulties in handling HBCs is evident in the limited techniques that can show the presence of these molecules, with the only confirmation available through MALDI-MS. Structural analyses for **62** and **64** are convincing due to a the parent ion displaying 100% signal intensity. **51**, however does possess a sufficient solubility in chloroform and toluene to acquire an acceptable ^1H NMR, confirming structural constitution and giving the molecule suitable solution properties to allow its use as an asphaltene model.

2.4. SYNTHESIS OF ALKYLATED TRIBENZOPENTAPHENES

Insertion of alkynes in place of a diphenylalkyne and subsequent aromatic oxidation of tetraphenylbenzene (TPB) derivatives was expected to afford a series of 8-ring peri-condensed functionalised tribenzopentaphenes (TBPs). Undecynoic acid was first inserted into **59** was performed in an analogous reaction to the generation of HPB derivatives (**Fig. 60**). Products from the transformation of **65** to **66** were found to possess a solubility too low for satisfactory purification however.

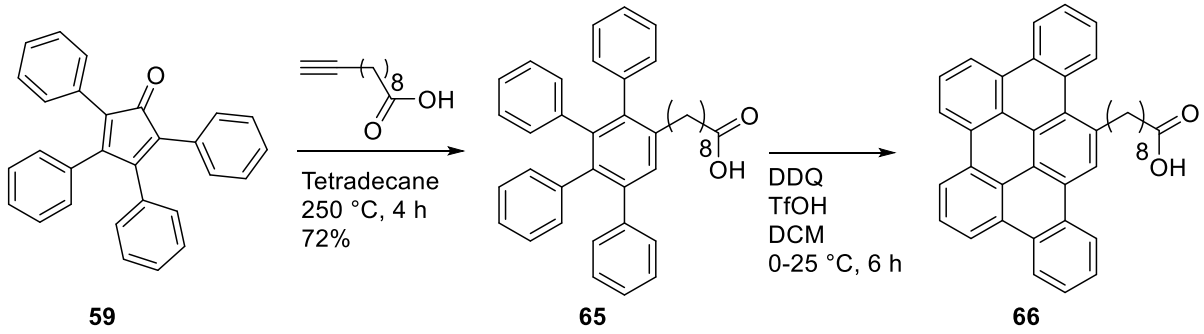

Figure 60. Reaction scheme for the synthesis of TBP **66**.

Initial attempts to increase the solubility of the **59** aimed to Kumada-Corriu cross-coupling upon **70** to install alkyl groups. Ketonic decarboxylation upon **67** afforded **68**, which was converted to **69** *via* a double aldol reaction. Diels-Alder cycloaddition afforded **70**. This synthetic route was not found to be viable due to the incompatibility of **70** as a coupling partner. **70** Was consumed in these attempted reactions, however the products generally proved to be diverse and indistinguishable.

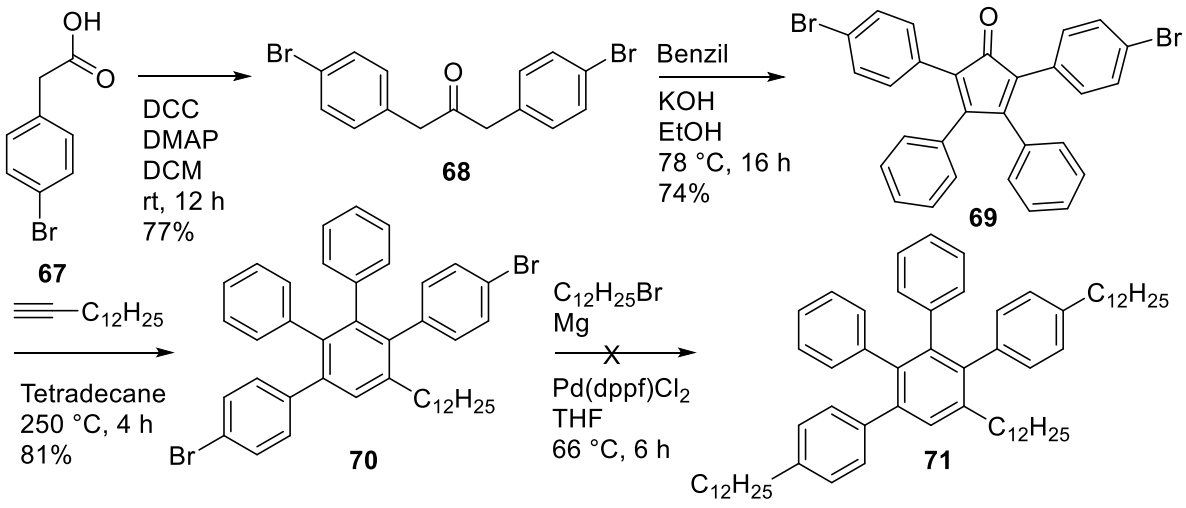

Figure 61. Unsuccessful synthetic route to alkylated TPB derivatives.

Alkyl functionality was instead built into **59** through carbonyl protection of **68** using acid-catalysed acetylisation, followed by *bis*-Kumada-Corriu coupling upon **72** to acquire **73**. The acetal protecting group was then removed utilising acid-catalysed hydrolysis to afford **74**. A further aldol reaction was then performed with benzil resulting in the desired diene **75**.

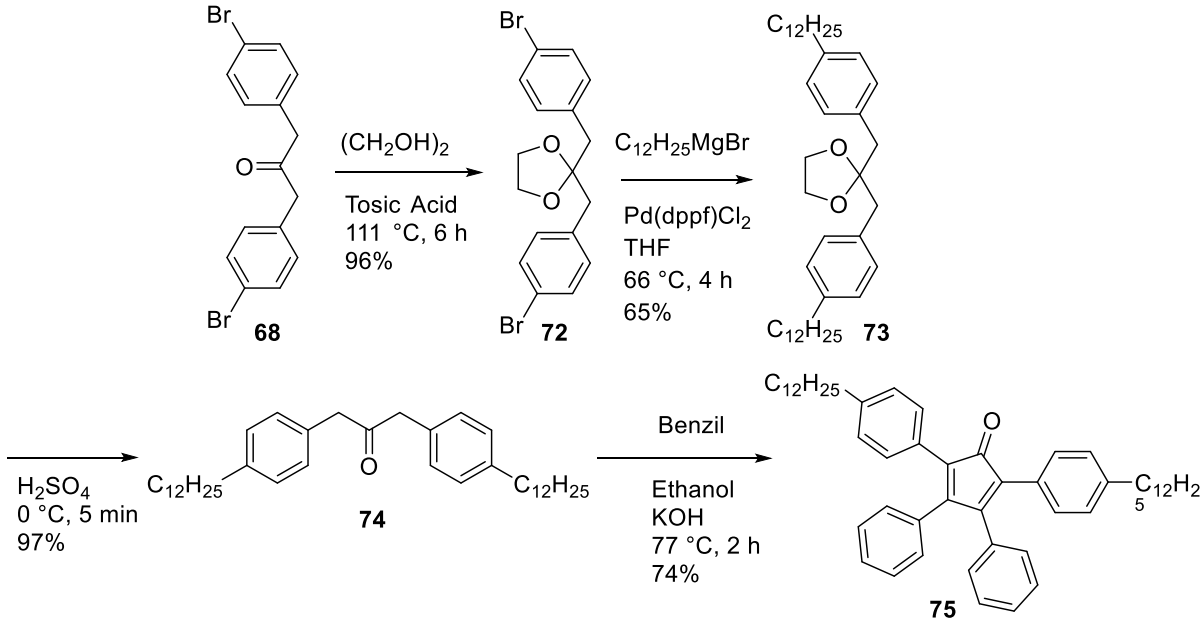

Figure 62. Synthetic route to **75**.

A series of alkynes were reacted with **75** in order to generate representative functionalities: these Diels-Alder reactions proceeded with varying levels of success (**Fig. 63**). Undec-10-ynoic acid and tetradec-1-yne performed as expected to afford HPB derivatives **71** and **76**.

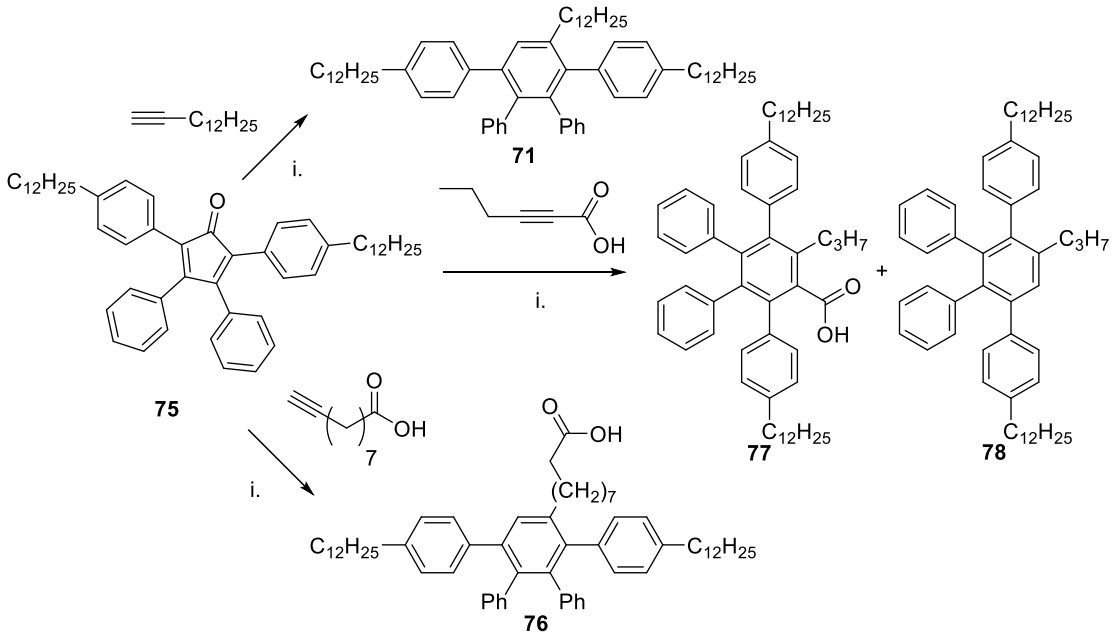

Figure 63. Products of Diels-Alder cycloaddition upon **75**. i. tetradecane, 250 °C, 4 h.

The Diels-Alder cycloaddition of **75** with hex-2-ynoic acid however resulted in the formation of **77** and **78** in a 35:65 ratio. In order to probe the mechanism for the formation of this derivative, carboxylic acid **77** was heated to 250 °C which resulted in its decarboxylation to **78**.

DDQ and triflic acid mediated oxidation to the fully condensed aromatic analogues of tetraphenyl benzyl derivatives proved largely unsuccessful. **71**, **77** and **78** produced intractable mixtures of oxidised aromatics that were not suitable for purpose as asphaltene model compounds given the requirements for a high level of purity. These compounds chromatographed poorly, precluding purification by HPLC and RP-HPLC. Solubility based purifications including trituration, recrystallisation and Soxhlet washing with various solvents also failed. Attempted purification by sublimation at 400 °C and under a high vacuum (5.2×10^{-7} Torr) was also found to be unsuccessful presumable due to its high molecular weight of 869 $gmol^{-1}$.

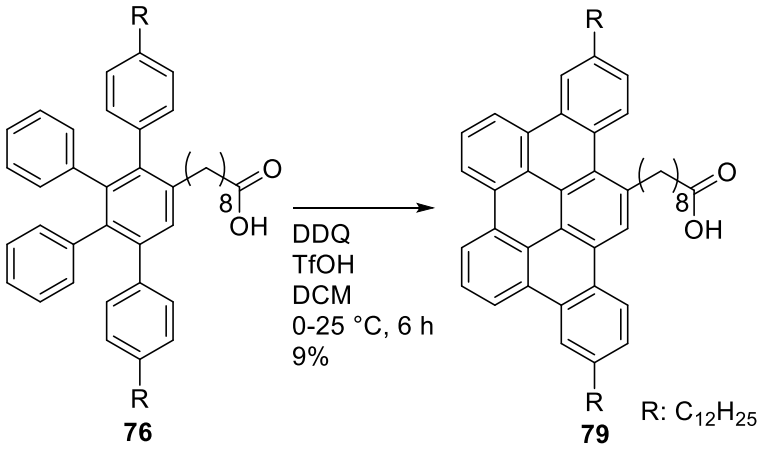

Figure 64. Successful OAC oxidation of **76** to **79**.

Carboxylic acid **79** was successfully purified, albeit in a 9% yield, upon successive recrystallisations with methanol (**Fig. 64**).

2.5. SYNTHESIS OF GEOLOGICALLY-INSPIRED ASPHALTENE 'ISLAND' MODEL

A synthetic target requested by industrial partners was based upon using compounds closely resembling those present in the natural system. Polyaromatic compounds representing products of catagenisis were to be fused with steroid derivatives, such as found in plant matter. In order to acquire such a molecule, pre-functionalisation of both the aromatic and aliphatic components is necessary in order to set up a viable coupling route. Once achieved, the steroidal system was intended to be oxidised in order to establish a single condensed aromatic system.

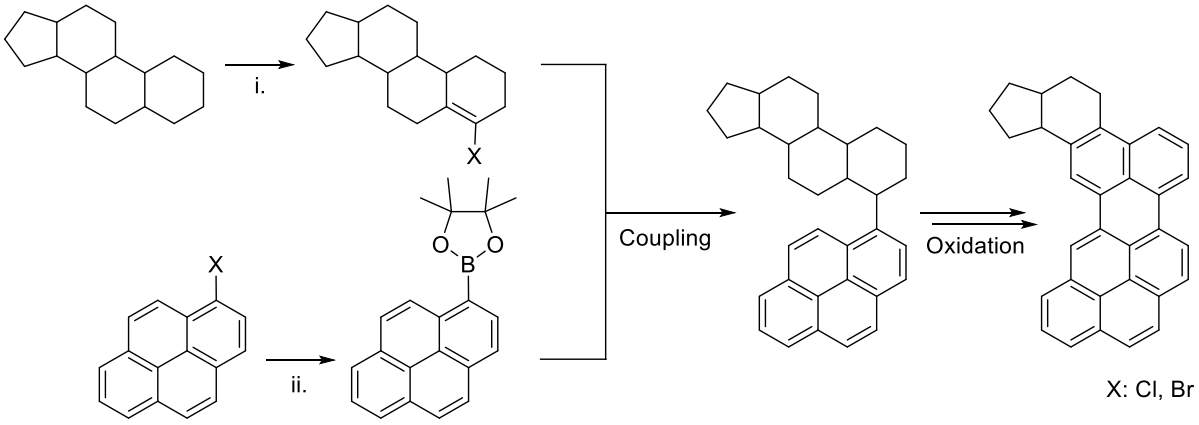

Figure 65. General scheme for the formation of an aromatic steroidal derivative.

2.5.1. PREPARATION OF 4-BROMOCHOLESTENONE

Cholesterol **80** was chosen as a suitable starting material as its oxidation to 4-bromo-4-cholesten-3-one **83** is well established.[186]

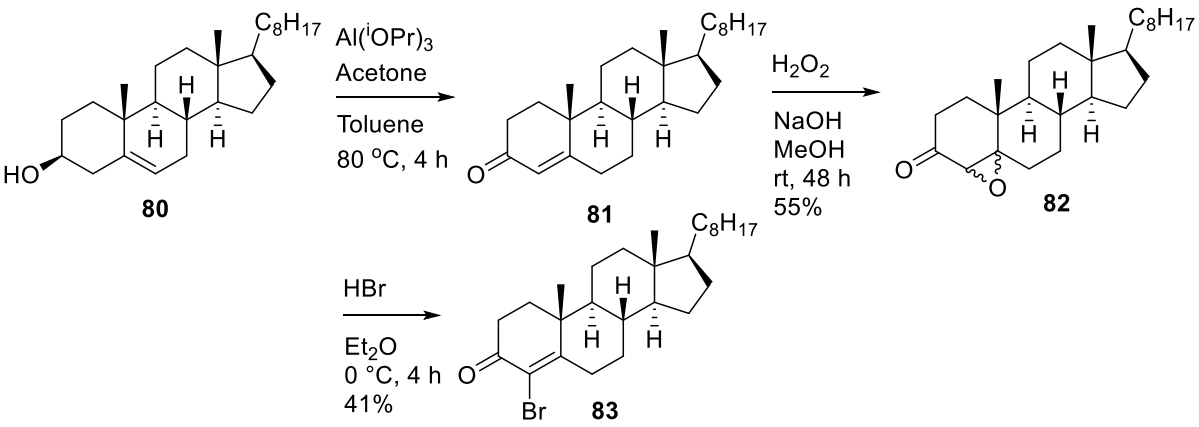

Figure 66. Reaction scheme for the synthesis of **83**.

Oppenauer oxidation of **80** afforded the corresponding α,β-unsaturated ketone **81**. This oxidation was driven in a forward direction due to the presence of excess acetone.[187]

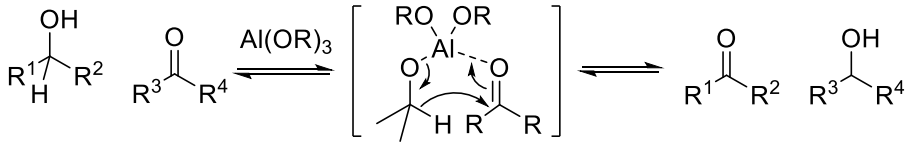

Figure 67. Mechanism for Oppenauer oxidation.

The Julià-Colonna epoxidation of **81** uses basic hydrogen peroxide to form a peroxide-enolate intermediate followed by the release of sodium hydroxide to afford epoxides **82a/b**.[188]

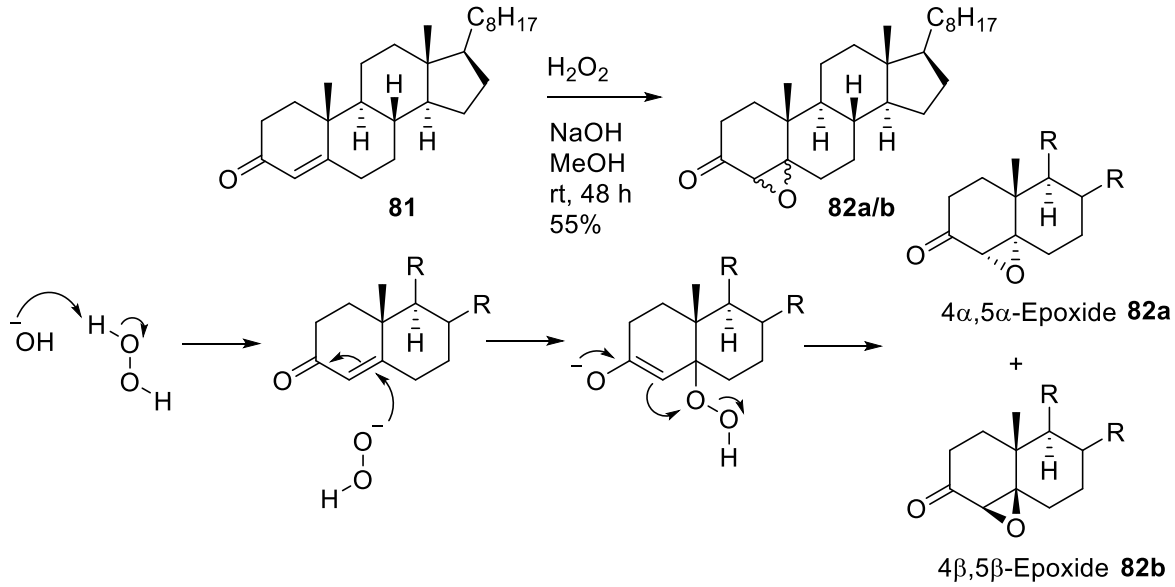

Figure 68. Reaction scheme and mechanism for the epoxidation of **81**.

The reaction sees **82b** form as the major isomer. It is plausible that this is due to a stereoelectronic preference for the enone to undergo axial attack by a peroxide anion during the initial reaction step, as steric factors inhibit equatorial approach of the anion.[189]

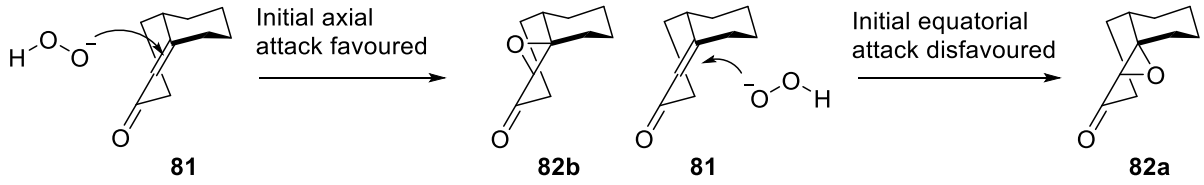

Figure 69. Plausible stereoelectronic explanation for disproportionate epoxide formation.

82b was then reacted with hydrogen bromide to form **83**. The reaction proceeds *via* diaxial opening of the epoxide followed by spontaneous dehydration of the intermediate β-hydroxyketone to form **83**, with no alternative bromination products seen.[190]

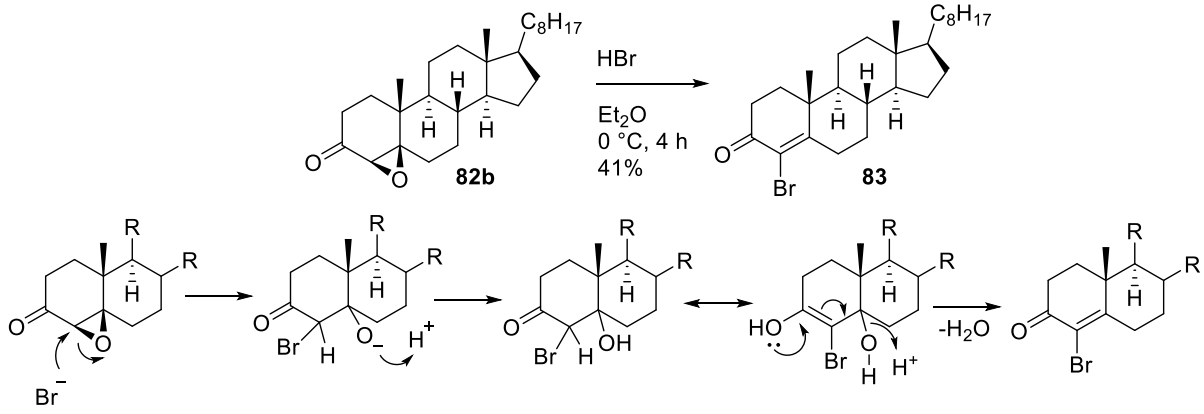

Figure 70. Reaction scheme of **82b** with HBr to yield **83**.

2.5.2. PREPARATION OF PYRENYE-1-YL BORONIC ACID

1-Bromopyrene was chosen as the coupling partner for Miyaura borylation due to its bromide functionality being situated ideally for post-coupling oxidation to potentially form a planar model molecule with a single condensed aromatic core unit (**Fig. 65**). Use of $Pd(PPh_3)_4$ to generate **84** in a Miyaura borylation required long reaction times and displayed poor conversion. Significantly higher yields were obtained with $Pd(dppf)Cl_2$.

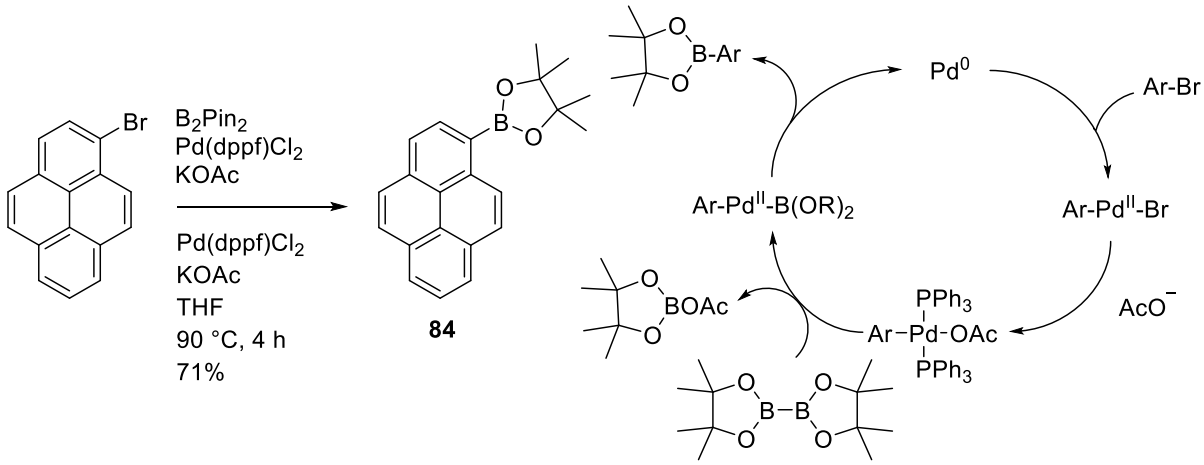

Figure 71. Reaction scheme and catalytic cycle to acquire **84**.[191]

The coupling reaction forms 1,1'-bipyrene **85** as a major by-product due to a competing Suzuki-Miyaura coupling between starting material and **84**.

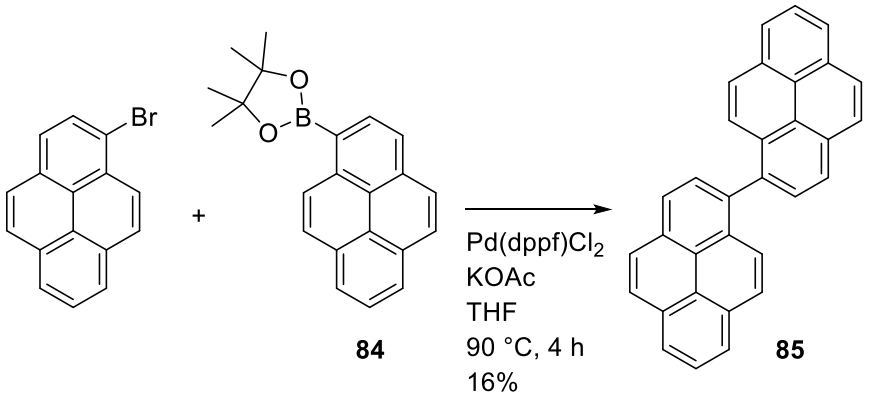

Figure 72. Competing Suzuki-Miyaura coupling produced **85** as a major by-product.

2.5.3. COUPLING OF STEROID TO PAH

An attempted Suzuki-Miyaura coupling of **84** with **83**, under standard conditions, afforded an intractable mixture of products.

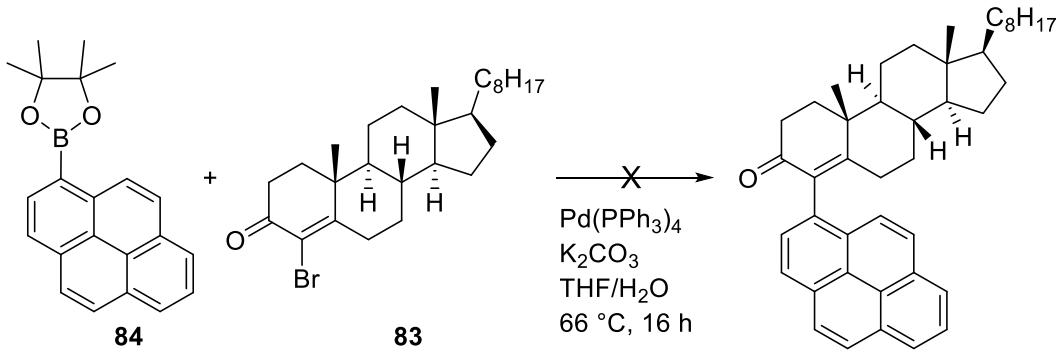

Figure 73. Unsuccessful coupling of **84** with **83**.

It is plausible that the vinylbromide functionality was rendered unreactive as a consequence of being positioned α- to carbonyl functionality. In order to capture a suitable asphaltene model compound of this design, various catalytic conditions need to be tested and evaluated. However, this may be fruitful in the future to provide an intriguing asphaltene model.

3. CONCLUSIONS AND FURTHER WORK

3.1. CONCLUSIONS

Classical nucleophilic aromatic substitution (S_NAR) reactions were employed in the preparation of a family of sulphurous 'archipelago' model compounds. A second generation synthesis of these molecules involved initial S_NAR of 1-bromopyrene with methanethiolate, followed by demethylation to afford pyrene-1-thiol **36** in high yield. Alkylation of this thiol with a variety of alkyl halides proceeded much more smoothly, and produced products devoid of impurities, compared to those obtained by the direct substitution of bromopyrene with thiols. Encouraging insights into the deposition mechanism of these derivatives have been demonstrated through preliminary AFM and adsorption isotherm experiments. A sulfur-free version of these derivatives was synthesised through the use organolithium precursors allowing for the impact of sulfur functionality to be evaluated.

The nitration of perylene was optimised and provided the versatile feedstock intermediate **27** which proved useful in the production of scaffolds containing pyridine **31**, thiophene **29** and carbazole **49** motifs. These structures are believed to be representative of those found in asphaltenes isolated from natural sources and provides material for further evaluation by other experimentalists associated with the BP ICAM 15 program. HPB derivatives (**50**, **60** and **61**) were generated through two synthetic pathways to arrive at hexabenzocoronene derivatives **51**, **63** and **64**. This procedure was adapted and key intermediate **75** synthesised used in the generation of a TBP aromatic core with appropriate functionality to serve as a suitable acidic asphaltene model compound **79**. The synthesis of a geologically inspired asphaltene model was attempted through coupling of **83** with **84**, however the system requires refining in order to achieve successful cross-coupling.

'Island' and 'archipelago' model compounds generated throughout this program are plotted alongside those previously synthesised and simulated in the literature (**Sect. 1.7.**) in terms of DBE (**Sect. 1.5.3**) and molecular weight generally showing a satisfactory fit within the structural parameters of the asphaltenes (**Fig. 74** and **75**).

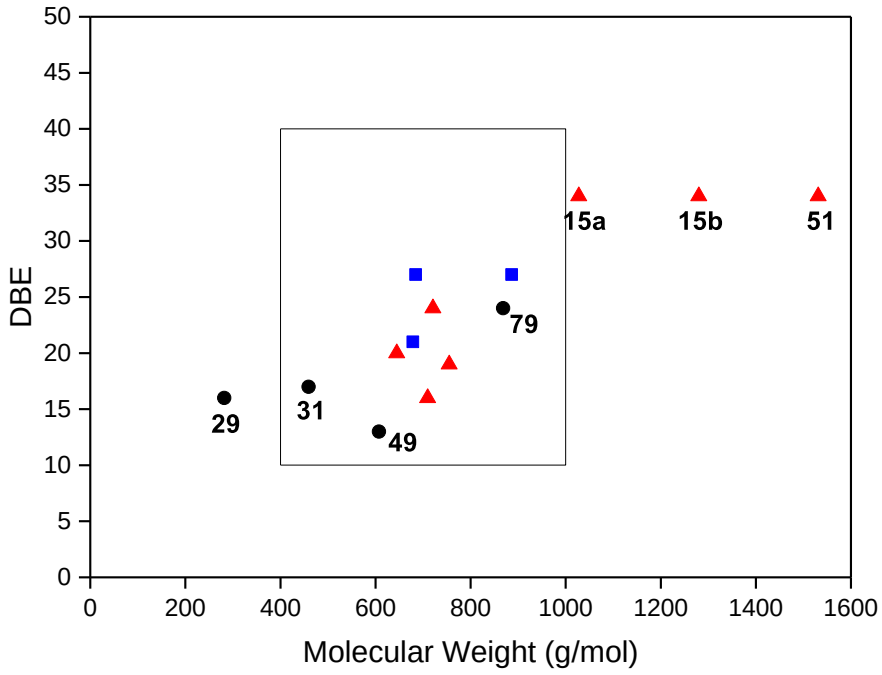

Figure 74. 'Island' molecules DBE plotted against molecular weight for models synthesised in this project (black circles), literature asphaltene models (red triangles) and simulated asphaltene models (blue squares).

Simulated model compounds (blue triangles), with no restriction on the synthetic feasibility or solubility properties occupy optimal locations on these maps. 'Island' molecules **51** and **31** possess 4 and 6 FARs respectively and occupy the lighter region of asphaltene chemical space. TBP **79** appears as a more suitable candidate molecule to analogous hexa-alkylated HBC model compounds **51** and **15a/b**. It is proposed that the molecules synthesised here will serve as superior asphaltene model compounds in comparison to literature examples (red triangles) due to the possession of specific and relevant functionalities alongside appropriate solubilities for deposition analysis from relevant solvents toluene and heptane. The atypically high solubility of **29** in toluene, contrary to other perylene derivatives, made alkyl functionalisation redundant and places this candidate as an outlier. However, **29** is still expected to perform adequately in future chemisorption studies of aromatic sulphur functionality upon relevant substrates.

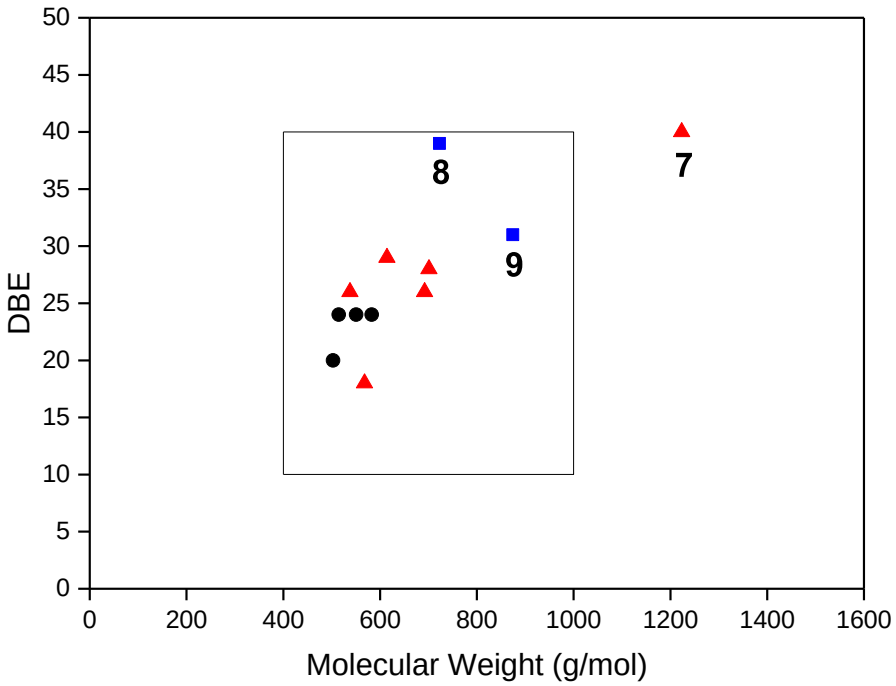

Figure 75. 'Archipelago' molecules DBE plotted against molecular weight for models synthesised in this project (black circles), literature asphaltene models (red triangles) and simulated asphaltene models (blue squares).

Archiepelago models synthesised in this project (black circles, **Fig. 78**) are chemically similar and occupy a condensed region of the plot within the average asphaltene region. Literature archipelago model compounds (red triangles) display an appropriate distribution and solubility properties. It is intended that models synthesised in this program will add to body of research produced by these materials and inform the discussion on the impact of alkyl sulphur in these types of asphaltene model motif.

3.2. FURTHER WORK

The compounds described within this thesis are expected to reveal insights into the mechanism of asphaltene deposition through the experimental methods described in ICAM 15 WPs.

AFM analysis is currently being undertaken to evaluate the affinity of synthesised model compounds for various surfaces through interpretation of morphology and adhesion force calculations. QCM analysis and adsorption isotherms is expected to provide complementary data in describing the mass adsorption of models upon the substrates under investigation. These data streams will inform computational simulations of asphaltenic molecules upon relevant surfaces and assist in the design of new experiments seeking to analyse other depositing organics of commercial interest.

Preliminary results observing the direct relationship of substrate upon deposit growth (**Sect. 2.1.5.**) provide an encouraging outlook towards reducing aromatic deposits. Further studies depositing the other model compounds and real asphaltenes under these experimental conditions are required to identify if certain morphologies or structural types conform to these principles. A suitable substrate identified by these methods would be of interest regarding the commercialisation of unconventional crude oils.

4. EXPERIMENTAL PROCEDURES

4.1. GENERAL REMARKS

All reactants and reagents were purchased from Sigma Aldrich, Fisher Scientific, Acros Organics, Apollo Scientific or Fluorochem and assayed by ^{1}H NMR and purified where necessary. THF was distilled from sodium benzophenone ketyl or purchased directly from Sigma Aldrich. Diethyl ether was dried over sodium wire. Acetone, DCM, chloroform and ethanol were dried over activated 4 Å molecular sieves. All other anhydrous solvents and reagents were purchased as such and used without purification. Petroleum ether, bp range 40-60 °C was used as supplied. Reactions that were conducted out under microwave irradiation were performed using a Biotage Initiator focused microwave reactor (400 W operating at 2.45 GHz). TLC was carried out using DC-Fertigfolie POLYGRAM® SIL G/UV_{254} precoated TLC sheets with substrate detection by UV light (254 and 365 nm). All reaction glassware was heated under vacuum prior to use unless otherwise noted.

All NMR spectra were recorded with using a Bruker Avance III 400, Bruker Avance III HD 400 (equipped with a broadband "prodigy" N_2 coldprobe), Bruker Avance II+ 500, Bruker Avance 500 DRX or Bruker Avance III HD 500 (equipped with a broadband "prodigy" N_2 coldprobe) spectrometer. ^{1}H and ^{13}C NMR spectra were referenced to the residual solvent peak as appropriate: $CDCl_3$ (7.27 or 77.00 ppm respectively), DMSO-d_6 (2.50 or 39.51 ppm respectively), benzene-d_6 (7.16 or 128.39 ppm). Chemical shifts (∂) are quoted in parts per million downfield from tetramethylsilane (0.00 ppm). Signal splitting patterns are described as singlet (s), doublet (d), triplet (t), quartet (q), multiplet (m) or any combination of the above. Coupling constants (J) are given in Hz.

MALDI mass spectra were recorded with a Shimadzu Biotech Axima Confidence spectrometer using a dithranol, or TCNQ matrix as stated. Atmospheric pressure chemical ionisation (APCI) mass spectra were recorded on a Micromass Platform II, Waters SQD2 Aquity System or Thermo Exactive Plus EMR Orbitrap spectrometer. Electrospray ionization (ESI) mass spectra were recorded on a Waters SQD2 Aquity System spectrometer. Gas chromatography (GC) mass spectra were recorded on a Perkin Elmer Auto System XL Arnel with a Perkin Elmer TurboMass Spectrometer or Agilent 5975C Triple Axis GC/MS spectrometer. Electron ionization (EI) high resolution mass spectra were recorded on a Thermo Finnigan MAT95XP

spectrometer. High resolution ESI, heated electrospray ionization (HESI), APCI and atmospheric pressure photoionization (APPI) mass spectra were recorded on a Thermo Exactive Plus EMR Orbitrap spectrometer. Atmospheric solids analysis probe (ASAP) high resolution mass spectra were recorded on a Thermofisher LTQ Orbitrap XL spectrometer. Infrared spectra were obtained using a Thermo Scientific Nicolet iS5 spectrometer with an iDS ATR accessory.

Melting points were recorded on a Stuart SMP10 melting point apparatus or Gallenkamp Griffen melting point apparatus with a thermocouple attached to an Extech 380224 multimeter. Gradient sublimation was performed using apparatus constructed by the Manchester Chemistry Department mechanical and electrical workshops. The gradient sublimation heating coil is controlled by a thermostat and a temperature gradient is maintained along a pathlength of 40 cm by air cooling over the cold zone. Vacuum was maintained by an Edwards TIC Pumping Station turbopump (pressure normally 1×10^{-7} to 1×10^{-6} mbar).

4.2. SYNTHETIC PROCEDURES

4.2.1. ARCHIPELAGO COMPOUNDS

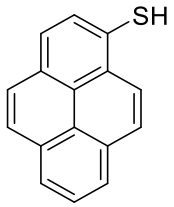

Pyrene-1-thiol (**36**)

Prepared by an adaptation of a literature synthesis.[192]

1-Bromopyrene (2.0 g, 7.2 mol) and sodium methanethiolate (1.5 g, 22 mmol) were dissolved in 80 mL of dry DMF under nitrogen. The reaction mixture was stirred at 150 °C overnight, then added to 150 mL of 0.5M HCl and extracted with ether (3x100 mL). The combined organic extracts were washed (2 x 50 mL 0.5M HCl, then brine 50 mL), dried ($MgSO_4$), and concentrated *in vacuo* to afford the *title compound* as a yellow coloured solid (1.69 g, 100%). This material was found to be of sufficient purity for further use.

MP 87-89 °C (Lit.[193] 86-89 °C). **^{1}H NMR** (400 MHz, Chloroform-*d*) ∂ 8.38 (d, *J* = 9.3 Hz, 1H), 8.23 (m, 3H), 8.06-7.99 (m, 5H), 3.87 (s, 1H). **^{13}C NMR** (101 MHz, Chloroform-*d*) ∂ 131.4, 130.9, 129.7, 129.4, 129.1, 127.9, 127.3, 127.0, 126.3, 125.6, 125.3, 125.2, 125.1, 124.9, 124.4, 124.2. **IR** $\tilde{\nu}_{max}/cm^{-1}$ 3039 (Ar C-H), 2545 (S-H), 1591 (Ar C=C). **MS** (GCMS) m/z 234.0 ($[M]^+$, 100%). **HR** *m/z* (ASAP$^+$) $C_{16}H_{10}$ + H calcd for 235.0676, found 235.0575.

General Procedure A: S_NAr of Alkyldithiol and Bromoaromatic

1-Bromopyrene or 9-bromophenanthrene (2.1 eq.), potassium carbonate (5 eq.) and dimethylformamide were added to a schlenk tube and the solution sparged with argon. Alkyldithiol (1 eq.) was then added and he solution heated to 140 ^oC for 16 h. The crude reaction mixture was then diluted with toluene and the organic layer washed with water and brine, then dried. The crude product was then recrystallised from heptane and toluene to afford the desired *bis*-arylsulfide in yields ranging from 12-46%.

General Procedure B: S_N2 Displacement of Dibromoalkyl using Aromatic thiol. Pyrene-1-thiol (2.1 mmol) was dissolved in DMF and potassium carbonate (10.0 mmol) added. 1,6-Dibromohexane (1.0 mmol) was then added dropwise and the mixture stirred for 5 min. The crude reaction mixture was then diluted with toluene and the organic layer washed with water and brine, then dried over magnesium sulfate. The crude product was then recrystallised from heptane and toluene to afford the desired *bis*-arylsulfide in yields ranging from 85-91%.

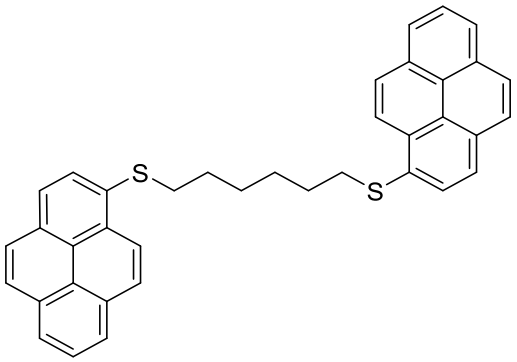

1,6-*Bis*-(pyren-1-ylthio)hexane (**32**)

Procedure A: Synthesised from 1-bromopyrene (500 mg, 1.78 mmol) and 1,6-hexanedithiol (127.4 mg, 0.847 mmol) affording an amorphous yellow coloured solid (333 mg, 34%).

Procedure B: Synthesised from pyrenyl-1-thiol (400 mg, 1.70 mmol) and 1,6-dibromohexane (124 μL, 0.81 mmol) affording the *title compound* as fine yellow coloured needles (405 mg, 91% yield).

MP 127-128 °C. **^{1}H NMR** (400 MHz, Chloroform-*d*) ∂ 8.67 (d, *J* = 9.3 Hz, 1H), 8.19 (dd, *J* = 7.3 Hz, 4H), 8.12 (d, *J* = 9.3 Hz, 2H), 8.08 (s, 4H), 8.08-7.99 (m, 6H), 3.07 (t, *J* = 7.0 Hz, C$\underline{H}_2$-Ar, 4H), 1.68-1.62 (m, C$\underline{H}_2$-CH_2-Ar, 4H), 1.50-1.42 (m, C$\underline{H}_2$-CH_2-CH_2-Ar, 4H). **^{13}C NMR** (101 MHz, Chloroform-*d*) ∂ 131.4, 130.93, 129.7, 129.4, 129.1, 127.9, 127.3, 127.0, 126.3,

125.6, 125.3, 125.2, 125.1, 124.9, 124.4, 124.2. N.B. 14 Aromatic carbons detected rather than 16, this is assumed to be due to overlap. **IR** $\tilde{\nu}_{max}/cm^{-1}$ 3049 and 2926 (Ar C-H), 1591 and 1481 (Ar C=C), 676 (C-S). **MS (**MALDI-Dithranol) m/z 550.2 ($[M]^+$, 100%). **HR** *m/z* (APCI$^+$) $C_{38}H_{40}$ + H calcd for 551.1862, found 551.1866. Structure determination confirmed by X-ray crystallography.

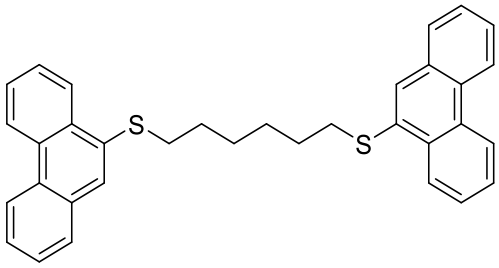

1,6-*Bis*-(phenanthren-9-ylthio)hexane (**34**)

Procedure A: Synthesised from 9-bromophenanthrene (500 mg, 1.95 mmol) and 1,6-hexanedithiol (142.2 μL, 0.93 mmol) to afford the *title compound* as a colourless, amorphous solid (215 mg, 46%).

MP 94-96 °C. **^{1}H NMR** (500 MHz, Chloroform-*d*) ∂ 8.71 (d, *J* = 7.5 Hz, 2H), 8.65 (d, *J* = 8.3 Hz, 2H), 8.49 (d, *J* = 7.5 Hz, 2H), 7.81 (d, *J* = 8.0 Hz, 2H), 7.69 (s, 2H), 7.73-7.53 (m, 8H), 3.06 (t, *J* = 7.3 Hz, C$\underline{H}_2$-Ar, 4H), 1.74-1.68 (m, C$\underline{H}_2$-CH_2-Ar, 4H), 1.27-1.24 (m, C$\underline{H}_2$-CH_2-CH_2-Ar, 4H). **^{13}C NMR** (101 MHz, Chloroform-*d*) 132.6, 131.8, 131.3, 130.6, 129.4, 127.9, 127.6, 127.0, 126.9, 126.9, 126.4, 125.6, 123.0, 122.6, 35.5, 28.8, 28.4. **IR** $\tilde{\nu}_{max}/cm^{-1}$ 3005 and 2824 (Ar C-H), 698 (C-S). **MS (**MALDI-Dithranol) m/z 502.4 ($[M]^+$, 100%). **HR** *m/z* (HESI)$^+$ $C_{34}H_{30}S_2$ calcd for 502.1783, found 502.1773.

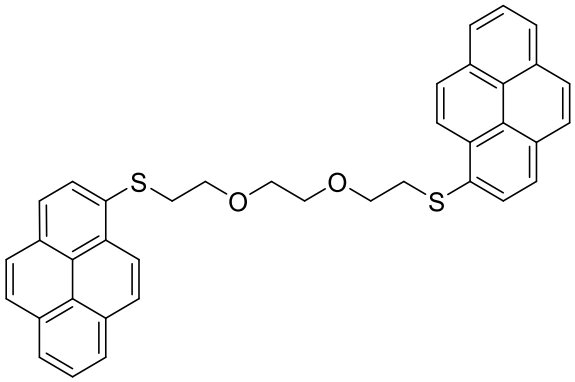

1,2-*Bis*-(2-(pyren-1-ylthio)ethoxy)ethane (**33**)

Procedure A: Synthesised from 1-bromopyrene (1.0 g, 3.56 mmol) and 3,6-dioxa-1,8-octanedithiol (0.193 mL, 1.19 mmol) to afford the *title compound* as an amorphous colourless solid (0.41 g, 20%).

MP 113-115 °C. **^{1}H NMR** (400 MHz, Benzene-d^6) ∂ 8.88 (d, J = 9.3 Hz, 2H) , 8.02 (d, J = 8.0 Hz, 2H), 7.87-7.83 (m, 6H), 7.75 (d, J = 9.0 Hz, 4H), 7.70 (m, 4H), 3.42 (t, J = 7.3 Hz, 4H), 3.42 (s, O-C$\underline{H}_2$-C$\underline{H}_2$-O, 4H), 3.03 (t, J = 7.3 Hz, 4H) ppm. **^{13}C NMR** (101 MHz, Benzene-d^6) ∂ 131.8, 131.4, 131.2, 130.9, 130.6, 129.8, 127.2, 126.0, 125.4, 125.3, 125.2, 124.9, 124.8, 124.8, 35.6, 33.4, 25.8. N.B. 14 Aromatic carbons detected rather than 16, this is assumed to be due to overlap. **IR** $\tilde{\nu}_{max}$/cm^{-1} 3085 and 2901 (Ar C-H), 1303 (Ar C=C), 1046 (C-O), 598 (C-S). **MS (**MALDI-Dithranol) m/z 582.6 ([M]$^+$, 70%).

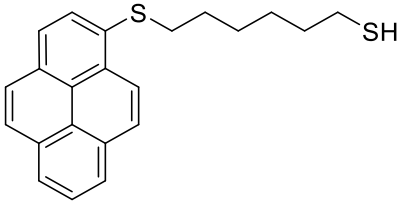

6-(Pyren-1-ylthio)hexane-1-thiol (**35**)

Modified Procedure A: Synthesised from 1-bromopyrene (500 mg, 1.78 mmol) and 1,6-hexanedithiol (2.72 mL, 17.8 mmol) dissolved in DMF (25 mL) and heated to reflux for 16 h. The crude material was purified by column chromatography on silica gel (10% toluene/hexanes) to afford the *title compound* as yellow coloured needles (193 mg, 31%).

MP 82-83 °C. **^{1}H NMR** (400 MHz, Benzene-d_6) ∂ 8.95 (d, *J* = 9.3 Hz, 1H), 8.06 (d, *J* = 8.1 Hz, 1H), 7.95 (d. *J* = 9.3 Hz, 1H), 7.91 (d, *J* = 7.7 Hz, 2H), 7.86 (d, *J* = 8.1 Hz, 1H), 7.79 (d, *J* = 9.2 Hz, 1H), 7.77 (d, *J* = 9.2 Hz, 1H), 7.73 (t, *J* = 7.2 Hz, 1H), 2.82 (t, *J* = 7.6 Hz, C$\underline{H}_2$-S-Ar, 2H), 2.06 (q, *J* = 7.5 Hz, C$\underline{H}_2$-SH, 2H), 1.50–0.86 (m, 8H). **^{13}C NMR** (101 MHz, Benzene-d^6) ∂ 132.1, 131.9, 131.5, 131.3, 130.5, 129.1, 128.2, 127.8, 127.7, 126.7, 125.7, 125.7, 125.6, 125.4, 125.0, 124.9, 35.5, 34.4, 29.7, 28.7, 28.4, 24.9. **MS (**MALDI-TCNQ) m/z 351.8 ([M]$^+$, 50%). Structure determination confirmed by X-ray crystallography.

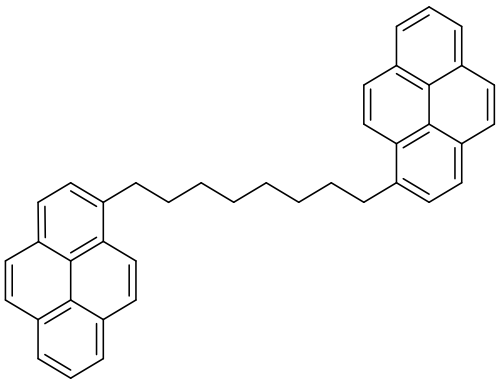

1,8-Di(pyren-1-yl)octane (**38**)

Anhydrous THF (250 mL)was added to a flame-dried reaction vessel charged with 1-bromopyrene (3.0 g, 10.67 mmol) and the resulting solution cooled to -78 °C under an atmosphere of nitrogen. *tert*-Butyl lithium solution (12.5 mL of a 1.7 M solution in hexanes; 21.4 mmol) was then added, dropwise, over a period of 0.5 h and the mixture stirred for a further 0.5 h at this temperature. 1,8-Dibromooctane (1.31 g, 4.80 mmol) was then added dropwise and the reaction temperature maintained at for 1 h before being allowed to reach room temperature and stirred overnight. The reaction was then quenched by the addition of ice-cold water (500 mL) and extracted with toluene. The combined organic extracts were dried ($MgSO_4$), concentrated *in vacuo* and the residue purified by column chromatography (silica gel; gradient 5-30% DCM/hexanes). Recrystallization of this material from heptane/toluene afforded the *title compound* as a colourless solid (475 mg, 11%).

MP 137-141 °C. **^{1}H NMR** (400 MHz, Chloroform-*d*) ∂ 8.28 (d, *J* = 9.0 Hz, 2H), 8.16 (dd, *J* = 7.5 Hz, 4H), 8.13-8.06 (m, 4H), 8.06-7.95 (m, 6H), 7.86 (d, *J* = 7.8 Hz, 2H), 3.33 (t, *J* = 7.5 Hz, C$\underline{H}_2$-Ar, 4H), 1.86 (quin, *J* = 7.5 Hz, C$\underline{H}_2$-CH$_2$-Ar, 4H), 1.54-1.38 (m, 8H). **^{13}C NMR** (101 MHz, Chloroform-*d*) ∂ 137.3, 131.4, 130.9, 129.7, 128.6, 127.6, 127.3, 127.1, 126.5, 125.7,

125.1, 124.8, 124.6, 123.5, 33.6 ($\underline{C}H_2$-Ar), 31.92, 29.8, 29.5. N.B. 14 Aromatic carbons detected rather than 16, this is assumed to be due to overlap. **MS** [APCI$^+$] m/z 514.3 ([M]$^+$, 100%). **HR** *m/z* (APCI$^+$) $C_{40}H_{34}$ + H calcd for 515.2733, found 515.2737. Structure determination confirmed by X-ray crystallography.

4.2.2. PERYLENE SCAFFOLD MOLECULES

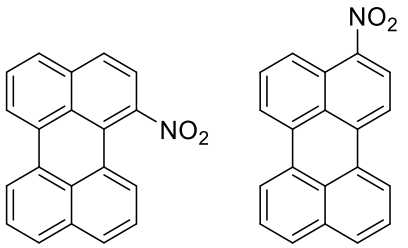

1-Nitroperylene (**27**) and 3-Nitroperylene (**28**)

Prepared from an adaption of a literature synthesis.[157]

Perylene (10.0 g, 39.7 mmol) was dissolved in 1,4-dioxane (1.50 L) heated to 70 °C. Water (20 mL) was then added, followed by dropwise fuming nitric acid (10 mL, ρ = 1.50 g/L) and the solution stirred for 3 h. The reaction was then quenched by addition of sat. $NaHCO_3$ solution (200 mL) and the organics extracted with toluene (3 x 1 L) and the combined extracts concentrated *in vacuo*. The crude product purified by column chromatography and the products eluted with a gradient solvent system (20-50% DCM/hexanes), to consecutively afford 1-nitroperylene (1.62 g, 17 %) as bright red crystals and 3-nitroperylene (4.21 g, 21%) as a dark red amorphous solid.

1-Nitroperylene **27**:

MP 205-211 °C (Lit.[194] 210 °C). **^{1}H NMR** (400 MHz, Chloroform-*d*) ∂ 8.29 (d, *J* = 7.8 Hz, 1H), 8.26 (d, *J* = 7.5 Hz, 1H), 7.85 (d, *J* = 7.0 Hz, 1H), 7.81 (dt, *J* = 8.5 Hz, 2H), 7.75 (d, *J* = 7.8 Hz, 1H), 7.73 (d, *J* = 8.5 Hz, 1H), 7.64 (t, *J* = 7.8 Hz, 1H), 7.59 (d, *J* = 7.8 Hz, 1H), 7.57 (d, *J* = 8.8 Hz, 1H), 7.46 (t, *J* = 7.8 Hz, 1H). **^{13}C NMR** (101 MHz, Chloroform-*d*) ∂ 134.8, 134.2, 132.4, 130.1, 129.7, 129.2, 128.8, 128.6, 128.5, 128.0, 127.4, 126.8, 126.6, 126.5, 125.7, 124.5, 122.2, 122.0, 121.5. **MS** (GCMS) m/z 297.0 ($[M]^+$, 60%). Characterisation data was in agreement with that in the literature.[195]

3-Nitroperylene **28**:

MP 210-215 °C. (Lit.[196] 208-210 °C). **^{1}H NMR** (400 MHz, Chloroform-*d*) ∂ 8.26 (d, *J* = 7.5 Hz, 1H), 8.23 (d , *J* = 7.5 Hz, 1H), 7.84 (d, *J* = 7.8 Hz, 1H), 7.80 (dt, *J* = 9.0 Hz, 2H), 7.73 (d, *J* = 8.0 Hz, 1H), 7.71 (d, *J* = 8.8 Hz, 1H), 7.62 (t, *J* = 8.0 Hz, 1H), 7.56 (t, *J* = 7.8 Hz, 1H), 7.54 (d, *J* = 8.8 Hz, 1H), 7.45 (t, *J* = 8.0 Hz, 1H). **^{13}C NMR** (101 MHz, Chloroform-*d*) ∂ 146.4,

134.8, 134.2, 132.3, 130.1, 129.7, 129.2, 128.8, 128.5, 128.4, 128.0, 127.3, 126.7, 126.6, 126.5, 125.7, 124.5, 122.1, 122.0, 121.5. **MS** (GCMS) m/z 297.1 ($[M]^+$, 100%).

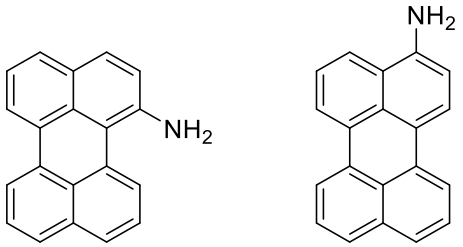

1-Aminoperylene (**43**) and 3-Aminoperylene (**43b**)

A mixture of isomers in 1-nitroperylene (400 mg, 1.35 mmol) and 3-nitroperylene (300 mg, 1.01 mmol) were dissolved in THF (100 mL) and the solution sparged with Ar. Pd/C (10% Pd, 100 mg) was then added and the solution charged with H_2. The mixture was stirred for 1 d and the organics collected as the eluent of filtration through Celite© using DCM. The crude products were then purified by column chromatography on silica gel (gradient 10-20% DCM/hexanes) to afford 1-aminoperylene (339 mg, 94%) and 3-aminoperylene (243 mg, 90%) as consecutive fractions.

1-Aminoperylene:

MP 190-196 °C (Lit.[197] 195-196 °C). **^{1}H NMR** (400 MHz, DMSO-d_6) ∂ 8.42 (d, J = 7.5 Hz, 1H), 8.16 (t, J = 6.5 Hz, 2H), 7.69 (d, J = 8.0 Hz, 1H), 7.64-7.53 (m, 3H), 7.52-7.43 (m, 2H), 7.27 (t, J = 7.8 Hz, 1H), 7.17 (d, J = 8.8 Hz, 1H), 6.04 (s, N-H, 2H). **^{13}C NMR** (101 MHz, DMSO-d_6) ∂ 143.0, 134.8, 132.2, 131.8, 130.6, 130.2, 129.8, 129.2, 128.8, 127.8, 126.8, 126.5, 126.3, 125.5, 123.4, 121.8, 121.4, 121.2, 119.1, 113.0. **MS** (GCMS) m/z 267.4 ([M]$^+$, 100%).

3-Aminoperylene:

MP 205-208 °C (Lit.[196] 208-210 °C). **^{1}H NMR** ∂ (400 MHz, DMSO-d_6) 8.28 (d, J = 7.5 Hz, 1H), 8.22 (d, J = 7.5 Hz, 1H), 8.09 (d, J = 8.3 Hz, 1H), 8.00 (d, J = 7.3 Hz, 1H), 7.96 (d, J = 8.3 Hz, 1H), 7.65 (d, J = 8.0 Hz, 1H), 7.52 (d, J = 8.0 Hz, 1H), 7.48-7.35 (m, 3H), 6.76 (d, J = 8.3 Hz, 1H), 6.11 (s, N-H, 2H). **^{13}C NMR** (101 MHz, Chloroform-d) ∂ 144.4, 142.1, 138.4, 134.9, 131.9, 131.6, 129.5, 127.7, 126.7, 126.4, 125.8, 125.6, 124.2, 121.4, 120.7, 120.6, 119.8, 118.1, 110.9. N.B. 19 Aromatic carbons detected rather than 20, this is assumed to be due to overlap. **MS** (GCMS) m/z 267.8 ([M]$^+$, 100%).

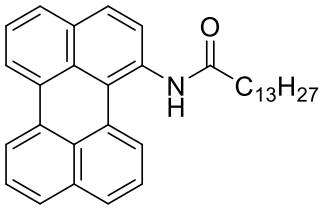

N-(perylen-1-yl)tetradecanamide (**44**)

To a solution of 1-aminoperylene (1.0 g, 3.74 mmol) was dissolved in THF (100 mL) was added pyridine (1.50 mL, 18.70 mmol). The solution was cooled to 0 °C and myristoyl chloride (2.24 mL, 8.24 mmol) was added dropwise. The reaction was stirred for 1 h and quenched upon addition of HCl (100 mL, 2 M). The organics were extracted with DCM and washed with water, then dried ($MgSO_4$). The crude product was then triturated with DCM/methanol to afford the *title compound* as a yellow coloured solid (1.4 g, 83%).

MP 152-154 °C. **^{1}H NMR** (400 MHz, DMSO-*d6*, 110 °C) ∂ 10.11 (s, 1H), 8.61 (d, *J* = 7.5 Hz, 1H), 8.34 (d, *J* = 6.5 Hz, 2H), 7.80-7.74 (m, 1H), 7.62-7.45 (m, 4H), 2.41 (t, *J* = 7.3 Hz, O=C-C$\underline{H}_2$, 2H), 1.68 (quin, *J* = 6.0 Hz, O=C-CH_2-C$\underline{H}_2$, 2H), 1.44-1.14 (m, 16H), 0.85 (t, *J* = 7.0 Hz, 3H). **^{13}C NMR** (101 MHz, DMSO-*d6*, 110 °C) ∂ 172.1 ($\underline{C}$=O), 133.9, 131.2, 129.9, 129.2, 128.2, 128.0, 127.0, 126.7, 126.6, 125.3, 121.6 120.8, 31.6, 29.5-29.3 (7C), 29.2, 29.0, 25.3, 22.4, 14.1. N.B. 12 Aromatic carbons detected rather than 20, this is assumed to be due to overlap. **IR** $\tilde{\nu}_{max}/cm^{-1}$ 3391 (N-H), 2914 and 2846 (Ar C-H), 1656 (C=O), 723 (Ar C=C). **MS** (MALDI-Dithranol) 500.6 ($[M+H]^+$, 100%). **HRMS** *m/z* (ASAP$^+$) $C_{34}H_{39}NO$ + H calcd for 478.3104, found 478.3091.

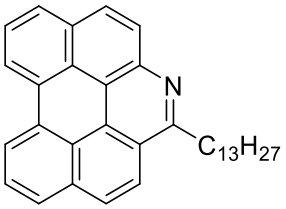

2-Tridecylphenanthro[1,10,9,8-*klmna*]phenanthridine (**31**)

N-(perylen-1-yl)dodecanamide (1.0 g, 2.22 mmol) and phosphorous pentoxide (1.16 g, 14.09 mmol) were dissolved in phosphoryl chloride (50 mL) and the solution heated to 100 °C overnight. The reaction mixture was then poured into water and the organics extracted with chloroform and concentrated *in vacuo*. The crude products were then triturated with DCM/methanol to afford the *title compound* as a yellow coloured solid (0.75 g, 78%).

MP 178-183 °C. **^{1}H NMR** (400 MHz, Chloroform-*d*) ∂ 8.84 (dd, *J* = 7.8, 7.5 Hz, 2H), 8.31 (d, *J* = 8.8 Hz, 1H), 8.25 (d, *J* = 9.0 Hz, 1H), 8.20 (d, *J* = 9.0 Hz, 1H), 8.17 (d, *J* = 7.8 Hz, 1H), 8.09 (d, *J* = 7.8 Hz, 1H), 8.05-7.98 (m, 2H), 7.95 (t, *J* = 7.8 Hz, 1H), 3.61 (t, *J* = 8.0 Hz, N=C-C$\underline{H}_2$, 2H), 2.03 (quin, *J* = 7.8 Hz, N=C-CH$_2$-C$\underline{H}_2$, 2H), 1.71-1.54 (m, 2H), 1.50-1.18 (m, 14H), 0.88 (t, *J* = 6.8, 3H). **^{13}C NMR** (101 MHz, Chloroform-*d*) ∂ 143.4, 133.0, 131.3, 131.1, 129.9, 129.7, 128.4, 128.0, 127.9, 127.8, 127.2, 126.3, 124.6, 124.6, 123.5, 121.3, 121.1, 120.9, 117.0, 36.6 (C$\underline{H}_2$-Ar), 31.9 (C$\underline{H}_2$-CH$_2$-Ar), 30.9, 30.1, 29.7-29.5 (6C), 29.4, 22.7, 14.1. N.B. 19 Aromatic carbons detected rather than 21, this is assumed to be due to overlap. **IR** $\tilde{\nu}_{max}$/cm^{-1} 2922 and 2851 (Ar C-H), 1741 (C=N), 730 (C=C). **HRMS** m/z (ASAP^{+}) $C_{34}H_{38}N$ + H calcd for 460.2999, found 460.2995.

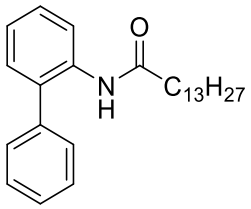

N-([1,1'-biphenyl]-2-yl)tetradecanamide (**41**)

Prepared from an adaption of a literature synthesis.[198]

(1,1'-Biphenyl)-2-amine (1.0 g, 5.91 mmol) was dissolved in DCM (50 mL) and pyridine (2 mL, 13.6 mmol) added. The solution was cooled to 0 °C and myristoyl chloride (2.5 mL, 9.20 mmol) added dropwise. The reaction was stirred for 1 h and quenched upon addition of HCl (100 mL, 2 M). The organics were extracted with ethyl acetate and washed with water, then concentrated *in vacuo*. The crude product was then purified by column chromatography on silica gel (5% EtOAc/hexanes) to give the title compound as a colourless solid (1.68 g, 81%).

MP 62-66 °C. **^{1}H NMR** (400 MHz, Chloroform-*d*) ∂ 8.22 (d, *J* = 8.0 Hz, 1H), 7.39-7.32 (m, 2H), 7.34 (d, *J* = 7.1 Hz, 1H), 7.29-7.26 (m, 3H), 7.18-7.14 (m, 1H), 7.12-7.06 (m, 1H) 2.09 (t, *J* = 7.6 Hz, 2H), 1.51-1.47 (m, 2H), 1.25-1.11 (m, 16H), 0.80 (t, *J* = 6.5 Hz, 3H). **^{13}C NMR** (101 MHz, Chloroform-*d*) ∂ 179.4 (C=O), 139.2, 139.0, 129.2, 127.9, 127.7, 126.5, 125.2, 125.0, 124.8, 124.0, 38.1, 26.6, 26.2, 26.0, 25.5, 22.4, 14.7. N.B. 10 Aromatic carbons detected rather than 12, this is assumed to be due to overlap. **MS** (GCMS) m/z 378.4 ($[M-H]^-$, 80%). Characterisation data was in agreement with that in the literature.[199]

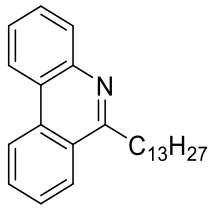

6-Tridecylphenanthridine (**42**)

N-([1,1'-biphenyl]-2-yl)dodecanamide (300 mg, 0.82 mmol) and phosphorous pentoxide (1.16 g, 4.09 mmol) were dissolved in phosphoryl chloride (10 mL) and the solution heated to 100 °C overnight. The reaction mixture was then poured into water and the organics extracted with EtOAc and concentrated *in vacuo* to afford the *title compound* as a colourless solid (273 mg, 97%) with no need for further purification.

MP 54-58 °C. **^{1}H NMR** (400 MHz, Chloroform-*d*) ∂ 8.66 (d, *J* = 8.5 Hz, 1H), 8.56 (d, *J* = 8.2 Hz, 1H), 8.27 (d, *J* = 8.2 Hz, 1H), 8.14 (d, *J* = 7.9 Hz, 1H), 7.85 (t, *J* = 7.9 Hz, 1H), 7.76-7.68 (m, 2H), 7.63 (t, *J* = 8.2 Hz, 1H), 3.38 (t, *J* = 7.8 Hz, C$\underline{H}_2$-Ar, 2H), 1.93 (quin, *J* = 7.8 Hz, C$\underline{H}_2$-CH_2-Ar, 2H), 1.54 (quin, *J* = 7.9 Hz, C$\underline{H}_2$-CH_2-CH_2-Ar, 2H), 1.40 (quin, *J* = 6.9 Hz, C$\underline{H}_2$-CH_2-CH_2-CH_2-Ar, 2H), 1.35-1.20 (m, 14H), 0.89 (t, *J* = 6.9 Hz, 3H). **^{13}C NMR** (101 MHz, Chloroform-*d*) ∂ 161.2, 145.2, 135.6, 130.2, 128.5, 128.2, 128.0, 127.5, 124.2, 123.5, 123.0, 121.8, 121.6, 35.8, 30.1, 29.7-29.4 (7C), 29.3, 29.0, 22.4, 14.5. **MS** (GCMS) m/z 361.3 (M^+, 100%). Characterisation data was in agreement with that in the literature.[199]

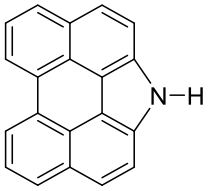

1*H*-Phenanthro[1,10,9,8-*cdefg*]carbazole (**30**)

1-Nitroperylene (1.0 g, 3.37 mmol) was dissolved in triethylphosphite (25 mL) and heated to 140 °C for 3 h. Upon cooling to rt the solids removed by filtration and washed with methanol to afford the *title compound* as a yellow coloured solid (741 mg, 83%).

MP 245-250 °C. **^{1}H NMR** (400 MHz, DMSO-d_6) ∂ 12.2 (s, N-H, 1H), 8.74 (d, J = 8.7 Hz, 2H), 8.17 (d, J = 8.2 Hz, 2H), 7.97 (d, J = 8.0 Hz, 2H), 7.94 (d, J = 7.9 Hz, 2H), 7.81 (t, J = 7.8 Hz, 2H). **^{13}C NMR** (101 MHz, DMSO-d_6) ∂ 138.1, 132.4, 131.8, 128.0, 127.8, 127.0, 124.8, 123.2, 123.0, 120.5. **MS** (GCMS) m/z 264.1 ([M-H]$^-$, 100%). Characterisation data was in agreement with that in the literature.[195]

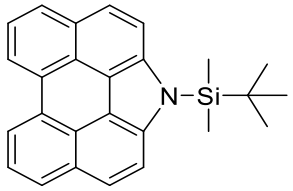

1-(*Tert*-butyldimethylsilyl)-1*H*-phenanthro[1,10,9,8-*cdefg*]carbazole (**47**)

To a flame-dried flask was added 1*H*-phenanthro[1,10,9,8-*cdefg*]carbazole (100 mg, 0.377 mmol), TBDMSCl (85 mg, 0.57 mmol), THF (50 mL) and the solution was sparged with Ar. Sodium hydride (60% dispersion in mineral oil, 41 mg, 0.57 mmol) was then added and the solution stirred for 1 h. The mixture was then poured into ice-water and the crude organics extracted with toluene. The organic extracts were concentrated *in vacuo* to afford the *title compound* as a yellow coloured solid with no need of further purification (142 mg, 99%)

MP 180-184 °C. **^{1}H NMR** (400 MHz, Chloroform-*d*) ∂ 8.61 (d, *J* = 7.6 Hz, 2H), 8.09 (d, *J* = 7.9 Hz, 2H), 7.92 (d, *J* = 8.8 Hz, 2H), 7.86 (d, *J* = 8.8 Hz, 2H), 7.80 (d, *J* = 7.6 Hz, 2H), 1.02 (s, 9H), 0.95 (s, 6H). **^{13}C NMR** (101 MHz, Chloroform-*d*) ∂ 139.3, 133.1, 131.4, 127.5, 127.4, 125.9, 123.4, 122.9, 119.7, 28.7, 22.6. N.B. 9 Aromatic carbons detected rather than 10, this is assumed to be due to overlap. 2 alkyl carbons detected rather than 3, this is assumed to be due to overlap. **MS** (GCMS) m/z 397.1 ([M]$^{+}$, 100%). **IR** $\tilde{\nu}_{max}$/cm^{-1} 2922 and 2851 (Ar C-H), 1199 (C-N), 651 (Ar C=C). **MS** (MALDI-TCNQ) m/z 379.0 ([M]$^{+}$, 100%). **HR** *m/z* (HESI)$^{+}$ $C_{26}H_{26}N_2Si$ + H calcd for 380.1829, found 380.1818.

Synthesis of Brominated Phenanthrocarbazoles

General procedure C: Mono- and dibromination of phenanthrocarbazoles using NBS

To a solution of the phenanthrocarbazole derivative (1 eq.) in sparged DMF (60 mL/g) was added a solution of NBS (1.05/2.10 eq. as specified) and the mixture stirred for 2 h at rt. The organics were then diluted with toluene, washed with water, then dried ($MgSO_4$). The crude products were then triturated with THF/heptane to yield the desired material.

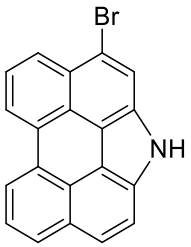

3-Bromo-1*H*-phenanthro[1,10,9,8-cdefg]carbazole (**45**)

Procedure C: 1*H*-Phenanthro[1,10,9,8-*cdefg*]carbazole (400 mg, 1.51 mmol) was reacted with NBS (282 mg, 1.58 mmol) in DMF (25 mL) to afford an inseparable mixture of unreacted starting material (63 mg, 15%), the desired mono-brominated (519 mg, 77%) and di-brominated products (66 mg 10%). Yields estimated from interpretation of ^{1}H NMR.

^{1}H NMR (400 MHz, DMSO-d_6) ∂ 12.31 (s, N-H, 1H), 8.88 (d, *J* = 7.5 Hz, 1H), 8.83 (d, *J* = 7.5 Hz, 1H), 8.37 (s, 1H), 8.26 (d, *J* = 8.0 Hz, 1H), 8.24 (d, *J* = 8.0 Hz, 1H), 7.98 (m, 3H), 7.87 (t, *J* = 7.8 Hz, 1H) – assigned by abstraction of those resonances that are associated with the alternate bromination products. **^{13}C NMR** (101 MHz, DMSO-d_6) ∂ 131.6, 130.6, 130.6, 129.6, 128.7, 127.6, 126.3, 126.1, 125.4, 124.9, 124.6, 124.5, 124.3, 122.4, 122.0, 119.8, 117.0, 116.8, 116.2. N.B. 19 Aromatic carbons detected rather than 20, this is assumed to be due to overlap. **MS** (MALDI-TCNQ) m/z 342.1 ([M(^{79}Br)-H]$^-$, 20%).

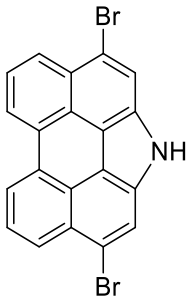

3,10-Dibromo-1H-phenanthro[1,10,9,8-cdefg]carbazole (**46**)

Procedure C: 1*H*-Phenanthro[1,10,9,8-*cdefg*]carbazole (420 mg, 1.58 mmol) was reacted with NBS (578 mg, 3.24 mmol) in DMF (25 mL) to exclusively afford the *title compound* as a yellow coloured solid (669 mg, 98%).

MP 152-156 °C. **^{1}H NMR** (400 MHz, Chloroform-*d*) ∂ 12.38 (s, N-H, 1H), 8.93 (d, J = 7.8 Hz, 2H), 8.38 (s, 2H), 8.31 (d, J = 8.3 Hz, 2H), 8.00 (t, J = 8.0 Hz, 2H). **^{13}C NMR** (101 MHz, Chloroform-*d*) ∂ 131.1, 129.9, 127.6, 126.6, 125.2, 124.1, 123.1, 119.9, 117.7, 116.5. **IR** $\tilde{\nu}_{max}/cm^{-1}$ 2917 and 2850 (Ar C-H), 565 (C-Br). Structure determination confirmed by X-ray crystallography. **MS** (MALDI-TCNQ) m/z 423.1 ([M(^{79}Br + ^{81}Br)]$^{+}$, 100%). **HRMS** *m/z* (APCI^{+}) $C_{20}H_{10}N(^{79}Br_2)$ calcd for 421.9166, found 421.9180.

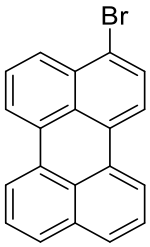

3-Bromoperylene (**46b**)

Procedure C: Perylene (2.0 g, 7.93 mmol) was reacted with NBS (1.41 g, 7.92 mmol) in DMF (120 mL) and the mixture stirred for 2 d to afford the *title compound* (90% pure by ^{1}H NMR) as a yellow solid (1.64 g, 62% yield).

^{1}H NMR (400 MHz, Chloroform-*d*) ∂ 8.20 (d, *J* = 7.5 Hz, 1H), 8.16 (d, *J* = 7.8 Hz, 1H), 8.10 (d, *J* = 7.5 Hz, 1H), 8.07 (d, *J* = 8.5 Hz, 1H), 7.95 (d, *J* = 8.0 Hz, 1H), 7.72 (d, *J* = 8.0 Hz, 1H), 7.70 (m, 2H), 7.55 (t, *J* = 7.5 Hz, 1H), 7.50-742 (m, 2H). **^{13}C NMR** (101 MHz, Chloroform-*d*) ∂ 134.6, 133.1, 131.6, 131.2, 130.7, 130.6, 129.9, 128.3, 128.2, 127.7, 127.0, 126.7, 126.6, 122.5, 121.0, 120.8, 120.5, 120.4. N.B. 18 Aromatic carbons detected rather than 20, this is assumed to be due to overlap. **MS** m/z (MALDI-TCNQ) 330.0 ([M(^{79}Br)]$^{+}$, 100%), 332.0 ([M(^{81}Br)]$^{+}$, 100%). Characterisation data was in agreement with that in the literature.[200]

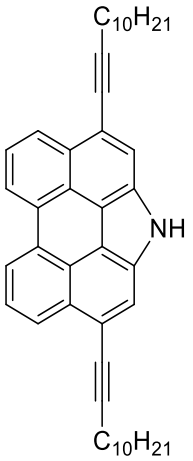

3,10-Di(dodec-1-yn-1-yl)-1*H*-phenanthro[1,10,9,8-*cdefg*]carbazole (**48**)

3,10-Dibromo-1H-phenanthro[1,10,9,8-cdefg]carbazole (2.0 g, 4.75 mmol), and copper iodide (91.4 mg, 0.48 mmol) were dissolved in a mixture of triethylamine (40 mL) and THF (60 mL) and the solution sparged with Ar. $Pd(PPh_3)_4$ (554.7 mg, 0.48 mmol) and dodecyne (1.02 mL, 4.75 mmol) were then added and the solution heated to 66 °C. Dodecyne (1.02 mL, 4.75 mmol) was continually added every 1 h for 5 h and the reaction quenched on pouring into water. The organics were extracted with toluene and washed with water, then dried. The crude products were purified by column chromatography on silica gel (gradient 10-25% toluene/hexanes) to afford the *title compound* as fine light yellow coloured crystals (1.15 g, 42%).

MP 91-94 °C. **^{1}H NMR** (400 MHz, Chloroform-*d*) ∂ 8.83 (broad s, N-H, 1H), 8.70-8.64 (m, 2H), 8.47-8.43 (m, 2H), 7.97 (s, 2H), 7.89 (t, *J* = 7.8 Hz, 2H), 2.66-2.62 (m, CH_2-C≡C, 4H) , 1.79 (quin, *J* = 7.3 Hz, CH_2-CH_2-C≡C, 4H), 1.61 (quin, *J* = 7.0 Hz, CH_2-CH_2-CH_2-C≡C, 4H), 1.38-130 (m, 28H), 0.88 (t, *J* = 7.0 Hz, 6H). **^{13}C NMR** (101 MHz, Chloroform-*d*) ∂ 130.4, 129.9, 125.3, 124.4, 124.0, 121.3, 117.9, 80.1 (C≡C), 31.9, 29.7, 29.4, 29.3-29.2 (4C), 22.7, 20.0, 14.1. N.B. 7 Aromatic carbons detected rather than 10, this is assumed to be due to overlap. **IR** $\tilde{\nu}_{max}/cm^{-1}$ 3695 (N-H), 2983 and 2843 (Ar C-H), 2010 (C≡C). **MS** (MALDI-TCNQ) m/z 593.6 ($[M]^+$, 100%). **HRMS** *m/z* (ASAP$^+$) $C_{44}H_{51}N$ calcd for 593.4016, found 593.4004.

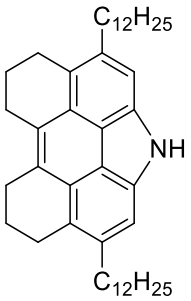

3,10-Didodecyl-4,5,6,7,8,9-hexahydro-1H-phenanthro[1,10,9,8-cdefg]carbazole (**49**)

3,10-Di(dodec-1-yn-1-yl)-1*H*-phenanthro[1,10,9,8-*cdefg*]carbazole (1.15 g, 1.94 mmol) was dissolved in THF (100 mL) and the solution sparged with Ar. Pd/C (10% Pd, 100 mg) was then added and the solution charged with H_2. The mixture was stirred for 2 d and the organics collected as the eluent of filtration through Celite©. The crude products were then purified by column chromatography on silica gel (gradient 5-20% DCM/hexanes) to afford the *title compound* as green coloured crystals (177 mg, 15%).

MP 114-118 °C. **^{1}H NMR** (400 MHz, Chloroform-*d*) ∂ 7.78 (s, N-H, 1H), 7.23 (s, 2H), 3.12 (dt, *J* = 5.7, 5.6 Hz, Ar-C$\underline{H}_2$-CH_2,-C$\underline{H}_2$-Ar, 8H), 2.94 (t, *J* = 8.2 Hz, C$\underline{H}_2$-Ar, 4H), 2.27 (quin, *J* = 6.0 Hz, Ar-CH_2-C$\underline{H}_2$,-CH_2-Ar, 4H), 1.69 (quin, *J* = 7.6 Hz, C$\underline{H}_2$- Ar, 4H), 1.46-1.21 (m, 36H), 0.88 (t, *J* = 6.9 Hz, 6H). **^{13}C NMR** (101 MHz, Chloroform-*d*) ∂ 151.5, 137.7, 129.2, 128.2, 124.7, 119.6, 106.2 (Ar$\underline{C}$-H), 40.5, 40.1, 39.7, 34.2, 32.0, 31.9, 30.0, 29.7, 29.6, 29.3, 26.2, 25.5, 24.8, 22.7, 14.1. **IR** $\tilde{\nu}_{max}$/cm^{-1} 3342 (broad N-H), 2916 and 2848 (Ar C-H), 1199 (C-N), 753 (Ar C=C). **MS** (MALDI-Dithranol) m/z 607.6 ([M]$^+$, 85%). **HRMS** m/z (ASAP$^+$) $C_{44}H_{66}N$ calcd for 608.5190 found 608.5190. Structure determination confirmed by X-ray crystallography.

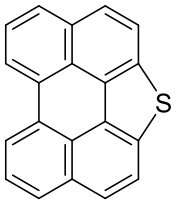

Peryleno[1,12-*bcd*]thiophene (**29**)

Prepared by adaption of a literature synthesis.[157]

1-Nitroperylene (400 mg, 1.35 mmol) and sulphur powder (430 mg, 13.50 mmol) were dissolved in NMP (50 mL) and the solution heated to 180 °C for 1 d. The reaction was quenched upon addition to HCl (200 mL, 2M) and the organics extracted with toluene. The combined organic extracts were then washed with water (2 x 100 mL) and dried ($MgSO_4$). The crude products were then purified by column chromatography on silica gel (gradient 5-20% DCM/hexanes) to yield the desired material as yellow solid (50 mg, 13%).

MP 270-280 °C. **^{1}H NMR** (400 MHz, Chloroform-*d*) ∂ 8.59 (d, *J* = 7.5 Hz, 2H), 8.10 (dd, *J* = 8.8 Hz, 2H), 8.07 (d, *J* = 8.0 Hz, 2H), 7.96 (d, *J* = 8.8 Hz, 2H), 7.83 (t, *J* = 7.8 Hz, 2H). **^{13}C NMR** (101 MHz, Chloroform-*d*) ∂ 134.0, 130.9, 130.6, 126.2, 126.1, 125.9, 125.7, 121.8, 120.7. N.B. 9 Aromatic carbons detected rather than 10, this is assumed to be due to overlap. **MS** (GCMS) m/z 281.2 ([M-H]$^-$, 100%). Characterisation data was in agreement with that in the literature.[157]

4.2.3. HEXABENZOCORONENE SYNTHESIS

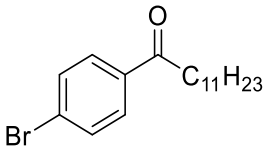

1-(4-Bromophenyl)dodecan-1-one (**56**)

A mixture of bromobenzene (24.4 mL, 0.23 mol) and DCM (500 mL) was sparged with Ar and cooled to 0 °C. Aluminium chloride (30.0 g, 0.23 mol) was added and the suspension stirred for 15 min. To the reaction mixture was added lauroyl chloride (52.1 mL, 0.23 mol) over 1 h. The reaction was the was stirred for 6 d then quenched with ice water (200 mL) and HCl (200 mL, 2M). The crude product was purified by column chromatography on silica gel (5% DCM/hexanes) and the eluent recrystallised from ethanol to afford the *title compound* as colourless crystals (46.8 g, 60%).

MP 60-64 °C (Lit.[201] 63-63 °C). **^{1}H NMR** (400 MHz, Chloroform-*d*) ∂ 7.84 (d, *J* = 8.5 Hz, 2H), 7.62 (d, *J* = 8.8 Hz, 2H), 2.92 (t, *J* = 7.3 Hz, C$\underline{H}_2$-C=O, 2H), 1.72 (quin, *J* = 7.3 Hz, C$\underline{H}_2$-CH_2-C=O, 2H), 1.44-1.19 (m, 16H), 0.88 (t, *J* = 7.0 Hz, 3H). **^{13}C NMR** (101 MHz, Chloroform-*d*) ∂ 199.6 (C=O), 135.9, 132.1, 129.9, 128.3, 38.7, 32.0, 29.9, 29.7, 29.6, 24.4, 23.0, 14.4. **MS** (GCMS) m/z 338.4 ([M]$^{+}$, 100%). Characterisation data was in agreement with that in the literature.[202]

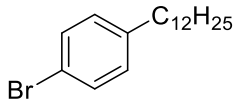

1-Bromo-4-dodecylbenzene (**57**)

1-(4-Bromophenyl)dodecan-1-one (2.80 g, 8.28 mmol), hydrazine monohydrate (0.82 mL, 64%) and potassium hydroxide (1.40 g, 24.8 mmol) were dissolved in triethylene glycol (50 mL) and heated to 110 °C for 2 h. The reaction temperature was then increased to 220 °C and the water removed by distillation for 30 min. The reaction mixture was then quenched with 2M HCl/ice water (500 ml). The combined organic extracts were diluted with DCM and washed with water (200 mL) then dried ($MgSO_4$). The crude products were then purified by column chromatography (hexanes) to afford the *title compound* as a colourless oil (1.93 g, 72%).

^{1}H NMR (400 MHz, Chloroform-*d*) ∂ 7.39 (d, *J* = 8.3 Hz, 2H), 7.06 (d, *J* = 8.3 Hz, 2H), 2.55 (t, *J* = 7.5 Hz, C$\underline{H}_2$-Ar, 2H), 1.58 (quin, *J* = 7.3 Hz, C$\underline{H}_2$-CH_2-Ar, 2H), 1.36-1.19 (m, 18H), 0.89 (t, *J* = 6.5 Hz, 3H). **^{13}C NMR** (101 MHz, Chloroform-*d*) ∂ 142.0, 131.3, 130.2, 119.2, 35.5, 31.9, 29.7, 29.6, 29.5, 29.4, 29.2, 22.7, 14.2. **MS (**GCMS) m/z 324.2 ($[M]^+$, 60%). Characterisation data was in agreement with that in the literature.[202]

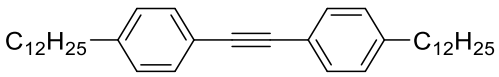

1,2-*Bis*-(4-dodecylphenyl)ethyne (**54**)

Prepared by adaption of a literature synthesis.[203]

But-2-ynedioic acid (1.68 g, 14.69 mmol), 1,8-diazabicyclo[5.4.0]undec-7-ene (4.34 mL, 30.85 mmol) and 1-bromo-4-dodecylbenzene (10.0 mL, 30.85 mmol) were dissolved in DMSO (100 mL) and the system sparged with Ar. $Pd(PPh_3)_2Cl_2$ (0.51 g, 0.73 mmol) and 1,4-*bis*-(diphenylphosphino)butane (0.63 g, 1.47 mmol) were then added and the reaction mixture heated to 110 °C for 5 h. The reaction was then quenched with saturated ammonium chloride solution and the organics extracted with diethyl ether. The organic layer was then washed with water and then dried ($MgSO_4$). The crude material was purified by column chromatography on silica gel (hexanes) and the eluent recrystallised from ethanol to give the *title compound* as yellow coloured crystals. (4.99 g, 66%).

MP 58-61 °C (Lit[204] 58-59 °C). **^{1}H NMR** (400 MHz, Chloroform-*d*) ∂ 7.44 (d, *J* = 8.0 Hz, 4H), 7.16 (d, *J* = 8.3 Hz, 4H), 2.16 (t, *J* = 7.8 Hz, C$\underline{H}_2$-Ar, 4H), 1.60 (m, 4H), 1.37-1.20 (m, 36H), 0.89 (t, *J* = 7.0 Hz, 6H). **^{13}C NMR** (101 MHz, Chloroform-*d*) ∂ 143.1, 131.5, 128.5, 120.6, 88.9 ($\underline{C}$≡C), 35.9, 31.9, 31.3, 29.9, 29.6, 29.3, 29.1, 22.7, 14.2. **MS (**MALDI-Dithranol) m/z 514.6 ($[M]^+$, 100%). Characterisation data was in agreement with that in the literature.[203]

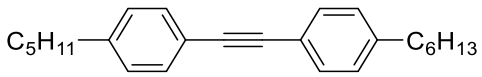

1-Hexyl-4-((4-pentylphenyl)ethynyl)benzene (**52**)

Copper iodide (44.0 mg, 0.23 mmol) was added to tetrahydrofuran (10 mL) and trimethylamine (10 mL) and the solution sparged with Ar. 1-Ethynyl-4-pentylbenzene (0.50 mL, 3.28 mmol) and 1-iodo-4-hexylbenzene (0.67 mL, 3.44 mmol) were then added followed by $Pd(PPh_3)_4$ (265 mg, 0.23 mmol) and the reaction heated to 66 °C for 16 h. The reaction mixture was filtered through Celite® and the eluent washed with water (200 mL), then brine (200 mL). The crude products were then concentrated *in vacuo* purified by chromatography on silica gel (hexanes) to afford the *title compound* as a colourless solid (806 mg, 74 %).

MP 87-89 °C. **^{1}H NMR** (400 MHz, Chloroform-*d*) ∂ 7.44 (d, *J* = 8.1 Hz, 4H), 7.16 (d, *J* = 8.0 Hz, 4H), 2.61 (t, *J* = 7.5 Hz, C$\underline{H}_2$-Ar, 4H), 1.62 (m, C$\underline{H}_2$-CH_2-Ar, 4H), 1.32 (m, 10H), 0.90 (m, 6H). **^{13}C NMR** (101 MHz, Chloroform-*d*) ∂ 143.6, 131.4, 128.4, 120.6, 88.9 ($\underline{C}$≡C), 35.9 ($\underline{C}H_2$-Ar), 31.7, 31.4, 31.2, 31.2, 30.9, 28.9, 22.6, 22.5, 14.1, 14.0. **MS** (GCMS) m/z 332.30 ($[M]^+$, 100%). Characterisation data was in agreement with that in the literature.[205]

General Procedure D: Diels-Alder Cycloaddition to Generate Dialkyl Hexaphenylbenzene Derivatives

Diphenylalkynes (1.2 eq.) were combined with tetraphenylcyclopentadieneone (TPCPD) (1 eq.) and tetradecane and heated to 250 °C for 4 h. The crude material was loaded directly onto silica gel and purified by column chromatography.

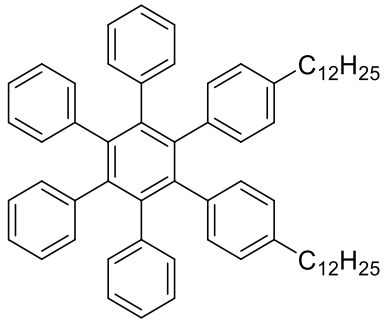

1,2-*Bis*-(4-dodecylbenzene)-3,4,5,6-tetraphenylbenzene (**61**)

Procedure D: 1,2-*Bis*-(4-dodecylphenyl)ethyne (1.50 g, 2.91 mmol) and TPCPD (924 mg, 2.42 mmol) were dissolved in tetradecane (10 mL) and heated to 250 °C for 4 h. The reaction mixture was loaded directly onto silica gel and chromatographed (20% DCM/hexanes) to give the *title compound* as a colourless solid (2.18 g, 86%).

MP 224-228 °C. **^{1}H NMR** (400 MHz, Chloroform-*d*) ∂ 6.91-6.80 (m, 20H), 6.68 (d, *J* = 8.3 Hz, 4H), 6.63 (d, *J* = 8.3 Hz, 4H), 2.34 (t, *J* = 7.5 Hz, C$\underline{H}_2$-Ar, 4H), 1.39 (quin, *J* = 7.5 Hz, C$\underline{H}_2$-CH_2-Ar, 4H), 1.34-1.01 (m, 36H), 0.89 (t, *J* = 7.0 Hz, 6H). **^{13}C NMR** (101 MHz, Chloroform-*d*) ∂ 140.8, 140.7, 140.6, 140.3, 140.0, 139.3, 137.8, 131.5, 131.2, 126.6, 126.5, 125.1, 125.0, 35.3 (C$\underline{H}_2$-Ar), 32.0 (C$\underline{H}_2$-CH_2-Ar), 31.2, 29.9, 29.8, 29.6, 29.4, 28.8, 22.7, 14.3. N.B. 13 Aromatic carbons detected rather than 15, this is assumed to be due to overlap. **MS (**MALDI-Dithranol) m/z 872.3 ($[M+H]^+$, 100%). Characterisation data was in agreement with that in the literature.[206]

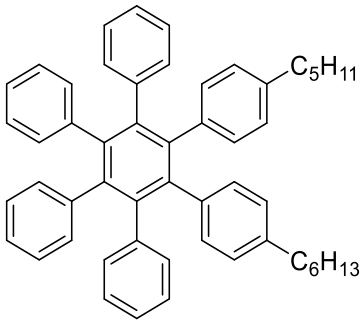

4-Hexyl-4’’-pentyl-3’,4’,5’,6’-tetraphenyl-1,1’:2’,1’’-terphenyl (**60**)

Procedure D: 1-Hexyl-4-((4-pentylphenyl)ethynyl)benzene (0.50 g, 1.50 mmol) and TPCPD (476 mg, 1.25 mmol) was dissolved in tetradecane (5 mL) and heated to 250 °C for 4 h. The reaction mixture was loaded directly onto silica gel and chromatographed (30% DCM/hexanes) to give the *title compound* as a colourless solid (703 mg, 82%).

MP 189-193 °C. **^{1}H NMR** (400 MHz, Chloroform-*d*) ∂ 6.84 (m, 20H), 6.69 (d, *J* = 8.3 Hz, 4H), 6.64 (d, *J* = 8.3 Hz, 4H), 2.35 (t, *J* = 7.3 Hz, C$\underline{H}_2$-Ar, 4H), 1.40 (m, C$\underline{H}_2$-CH_2-Ar, 4H), 1.23 (m, 6H), 1.09 (m, 4H), 0.85 (m, 6H). **^{13}C NMR** (101 MHz, Chloroform-*d*) ∂ 140.8, 140.7, 140.5, 140.3, 140.0, 139.3, 137.9, 137.5, 137.2, 131.5, 126.5, 125.0, 35.1, 31.7, 30.9, 29.4, 22.6, 14.5. N.B. 13 Aromatic carbons detected rather than 15, this is assumed to be due to overlap. **MS** (MALDI-Dithranol) m/z 712.0 ($[M+Na]^+$, 100%).

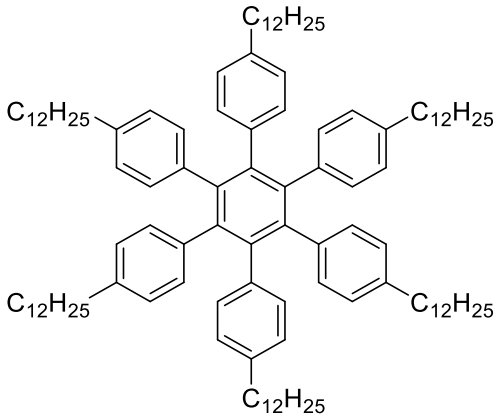

Hexakis(4-dodecylphenyl)benzene (**50**)

1,2-*Bis*-(4-dodecylphenyl)ethyne (1.00 g, 1.94 mmol) was dissolved in tetradecane (10 mL) and sparged with Ar. Cobalt carbonyl (65.0 mg, 0.19 mmol) was then added and the mixture heated to 250 °C for 4 h. The reaction mixture was cooled and the crude product loaded directly onto a silica plug and the organics extracted (10% DCM/hexanes). The resultant oil was then dissolved in diethyl ether (50 mL) and triturated with hot methanol (250 mL). The precipitated solids were then filtered and washed with methanol (3 x 50 mL) to give the *title compound* as a colourless powder (590 mg, 59%).

MP 79-84 °C. **^{1}H NMR** (400 MHz, Chloroform-*d*) ∂ 6.67 (d, *J* = 8.2 Hz, 12H), 6.62 (d, *J* = 8.2 Hz, 12H), 2.34 (t, *J* = 7.6 Hz, C$\underline{H}_2$-Ar, 12H), 1.40 (quin, *J* = 7.6 Hz, C$\underline{H}_2$-CH_2-Ar, 12H), 1.35-1.06 (m, C-H, 108H) 0.89 (t, *J* = 6.9 Hz, 18H). **^{13}C NMR** (101 MHz, Chloroform-*d*) ∂ 140.3, 138.3, 131.4, 126.4, 126.3, 35.3, 31.9, 31.2, 30.1, 29.8, 29.6, 29.5, 29.3, 29.2, 28.9, 22.7, 14.1. **MS (**MALDI-Dithranol) m/z 1545.4 ($[M+H]^+$, 100%). Characterisation data was in agreement with that in the literature.[207]

General Procedures E and F: Intramolecular oxidative cyclodehydrogenation of hexaphenylbenzenes (HPB)

General procedure E – an adaptation of a literature synthesis.[150]

HPB (1 eq.) was dissolved in DCM and the solution sparged with Ar an ice/water bath. To this solution, $FeCl_3$ (30 eq.) in nitromethane was added dropwise. The mixture was stirred for 12 h before being quenched with MeOH (30 mL). The organics were then diluted with toluene and washed with water. The crude material was then loaded onto silica gel and washed with 30% DCM/hexanes and then extracted with hot toluene. The filtrate was then dissolved in DCM and triturated with hot methanol. The precipitated solids were then filtered and washed with hot methanol.

General procedure F – an adaptation of a literature synthesis.[208]

HPB (1 eq.) was dissolved in ice-cooled DCM and sparged with Ar. DDQ (8 eq.) was then added followed by the dropwise addition of triflic acid (8 eq.). The reaction was stirred for 6 h then quenched with saturated $NaHCO_3$ solution. The organics were then diluted with $CHCl_3$, washed with water, then dried. The crude material was loaded onto silica gel and washed with 30% DCM/hexanes, then extracted with hot toluene. The filtrate was diluted with DCM and triturated with hot methanol. The precipitated solids were filtered and washed with hot methanol.

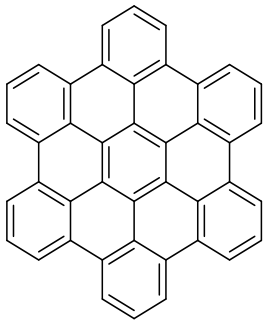

Hexabenzocoronene (**62**)

Procedure E: Hexaphenylbenzene (100 mg, 0.19 mmol) was reacted with ferric chloride (930mg, 5.74 mmol) in nitrobenzene (5 mL) to yield the desired material as yellow coloured solid (8 mg, 10%).

Procedure F: Hexaphenylbenzene (100 mg, 0.19 mmol) was reacted with DDQ (152 mg, 0.67 mmol) and triflic acid (58 μL, 0.67 mmol) to yield the desired material as an off-white coloured solid (44 mg, 45%).

The poor solubility of this compound in deuterated solvents precludes analysis by NMR. **MP** >400 °C (Lit[209] >600°C). **MS** (MALDI-Dithranol) m/z 523.1 ($[M+H]^+$, 100%). Characterisation data was in agreement with that in the literature.

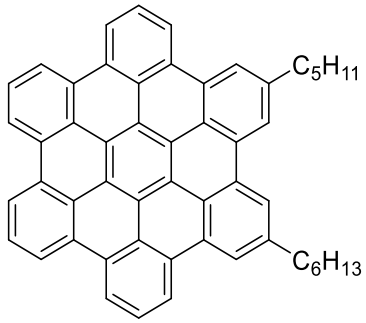

2-Hexyl-5-pentylhexabenzo[*bc,ef,hi,kl,no,qr*]coronene (**63**)

Procedure E: 4-Hexyl-4’’-pentyl-3’,4’,5’,6’-tetraphenyl-1,1’:2’,1’’-terphenyl (100 mg, 0.15 mmol) was reacted with ferric chloride (715 mg, 4.41 mmol) to yield the desired material as yellow coloured solid (7 mg, 7%).

Procedure F: 2-Hexyl-5-pentylhexabenzo[*bc,ef,hi,kl,no,qr*]coronene (100 mg, 0.15 mmol) was reacted with DDQ (263.3 mg, 1.16 mmol) to yield the desired material as a colourless solid (38 mg, 39%).

The poor solubility of this compound in deuterated solvents precludes analysis by NMR. **MP** 215-221 °C. **MS** (MALDI-Dithranol) m/z 677.1 ($[M+H]^+$, 100%).

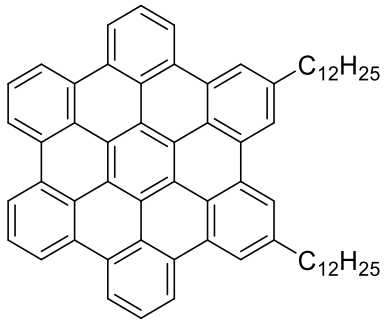

2,5-Didodecylhexabenzo[*bc*,*ef*,*hi*,*kl*,*no*,*qr*]coronene (**64**)

Procedure E: 1,2-*Bis*-(4-dodecylbenzene)-3,4,5,6-tetraphenylbenzene (100 mg, 0.12 mmol) was reacted with $FeCl_3$ (550 mg, 3.60 mmol) to yield the desired material as yellow coloured solid (11 mg, 11%).

P**rocedure F**: 1,2-*Bis*-(4-dodecylbenzene)-3,4,5,6-tetraphenylbenzene (1 g, 1.15 mmol) was reacted with DDQ (1.69 g, 8.97 mmol) to yield the desired material as a colourless solid (316 mg, 32%).

The poor solubility of this compound in deuterated solvents precludes analysis by NMR. **MP** 174-178 °C. (MALDI-Dithranol) m/z 859.1 ($[M+H]^+$, 100%). Characterisation data was in agreement with that in the literature.[206]

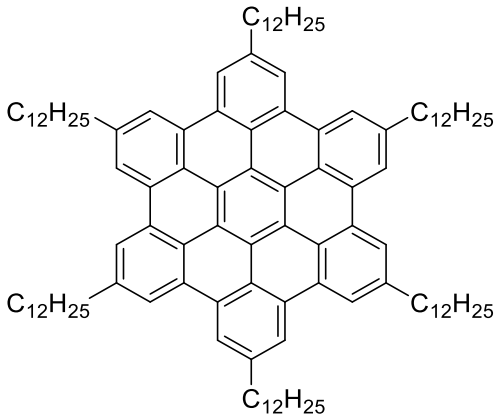

2,5,8,11,14,17-Hexadodecyldexabenzo[*bc*,*ef*,*hi*,*kl*,*no*,*qr*]coronene (**51**)

Procedure E: Hexakis(4-dodecylphenyl)benzene (500 mg, 0.32 mmol) was reacted with ferric chloride (715 mg, 4.411 mmol) to yield the desired material as yellow coloured solid (31 mg, 6%).

Procedure F: Hexakis(4-dodecylphenyl)benzene (695 mg, 0.454 mmol) was reacted with DDQ (670 mg, 2.948 mmol) to yield the desired material as a yellow coloured solid (271 mg, 35%).

MP 195-201 °C. **^{1}H NMR** (400 MHz, Chloroform-*d*) ∂ 8.44 (s, 12H), 3.03 (t, *J* = 7.6 Hz, C$\underline{H}_2$-Ar, 12H), 1.64 (quin, *J* = 7.6 Hz, C$\underline{H}_2$-CH_2-Ar, 12H), 1.52-1.19 (m, 108H) 0.88 (t, *J* = 6.9 Hz, 18H). The poor solubility of this compound in deuterated solvents precludes analysis by ^{13}C NMR. **MS** (MALDI-Dithranol) m/z 1533.0 ([M+H]$^{+}$, 100%). Characterisation data was in agreement with that in the literature.[210]

4.2.4. SYNTHESIS OF TRIBENZOPENTAPHENES: PRECURSORS AND DERIVATIVES

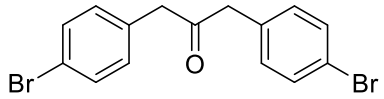

1,3-*Bis*-(4-bromophenyl)propan-2-one (**68**)

4-Bromophenylacetic acid (50.0 g, 0.23 mol), dicyclohexylcarbodiimide (15.0 g, 1.03 mol) and DMAP (12.50 g, 1.03 mol) were dissolved in DCM (1 L) and the solution sparged with Ar. The reaction mixture was stirred for 24 h at rt. Major by-product dicyclohexylurea was removed *via* vacuum filtration and the filtrate concentrated *in vacuo*. The crude product was then recrystallised from ethanol/water to give the desired product as white crystals (64.6 g, 77%).

MP 118-124 °C (Lit.[211] 116-118 °C). **^{1}H NMR** (400 MHz, Chloroform-*d*) ∂ 7.46 (d, J = 8.5 Hz, 4H), 7.03 (4H, d, J = 8.5 Hz, 4H), 3.69 (4H, s, C$\underline{H}_2$-Ar, 4H). **^{13}C NMR** (101 MHz, Chloroform-*d*) ∂ 204.2 ($\underline{C}$=O), 132.6, 131.9, 131.2, 121.3 ($\underline{C}$-Br), 48.5 ($\underline{C}H_2$-Ar). **MS** (MALDI-Dithranol) m/z 366.9 ($[M+H]^+$, 100%). Characterisation in agreement with that in the literature.[212]

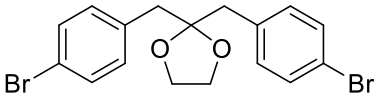

2,2-*Bis*-(4-bromobenzyl)-1,3-dioxolane (**72**)

1,3-*Bis*-(4-bromophenyl)propan-2-one (5.0 g, 13.68 mmol), ethylene glycol (0.92 mL, 16.41 mmol) and *para*-toluenesulfonic acid monohydrate (260 mg, 1.37 mmol) were dissolved in toluene (50 mL) and the solution sparged with Ar. The reaction mixture was heated at reflux for 16 h. The solvent was removed *in vacuo* and the crude material purified by recrystallisation from ethanol/water to give the *title compound* as colourless crystals (5.41 g, 96%).

MP 108-112 °C. **^{1}H NMR** (400 MHz, Chloroform-*d*) ∂ 7.40 (d, *J* = 8.3 Hz, 4H), 7.14 (d, *J* = 8.5 Hz, 4H), 3.45 (s, C$\underline{H}_2$-Ar, 4H), 2.88 (s, O-C$\underline{H}_2$-C$\underline{H}_2$-O, 4H). **^{13}C NMR** (101 MHz, Chloroform-*d*) ∂ 135.4, 132.5, 131.1, 120.5 ($\underline{C}$-Br), 110.2 ($\underline{C}$-O_2), 65.5 (O-$\underline{C}H_2$-$\underline{C}H_2$-O), 44.0 ($\underline{C}H_2$-Ar). **MS** (MALDI-Dithranol) m/z 410.0 ([M(^{79}Br + ^{79}Br]$^{+}$, 100%). Characterisation data was in agreement with that in the literature.[213]

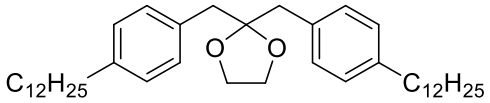

2,2-*Bis*-(4-dodecylbenzyl)-1,3-dioxolane (**73**)

Prepared by an adaptation of a literature synthesis.[214]

To a solution of magnesium (1.20 g, 49.0 mmol) in THF (25 mL) was added dropwise 4-octylbromobenzene (4.67 mL, 19.52 mmol). The mixture was stirred at 60 °C for 1 h to afford a solution of 4-dodecylphenyl magnesium bromide. To a homogeneous solution of 2,2-*bis*-(4-bromobenzyl)-1,3-dioxolane (1.0 g, 2.44 mmol) and Pd(dppf)Cl_2 (215 mg, 0.29 mmol) in THF (25 mL) was added dropwise 4-dodecylphenyl magnesium bromide in THF fresh prepared in describing above at 0 °C. The reaction mixture was heated to reflux for 2 h then quenched with methanol (50 mL). The organics were extracted with DCM and washed with water. The crude products were concentrated *in vacuo* then purified by chromatography on silica gel (5% DCM/Hexanes) to give the *title compound* as a colourless solid (937 mg, 65%).

MP 64-69 °C. **^{1}H NMR** (400 MHz, Chloroform-*d*) ∂ 7.19 (d, *J* = 8.0 Hz, 4H), 7.09 (d, *J* = 8.0 Hz, 4H), 3.45 (s, CO_2-C$\underline{H}_2$-Ar, 4H), 2.91 (s, C$\underline{H}_2$-O, 4H), 2.57 (t, *J* = 7.8 Hz, CH_2-C$\underline{H}_2$-Ar, 4H), 1.59 (4H, quin, *J* = 7.0 Hz, C$\underline{H}_2$-CH_2-Ar, 4H), 1.38-1.14 (m, 36H), 0.89 (t, *J* = 7.0 Hz, 6H). **^{13}C NMR** (101 MHz, Chloroform-*d*) ∂ 141.0, 133.8, 130.5, 127.9, 111.0 (C-O_2), 65.4 ($\underline{C}H_2$-O), 44.2 (CO_2-$\underline{C}H_2$-Ar)), 35.7 (CH_2-$\underline{C}H_2$-Ar), 32.0, 31.6, 29.8-29.3 (8C), 22.8, 14.2. **IR** $\tilde{\nu}_{max}$/cm^{-1} 2952 and 2847 (Ar C-H), 1514 (Ar C=C), 1040 (C-O). **MS** [APCI$^+$] m/z 591.6 ([M]$^+$, 100%). **HR** *m/z* (ASAP)$^+$ $C_{41}H_{67}O_2$ calcd for 591.5136, found 591.5124.

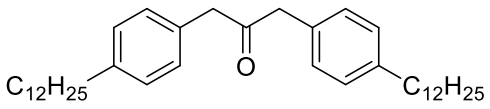

1,3-*Bis*-(4-dodecylphenyl)propan-2-one (**74**)

Prepared by an adaptation of a literature synthesis.[215]

2,2-*Bis*-(4-dodecylbenzyl)-1,3-dioxolane (10.0 g, 16.90 mmol) was stirred in sulphuric acid (30 mL, 18.4 M) at 0 °C for 5 min. The reaction was quenched by slow addition to saturated $NaHCO_3$ solution (200 mL). The solids were removed by filtration and washed with methanol (2 x 100 mL). The crude product was then extracted with DCM (200 mL) and triturated with hot methanol (300 mL). The *title compound* was then collected by filtration as a colourless solid (8.96 g, 97%).

MP 71-74 °C. **^{1}H NMR** (400 MHz, Chloroform-*d*) ∂ 7.13 (d, *J* = 8.0 Hz, 4H), 7.06 (d, *J* = 8.3 Hz, 4H), 3.68 (s, O=C-C$\underline{H}_2$-Ar, 4H), 2.57 (t, *J* = 8.0 Hz, CH_2-C$\underline{H}_2$-Ar, 4H), 1.59 (m, C$\underline{H}_2$-CH_2-Ar, 4H), 1.36-1.18 (m, 36H), 0.89 (t, *J* = 6.8 Hz, 6H). **^{13}C NMR** (101 MHz, Chloroform-*d*) ∂ 206.5 ($\underline{C}$=O), 141.6, 131.2, 129.4, 128.8, 48.7 (O=C-$\underline{C}H_2$-Ar), 35.6 (CH_2-$\underline{C}H_2$-Ar), 32.0, 31.9, 29.9-29.2 (7C), 22.7, 14.2. **MS** [APCI$^+$] m/z 546.8 ([M]$^+$, 100%). Characterisation data was in agreement with that in the literature.[216]

General procedure G: **Aldol Reaction of Functionalised *Bis*-phenylpropanone Derivatives with Benzil**

To an Ar sparged volume of ethanol was added 1,3-*bis*-(4-dodecylphenyl)propan-2-one (1 eq.), benzil (1.05 eq) and KOH (0.1 eq.). The reaction mixture was heated to reflux overnight then cooled to 0 °C. The precipitated solids were then collected *via* filtration and washed with chilled ethanol. Prepared by adaption of a literature synthesis.[216]

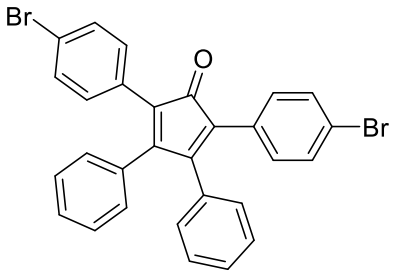

2,5-*Bis*-(4-bromophenyl)-3,4-diphenylcylopenta-2,4-dien-1-one (**69**)

Procedure G: 1,3-*Bis*-(4-bromophenyl)propan-2-one (1.0 g, 2.78 mmol) was reacted with benzil (615 mg, 2.92 mmol) and potassium hydroxide added (15 mg, 0.28 mmol) to yield the *title compound* as purple coloured crystals (1.12 g, 74%).

MP 245-251 °C (Lit.[179] 247 °C). **^{1}H NMR** (400 MHz, Chloroform-*d*) ∂ 7.38 (d, *J* = 8.5 Hz, 4H), 7.31-7.25 (m, 2H), 7.20 (t, *J* = 7.0 Hz, 4H), 7.11 (d, *J* = 8.8 Hz, 4H), 6.91 (d, *J* = 8.5 Hz, 4H). **^{13}C NMR** (101 MHz, Chloroform-*d*) ∂ 199.5 (C=O), 155.0, 132.6, 131.6, 131.3, 129.5, 129.2, 128.9, 128.2, 124.4, 122.0. **MS** (MALDI-TCNQ) 541.1 ([M(^{79}Br + ^{81}Br)-H]$^{+}$, 80%).

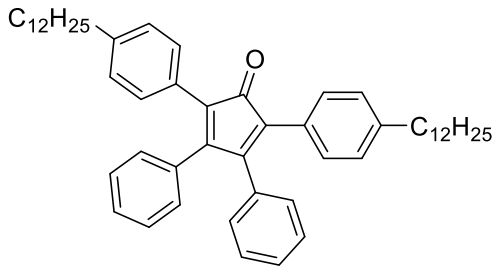

2,5-*Bis*-(4-dodecylphenyl)-3,4-diphenylcyclopenta-2,4-dien-1-one (**75**)

Procedure G: 1,3-*Bis*-(4-dodecylphenyl)propan-2-one (8.5 g, 15.55 mmol) was reacted with benzil (3.43 g, 16.33 mmol) and potassium hydroxide added (100 mg, 1.73 mmol) to yield the isolated product as purple coloured crystals (8.30 g, 74%).

MP 104-106 °C. **^{1}H NMR** (400 MHz, Chloroform-*d*) ∂ 7.23 (d, *J* = 7.3 Hz, 2H), 7.17 (m 2H), 7.05 (d, *J* = 8.3 Hz), 6.94 (m, 4H), 2.55 (t, *J* = 7.5 Hz, CH_2-C<u>H</u>$_2$-Ar, 4H), 1.59 (quin, *J* = 7.0 Hz, C<u>H</u>$_2$-CH_2-Ar, 4H), 1.36-1.21 (m, 36H), 0.89 (t, *J* = 6.8 Hz, 6H). **^{13}C NMR** (101 MHz, Chloroform-*d*) ∂ 154.0, 142.4, 131.2, 129.9, 129.3, 128.3, 128.1, 128.0, 127.9, 125.1, 35.8, 32.0, 31.3, 29.8, 29.6, 29.4, 29.2, 29.1, 22.6, 14.1. **MS** (MALDI-Dithranol) 720.9 ($[M]^+$, 100%). Characterisation data was in agreement with that in the literature.[217]

Synthesis of Tetraphenylbenzene Derivatives

General Procedure H - Diels-Alder [4+2] Cycloadditions of CPD Derivatives

Tetradecane (5 mL) was added to CPD (1 eq.) and alkyne (1.1 eq.). The reaction mixture was then heated to 250 °C for 4 h. Once cooled, the solution was loaded directly onto silica gel and purified by column chromatography. Prepared by adaption of a literature synthesis.[179]

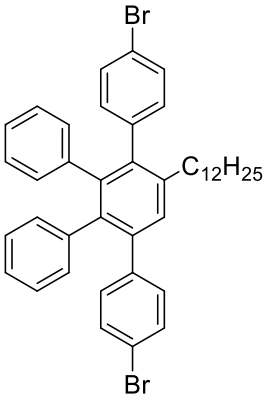

4-Bromo-4'-(4-bromophenyl)-5'-dodecyl-3'-phenyl-1,1':2',1''-terphenyl (**70**)

Procedure H: 2,5-*Bis*-(4-bromophenyl)-3,4-diphenylcylopenta-2,4-dien-1-one (750 mg, 1.38 mmol) was reacted with 1-tetradecyne (380 μL, 1.45 mmol) and chromatographed (20% DCM/hexanes) to afford the *title compound* as fine grey coloured crystals (790 mg, 81%).

MP 144-149 °C. **^{1}H NMR** (400 MHz, Chloroform-*d*) ∂ 7.35 (s, 1H), 7.31-7.25 (m, 5H), 7.00 (d, *J* = 8.3 Hz, 2H), 6.95-6.89 (m, 4H), 6.86 (m, 3H), 6.79 (m, 2H), 6.72 (m, 2H), 2.48 (t, *J* = 8.0 Hz, C$\underline{H}_2$-Ar, 2H), 1.53 (m, C$\underline{H}_2$-CH_2-Ar, 2H), 1.37-1.13 (m, 18H), 0.91 (t, *J* = 6.8 Hz, 3H) **^{13}C NMR** (101 MHz, Chloroform-*d*) ∂ 141.6, 140.9, 140.3, 140.0, 139.6, 139.5, 139.2, 137.5, 132.0, 131.5, 131.1, 130.7, 130.5, 129.9, 129.7, 127.1, 126.7, 125.7, 125.5, 120.5, 120.2, 33.7, 31.9, 31.3, 29.7, 29.6, 29.5, 29.4, 29.3, 22.7, 14.1. **IR** $\tilde{\nu}_{max}$/cm^{-1} 2919 and 2850 (Ar C-H), 1742 (C=O), 1434 (Ar C=C), 667 (C-Br). **MS** (MALDI-TCNQ) 708.7 ([M(^{79}Br + ^{81}Br)]$^{+}$, 25%). **HR** *m/z* (ASAP)$^{+}$ $C_{42}H_{45}{}^{79}Br_2$ calcd for 707.1883, found 707.1886.

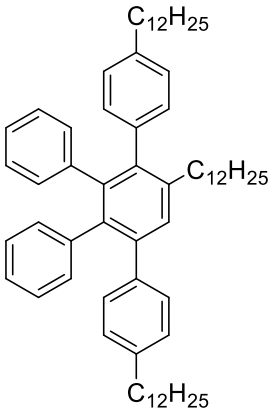

4,5’-Didodecyl-4’-(4-dodecylphenyl)-3’-phenyl-1,1’:2’,1’’-terphenyl (**71**)

Procedure H: 2,5-*Bis*-(4-dodecylphenyl)-3,4-diphenylcyclopenta-2,4-dien-1-one (2.0 g, 2.78 mmol) was reacted with 1-tetradecyne (1.36 mL, 5.55 mmol) and chromatographed (5% DCM/hexanes) to afford the *title compound* as a colourless oil. (1.83 g, 74%).

^{1}H NMR (400 MHz, Chloroform-*d*) ∂ 7.45 (s, 1H), 7.10 (d, *J* = 8.2 Hz, 2H), 7.02 (d, *J* = 8.2 Hz, 2H), 6.98 (s, 4H), 6.93 (m, 3H), 6.89-6.77 (m, 7H), 2.57 (m, C$\underline{H}_2$-Ar, 6H), 1.60 (m, 6H), 1.48-1.13 (m, 54H), 0.92 (m, 9H). **^{13}C NMR** (101 MHz, Chloroform-*d*) ∂ 141.3, 140.6, 140.3, 140.2, 140.1, 139.9, 139.2, 137.2, 137.1, 131.5, 131.1, 130.1, 129.8, 129.6, 127.3, 127.0, 126.5, 126.1, 125.0, 124.7, 41.2, 35.9, 35.2, 33.7, 31.8, 31.3, 31.0, 29.7, 28.5, 27.5, 22.5, 20.2, 19.2, 18.5, 14.07, 13.9, 11.14. **MS** (MALDI-Dithranol) 886.9 ([M)]$^{+}$, 70%). **HR** *m/z* (ASAP)$^{+}$ $C_{66}H_{95}$ calcd for 887.7428, found 887.7405.

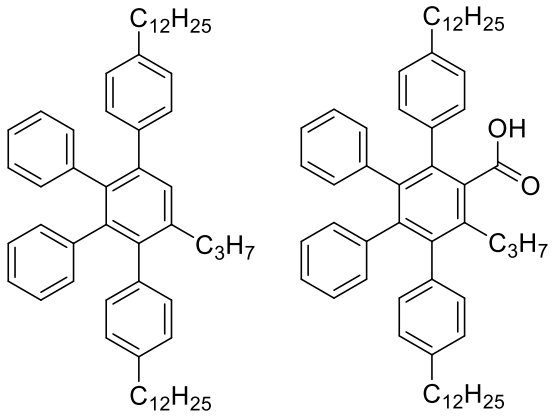

4-Dodecyl-4’-(4-dodecylphenyl)-3’-phenyl-5’-propyl-1,1’:2’,1’’-terphenyl (**78**) and 4’-Butyl-4’’-dodecyl-5’-(4-dodecylphenyl)-6’-phenyl-[1,1’:2’,1’-terphenyl]-3’-carboxylic acid (**77**)

Procedure H: 2,5-*Bis*-(4-dodecylphenyl)-3,4-diphenylcyclopenta-2,4-dien-1-one (3.0 g, 4.16 mmol) was reacted with hex-2-ynoic acid (930 mg, 8.33 mmol) and the crude products purified by column chromatography on silica gel (15% DCM/hexanes) to afford 5’-butyl-4-dodecyl-4’-(4-dodecylphenyl)-3’-phenyl-1,1’:2’,1’’-terphenyl as a colourless oil (1.86 g, 55%) and 4’-butyl-4’’-dodecyl-5’-(4-dodecylphenyl)-6’-phenyl-[1,1’:2’,1’-terphenyl]-3’-carboxylic acid as a yellow coloured solid (1.01 g, 30%) in consecutive fractions.

4-Dodecyl-4’-(4-dodecylphenyl)-3’-phenyl-5’-propyl-1,1’:2’,1’’-terphenyl:

^{1}H NMR (400 MHz, Chloroform-*d*) ∂ 7.06 (d, *J* = 8.3 Hz, 2H), 6.99 (d, *J* = 8.3 Hz, 2H), 6.95 (s, 4H), 6.91-6.85 (m, 3H), 6.83-6.79 (m, 5H), 6.75-6.70 (m, 2H), 2.54-2.50 (m, C$\underline{H}_2$-Ar, 6H), 1.71-1.65 (m, 6H), 1.40-1.09 (m, 38H), 0.91-0.84 (m, 9H). **^{13}C NMR** (101 MHz, Chloroform-*d*) ∂ 141.6, 140.78, 140.6, 140.5, 140.4, 140.2, 140.0, 139.4, 137.5, 137.4, 131.7, 131.3, 130.3, 130.0, 129.7, 127.6, 127.3, 126.7, 126.4, 125.2, 124.9, 41.4, 36.1, 36.0, 35.5, 35.5, 34.1, 31.9, 31.6, 31.3, 31.2, 29.7, 29.6, 29.5, 29.4, 29.3, 29.1, 29.0, 27.7, 24.4, 22.7, 22.7, 22.6, 22.3, 20.5, 19.5, 18.8, 14.3, 14.1, 11.4. **MS** (MALDI-TCNQ) 761.2 ($[M+H]^+$, 100%). **HRMS** *m/z* $(HESI)^+$ $C_{55}H_{77}$ calcd for 761.6020, found 761.5999.

4’-Butyl-4’’-dodecyl-5’-(4-dodecylphenyl)-6’-phenyl-[1,1’:2’,1’-terphenyl]-3’-carboxylic acid:

MP 156-161 °C. **^{1}H NMR** (400 MHz, Chloroform-*d*) ∂ 7.28 (s, 1H), 7.04 (d, *J* = 8.2 Hz, 2H), 6.96 (s, 4H), 6.92 (d, *J* = 8.2 Hz, 2H), 6.86-6.78 (m, 6H), 6.77-6.71 (m, 4H), 2.52 (m, C$\underline{H}_2$-Ar, 6H), 1.53 (m, 6H), 1.36-1.13 (m, 38H), 0.90 (t, *J* = 6.9 Hz, 6H), 0.73 (t, *J* = 7.6 Hz, 3H). **^{13}C NMR** (101 MHz, Chloroform-*d*) ∂ 173.0 (C=O), 142.9, 141.2, 141.1, 140.6, 140.2, 139.6,

139.0, 137.8, 136.8, 136.7, 136.3, 133.1, 131.3, 130.9, 130.2, 130.1, 127.3, 127.3, 126.5, 126.4, 125.3, 125.2, 35.5, 35.4, 34.2, 31.9, 31.1, 31.1, 29.7, 29.7, 29.7, 29.6, 29.5, 29.4, 29.1, 28.9, 24.6, 22.7, 14.6, 14.1. **IR** $\tilde{\nu}_{max}/cm^{-1}$ 2919 and 2849 (Ar C-H), 1704 (C=O), 1409 (Ar C=C). **MS** (MALDI-TCNQ) 804.6 $([M)]^+$, 100%).

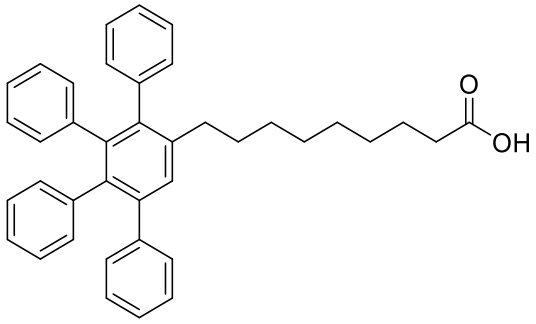

9-(3',6'-Diphenyl-[1,1':2',1'-terphenyl]-4'-yl)nonanoic acid (**65**)

Procedure H: TPCPD (500 mg, 1.30 mmol) was reacted with undec-10-ynoic acid (250 mg, 1.43 mmol) and the crude products purified by column chromatography on silica gel (gradient system 15-50% DCM/hexanes) to afford the *title compound* as colourless solid (530 mg, 76%).

MP 174 °C. **^{1}H NMR** (400 MHz, Chloroform-*d*) ∂ 7.41 (s, 1H), 7.21-7.02 (m, 10H), 6.92-6.74 (m, 10H), 2.50 (t, *J* = 8.0 Hz, 2H), 2.33 (t, *J* = 7.5 Hz, 2H), 1.67-1.48 (m, 4H), 1.38-1.12 (m, 4H), 0.91 (t, *J* = 6.8 Hz, 6H). **^{13}C NMR** (101 MHz, Chloroform-*d*) ∂ 179.2 (C=O), 142.2, 141.4, 140.6, 140.5, 140.3, 140.1, 137.5, 131.7, 131.3, 130.5, 130.0, 127.5, 127.2, 126.8, 126.5, 126.1, 126.0, 125.4, 125.1, 33.9, 33.4, 31.3, 31.0, 29.6, 29.1, 24.7. **IR** $\tilde{\nu}_{max}/cm^{-1}$ 3695 (broad O-H), 2951 and 2826 (Ar C-H), 1685 (C=O), 1345 (Ar C=C). **MS** [MALDI-TCNQ] 539.4 $([M+H]^+$, 100%). **HRMS** *m/z* $(ASAP)^+$ $C_{39}H_{39}O_2$ calcd for 539.2945, found 539.2933.

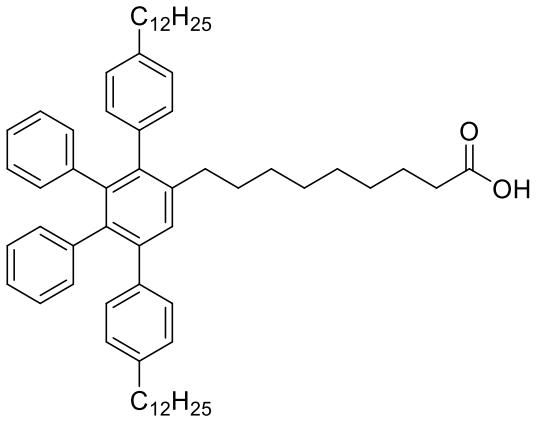

9-(3',6'-*Bis*-(4-dodecylphenyl)-[1,1':2',1''-terphenyl]-4'-yl)nonanoic acid (**76**)

Procedure H: 2,5-*Bis*-(4-dodecylphenyl)-3,4-diphenylcyclopenta-2,4-dien-1-one (450 mg, 0.62 mmol) was reacted with undec-10-ynoic acid (119 mg, 0.66 mmol) and the crude products purified by column chromatography on silica gel (gradient system 15-50% DCM/hexanes) to afford the *title compound* as an orange coloured oil (461 mg, 85%).

^{1}H NMR (400 MHz, Chloroform-*d*) ∂ 7.41 (s, 1H), 7.06 (d, *J* = 8.2 Hz, 2H), 6.98 (d, *J* = 8.3 Hz, 2H), 6.95 (s, 4H), 6.90 (m, 3H), 6.83 (m, 5H), 6.76 (m, 2H), 2.53 (m, C$\underline{H}_2$-Ar, 6H), 2.35 (t, C$\underline{H}_2$-C=O, 2H), 1.67-1.49 (m, 8H), 1.38-1.15 (m, 45H), 0.91 (t, *J* = 6.8 Hz, 6H). **^{13}C NMR** (101 MHz, Chloroform-*d*) ∂ 179.7 ($\underline{C}$=O), 141.5, 140.8, 140.6, 140.5, 140.1, 139.4, 137.5-137.3, 131.7, 131.3, 130.2, 129.9, 129.8, 127.5, 127.2, 126.7, 126.3, 125.2, 124.9, 35.5, 35.4, 34.0, 33.8, 31.9, 31.3, 31.2, 29.8, 29.2, 29.1, 28.8, 24.6, 22.6, 14.12. **IR** $\tilde{\nu}_{max}$/cm^{-1} 3695 (broad O-H), 2951 and 2826 (Ar C-H), 1685 (C=O), 1345 (Ar C=C). **MS** [MALDI-Dithranol] 874.9 ([M]$^{+}$, 100%). **HRMS** *m/z* (ASAP)$^{+}$ $C_{63}H_{87}O_2$ calcd for 875.6701, found 875.6690.

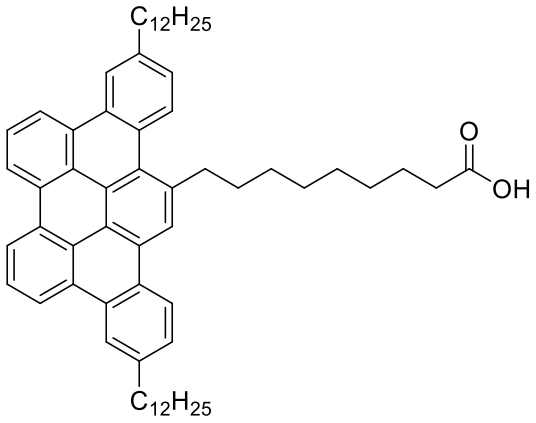

9-(3,12-Didodecyltribenzo[*fg,ij,rst*]pentaphen-15-ylnonanoic acid (**79**)

To a sparged, 0 °C solution of **76** (600 mg, 0.69 mmol) in DCM (50 mL) was added DDQ (545 mg, 2.80 mmol) and the mixture stirred for 15 min. Triflic acid (210 μL, 2.80 mmol) was then added and the reaction allowed to warm to rt over 6 h, then quenched by the addition of sat. $NaHCO_3$ solution (100 mL). The organic layer was separated, washed with water (2 x 100 mL), dried ($MgSO_4$), then concentrated *in vacuo*. The crude product was concentrated *in vacuo* and purified by column chromatography on silica gel then (3% methanol/DCM). Concentration of these extracts *in vacuo* and further purification by fractional recrystallisation (DCM/methanol) afforded the *title compound* as a microcrystalline, colourless solid (53 mg, 9%).

MP 186-189 °C. **^{1}H NMR** (400 MHz, Chloroform-*d*) ∂ 10.46 (broad s, HO-C=O, 1H) 8.93-8.85 (m, 5H), 8.75 (d, *J* = 8.5 Hz, 2H), 8.59-8.53 (m, 2H), 8.47 (d, *J* = 8.3 Hz, 1H), 8.00 (t, *J* = 7.8 Hz, 1H) , 7.99 (t, *J* = 8.0 Hz, 1H) ,7.57 (d, *J* = 8.3 Hz, 1H), 7.46 (d, *J* = 8.3 Hz, 1H), 3.63 (t, *J* = 8.0 Hz, CH_2-C=O, 2H), 2.90 (t, *J* = 7.8 Hz, CH_2-Ar, 4H), 2.34 (t, *J* = 7.3 Hz, CH_2-Ar, 2H), 2.09-2.00 (m, 2H), 1.86-1.79 (m, 4H), 1.66-1.60 (m, 3H), 1.55-1.16 (m, 44H), 0.88 (t, *J* = 6.5 Hz, 6H). **^{13}C NMR** (101 MHz, Chloroform-*d*) ∂ 179.7 (C=O), 141.5, 140.8, 140.6, 140.5, 140.1, 139.4, 137.5, 137.3, 131.7, 131.3, 130.2, 129.9, 129.8, 127.5, 127.2, 126.7, 126.3, 125.2, 124.9, 35.5, 35.4, 34.0, 33.8, 31.9, 31.3, 31.2, 29.8, 29.2, 29.1, 28.8, 24.6, 22.6, 14.1. **IR** $\tilde{\nu}_{max}/cm^{-1}$ 2918 and 2848 (Ar C-H), 1705 (C=O). **MS** (MALDI-TCNQ) m/z 868.8 ($[M]^+$, 80%). **HRMS** *m/z* (ASAP$^-$) $C_{63}H_{79}O_2$ calcd for 867.6086, found 867.6067.

4.2.5. GEOLOGICALLY-INSPIRED ASPHALTENE MODEL PRECURSORS

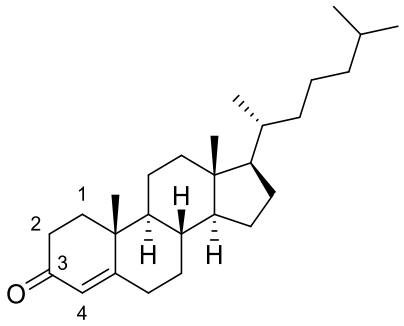

4-Cholesten-3-one (**81**)

Cholesterol (1.00 g, 2.58 mmol) and then aluminium isopropoxide (1.06 g, 5.19 mmol) was added to acetone (50 mL) which had previously been sparged with argon. The reaction mixture was then heated to 80 °C for 72 h. On cooling to ambient temperature the reaction mixture was filtered through Celite© with the aid of DCM and the filtrate washed with water and then brine. The combined organic extracts were dried ($MgSO_4$) and concentrated *in vacuo*. Recrystallisation of the residue from methanol afforded the *title compound* as a colourless solid (0.77 g, 78%).

MP 84-85 °C (Lit.[218] 82-84 °C). **^{1}H NMR** (500 MHz, Chloroform-*d*) ∂ 5.73 (s, C_4H, 1H), 2.47 (dd, *J* = 17.7, 4.8 Hz, C_2H, 1H), 2.41 (dd, *J* = 14.3, 5.2 Hz, C_1H, 1H), 1.65-0.95 (m, 22H), 0.93 (d, *J* = 6.6 Hz, 3H), 0.89 (d, *J* = 6.6 Hz, 3H), 0.88 (d, *J* = 6.6 Hz, 3H), 0.73 (s, 3H). **^{13}C NMR** (101 MHz, Chloroform-*d*) ∂ 173.5 (C5), 124.6 (C4), 117.8 (C3). **MS** (APCI) m/z 385.5 ($[M+H]^+$, 100%). Characterisation data was in agreement with that in the literature.[219]

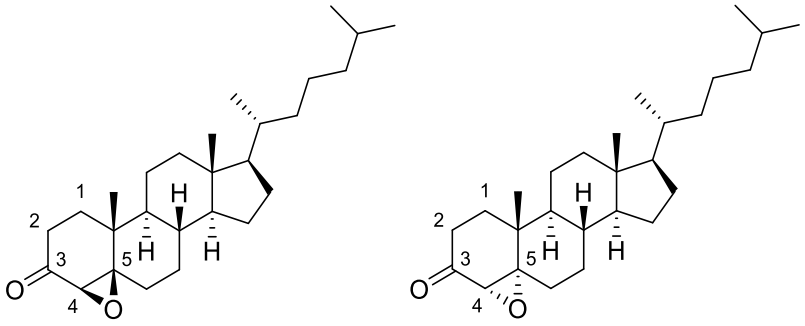

4β,5-Epoxy-5β-cholest-3-one (**82b**) and 4α,5-Epoxy-5α-cholest-3-one (**82a**)

Cholest-4-en-3-one (1 g, 2.60 mmol) was dissolved in methanol (20 mL) and the solution cooled to 0 °C. Hydrogen peroxide (0.78 mL, 30%) was added dropwise and the solution stirred for 15 min. Sodium hydroxide solution (0.22 mL, 10%) was then added dropwise. The reaction was then allowed to reach room temperature and stirred for 48 h. The reaction mixture was diluted with water (100 mL) and the organics extracted with ethyl acetate (100 mL). The combined organic extracts were dried ($MgSO_4$). The crude product was then purified by chromatography on silica gel (5% EtOAc/Hexane) to give 4β,5-Epoxy-5β-cholest-3-one (0.51 g, 51%) and 4α,5-Epoxy-5α-cholest-3-one (0.04 g, 4 %) consecutively as colourless solids.

4β,5-Epoxy-5β-cholest-3-one, **82b**:

^{1}H NMR (500 MHz, Chloroform-*d*) ∂ 2.98 (s, C_4H, 1H), 2.19 (m, 3H), 2.02 (dt, *J* = 12.6 Hz, 3.47, C_2H, 1H), 1.85 (m, 3H), 1.65-0.95 (m, 22H), 1.16 (s, 3H), 0.91 (d, *J* = 6.6 Hz, 3H), 0.70 (s, 3H).

4α,5-Epoxy-5α-cholest-3-one, **82a:**

MP 118-120 °C. **^{1}H NMR** (500 MHz, Chloroform-*d*) ∂ 3.02 (s, C_4H, 1H), 2.26-2.20 (m, 3H), 2.08 (dt, *J* = 12.6, 3.5 Hz, C_2H, 1H), 1.94-1.88 (m, 3H), 1.67-0.96 (m, 22H), 1.18 (s, 3H), 0.94 (d, *J* = 6.6 Hz, 3H), 0.71 (s, 3H).

4β,5β-epoxide and 4α,5α-epoxide:

MP 118-120 °C (Lit.[220] 119-121 °C). **^{13}C NMR** (101 MHz, Chloroform-*d*) ∂ 200.9 (C3), 72.9 (C5), 64.8 (C4). **MS** (APCI) m/z 487.4 ($[M+Na]^+$, 100%).

Characterisation data was in agreement with that in the literature.[188]

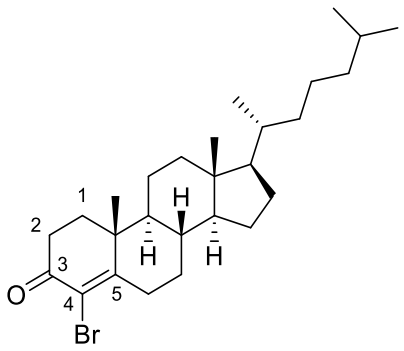

4-Bromocholest-4-en-3-one (**83**)

Prepared by an adaptation of a literature synthesis[188]

To a solution of 4α,5-epoxy-5α-cholest-3-one (50 mg, 0.125 mmol) in acetone (5 mL), pre-cooled in an ice/water bath, aqueous hydrogen bromide solution (16%, 0.125 mL) was added dropwise and the solution stirred for 4 h. The reaction mixture was then diluted with EtOAc (100 mL) and washed with water (100 mL). The organics were then dried ($MgSO_4$) and purified by column chromatography on silica gel (5% EtOAc/hexanes) to afford the *title compound* as a yellow coloured solid (24 mg, 41%).

MP 113-116 °C (Lit.[188] 112-114 °C). **^{1}H NMR** (400 MHz, Chloroform-*d*) ∂ 3.27 (dt, *J* = 15.1, 2.8 Hz, C_2H, 1H), 2.26 (td, *J* = 14.8, 5.4 Hz, 1H), 2.05-0.97 (m, 24H), 1.22 (s, 3H), 0.91 (d, *J* = 6.6 Hz, 3H), 0.90-0.84 (m, 9H), 0.72 (s, 3H). **^{13}C NMR** (101 MHz, Chloroform-*d*) 190.7 (C3), 168.3 (C4), 121.7 (C5). **MS** (MALDI-Dithranol) m/z 463.2 ($[M+H]^+$, 100%). Characterisation data was in agreement with that in the literature.[186]

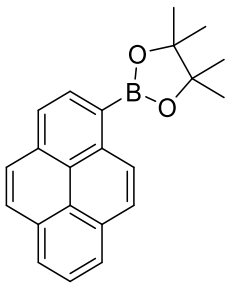

4,4,5,5-Tetramethyl-2-(pyren-1-yl)-1,3,2-dioxaborolane (**84**)

1-Bromopyrene (500.0 mg, 1.778 mmol), *bis*(pinnacolato)diboron (629.9 mg, 1.778 mmol), KOAc (383.8 mg, 0.132 mmol) and THF (20 mL) were added to a reaction vial and the reaction mixture sparged with argon. Pd(dppf)Cl_2 (96.6 mg, 0.132 mmol) was then added and the vessel sealed. The solution was heated to reflux for 4 h, then cooled. Insoluble material was removed by filtration through Celite© (50% DCM/hexanes) and the filtrate concentrated *in vacuo*.Chromatography of the residue (20% EtOAc/hexanes) afforded the *title compound* (420 mg, 71%), as a colourless solid, followed by a minor quantity of 1,1'-bipyrene as a minor by-product (40 mg, 16%).

4,4,5,5-Tetramethyl-2-(pyren-1-yl)-1,3,2-dioxaborolane:

MP 204-210 °C. **^{1}H NMR** (400 MHz, Chloroform-*d*) ∂ 9.11 (d, *J* = 9.29 Hz, 1H), 7.53 (d, *J* = 7.5 Hz, 1H), 8.26-7.99 (m, 7H), 1.52 (s, 12H). **^{13}C NMR** (101 MHz, Chloroform-*d*) 136.5, 133.9, 133.5, 131.2, 130.8, 128.7, 128.1, 127.8, 127.5, 127.4, 125.7, 125.4, 125.2, 124.9, 124.7, 124.1, 83.2, 24.8. **MS (**MALDI-Dithranol) m/z 246.1 ($[M]^+$, 40%). Characterisation data was in agreement with that in the literature.[221]

1,1'-Bipyrene (**85**):

MP 325-331 °C (Lit.[222] 327-328 °C). **^{1}H NMR** (400 MHz, Chloroform-*d*) ∂ 8.37 (d, *J* = 7.57 Hz, 2H), 8.30-8.16 (m, 10H), 8.04 (t, *J* = 7.24 Hz, 2H), 7.87 (d, *J* = 7.53 Hz, 2H), 7.67 (d, *J* = 7.57 Hz, 2H). **^{13}C NMR** (101 MHz, Chloroform-*d*) 136.7, 135.8, 135.1, 134.6, 134.0, 133.3, 132.1, 130.7, 128.6, 124.5. **MS (**MALDI-Dithranol) m/z 402.4 ($[M]^+$, 65%). Characterisation data was in agreement with that in the literature.[223]

5. APPENDIX

5.1. ICAM 15 WORK PACKAGES

Work Package 1 (WP1) – Reference Materials and Properties

Pure compounds representing asphaltenes in terms of molecular shape, size, functionality and aggregation/adhesion behaviours are to be specifically prepared and characterised. Novel molecular cores are to be synthesised and derivatised to provide an array of new model materials which are expected to be excellent asphaltene models. These molecular cores' function utility allows the inclusion of all chemical groups of interest to the programme. They can be readily modified to give a range of large molecular weights, variable solubility and site specific polarity.

Work Package 2 (WP2) – Understanding Deposition of Carbonaceous Materials in Fluids and at the Solid/Liquid Interface

This experimental work aims to gain a key understanding of the nature of carbonaceous nucleation, aggregate growth and deposition from observation at both laboratory and near-operation conditions of temperature and pressure. It will cover the interaction of model compounds/model fluids and crude oils with metal, metal oxide and metal sulphide surfaces. This will build upon the understanding of intermolecular interactions and consider carbonaceous deposits at the solid-fluid interface. These deposits can either; (a) nucleate in bulk fluids and deposit at the solid-fluid interface; or (b) nucleate and grow at the interface; or (c) both. To understand the mechanisms of deposition at the metal-fluid interface a number of approaches will be pursued. The nature of interactions and binding energy between carbonaceous compounds and various surfaces will be examined with scanning probe microscopy, light spectroscopies, calorimetry, neutron (SANS, NR), X-ray scattering, sum frequency generation spectroscopy (SFG) and langmuir adsorption isotherms. A quartz crystal microbalance (QCM) will be employed to investigate how surface condition, flow rate, pressure, and temperature affect deposition rate. The distribution of deposit growth will be studied using high resolution imaging methods. *Ex-situ* chemical methods using a multi-technique forensic approach aim to identify relevant chemical parameters in the formation of carbonaceous deposits using a 'top-down' deconstruction approach.

A designated pressure cell for QCM will be designed and commissioned that will allow investigation of adsorption kinetics, adsorption amount and the viscoelastic property of the adsorbed layers at pressure and temperatures and on surfaces relevant to BP operations. The influence and effectiveness of surface active additives and dispersants will also be investigated. Model compounds prepared will be analysed. The effect of surface oxide and sulphide will be examined in parallel, where the effect of surface polarity, wettability and surface texture of deposition will be studied. Deposition will take place on model surfaces including metal surfaces gold, iron, titanium, nickel and chromium, and on oxide surfaces, such as aluminium oxide, zirconium oxide, and textured oxide surfaces.

Work Package 2.2 (WP 2.2) - Molecular Interactions between Carbonaceous Materials and Surfaces

These experiments focus on carbonaceous material adsorption at interfaces. Sum frequency generation (SFG), calorimetry and neutron reflectivity (NR) is used to monitor adsorption, the adsorbed layer structure (single molecules or aggregates), molecular orientation and behaviour with time. The nature of the chemical group binding to the surface will be investigated, requiring band identification of SFG, Reflection-Absorption IR Spectroscopy (RAIRS), Attenuated Total Reflectance (ATR) spectroscopy and related spectroscopic methods. The strength of binding to surfaces is obtained both by adsorption isotherms at different temperature and by direct measurement of enthalpies of adsorption (exchange) using calorimetry. The mechanism and effectiveness of potential deposition inhibitors are to be investigated.

Work Package 2.3 (WP 2.3) - Surface and Deposit Characterisation at the Nanoscale

Deposition of real asphaltenes and model molecules upon surfaces are to be analysed through Optical Microscopy, scanning electron microscopy (SEM), environmental scanning electron microscopy (ESEM), transmission electron microscopy (TEM) and scanning probe microscopy (both atom-force microscopy (AFM) and scanning tunnelling microscopy (STM)). High-resolution images of the deposits and surfaces gain morphological information and will assess the efficacy of surface modification in influencing deposit formation. This will be performed for a variety of different surface conditions in a ‘post-mortem’ approach. FE-SEM and Titan aberration-corrected TEM is also utilised. The output from this part of the programme together with the detailed chemical analysis in work packages feeds into the novel surfaces programme to inform it of relevant surface design parameters.

Work Package 2.4 (WP 2.4) - Chemical Compositional Analysis of Deposits Formed in Flow Cells

Focuses on analytical techniques that provide most information about the chemical composition of surface deposits. The work will focus on field samples and deposits of pure compounds prepared by WS1. Applying a multi-technique forensic approach, this work will aim to identify relevant chemical parameters in the formation of carbonaceous deposits using a 'top-down' deconstruction, thereby linking also with work performed in work streams WS1 and WS3. Analytical techniques include Raman, X-ray diffraction, fluorescence/luminescence and UV-vis techniques, surface analysis techniques (XPS, NEXAFS, SIMS) as well as optical and electron microscopies. 2D imaging, radiography, tomographic imaging or trace element analysis are also considered.

With a conclusion drawn upon the most successful analytical techniques in providing information about the chemical state of deposits and interfaces, these practices will be applied in-situ in small scale laboratory simulation experiments and examine the chemical nature of deposits formed on metal coupons, and moving/oscillating elements due to exposure to selected field liquids (oils) and model liquids as a function of flow and pressure. Transfer cells set up to permit quasi in-situ surface analysis use environmental cells coupled to the analysis chambers to maintain the integrity and solvation of deposits. This work will link closely to work performed in WP1 and inform the 'bottom-up' approach with model systems of comparatively lower complexity, providing a constructive 'reality check' on the relevance of parameters investigated.

Work Package 3 (WP 3) – Novel Surfaces Preparation and Surface Characterisation

A fundamental understanding and modelling of fluid-surface interaction through fabrication of surfaces with specific functionalities and morphologies that enable systematic inquiry of surface interaction. Surfaces with specific polarity, potential or hydrophobicity/philicity will be created on typical structural alloy coupons and customised substrates for integration into the QCM studies detailed in WS2. While the rate of deposition will be monitored via QCM, the specific topology of deposits and the influence of surface structure and chemistry will be analysed via in-situ scanning probe microscopies. Insight gained from these characterisation efforts, including characterisation of binding energies between deposits and various surfaces will be used to develop novel protective coating concepts for up-stream components.

Materials and surfaces displaying functionalities/textures of interest will be identified and fabricated and characterised. Novel and industrial surfaces of relevance to the problem of carbonaceous deposits will be analysed by AFM. High-resolution real-time imaging will observe the liquid-solid interface to observe the influence of surface morphology upon deposit growth. Real asphaltenes and model compounds from WP1 are to be used. A liquid flow cell will also be used to investigate the effects of temperature impacts this phenomena.

Work Package 4 (WP 4) - Molecular Modelling of Asphaltene Aggregation and Deposition on Surfaces

WP 4 will explore the fundamental molecular-level aspects of asphaltene aggregation and deposition of surfaces where the molecular structure/composition, size and energy differences with respect to the solvent are the driving force for self-assembly and, in some cases, posterior precipitation from crude oils and build-up on surfaces. The modelling will span detailed atomistic-level to coarse grained approach that allows the study of large collectives of molecules and mixtures that will allow for the study of deposition mechanism onto surfaces.

A representative synthetic reservoir fluid will be studied by means of molecular simulations spanning multiple length and timescales of both the fluid phase aggregation and the impact of surfaces forces on the ultimate deposition. The pressure and temperature condition will correspond to the situation of interest for reservoirs (high pressure, moderate temperature). The effect of relevant surfaces (carbon steel, iron sulphide) will be considered and focus on the mesoscopic scale (coarse grained modelling) to understand the kinetics of carbonaceous deposit formation.

5.2. ^{1}H AND ^{13}C SPECTRA OF KEY COMPOUNDS

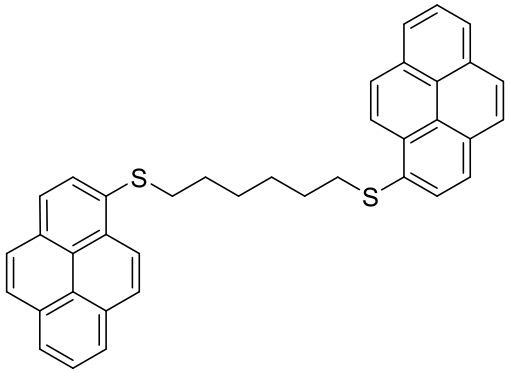

1,6-*Bis*-(pyren-1-ylthio)hexane (**32**)

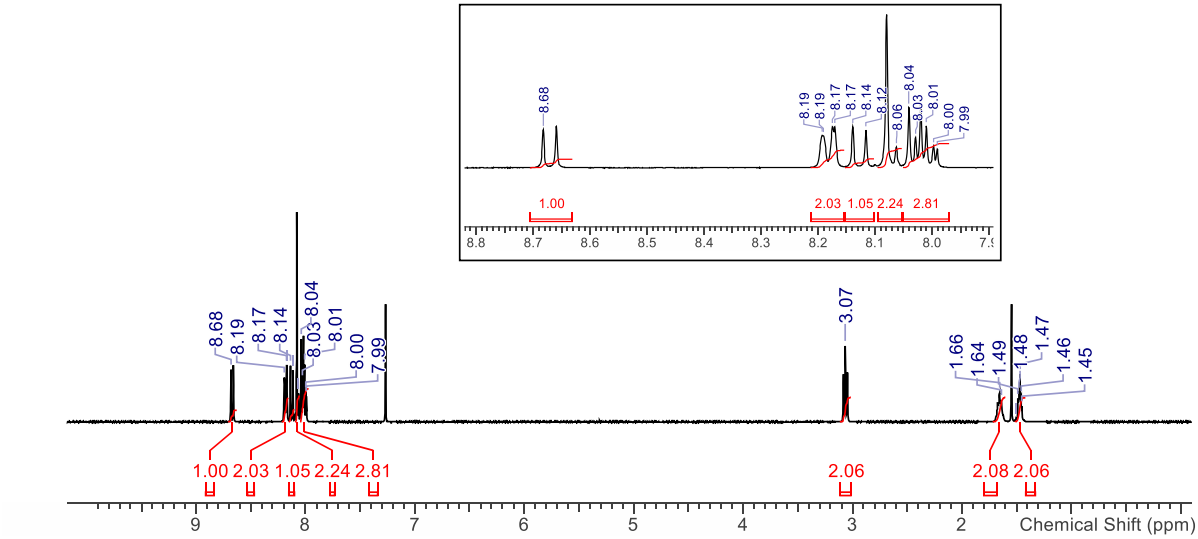

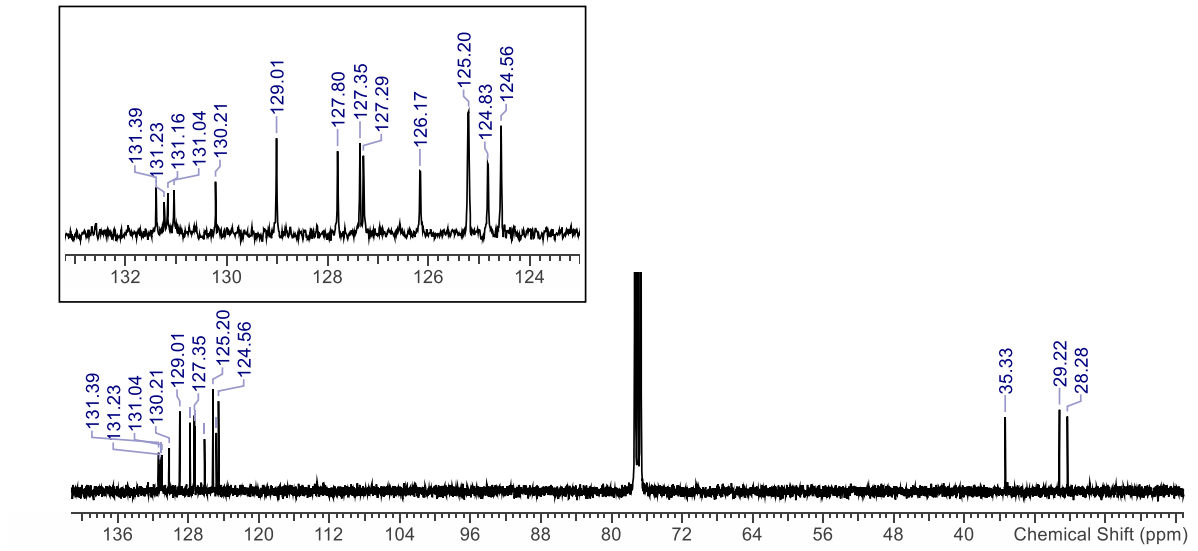

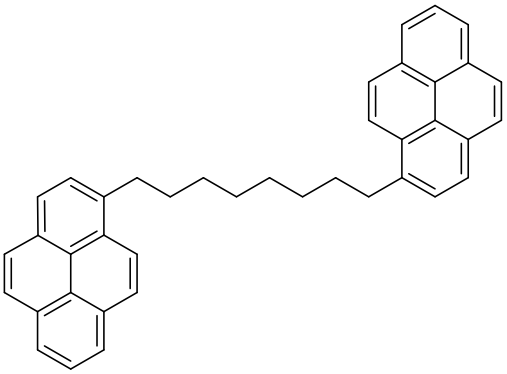

1,8-Di(pyren-1-yl)octane (**38**)

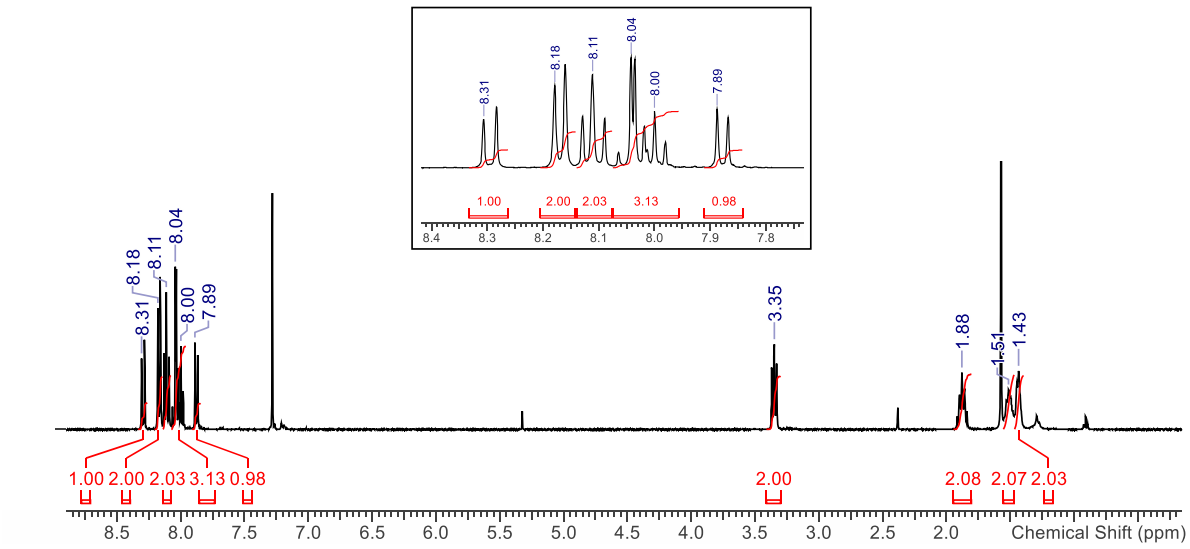

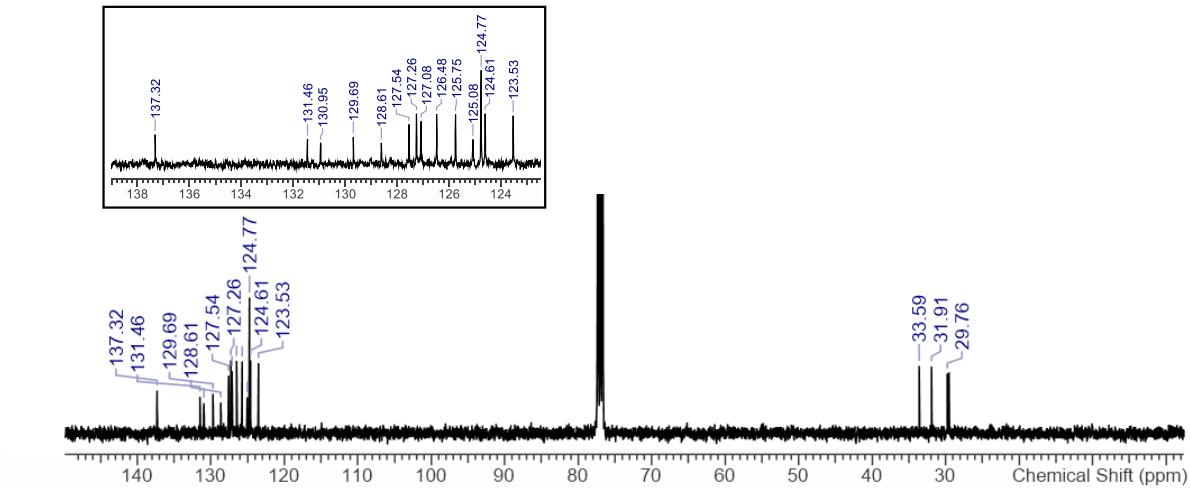

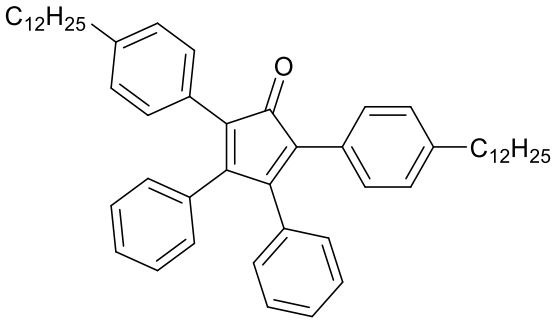

2,5-*Bis*-(4-dodecylphenyl)-3,4-diphenylcyclopenta-2,4-dien-1-one (**75**)

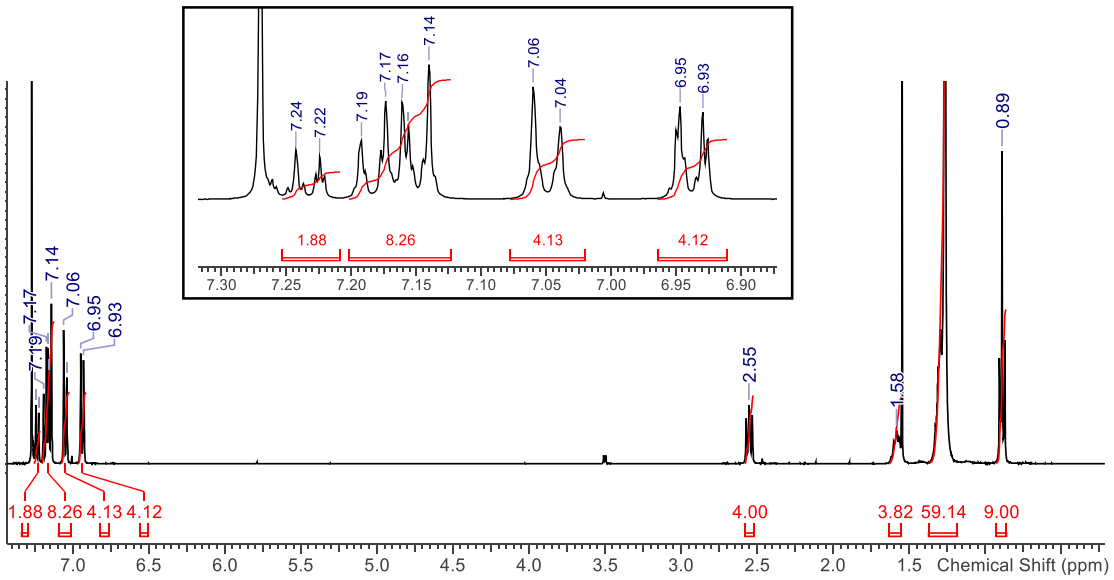

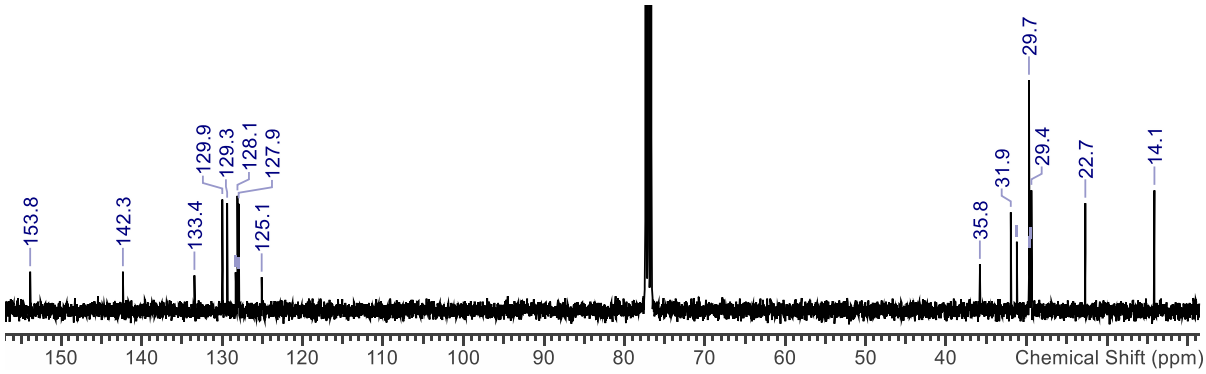

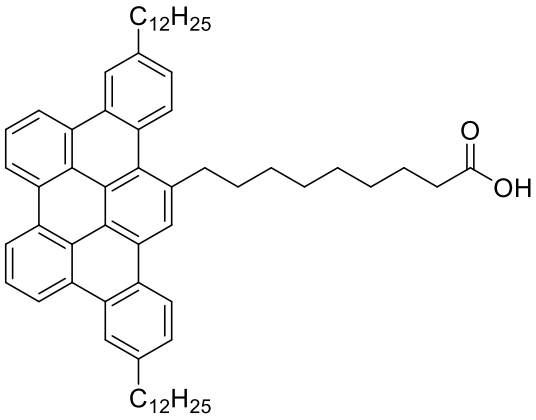

9-(3,12-didodecyltribenzo[*fg*,*ij*,*rst*]pentaphenyl-15-yl)nonanoic acid (**79**)

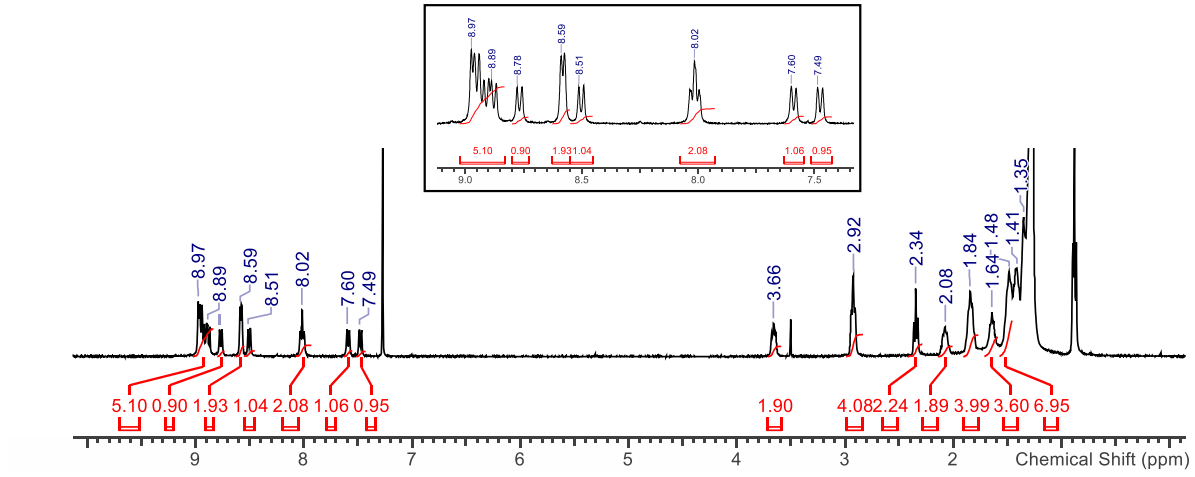

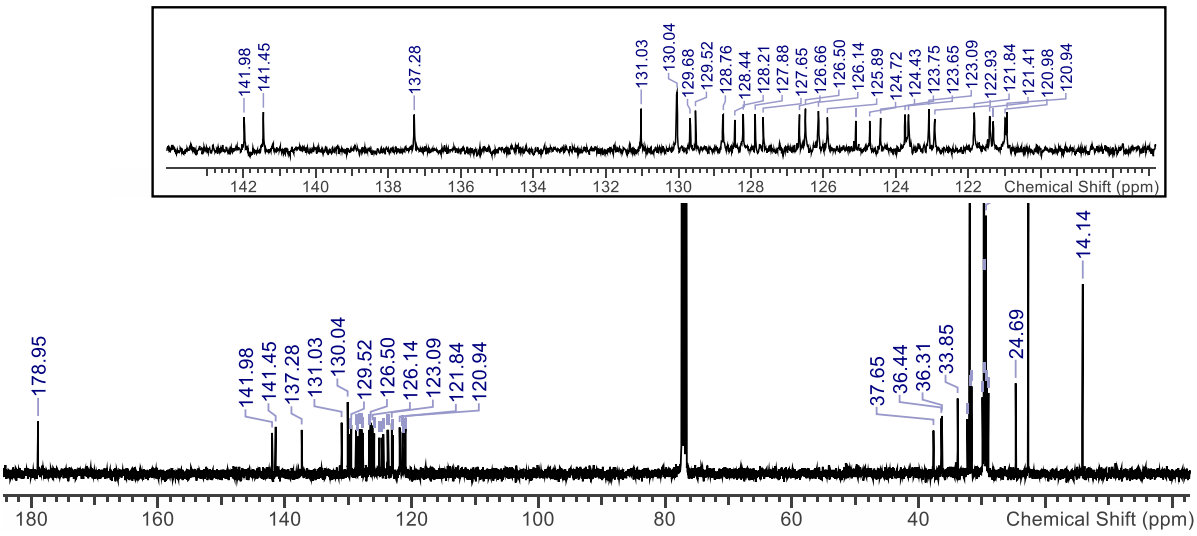

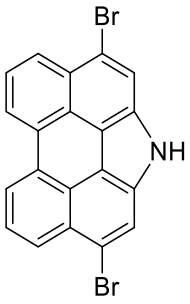

3,10-Dibromo-1H-phenanthro[1,10,9,8-cdefg]carbazole (**46**)

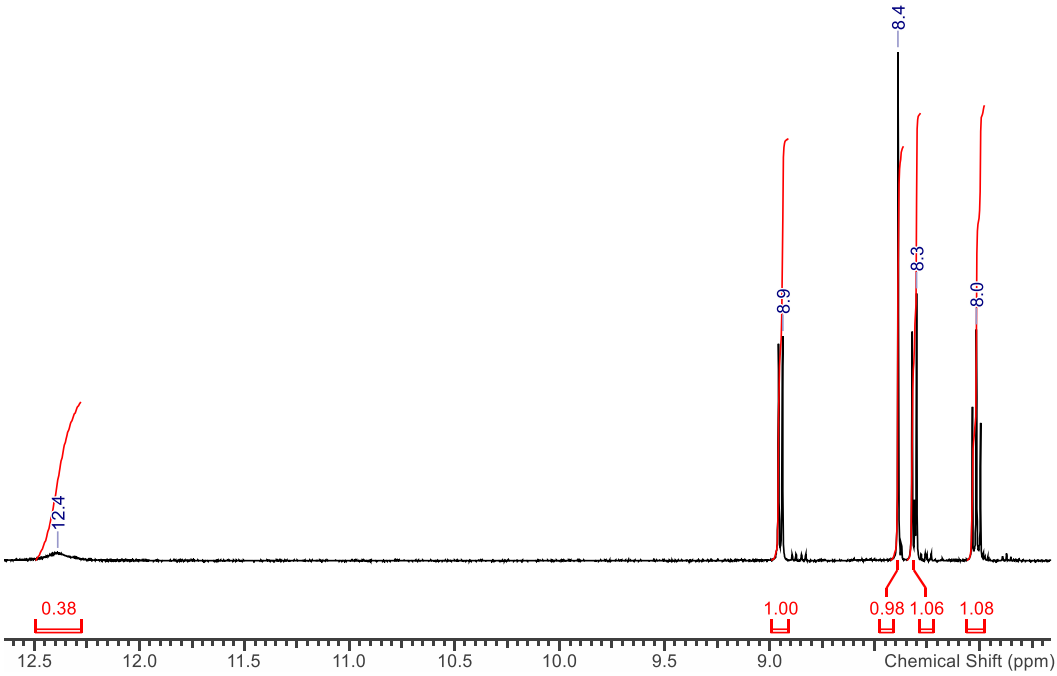

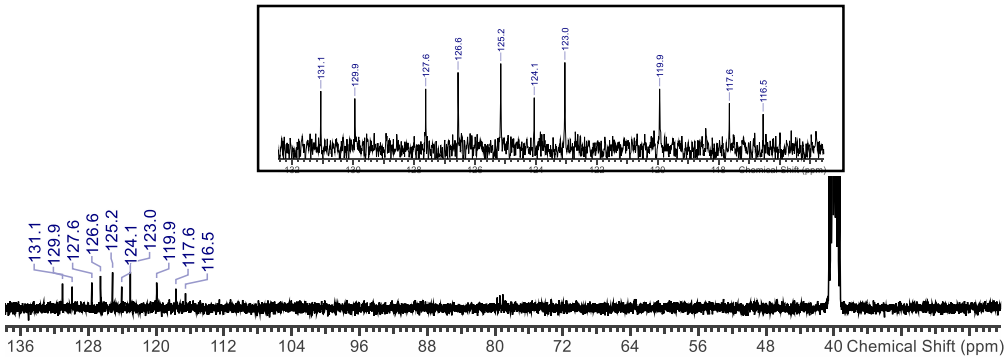

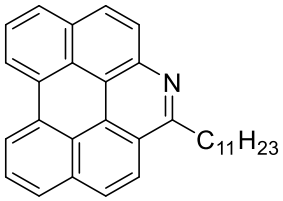

2-Undecylphenanthro[1,10,9,8-*klmna*]phenanthridine (**31**)

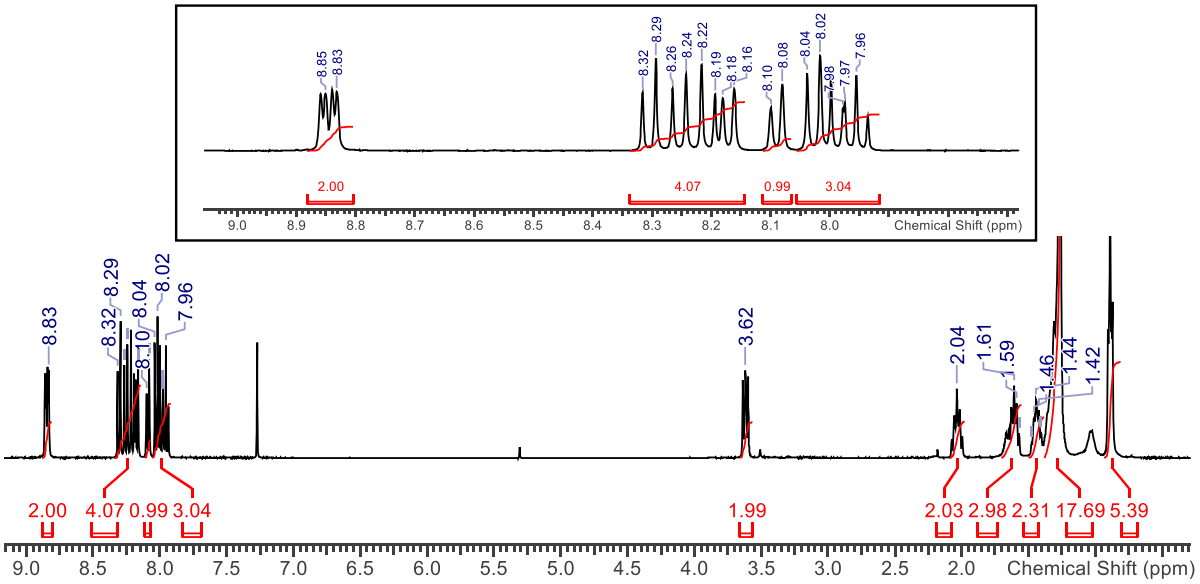

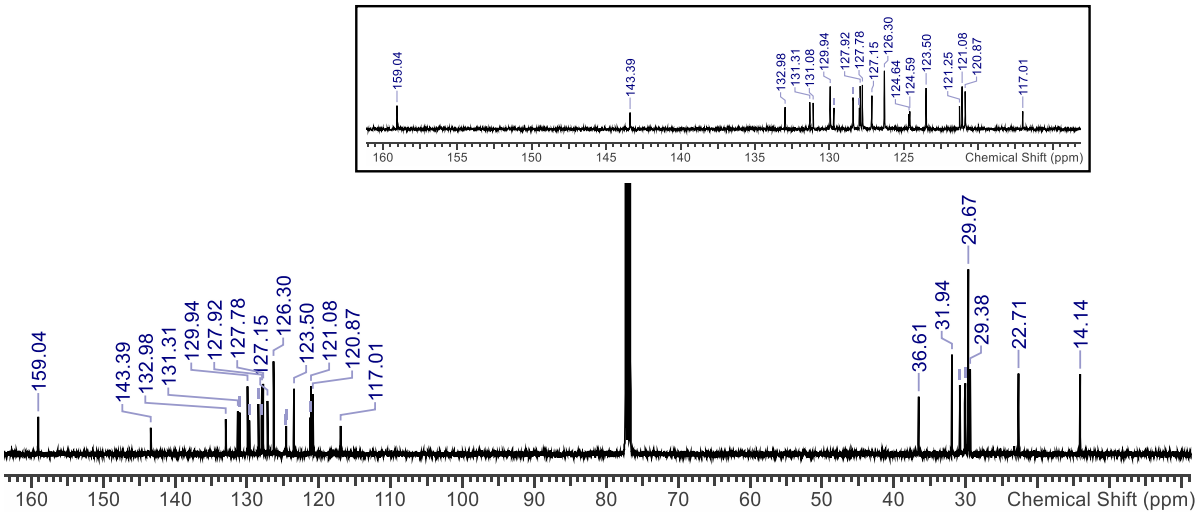

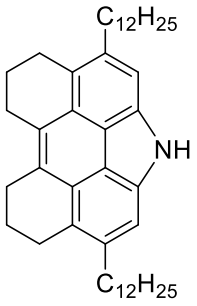

3,10-Didodecyl-4,5,6,7,8,9-hexahydro-1*H*-phenanthro[1,10,9,8-*cdefg*]carbazole (**49**)

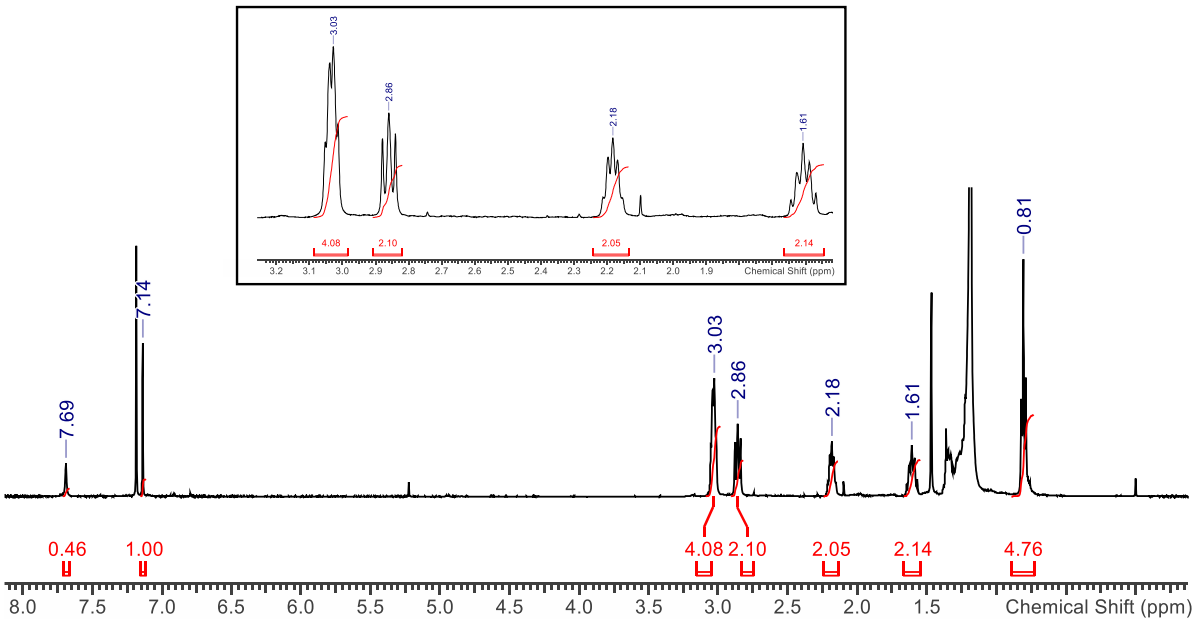

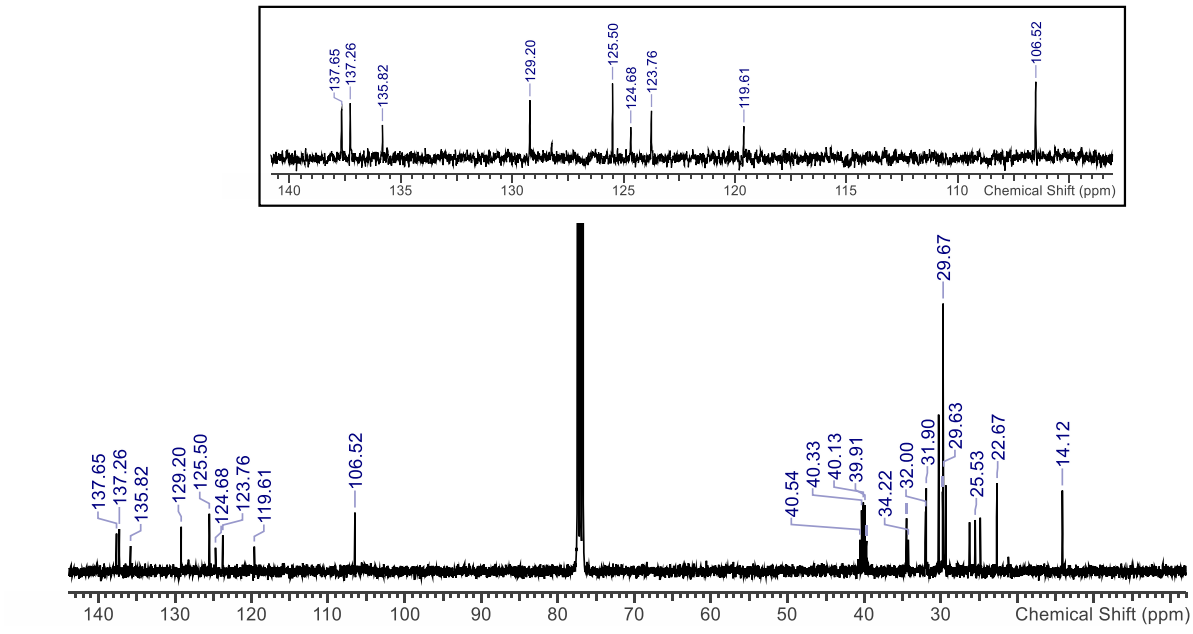

5.3. CRYSTALLOGRAPHIC AND STRUCTURAL REFINEMENT DATA

5.3.1. 1,6-*BIS*-(PHENANTHREN-9-YLTHIO)HEXANE

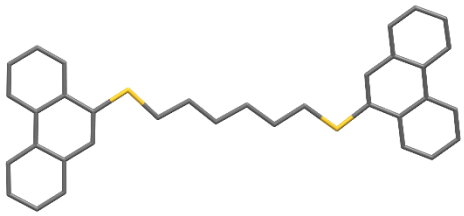

Identification code	S5026R
Empirical formula	$C_{41}H_{38}S_2$
Formula weight	594.83
Temperature/K	150
Crystal system	monoclinic
Space group	$P2_1/c$
a/Å	7.6663(2)
b/Å	22.5943(5)
c/Å	18.0159(4)
α/°	90
β/°	93.760(2)
γ/°	90
Volume/Å^3	3113.90(13)
Z	4
ρ_{calc}g/cm^3	1.269
μ/mm^{-1}	0.200
F(000)	1264.0
Crystal size/mm^3	0.5 × 0.5 × 0.34
Radiation	MoKα (λ = 0.71073)
2Θ range for data collection/°	4.258 to 60.326
Index ranges	$-10 \leq h \leq 10$, $-31 \leq k \leq 31$, $-24 \leq l \leq 25$
Reflections collected	46303
Independent reflections	8131 [R_{int} = 0.0350, R_{sigma} = 0.0299]

Data/restraints/parameters	8131/99/414
Goodness-of-fit on F^2	1.032
Final R indexes [I>=2σ (I)]	R_1 = 0.0503, wR_2 = 0.1241
Final R indexes [all data]	R_1 = 0.0654, wR_2 = 0.1315
Largest diff. peak/hole / e $Å^{-3}$	0.50/-0.62

5.3.2. 1,6-*BIS*-(PYREN-1-YLTHIO)HEXANE

Identification code	S4058QA
Empirical formula	$C_{38}H_{30}S_2$
Formula weight	550.74
Temperature/K	100(2)
Space group	$Pna2_1$
a/Å	10.5445(3)
b/Å	6.5897(2)
c/Å	38.6840(11)
α/°	90.00
β/°	90.00
γ/°	90.00
Volume/Å^3	2687.96(14)
Z	4
ρ_{calc}g/cm^3	1.361
μ/mm^{-1}	1.990
F(000)	1160.0
Crystal size/mm^3	0.26 × 0.17 × 0.09
Radiation	CuKα (λ = 1.54178)
2Θ range for data collection/°	4.56 to 144.42
Index ranges	$-12 \leq h \leq 12$, $-8 \leq k \leq 7$, $-41 \leq l \leq 47$
Reflections collected	10965
Independent reflections	4441 [R_{int} = 0.0344]
Data/restraints/parameters	4441/13/362
Goodness-of-fit on F^2	1.049
Final R indexes [I>=2σ (I)]	R_1 = 0.0617, wR_2 = 0.1510
Final R indexes [all data]	R_1 = 0.0641, wR_2 = 0.1541

Largest diff. peak/hole / e $Å^{-3}$	2.53/-0.39
Flack parameter	0.28(3)

5.3.3. 1,2-*BIS*-(2-(PYREN-1-YLTHIO)ETHOXY)ETHANE

Identification code	S4113NA
Empirical formula	$C_{38}H_{30}O_2S_2$
Formula weight	582.74
Temperature/K	180(2)
Space group	$P2_1/c$
a/Å	22.7430(13)
b/Å	6.9451(5)
c/Å	9.0284(5)
α/°	90.00
β/°	96.876(4)
γ/°	90.00
Volume/Å^3	1415.80(15)
Z	2
ρ_{calc}g/cm^3	1.367
μ/mm^{-1}	1.975
F(000)	612.0
Crystal size/mm^3	0.18 × 0.16 × 0.07
Radiation	CuKα (λ = 1.54178)
2Θ range for data collection/°	3.92 to 144.28
Index ranges	$-26 \leq h \leq 28$, $-5 \leq k \leq 8$, $-11 \leq l \leq 10$
Reflections collected	7424
Independent reflections	2728 [R_{int} = 0.0247]
Data/restraints/parameters	2728/0/190
Goodness-of-fit on F^2	1.043

Final R indexes [I>=2σ (I)]	R_1 = 0.0341, wR_2 = 0.0902
Final R indexes [all data]	R_1 = 0.0397, wR_2 = 0.0941
Largest diff. peak/hole / e $Å^{-3}$	0.40/-0.18

5.3.4. 6-(PYREN-1-YLTHIO)HEXANE-1-THIOL

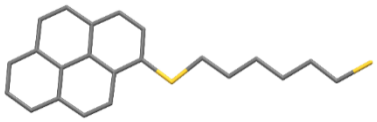

Identification code	S4097MA
Empirical formula	$C_{22}H_{22}S_2$
Formula weight	350.52
Temperature/K	100(2)
Space group	P-1
a/Å	7.5036(8)
b/Å	7.6007(7)
c/Å	17.7695(17)
α/°	93.842(4)
β/°	90.257(5)
γ/°	117.905(4)
Volume/Å^3	892.85(15)
Z	2
ρ_{calc}g/cm^3	1.304
μ/mm^{-1}	2.673
F(000)	372.0
Crystal size/mm^3	0.28 × 0.11 × 0.03
Radiation	CuKα (λ = 1.54178)
2Θ range for data collection/°	13.22 to 144.68
Index ranges	$-9 \leq h \leq 8$, $-9 \leq k \leq 9$, $-21 \leq l \leq 21$
Reflections collected	9239
Independent reflections	3382 [R_{int} = 0.0299]
Data/restraints/parameters	3382/0/221
Goodness-of-fit on F^2	1.097
Final R indexes [I>=2σ (I)]	R_1 = 0.0321, wR_2 = 0.0906
Final R indexes [all data]	R_1 = 0.0359, wR_2 = 0.0991

Largest diff. peak/hole / e $Å^{-3}$	0.33/-0.35

5.3.5. 1,8-Di(pyren-1-yl)octane

Identification code	S5028l
Empirical formula	$C_{40}H_{34}$
Formula weight	514.67
Temperature/K	100.03(10)
Crystal system	Monoclinic
Space group	$P2_1/c$
a/Å	8.8074(6)
b/Å	32.371(3)
c/Å	9.5281(6)
α/°	90
β/°	90.974(6)
γ/°	90
Volume/Å^3	2716.1(3)
Z	4
ρ_{calc}g/cm^3	1.259
μ/mm^{-1}	0.071
F(000)	1096.0
Crystal size/mm^3	0.08 × 0.043 × 0.014
Radiation	MoKα (λ = 0.71073)
2Θ range for data collection/°	4.456 to 57.112
Index ranges	$-11 \leq h \leq 11$, $-42 \leq k \leq 35$, $-7 \leq l \leq 12$
Reflections collected	15263
Independent reflections	6169 [R_{int} = 0.0622, R_{sigma} = 0.1129]
Data/restraints/parameters	6169/0/361
Goodness-of-fit on F^2	0.913
Final R indexes [I>=2σ (I)]	R_1 = 0.0552, wR_2 = 0.1082

Final R indexes [all data] $R_1 = 0.1616$, $wR_2 = 0.1402$

Largest diff. peak/hole / e $Å^{-3}$ 0.19/-0.19

5.3.6. 1-NITROPERYLENE

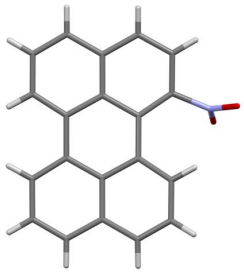

Identification code	S4879A
Empirical formula	$C_{20}H_{11}NO_2$
Formula weight	297.30
Temperature/K	149.9(3)
Crystal system	monoclinic
Space group	$P2_1/c$
a/Å	5.1980(4)
b/Å	14.7881(11)
c/Å	17.4042(15)
α/°	90
β/°	96.864(9)
γ/°	90
Volume/Å^3	1328.24(19)
Z	4
ρ_{calc}g/cm^3	1.487
μ/mm^{-1}	0.097
F(000)	616.0
Crystal size/mm^3	0.76 × 0.099 × 0.066
Radiation	MoKα (λ = 0.71073)
2Θ range for data collection/°	7.254 to 52.742
Index ranges	$-6 \leq h \leq 6$, $-18 \leq k \leq 18$, $-21 \leq l \leq 21$
Reflections collected	9689
Independent reflections	2720 [R_{int} = 0.0603, R_{sigma} = 0.0669]
Data/restraints/parameters	2720/0/208
Goodness-of-fit on F^2	1.044

Final R indexes [I>=2σ (I)]	R_1 = 0.0653, wR_2 = 0.1495
Final R indexes [all data]	R_1 = 0.0977, wR_2 = 0.1711
Largest diff. peak/hole / e $Å^{-3}$	0.55/-0.25

5.3.7. 3,10-DIBROMO-1*H*-PHENANTHRO[1,10,9,8-*CDEFG*]CARBAZOLE

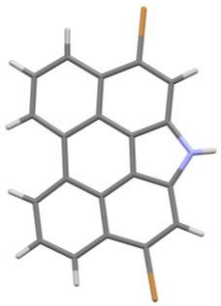

Identification code	S5025l
Empirical formula	$C_{20}H_9Br_2N$
Formula weight	423.10
Temperature/K	150
Crystal system	orthorhombic
Space group	$P2_12_12_1$
a/Å	3.9370(2)
b/Å	15.3357(8)
c/Å	22.7044(16)
α/°	90
β/°	90
γ/°	90
Volume/Å^3	1370.82(14)
Z	4
ρ_{calc}g/cm^3	2.050
μ/mm^{-1}	5.910
F(000)	824.0
Crystal size/mm^3	0.3 × 0.08 × 0.07
Radiation	MoKα (λ = 0.71073)
2Θ range for data collection/°	4.464 to 57.196
Index ranges	$-5 \leq h \leq 5$, $-20 \leq k \leq 20$, $-30 \leq l \leq 27$
Reflections collected	8170
Independent reflections	3145 [R_{int} = 0.0513, R_{sigma} = 0.0732]

Data/restraints/parameters	3145/0/208
Goodness-of-fit on F^2	1.025
Final R indexes [I>=2σ (I)]	R_1 = 0.0391, wR_2 = 0.0667
Final R indexes [all data]	R_1 = 0.0513, wR_2 = 0.0693
Largest diff. peak/hole / e $Å^{-3}$	0.48/-0.63
Flack parameter	0.019(12)

5.3.8. 3,10-DIDODECYL-4,5,6,7,8,9-HEXAHYDRO-1H-PHENANTHRO[1,10,9,8-*CDEFG*]CARBAZOLE

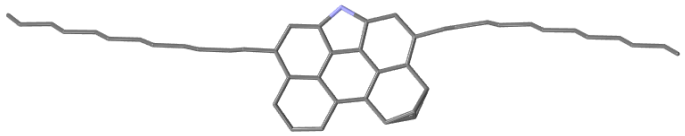

Identification code	S4936l
Empirical formula	$C_{44}H_{65}N$
Formula weight	607.97
Temperature/K	200.01(10)
Crystal system	Monoclinic
Space group	$P2_1$
a/Å	9.1892(5)
b/Å	8.0498(4)
c/Å	25.0877(16)
α/°	90
β/°	99.006(6)
γ/°	90
Volume/Å^3	1832.89(18)
Z	2
ρ_{calc}g/cm^3	1.102
μ/mm^{-1}	0.455
F(000)	672.0
Crystal size/mm^3	0.1 × 0.1 × 0.02
Radiation	CuKα (λ = 1.54184)
2Θ range for data collection/°	7.136 to 144.662
Index ranges	$-11 \leq h \leq 11$, $-9 \leq k \leq 9$, $-30 \leq l \leq 27$
Reflections collected	19044
Independent reflections	7019 [R_{int} = 0.0647, R_{sigma} = 0.0788]
Data/restraints/parameters	7019/3/421
Goodness-of-fit on F^2	0.979
Final R indexes [I>=2σ (I)]	R_1 = 0.0506, wR_2 = 0.1233

Final R indexes [all data]	R_1 = 0.0844, wR_2 = 0.1437
Largest diff. peak/hole / e Å^{-3}	0.13/-0.15
Flack parameter	-0.4(9)

6. REFERENCES

(1) McCabe, E. M.Chem Report, University of Manchester, 2017.

(2) Huc, A. Y. *Heavy Crude Oils: From Geology to Upgrading*; Editions Technip, 2011.

(3) Kolobov, A. V.; Tominaga, J. *Two-Dimensional Transition-Metal Dichalcogenides*; Springer Series in Materials Science; Springer International Publishing: Cham, 2016; Vol. 239.

(4) Aadony, B.; Looyeh, R. Fundamentals of Solid Mechanics. *Pet. Rock Mech.* **2011**, 1–12.

(5) Schenk, C. J.; Cook, T. A.; Charpentier, R. R.; Pollastro, R. M.; Klett, T. R.; Tennyson, M. E.; Kirschbaum, M. A.; Brownfield, M. E.; Pitman, J. K. An Estimate of Recoverable Heavy Oil Resources of the Orinoco Oil Belt, Venezuela. **2009**.

(6) Agrawal, P. India's Petroleum Demand: Estimations and Projections. *Appl. Econ.* **2015**, *47*, 1199–1212.

(7) Buenrostro-Gonzalez, E.; Groenzin, H.; Lira-Galeana, C.; Mullins, O. C. The Overriding Chemical Principles That Define Asphaltenes. *Energy and Fuels* **2001**, *15*, 972–978.

(8) Coletti, F.; Joshi, H. M.; Macchietto, S.; Hewitt, G. F. Introduction. In *Crude Oil Fouling*; Elsevier, 2015; pp 1–22.

(9) Sinnathambi, C. M.; Nor, N. M. Relationship between SARA Fractions and Crude Oil Fouling. *J. Appl. Sci.* **2012**, *12*, 2479–2483.

(10) Schantz, S. S.; Stephenson, W. K. Asphaltene Deposition: Development and Application of Polymeric Asphaltene Dispersants. In *SPE Annual Technical Conference and Exhibition*; Society of Petroleum Engineers: Dallas, TX, 1991.

(11) Villard, Y.; Fajardo, F.; Milne, A. Enhanced Oil Recovery Using Innovative Asphaltene Inhibitors in East Venezuela. In *SPE International Conference and Exhibition on Formation Damage Control*; Society of Petroleum Engineers: Lafayette, Louisiana, 2016.

(12) Kelland, M. *Production Chemicals for the Oil and Gas Industry*, 2nd ed.; CRC Press:

Baton Rouge, 2014.

(13) Montoya, T.; Coral, D.; Franco, C. A.; Nassar, N. N.; Cortés, F. B. A Novel Solid–Liquid Equilibrium Model for Describing the Adsorption of Associating Asphaltene Molecules onto Solid Surfaces Based on the "Chemical Theory." *Energy and Fuels* **2014**, *28*, 4963–4975.

(14) Abdallah, W. A.; Taylor, S. D. Surface Characterization of Adsorbed Asphaltene on a Stainless Steel Surface. *Nucl. Instruments Methods Phys. Res. Sect. B Beam Interact. with Mater. Atoms* **2007**, *258*, 213–217.

(15) Al-Jabari, M.; Husien, M. Review of Adsorption of Asphaltenes onto Surfaces and Its Application in Heavy Oil Recovery/Upgrading and Environmental Protection. In *3rd International Congress of Chemistry and Environment ICCE*; 2007.

(16) Dickie, J. P.; Yen, T. F. Macrostructures of the Asphaltic Fractions by Various Instrumental Methods. *Anal. Chem.* **1967**, *39*, 1847–1852.

(17) Mullins, O. C. The Modified Yen Model †. *Energy and Fuels* **2010**, *24*, 2179–2207.

(18) Mullins, O. C.; Sabbah, H.; Eyssautier, J.; Pomerantz, A. E.; Barré, L.; Andrews, A. B.; Ruiz-Morales, Y.; Mostowfi, F.; McFarlane, R.; Goual, L.; et al. Advances in Asphaltene Science and the Yen–Mullins Model. *Energy and Fuels* **2012**, *26*, 3986–4003.

(19) Sjöblom, J.; Simon, S.; Xu, Z. Model Molecules Mimicking Asphaltenes. *Adv. Colloid Interface Sci.* **2015**, *218*, 1–16.

(20) Xiong, Y.; Cao, T.; Chen, Q.; Li, Z.; Yang, Y.; Xu, S.; Yuan, S.; Sjöblom, J.; Xu, Z. Adsorption of a Polyaromatic Compound on Silica Surfaces from Organic Solvents Studied by Molecular Dynamics Simulation and AFM Imaging. *J. Phys. Chem. C* **2017**, *121*, 5020–5028.

(21) Tissot, B. P.; Welte, D. T. *Petroleum Formation and Occurrence*, 2nd ed.; Springer-Verlag: Berlin, 1984.

(22) Bjorlykke, K. *Petroleum Geoscience: From Sedimentary Environments to Rock Physics*; Springer International Publishing, 2010.

(23) Galwey, A. Some Chemical and Mechanistic Aspects of Petroleum Formation. *Trans. R. Soc. South Africa* **2015**, *70*, 9–24.

(24) Nan, Z. D.; Xiang X-C; Zeng, H. L.; Zhang, H. T.; Sun, Y. Thermo-Kinetic Investigation of Optimum Growth Temperature of Petroleum Bacteria. *J. Therm. Anal. Calorim.* **2001**, *63*, 291–296.

(25) Rocks, P.; Stresses, E. *Petroleum Rock Mechanics*; Elsevier, 2011.

(26) Drummond, C.; Israelachvili, J. Fundamental Studies of Crude Oil–surface Water Interactions and Its Relationship to Reservoir Wettability. *J. Pet. Sci. Eng.* **2004**, *45*, 61–81.

(27) Speight, J. G. Thermal Methods of Recovery. In *Heavy Oil Production Processes*; Elsevier, 2013; pp 93–130.

(28) Pourabdollah, K.; Mokhtari, B. The VAPEX Process, from Beginning up to Date. *Fuel* **2013**, *107*, 1–33.

(29) Mullins, O. C.; Sheu, E. Y.; Hammami, A.; Marshall, A. G. *Asphaltenes, Heavy Oils, and Petroleomics*; Springer, 2007; Vol. 8.

(30) Knight, A. *Enhanced Oil Recovery: Methods, Economic Benefits and Impacts on the Environment*; Nova Science Pub. Inc., 2015.

(31) Tiratsoo, J. Pigging Research. In *Pipeline Pigging and Inspection Technology*; Elsevier, Ed.; Elsevier, 1999; pp 449–459.

(32) Jones, D. S. J. S. Handbook of Petroleum Processing. In *Handbook of Petroleum Processing*; Springer Netherlands: Dordrecht, 2008; pp 47–109.

(33) Mozdianfard, M. R.; Behranvand, E. Fouling at Post Desalter and Preflash Drum Heat Exchangers of CDU Preheat Train. *Appl. Therm. Eng.* **2015**, *89*, 783–794.

(34) Coletti, F.; Macchietto, S. Refinery Pre-Heat Train Network Simulation Undergoing Fouling: Assessment of Energy Efficiency and Carbon Emissions. *Heat Transf. Eng.* **2011**, *32*, 228–236.

(35) Jones, D. S. J. S. Handbook of Petroleum Processing. In *Handbook of Petroleum Processing*; Springer Netherlands: Dordrecht, 2008; pp 111–187.

(36) Ludwig, E. E. *Applied Process Design for Chemical and Petrochemical Plants*; Gulf Pub. Co, 1995.

(37) Speight, J. G. *Fouling in Refineries*; Elsevier: Oxford, 2015.

(38) Palmer, K. A.; Hale, W. T.; Such, K. D.; Shea, B. R.; Bollas, G. M. Optimal Design of Tests for Heat Exchanger Fouling Identification. *Appl. Therm. Eng.* **2016**, *95*, 382–393.

(39) Bott, T. R. *Fouling of Heat Exchangers*; Elsevier, 1995.

(40) Demirbas, A.; Alidrisi, H.; Balubaid, M. A. API Gravity, Sulfur Content, and Desulfurization of Crude Oil. *Pet. Sci. Technol.* **2015**, *33*, 93–101.

(41) Fahim, M. A.; Alsahhaf, T. A.; Elkilani, A. S. *Fundamentals of Petroleum Refining*; Elsevier, 2010.

(42) Fan, T.; Wang, J.; Buckley, J. S. Evaluating Crude Oils by SARA Analysis. In *SPE/DOE Improved Oil Recovery Symposium*; Society of Petroleum Engineers: Tulsa, Oklahoma, 2002.

(43) Santos, R. G.; Loh, W.; Bannwart, A. C.; Trevisan, O. V. An Overview of Heavy Oil Properties and Its Recovery and Transportation Methods. *Brazilian J. Chem. Eng.* **2014**, *31*, 571–590.

(44) Khaksar, L.; Shirokoff, J. Effect of Elemental Sulfur and Sulfide on the Corrosion Behavior of Cr-Mo Low Alloy Steel for Tubing and Tubular Components in Oil and Gas Industry. *Materials (Basel).* **2017**, *10*, 430.

(45) Parisotto, G.; Ferrão, M. F.; Müller, A. L. H.; Müller, E. I.; Santos, M. F. P.; Guimarães, R. C. L.; Dias, J. C. M.; Flores, E. M. M. Total Acid Number Determination in Residues of Crude Oil Distillation Using ATR-FTIR and Variable Selection by Chemometric Methods. *Energy and Fuels* **2010**, *24*, 5474–5478.

(46) Moschopedis, S. E.; Speight, J. G. Oxygen Functions in Asphaltenes. *Fuel* **1976**, *55*, 334–336.

(47) Sheu, E. Y.; Mullins, O. C. Asphaltenes: Fundamentals and Applications. In *Asphaltenes: fundamentals and applications*; Fine Particle Society: Chicago, Illinois, 1993.

(48) Zhao, X.; Shi, Q.; Gray, M. R.; Xu, C. New Vanadium Compounds in Venezuela Heavy Crude Oil Detected by Positive-Ion Electrospray Ionization Fourier Transform Ion Cyclotron Resonance Mass Spectrometry. *Sci. Rep.* **2015**, *4*, 5373.

(49) Ashoori, S.; Sharifi, M.; Masoumi, M.; Mohammad Salehi, M. The Relationship between SARA Fractions and Crude Oil Stability. *Egypt. J. Pet.* **2017**, *26*, 209–213.

(50) Klein, G. C.; Kim, S.; Rodgers, R. P.; Marshall, A. G.; Yen, A.; Asomaning, S. Mass Spectral Analysis of Asphaltenes. I. Compositional Differences between Pressure-Drop and Solvent-Drop Asphaltenes Determined by Electrospray Ionization Fourier Transform Ion Cyclotron Resonance Mass Spectrometry. *Energy and Fuels* **2006**, *20*, 1965–1972.

(51) Wang, P.; Dong, Z.; Tan, Y.; Liu, Z. Investigating the Interactions of the Saturate, Aromatic, Resin, and Asphaltene Four Fractions in Asphalt Binders by Molecular Simulations. *Energy and Fuels* **2015**, *29*, 112–121.

(52) Andersen, S. I.; Hofsäss, T.; Kleinitz, W.; Rahimian, I. Organic Precipitates in Oil Production of a Venezuelan Oil Field. *Pet. Sci. Technol.* **2001**, *19*, 55–74.

(53) Spiecker, P. M.; Gawrys, K. L.; Kilpatrick, P. K. Aggregation and Solubility Behavior of Asphaltenes and Their Subfractions. *J. Colloid Interface Sci.* **2003**, *267*, 178–193.

(54) Rubinstein, I.; Strausz, O. P. Thermal Treatment of the Athabasca Oil Sand Bitumen and its Component Parts. *Geochim. Cosmochim. Acta* **1979**, *43*, 1887–1893.

(55) Ali, M. F.; Saleem, M. Thermal Decomposition of Saudi Crude Oil Asphaltenes. *Fuel Sci. Technol. Int.* **1991**, *9*, 461–484.

(56) Zuo, P.; Shen, W. Identification of Nitrogen-Polyaromatic Compounds in Asphaltene from Co-Processing of Coal and Petroleum Residue Using Chromatography with Mass Spectrometry. *Int. J. Coal Sci. Technol.* **2017**, *4*, 281–299.

(57) Mitra-Kirtley, S.; Mullins, O. C.; Van Elp, J.; George, S. J.; Chen, J.; Cramer, S. P. Determination of the Nitrogen Chemical Structures in Petroleum Asphaltenes Using XANES Spectroscopy. *J. Am. Chem. Soc.* **1993**, *115*, 252–258.

(58) Yen, T. F.; Chilingarian, G. *Asphaltenes and Asphalts 2*; Elsevier: Los Angeles, 2000.

(59) H. Ali, L.; A. Al-Ghannam, K.; M. Al-Rawi, J. Chemical Structure of Asphaltenes in Heavy Crude Oils Investigated by NMR. *Fuel* **1990**, *69*, 519–521.

(60) Hortal, A. R.; Martínez-Haya, B.; Lobato, M. D.; Pedrosa, J. M.; Lago, S. On the Determination of Molecular Weight Distributions of Asphaltenes and Their Aggregates in Laser Desorption Ionization Experiments. *J. Mass Spectrom.* **2006**, *41*, 960–968.

(61) Bunger, J. W.; Li, N. C. *Chemistry of Asphaltenes*; Bunger, J. W., Li, N. C., Eds.; Advances in Chemistry; American Chemical Society: Washington, D.C., 1982; Vol. 195.

(62) Mullins, O. C.; Martínez-Haya, B.; Marshall, A. G. Contrasting Perspective on Asphaltene Molecular Weight. This Comment vs the Overview of A. A. Herod, K. D. Bartle, and R. Kandiyoti. *Energy and Fuels* **2008**, *22*, 1765–1773.

(63) Pomerantz, A. E.; Hammond, M. R.; Morrow, A. L.; Mullins, O. C.; Zare, R. N. Two-Step Laser Mass Spectrometry of Asphaltenes. *J. Am. Chem. Soc.* **2008**, *130*, 7216–7217.

(64) Schneider, M. H.; Andrews, a. B.; Mitra-Kirtley, S.; Mullins, O. C. Asphaltene Molecular Size by Fluorescence Correlation Spectroscopy. *Energy and Fuels* **2007**, *21*, 2875–2882.

(65) Kawashima, H.; Takanohashi, T.; Iino, M.; Matsukawa, S. Determining Asphaltene Aggregation in Solution from Diffusion Coefficients as Determined by Pulsed-Field Gradient Spin-Echo 1H NMR. *Energy and Fuels* **2008**, *22*, 3989–3993.

(66) Groenzin, H.; Mullins, O. C.; Eser, S.; Mathews, J.; Yang, M. G.; Jones, D. Molecular Size of Asphaltene Solubility Fractions. *Energy and Fuels* **2003**, *17*, 498–503.

(67) Badre, S.; Carla Goncalves, C.; Norinaga, K.; Gustavson, G.; Mullins, O. C. Molecular Size and Weight of Asphaltene and Asphaltene Solubility Fractions from Coals, Crude Oils and Bitumen. *Fuel* **2006**, *85*, 1–11.

(68) Andrews, A. B.; Guerra, R. E.; Mullins, O. C.; Sen, P. N. Diffusivity of Asphaltene Molecules by Fluorescence Correlation Spectroscopy. *J. Phys. Chem. A* **2006**, *110*, 8093–8097.

(69) Guerra, R. E.; Ladavac, K.; Andrews, A. B.; Mullins, O. C.; Sen, P. N. Diffusivity of

Coal and Petroleum Asphaltene Monomers by Fluorescence Correlation Spectroscopy. *Fuel* **2007**, *86*, 2016–2020.

(70) Lisitza, N. V.; Freed, D. E.; Sen, P. N.; Song, Y.-Q. Study of Asphaltene Nanoaggregation by Nuclear Magnetic Resonance. *Energy and Fuels* **2009**, *23*, 1189–1193.

(71) Tissot, B.; Welte, D. *Petroleum Formation and Occurrence: A New Approach to Oil and Gas Exploration*; Springer Science and Business Media, 2012.

(72) Murgich, J.; Abanero, J. A.; Strausz, O. P. Molecular Recognition in Aggregates Formed by Asphaltene and Resin Molecules from the Athabasca Oil Sand. *Energy and Fuels* **1999**, *13*, 278–286.

(73) Sedghi, M.; Goual, L. PC-SAFT Modeling of Asphaltene Phase Behavior in the Presence of Nonionic Dispersants. *Fluid Phase Equilib.* **2014**, *369*, 86–94.

(74) Alvarez-Ramírez, F.; Ruiz-Morales, Y. Island versus Archipelago Architecture for Asphaltenes: Polycyclic Aromatic Hydrocarbon Dimer Theoretical Studies. *Energy and Fuels* **2013**, *27*, 1791–1808.

(75) Alemany, L. B.; Verma, M.; Billups, W. E.; Wellington, S. L.; Shammai, M. Solid- and Solution-State Nuclear Magnetic Resonance Analyses of Ecuadorian Asphaltenes: Quantitative Solid-State Aromaticity Determination Supporting the "Island" Structural Model. Aliphatic Structural Information from Solution-State NMR *Energy and Fuels* **2015**, *29*, 6317–6329.

(76) Ungerer, P.; Rigby, D.; Leblanc, B.; Yiannourakou, M. Sensitivity of the Aggregation Behaviour of Asphaltenes to Molecular Weight and Structure Using Molecular Dynamics. *Mol. Simul.* **2014**, *40*, 115–122.

(77) Borton, D.; Pinkston, D. S.; Hurt, M. R.; Tan, X.; Azyat, K.; Scherer, A.; Tykwinski, R.; Gray, M.; Qian, K.; Kenttämaa, H. I. Molecular Structures of Asphaltenes Based on the Dissociation Reactions of Their Ions in Mass Spectrometry. *Energy and Fuels* **2010**, *24*, 5548–5559.

(78) Ancheyta Juárez, J.; Trejo, F.; Rana, M. S. *Asphaltenes : Chemical Transformation during Hydroprocessing of Heavy Oils*; CRC Press/Taylor and Francis, 2009.

(79) Strausz, O. P.; Mojelsky, T.; Lown, E. M. The Molecular Structure Unfolding Story of Asphaltene: An Unfolding Story. *Fuel* **1992**, *71*, 1355–1363.

(80) Gray, M. R.; Tykwinski, R. R.; Stryker, J. M.; Tan, X. Supramolecular Assembly Model for Aggregation of Petroleum Asphaltenes. *Energy and Fuels* **2011**, *25*, 3125–3134.

(81) Alshareef, A. H.; Scherer, A.; Tan, X.; Azyat, K.; Stryker, J. M.; Tykwinski, R. R.; Gray, M. R. Formation of Archipelago Structures during Thermal Cracking Implicates a Chemical Mechanism for the Formation of Petroleum Asphaltenes. *Energy and Fuels* **2011**, *25*, 2130–2136.

(82) Karimi, A.; Qian, K.; Olmstead, W. N.; Freund, H.; Yung, C.; Gray, M. R. Quantitative Evidence for Bridged Structures in Asphaltenes by Thin Film Pyrolysis. *Energy and Fuels* **2011**, *25*, 3581–3589.

(83) Bae, E.; Yeo, I. J.; Jeong, B.; Shin, Y.; Shin, K.-H.; Kim, S. Study of Double Bond Equivalents and the Numbers of Carbon and Oxygen Atom Distribution of Dissolved Organic Matter with Negative-Mode FT-ICR MS. *Anal. Chem.* **2011**, *83*, 4193–4199.

(84) Li, D. D.; Greenfield, M. L. High Internal Energies of Proposed Asphaltene Structures. *Energy and Fuels* **2011**, *25*, 3698–3705.

(85) Maksić, Z. B.; Barić, D.; Müller, T. Clar's Sextet Rule Is a Consequence of the σ-Electron Framework. *J. Phys. Chem. A* **2006**, *110*, 10135–10147.

(86) Ruiz-Morales, Y. HOMO−LUMO Gap as an Index of Molecular Size and Structure for Polycyclic Aromatic Hydrocarbons and Asphaltenes: A Theoretical Study. I. *J. Phys. Chem. A* **2002**, *106*, 11283–11308.

(87) Mondal, R.; Adhikari, R. M.; Shah, B. K.; Neckers, D. C. Revisiting the Stability of Hexacenes. *Org. Lett.* **2007**, *9*, 2505–2508.

(88) Mondal, R.; Shah, B. K.; Neckers, D. C. Photogeneration of Heptacene in a Polymer Matrix. *J. Am. Chem. Soc.* **2006**, *128*, 9612–9613.

(89) Zajac, G. Maya Petroleum Asphaltene Imaging by Scanning Tunneling Microscopy: Verification of Structure from Carbon and Proton NMR: https://web.anl.gov/PCS/acsfuel/preprint archive/Files/42_2_SAN FRANCISCO_04-97_0423.pdf.

(90) Sharma, A.; Groenzin, H.; Tomita, A.; Mullins, O. C. Probing Order in Asphaltenes and Aromatic Ring Systems by HRTEM. *Energy and Fuels* **2002**, *16*, 490–496.

(91) Andrews, A. B.; Edwards, J. C.; Pomerantz, A. E.; Mullins, O. C.; Nordlund, D.; Norinaga, K. Comparison of Coal-Derived and Petroleum Asphaltenes by 13 C Nuclear Magnetic Resonance, DEPT, and XRS. *Energy and Fuels* **2011**, *25*, 3068–3076.

(92) Schuler, B.; Meyer, G.; Peña, D.; Mullins, O. C.; Gross, L. Unraveling the Molecular Structures of Asphaltenes by Atomic Force Microscopy. *J. Am. Chem. Soc.* **2015**, *137*, 9870–9876.

(93) Carlos da Silva Ramos, A.; Haraguchi, L.; Notrispe, F. R.; Loh, W.; Mohamed, R. S. Interfacial and Colloidal Behavior of Asphaltenes Obtained from Brazilian Crude Oils. *J. Pet. Sci. Eng.* **2001**, *32*, 201–216.

(94) Evdokimov, I.; Eliseev, N. Y. Rheological Evidence of Structural Phase Transitions in Asphaltene-Containing Petroleum Fluids. *J. Pet. Sci. Eng.* **2001**, *30*, 199–211.

(95) Evdokimov, I. N.; Eliseev, N. Y.; Akhmetov, B. R. Assembly of Asphaltene Molecular Aggregates as Studied by near-UV/visible Spectroscopy: I. Structure of the Absorbance Spectrum. *J. Pet. Sci. Eng.* **2003**, *37*, 135–143.

(96) Wiehe, I. A.; Liang, K. S. Asphaltenes, Resins, and Other Petroleum Macromolecules. *Fluid Phase Equilib.* **1996**, *117*, 201–210.

(97) Siddiqui, M. N. Infrared Study of Hydrogen Bond Types in Asphaltenes. *Pet. Sci. Technol.* **2006**, *21*, 1601–1615.

(98) Siffert, B.; Kuczinski, J.; Papirer, E. Relationship between Electrical Charge and Flocculation of Heavy Oil Distillation Residues in Organic Medium. *J. Colloid Interface Sci.* **1990**, *135*, 107–117.

(99) Gray, M. R.; Tykwinski, R. R.; Stryker, J. M.; Tan, X. Supramolecular Assembly Model for Aggregation of Petroleum Asphaltenes. *Energy and Fuels* **2011**, *25*, 3125–3134.

(100) Bouhadda, Y.; Bormann, D.; Sheu, E.; Bendedouch, D.; Krallafa, A.; Daaou, M. Characterization of Algerian Hassi-Messaoud Asphaltene Structure Using Raman Spectrometry and X-Ray Diffraction. *Fuel* **2007**, *86*, 1855–1864.

(101) Sheu, E. Y. Small Angle Scattering and Asphaltenes. *J. Phys. Condens. Matter* **2006**, *18*, 2485–2498.

(102) Eyssautier, J.; Levitz, P.; Espinat, D.; Jestin, J.; Gummel, J.; Grillo, I.; Barré, L. Insight into Asphaltene Nanoaggregate Structure Inferred by Small Angle Neutron and X-Ray Scattering. *J. Phys. Chem.* **2011**, *115*, 6827–6837.

(103) Szymula, M.; Marczewski, A. W. Adsorption of Asphaltenes from Toluene on Typical Soils of Lublin Region. *Appl. Surf. Sci.* **2002**, *196*, 301–311.

(104) Kor, P.; Kharrat, R. Modeling of Asphaltene Particle Deposition from Turbulent Oil Flow in Tubing: Model Validation and a Parametric Study. *Petroleum* **2016**, *2*, 393–398.

(105) Nielsen, B. B.; Svrcek, W. Y.; Mehrotra, A. K. Effects of Temperature and Pressure on Asphaltene Particle Size Distributions in Crude Oils Diluted with N-Pentane. *Ind. Eng. Chem. Res.* **1994**, *33*, 1324–1330.

(106) Andersen, S. I.; Christensen, S. D. The Critical Micelle Concentration of Asphaltenes As Measured by Calorimetry. *Energy and Fuels* **2000**, *14*, 38–42.

(107) Castillo, J.; Goncalves, S.; Fernández, A.; Mujica, V. Applications of Photothermal Displacement Spectroscopy to the Study of Asphaltenes Adsorption. *Opt. Commun.* **1998**, *145*, 69–75.

(108) Angle, C. W.; Long, Y.; Hamza, H.; Lue, L. Precipitation of Asphaltenes from Solvent-Diluted Heavy Oil and Thermodynamic Properties of Solvent-Diluted Heavy Oil Solutions. *Fuel* **2006**, *85*, 492–506.

(109) Yudin, I. K.; Nikolaenko, G. L.; Gorodetskii, E. E.; Kosov, V. I.; Melikyan, V. R.; Markhashov, E. L.; Frot, D.; Briolant, Y. Mechanisms of Asphaltene Aggregation in Toluene–heptane Mixtures. *J. Pet. Sci. Eng.* **1998**, *20*, 297–301.

(110) Bockrath, B. C.; LaCount, R. B.; Noceti, R. P. Coal-Derived Asphaltenes: Effect of Phenol Content and Molecular Weight on Viscosity of Solutions. *Fuel* **1980**, *59*, 621–626.

(111) Molina V., D.; Ariza, E.; Poveda, J. C. Structural Differences among the Asphaltenes in Colombian Light Crudes from the Colorado Oil Field. *Energy and Fuels* **2017**, *31*, 133–

139.

(112) González, G.; Moreira, M. B. C. The Wettability of Mineral Surfaces Containing Adsorbed Asphaltene. *Colloids and Surfaces* **1991**, *58*, 293–302.

(113) Jeribi, M.; Almir-Assad, B.; Langevin, D.; Hénaut, I.; Argillier, J. F. Adsorption Kinetics of Asphaltenes at Liquid Interfaces. *J. Colloid Interface Sci.* **2002**, *256*, 268–272.

(114) Dudášová, D.; Simon, S.; Hemmingsen, P. V.; Sjöblom, J. Study of Asphaltenes Adsorption onto Different Minerals and Clays: Part 1. Experimental Adsorption with UV Depletion Detection. *Colloids Surfaces A Physicochem. Eng. Asp.* **2008**, *317*, 1–9.

(115) Araújo, R. S.; Azevedo, D. C. S.; Cavalcante, C. L.; Jiménez-López, A.; Rodríguez-Castellón, E. Adsorption of Polycyclic Aromatic Hydrocarbons (PAHs) from Isooctane Solutions by Mesoporous Molecular Sieves: Influence of the Surface Acidity. *Microporous Mesoporous Mater.* **2008**, *108*, 213–222.

(116) Murrell, L, Grenoble, D, Long, R. Separating Basic Asphaltenes Using Bronsted Acid Transition Metal Oxide Acid Catalysts. U.S. Patent 4424114, September 24, 1981.

(117) Raj, G.; Lesimple, A.; Whelan, J.; Naumov, P. Direct Observation of Asphaltene Nanoparticles on Model Mineral Substrates. *Langmuir* **2017**, *33*, 6248–6257.

(118) Alboudwarej, H.; Beck, J.; Svrcek, W. Y.; Yarranton, H. W.; Akbarzadeh, K. Sensitivity of Asphaltene Properties to Separation Techniques. *Energy and Fuels* **2002**, *16*, 462–469.

(119) Nassar, N. N. Asphaltene Adsorption onto Alumina Nanoparticles: Kinetics and Thermodynamic Studies. *Energy and Fuels* **2010**, *24*, 4116–4122.

(120) Goual, L.; Horváth-Szabó, G.; Masliyah, J. H.; Xu, Z. Adsorption of Bituminous Components at Oil/Water Interfaces Investigated by Quartz Crystal Microbalance: Implications to the Stability of Water-in-Oil Emulsions. *Langmuir* **2005**, *21*, 8278–8289.

(121) Ekholm, P.; Blomberg, E.; Claesson, P.; Auflem, I. H.; Sjöblom, J.; Kornfeldt, A. A Quartz Crystal Microbalance Study of the Adsorption of Asphaltenes and Resins onto a Hydrophilic Surface. *J. Colloid Interface Sci.* **2002**, *247*, 342–350.

(122) Fritschy, G.; Papirer, E. Interactions between a Bitumen, Its Components and Model Fillers. *Fuel* **1978**, *57*, 701–704.

(123) Tan, X.; Fenniri, H.; Gray, M. R. Pyrene Derivatives of 2,2′-Bipyridine as Models for Asphaltenes: Synthesis, Characterization, and Supramolecular Organization. *Energy and Fuels* **2008**, *22*, 715–720.

(124) Diner, C.; Scott, D. E.; Tykwinski, R. R.; Gray, M. R.; Stryker, J. M. Scalable, Chromatography-Free Synthesis of Alkyl-Tethered Pyrene-Based Materials. Application to First-Generation "Archipelago Model" Asphaltene Compounds. *J. Org. Chem.* **2015**, *80*, 1719–1726.

(125) Akbarzadeh, K.; Bressler, D. C.; Wang, J.; Gawrys, K. L.; Gray, M. R.; Kilpatrick, P. K.; Yarranton, H. W. Association Behavior of Pyrene Compounds as Models for Asphaltenes. *Energy and Fuels* **2005**, *19*, 1268–1271.

(126) Schulze, M.; Lechner, M. P.; Stryker, J. M.; Tykwinski, R. R. Aggregation of Asphaltene Model Compounds Using a Porphyrin Tethered to a Carboxylic Acid. *Org. Biomol. Chem.* **2015**, *13*, 6984–6991.

(127) Alshareef, A. H.; Scherer, A.; Stryker, J. M.; Tykwinski, R. R.; Gray, M. R. Thermal Cracking of Substituted Cholestane–Benzoquinoline Asphaltene Model Compounds. *Energy and Fuels* **2012**, *26*, 3592–3603.

(128) Schulze, M.; Scherer, A.; Hampel, F.; Stryker, J. M.; Tykwinski, R. R. Synthesis and Aggregation Behavior of Chiral Naphthoquinoline Petroporphyrin Asphaltene Model Compounds. *Chemistry* **2016**, *22*, 3378–3386.

(129) Nordgård, E. L.; Sjöblom, J. Isoprenoid Tetraacids. Part I: Synthesis and Interfacial Activities. *J. Dispers. Sci. Technol.* **2008**, *29*, 1114–1122.

(130) Martín-Martínez, F. J.; Fini, E. H.; Buehler, M. J. Molecular Asphaltene Models Based on Clar Sextet Theory. *RSC Adv.* **2015**, *5*, 753–759.

(131) Jian, C.; Liu, Q.; Zeng, H.; Tang, T. Effect of Model Polycyclic Aromatic Compounds on the Coalescence of Water-in-Oil Emulsion Droplets. *J. Phys. Chem. C* **2017**, *121*, 10382–10391.

(132) Lahive, C. W.; Deuss, P. J.; Lancefield, C. S.; Sun, Z.; Cordes, D. B.; Young, C. M.;

Tran, F.; Slawin, A. M. Z.; de Vries, J. G.; Kamer, P. C. J.; et al. Advanced Model Compounds for Understanding Acid-Catalyzed Lignin Depolymerization: Identification of Renewable Aromatics and a Lignin-Derived Solvent. *J. Am. Chem. Soc.* **2016**, *138*, 8900–8911.

(133) Collman, J. P.; Brauman, J. I.; Doxsee, K. M.; Halbert, T. R.; Suslick, K. S. Model Compounds for the T State of Hemoglobin. *Proc. Natl. Acad. Sci.* **1978**, *75*, 564–568.

(134) Stern, J. O.; Peisach,: Study of Cytochrome of the CO-Adduct. *J. Biol. Chem.* **1974**, *249*, 7495–7498.

(135) Rakotondradany, F.; Fenniri, H.; Rahimi, P.; Gawrys, K. L.; Kilpatrick, P. K.; Gray, M. R. Hexabenzocoronene Model Compounds for Asphaltene Fractions: Synthesis and Characterization. *Energy and Fuels* **2006**, *20*, 2439–2447.

(136) Jian, C.; Tang, T.; Bhattacharjee, S. Probing the Effect of Side-Chain Length on the Aggregation of a Model Asphaltene Using Molecular Dynamics Simulations. *Energy and Fuels* **2013**, *27*, 2057–2067.

(137) Dynarowicz-Łątka, P.; Dhanabalan, A.; Oliveira, O. N. Modern Physicochemical Research on Langmuir Monolayers. *Adv. Colloid Interface Sci.* **2001**, *91*, 221–293.

(138) Nordgård, E. L.; Landsem, E.; Sjöblom, J. Langmuir Films of Asphaltene Model Compounds and Their Fluorescent Properties. *Langmuir* **2008**, *24*, 8742–8751.

(139) Wang, J.; van der Tuuk Opedal, N.; Lu, Q.; Xu, Z.; Zeng, H.; Sjöblom, J. Probing Molecular Interactions of an Asphaltene Model Compound in Organic Solvents Using a Surface Forces Apparatus (SFA). *Energy and Fuels* **2012**, *26*, 2591–2599.

(140) Wang, J.; Lu, Q.; Harbottle, D.; Sjöblom, J.; Xu, Z.; Zeng, H. Molecular Interactions of a Polyaromatic Surfactant C5Pe in Aqueous Solutions Studied by a Surface Forces Apparatus. *J. Phys. Chem. B* **2012**, *116*, 11187–11196.

(141) Nordgård, E. L.; Sørland, G.; Sjöblom, J. Behavior of Asphaltene Model Compounds at W/O Interfaces. *Langmuir* **2010**, *26*, 2352–2360.

(142) Tùng, Đ. T.; Tuân, Đ. T.; Rasool, N.; Villinger, A.; Reinke, H.; Fischer, C.; Langer, P. Regioselective Palladium(0)-Catalyzed Cross-Coupling Reactions and Metal-Halide Exchange Reactions of Tetrabromothiophene: Optimization, Scope and Limitations.

Adv. Synth. Catal. **2009**, *351*, 1595–1609.

(143) Badger, G. M.; Christie, B. J.; Pryke, J. M.; Sasse, W. H. F. 890. Synthetic Applications of Activated Metal Catalysts. Part V. The Desulphurisation of Flavophen and of Tetraphenylthiophen. *J. Chem. Soc.* **1957**, 4417-4419.

(144) Chen, T.-A.; Liu, R.-S. Synthesis of Polyaromatic Hydrocarbons from Bis(biaryl)diynes: Large PAHs with Low Clar Sextets. *Chem. Eur. J.* **2011**, *17*, 8023–8027.

(145) Little, M. S.; Yeates, S. G.; Alwattar, A. A.; Heard, K. W. J.; Raftery, J.; Edwards, A. C.; Parry, A. V. S.; Quayle, P. Insights into the Scholl Coupling Reaction: A Key Transformation of Relevance to the Synthesis of Graphenes and Related Systems. *European J. Org. Chem.* **2017**, *83*, 1694–1703.

(146) King, B. T.; Kroulík, J.; Robertson, C. R.; Rempala, P.; Hilton, C. L.; Korinek, J. D.; Gortari, L. M. Controlling the Scholl Reaction. *J. Org. Chem.* **2007**, *72*, 2279–2288.

(147) Zhai, L.; Shukla, R.; Wadumethrige, S. H.; Rathore, R. Probing the Arenium-Ion (ProtonTransfer) versus the Cation-Radical (Electron Transfer) Mechanism of Scholl Reaction Using DDQ as Oxidant. *J. Org. Chem.* **2010**, *75*, 4748–4760.

(148) Grzybowski, M.; Skonieczny, K.; Butenschön, H.; Gryko, D. T. Comparison of Oxidative Aromatic Coupling and the Scholl Reaction. *Angew. Chem. Int. Ed.* **2013**, *52*, 9900–9930.

(149) Ito, S.; Wehmeier, M.; Brand, J. D.; Kübel, C.; Epsch, R.; Rabe, J. P.; Müllen, K. Synthesis and Self-Assembly of Functionalized Hexa-Peri-Hexabenzocoronenes. *Chemistry* **2000**, *6*, 4327–4342.

(150) Yamaguchi, R.; Ito, S.; Lee, B. S.; Hiroto, S.; Kim, D.; Shinokubo, H. Functionalization of Hexa- Peri -Hexabenzocoronenes: Investigation of the Substituent Effects on a Superbenzene. *Chem. Asian J.* **2013**, *8*, 178–190.

(151) Seyler, H.; Purushothaman, B.; Jones, D. J.; Holmes, A. B.; Wong, W. W. H. Hexa-Peri-Hexabenzocoronene in Organic Electronics. *Pure Appl. Chem.* **2012**, *84*, 1047–1067.

(152) Alameddine, B.; Caba, S.; Schindler, M.; Jenny, T. Synthesis of Alkyl-Substituted Tribenzopentaphenes as Versatile Polycondensed Aromatic Hydrocarbon π-π Stacking

Building Blocks. *Synthesis* **2012**, *44*, 1928–1934.

(153) Alameddine, B.; Anju, R. S.; Al-Sagheer, F.; Jenny, T. A. Tribenzopentaphene Derivatives with Lateral Aromatic Groups: The Effect of the Nature and Position of Substituents on Emission Properties. *New J. Chem.* **2016**, *40*, 10363–10370.

(154) Alameddine, B.; Sobhana Anju, R.; Shetty, S.; Baig, N.; Al-Mousawi, S.; Al-Sagheer, F. Direct Synthesis of Polyaromatic Chains of Tribenzopentaphene Copolymers through Cyclodehydrogenation of Their Poly-Tetraphenylbenzene Precursors. *J. Polym. Sci. Part A Polym. Chem.* **2017**, *55*, 3565–3572.

(155) Xu, Y.; Mao, N.; Feng, S.; Zhang, C.; Wang, F.; Chen, Y.; Zeng, J.; Jiang, J.-X. Perylene-Containing Conjugated Microporous Polymers for Photocatalytic Hydrogen Evolution. *Macromol. Chem. Phys.* **2017**, *218*, 1700-1749.

(156) Torres, É.; Berberan-Santos, M. N.; Brites, M. J. Synthesis, Photophysical and Electrochemical Properties of Perylene Dyes. *Dye. Pigment.* **2015**, *112*, 298–304.

(157) Jiang, W.; Qian, H.; Li, Y.; Wang, Z. Heteroatom-Annulated Perylenes: Practical Synthesis, Photophysical Properties, and Solid-State Packing Arrangement. *J. Org. Chem.* **2008**, *73*, 7369–7372.

(158) Głodek, M.; Makal, A.; Kłys, A.; Zakrzewski, J.; Plażuk, D. Direct Synthesis of Perylene-Fused Cyclic Ketones from Perylene and 2-Alkenoic Acids. *European J. Org. Chem.* **2016**, 4215–4223.

(159) Clayden, J.; Greeves, N.; Warren, S. *Organic Chemistry*; OUP Oxford, 2012.

(160) Jiang, W.; Zhou, Y.; Geng, H.; Jiang, S.; Yan, S.; Hu, W.; Wang, Z.; Shuai, Z.; Pei, J. Solution-Processed, High-Performance Nanoribbon Transistors Based on Dithioperylene. *J. Am. Chem. Soc.* **2011**, *133*, 1–3.

(161) Chen, Z. J.; Wang, L. M.; Zou, G.; Zhang, L.; Zhang, G. J.; Cai, X. F.; Teng, M. S. Colorimetric and Ratiometric Fluorescent Chemosensor for Fluoride Ion Based on Perylene Diimide Derivatives. *Dye. Pigment.* **2012**, *94*, 410–415.

(162) Adachi, S.; Onozuka, M.; Yoshida, Y.; Ide, M.; Saikawa, Y.; Nakata, M. Smooth Isoindolinone Formation from Isopropyl Carbamates via Bischler-Napieralski-Type Cyclization. *Org. Lett.* **2014**, *16*, 358–361.

(163) Wei, H.; Zhang, L.; Phan, H.; Huang, X.; Herng, T. S.; Zhou, J.; Zeng, W.; Ding, J.; Luo, S.; Wu, J.; et al. A Stable *N* -Annulated Perylene-Bridged Bisphenoxyl Diradicaloid and the Corresponding Boron Trifluoride Complex. *Chem. Eur. J.* **2017**, *23*, 9419–9424.

(164) Kathayat, R. S.; Finney, N. S. Sulfoxides as Response Elements for Fluorescent Chemosensors. *J. Am. Chem. Soc.* **2013**, *135*, 12612–12614.

(165) Kathayat, R. S.; Yang, L.; Sattasathuchana, T.; Zoppi, L.; Baldridge, K. K.; Linden, A.; Finney, N. S. On the Origins of Nonradiative Excited State Relaxation in Aryl Sulfoxides Relevant to Fluorescent Chemosensing. *J. Am. Chem. Soc.* **2016**, *138*, 15889–15895.

(166) Malashikhin, S.; Finney, N. S. Fluorescent Signaling Based on Sulfoxide Profluorophores: Application to the Visual Detection of the Explosive TATP. *J. Am. Chem. Soc.* **2008**, *130*, 12846–12847.

(167) Li, J.-R.; Bu, X.-H.; Zhang, R.-H.; Duan, C.-Y.; Man-Chung Wong, K.; Wing-Wah Yam, V. Lanthanide Perchlorate Complexes with 1,4-Bis(phenylsulfinyl)butane: Structures and Luminescent Properties. *New J. Chem.* **2004**, *28*, 261-265.

(168) Desgranges, C.; Delhommelle, J. Coarse-Grained Model and Boiling Point Prediction for Asphaltene Model Compounds via HMC-WL Simulations. *Energy and Fuels* **2017**, *31*, 10699–10705.

(169) Zhang, X.; Tan, H.; Yan, Y.; Hang, Y.; Yu, F.; Qu, X.; Hua, J. Targetable N-Annulated Perylene-Based Colorimetric and Ratiometric near-Infrared Fluorescent Probes for the Selective Detection of Hydrogen Sulfide in Mitochondria, Lysosomes, and Serum. *J. Mater. Chem. B* **2017**, *5*, 2172–2180.

(170) Usuki, T.; Komatsu, A. Preparation of Monoalkylpiperidines via the Mild Hydrogenation of Monoalkynylpyridines. *Tetrahedron Lett.* **2017**, *58*, 2856–2858.

(171) Heard, K. PhD Thesis: Novel Polyaromatics for Organic Electronics and Graphene Exfoliation: Synthetic Approaches Utilising Regioselective Aromatic C-H Borylation, University of Manchester, 2016.

(172) Grinko, A. A.; Min, R. S.; Sagachenko, T. A.; Golovko, A. K. Aromatic Sulfur-

Containing Structural Units of Resins and Asphaltenes in Heavy Hydrocarbon Feedstock. *Pet. Chem.* **2012**, *52*, 221–227.

(173) Ruiz-Morales, Y.; Mullins, O. C. Measured and Simulated Electronic Absorption and Emission Spectra of Asphaltenes. *Energy and Fuels* **2009**, *23*, 1169–1177.

(174) Meng, L.; Fujikawa, T.; Kuwayama, M.; Segawa, Y.; Itami, K. Thiophene-Fused π-Systems from Diarylacetylenes and Elemental Sulfur. *J. Am. Chem. Soc.* **2016**, *138*, 10351–10355.

(175) Nguyen, T. B.; Retailleau, P. Redox-Neutral Access to Sultams from 2-Nitrochalcones and Sulfur with Complete Atom Economy. *Org. Lett.* **2017**, *19*, 3879–3882.

(176) McKenna, A. M.; Donald, L. J.; Fitzsimmons, J. E.; Juyal, P.; Spicer, V.; Standing, K. G.; Marshall, A. G.; Rodgers, R. P. Heavy Petroleum Composition. 3. Asphaltene Aggregation. *Energy and Fuels* **2013**, *27*, 1246–1256.

(177) Kim, H.-S.; Lee, J.-H.; Kim, T.-H.; Okabe, S.; Shibayama, M.; Choi, S.-M. Phase Behavior of Hexa- *Peri* -Hexabenzocoronene Derivative in Organic Solvent. *J. Phys. Chem. B* **2011**, *115*, 7314–7320.

(178) de Souza, A. L. F.; da Silva, L. C.; Oliveira, B. L.; Antunes, O. A. C. Microwave- and Ultrasound-Assisted Suzuki–Miyaura Cross-Coupling Reactions Catalyzed by Pd/PVP. *Tetrahedron Lett.* **2008**, *49*, 3895–3898.

(179) Vanel, R.; Berthiol, F.; Bessières, B.; Einhorn, C.; Einhorn, J. Efficient Synthesis of Substituted Polyarylphthalimides *via* Cycloaddition of Cyclopentadienones with 2-Bromomaleimide. *Synlett* **2011**, *22*, 1293–1295.

(180) Zhu, S.; Wang, L.; Li, B.; Song, Y.; Zhao, X.; Zhang, G.; Zhang, S.; Lu, S.; Zhang, J.; Wang, H.; et al. Investigation of Photoluminescence Mechanism of Graphene Quantum Dots and Evaluation of Their Assembly into Polymer Dots. *Carbon N. Y.* **2014**, *77*, 462–472.

(181) Kadu, R. K.; Patil, V. R. New Strategy for Synthesis of Polyphenylene Substituted Dendronized Monomers Containing Fluorene Unit and the Study of Their Properties. *Polycycl. Aromat. Compd.* **2017**, *37*, 395–406.

(182) Gagnon, E.; Halperin, S. D.; Métivaud, V.; Maly, K. E.; Wuest, J. D. Tampering with

Molecular Cohesion in Crystals of Hexaphenylbenzenes. *J. Org. Chem.* **2010**, *75*, 399–406.

(183) Dötz, F.; Brand, J. D.; Ito, S.; Gherghel, L.; Müllen, K. Synthesis of Large Polycyclic Aromatic Hydrocarbons: Variation of Size and Periphery. *J. Am. Chem. Soc.* **2000**, *122*, 7707–7717.

(184) Sarhan, A. A. O.; Bolm, C. Iron Chloride in Oxidative C–C Coupling Reactions. *Chem. Soc. Rev.* **2009**, *38*, 2730.

(185) Rempala, P.; Kroulík, J.; King, B. T. Investigation of the Mechanism of the Intramolecular Scholl Reaction of Contiguous Phenylbenzenes. *J. Org. Chem.* **2006**, *71*, 5067–5081.

(186) Fei, X.-S.; Tian, W.-S.; Chen, Q.-Y. New, Convenient Route for Trifluoromethylation of Steroidal Molecules. *J. Chem. Soc. Perkin Trans. 1* **1998**, *6*, 1139–1142.

(187) Mandell, L. The Mechanism of the Wettstein-Oppenauer Oxidation. *J. Am. Chem. Soc.* **1956**, *78*, 3199–3201.

(188) Chochrek, P.; Wicha, J. 1,3-Chirality Transfer by Fragmentation of Allylsulfinic Acids: A Diastereoselective Approach to Vinyl Bromides Related Totrans-Hydrindane Ortrans-Decalin. *European J. Org. Chem.* **2007**, *2007*, 2534–2542.

(189) Kirby, A. J. *Stereoelectronic Effects*; Oxford University Press, 1996.

(190) Fairfull, A. E. S.; Petrow, V.; Short, W. F.; Shaw, J. I.; Stevenson, R.; Janus, J. W.; Clemo, G. R.; Howe, R.; Edington, R. A.; Percival, E. *J. Chem. Soc.* **1955**, 3549.

(191) Ishiyama, T.; Murata, M.; Miyaura, N. Palladium(0)-Catalyzed Cross-Coupling Reaction of Alkoxydiboron with Haloarenes: A Direct Procedure for Arylboronic Esters. *J. Org. Chem.* **1995**, *60*, 7508–7510.

(192) Lemcoff, G.; Ben-Asuly, A. Sulfur Chelated Ruthenium Compounds Useful as Olefin Metathesis Catalysts. US20100113722, 2010.

(193) Zhang, R.; Xu, L.; Chen, H.; Qin, Z.; Zhao, Y.; Ni, Z. Convenient Synthesis of 1-Thiohydroxypyrene by Newman-Kwart Rearrangement. *Chem. Res. Chinese Univ.* **2015**, *31*, 224–227.

(194) Hopff, H.; Schweizer, H. R. Zur Kenntnis Des Coronens. 2. Mitteilung. Dien-Anlagerungen in Der Perylen- Und Benzperylenreihe. *Helv. Chim. Acta* **1959**, *42*, 2315–2333.

(195) Madhu, S.; Evans, H. A.; Doan-Nguyen, V. V. T.; Labram, J. G.; Wu, G.; Chabinyc, M. L.; Seshadri, R.; Wudl, F. Infinite Polyiodide Chains in the Pyrroloperylene-Iodine Complex: Insights into the Starch-Iodine and Perylene-Iodine Complexes. *Angew. Chem. Int. Ed.* **2016**, *55*, 8032–8035.

(196) Almonasy, N.; Nepraš, M.; Hyková, Š.; Lyčka, A.; Čermák, J.; Dvořák, M.; Michl, M. The Synthesis of N-Derivatives of 3-Aminoperylene and Their Absorption and Fluorescence Properties. *Dye. Pigment.* **2009**, *82*, 164–170.

(197) Stephenson, M. T.; Shine, H. J. Cation Radicals. 47. Reaction of Perylene Cation Radical with Fluoride Ion and of Perylene with Xenon Difluoride. Formation of 1-Fluoro-, 3-Fluoro-, and a Difluoroperylene. Complications with Chloride Ion Impurity. *J. Org. Chem.* **1981**, *46*, 3139–3141.

(198) Broese, T.; Francke, R. Electrosynthesis Using a Recyclable Mediator–Electrolyte System Based on Ionically Tagged Phenyl Iodide and 1,1,1,3,3,3-Hexafluoroisopropanol. *Org. Lett.* **2016**, *18*, 5896–5899.

(199) Buu-Hoï, N. P.; Jacquignon, P.; Long, C. T. 99. Carcinogenic Nitrogen Compounds. Part XXI. New Alkyl Homologues of Phenanthridine, Benzacridines, and Related Nuclei. *J. Chem. Soc.* **1957**, 505–509.

(200) Markoulides, M. S.; Venturini, C.; Neumeyer, D.; Gourdon, A. Oxidative Cyclodehydrogenation of a Perylene Derivative: Different Reagents Give Different Products. *New J. Chem.* **2015**, *39*, 6498–6503.

(201) Truce, W. E.; Lyons, J. F. Sulfination of Aryllithium Compounds. The Preparation of Sodium O-, M- and P-N-Dodecylbenzenesulfonates. *J. Am. Chem. Soc.* **1951**, *73*, 126–128.

(202) Gabka, G.; Bujak, P.; Gryszel, M.; Kotwica, K.; Pron, A. Anchor Groups Effect on Spectroscopic and Electrochemical Properties of Quaternary Nanocrystals Cu–In–Zn–S Capped with Arylamine Derivatives. *J. Phys. Chem. C* **2015**, *119*, 9656–9664.

(203) Park, K.; Bae, G.; Moon, J.; Choe, J.; Song, K. H.; Lee, S. Synthesis of Symmetrical and Unsymmetrical Diarylalkynes from Propiolic Acid Using Palladium-Catalyzed Decarboxylative Coupling. *J. Org. Chem.* **2010**, *75*, 6244–6251.

(204) Shan, L.; Liu, D.; Li, H.; Xu, X.; Shan, B.; Xu, J.-B.; Miao, Q. Monolayer Field-Effect Transistors of Nonplanar Organic Semiconductors with Brickwork Arrangement. *Adv. Mater.* **2015**, *27*, 3418–3423.

(205) Xu, H.; Zhang, H.; Wu, F. Liquid Crystal Composition with High Optical Anisotropy and Liquid Crystal Display Element. CN102634347B, 2012.

(206) Jin, W.; Yamamoto, Y.; Fukushima, T.; Ishii, N.; Kim, J.; Kato, K.; Takata, M.; Aida, T. Systematic Studies on Structural Parameters for Nanotubular Assembly of Hexa- Peri -Hexabenzocoronenes. *J. Am. Chem. Soc.* **2008**, *130*, 9434–9440.

(207) Fechtenkötter, A.; Saalwächter, K.; Harbison, M. A.; Müllen, K.; Spiess, H. W. Highly Ordered Columnar Structures from Hexa-Peri-hexabenzocoronenes—Synthesis, X-Ray Diffraction, and Solid-State Heteronuclear Multiple-Quantum NMR Investigations. *Angew. Chem. Int. Ed.* **1999**, *38*, 3039–3042.

(208) Jones, D. J.; Purushothaman, B.; Ji, S.; Holmes, A. B.; Wong, W. W. H. Synthesis of Electron-Poor Hexa-Peri-Hexabenzocoronenes. *Chem. Commun.* **2012**, *48*, 8066–8068.

(209) Halleux, A.; Martin, R. H.; King, G. S. D. Synthèses Dans La Série Des Dérivés Polycycliques Aromatiques Hautement Condensés. L'hexabenzo-1,12; 2,3; 4,5; 6,7; 8,9; 10,11-Coronène, Le Tétrabenzo-4,5; 6,7; 11,12; 13,14-Péropyrène et Le Tétrabenzo-1,2; 3,4; 8,9; 10,11-Bisanthène. *Helv. Chim. Acta* **1958**, *41*, 1177–1183.

(210) Wu, J.; Fechtenkötter, A.; Gauss, J.; Watson, M. D.; Kastler, M.; Fechtenkötter, C.; Wagner, M.; Müllen, K. Controlled Self-Assembly of Hexa- P Eri - Hexabenzocoronenes in Solution. *J. Am. Chem. Soc.* **2004**, *126*, 11311–11321.

(211) Sauriat-Dorizon, H.; Maris, T.; Wuest, J. D.; Enright, G. D. Molecular Tectonics. Construction of Porous Hydrogen-Bonded Networks from Bisketals of Pentaerythritol. *J. Org. Chem.* **2003**, *68*, 240–246.

(212) Li, J.; Hu, B.; Hu, G.; Li, X.; Lu, P.; Wang, Y. An Efficient Synthesis of Heptaaryldipyrromethenes from Tetraarylcyclopentadienones and Ammonium Acetate

and Their Extension to the Corresponding BODIPYs. *Org. Biomol. Chem.* **2012**, *10*, 8848–8859.

(213) Fechtenkötter, A.; Tchebotareva, N.; Watson, M.; Müllen, K. Discotic Liquid Crystalline Hexabenzocoronenes Carrying Chiral and Racemic Branched Alkyl Chains: Supramolecular Engineering and Improved Synthetic Methods. *Tetrahedron* **2001**, *57*, 3769–3783.

(214) Byrne, B.; Wengenroth, K. J. A Convenient Preparation of Ethyl Vinyl Ketone. *Synthesis*, **1986**, 870–871.

(215) Adam, W.; Sahin, C.; Schneider, M. Mechanism of the Diastereoselective, Boron Trifluoride-Catalyzed Cyclization of Olefinic Tosylhydrazones to Stereolabeled, Bridgehead-Substituted Azoalkanes. *J. Am. Chem. Soc.* **1995**, *117*, 1695–1702.

(216) Lim, Z. B.; Tan, K. S.; Lunchev, A. V.; Li, H.; Cho, S. J.; Grimsdale, A. C.; Yazami, R. Synthesis and Assessment of New Cyclopenta-2,4-Dienone Derivatives for Energy Storage Applications. *Synth. Met.* **2015**, *200*, 85–90.

(217) Loi, S.; Wiesler, U.-M.; Butt, H.-J.; Müllen, K. Self-Assembly of Alkyl-Substituted Polyphenylene Dendrimers on Graphite. *Macromolecules* **2001**, *34*, 3661–3671.

(218) Ruzicka, L.; Plattner, P. A.; Aeschbacher, R. Über Steroide Und Sexualhormone. 44. Mitteilung. Zur Abspaltung von Bromwasserstoff Aus 2-Brom-Cholestanon Und 2-Brom-Androstandion. *Helv. Chim. Acta* **1938**, *21*, 866–872.

(219) Ohgane, K.; Karaki, F.; Noguchi-Yachide, T.; Dodo, K.; Hashimoto, Y. Structure-Activity Relationships of Oxysterol-Derived Pharmacological Chaperones for Niemann-Pick Type C1 Protein. *Bioorg. Med. Chem. Lett.* **2014**, *24*, 3480–3485.

(220) Tomoeda, M.; Ishizaki, M.; Kobayashi, H.; Kanatomo, S.; Koga, T.; Inuzuka, M.; Furuta, T. Studies on Conformation and reactivity—I : The Polyphosphoric Acid-Catalyzed Ring Opening of 4,5-Epoxy-3-Oxo Steroids—the Synthesis of 4-Ethylthiocholest-4-EN-3-One and Its Analogs. *Tetrahedron* **1965**, *21*, 733–742.

(221) Diev, V. V.; Schlenker, C. W.; Hanson, K.; Zhong, Q.; Zimmerman, J. D.; Forrest, S. R.; Thompson, M. E. Porphyrins Fused with Unactivated Polycyclic Aromatic Hydrocarbons. *J. Org. Chem.* **2012**, *77*, 143–159.

(222) Ammerer, L.; Zinke, A. Untersuchungen Uber Perylen Und Seine Derivate. *Monatshefte fur Chemie* **1953**, *84*, 25–31.

(223) Nefedov, V. A. Pyrene Dimerization into 1,1′-Dipyrenyl. *Russ. J. Org. Chem.* **2007**, *43*, 1163–1166.